

**DEVELOPMENT OF ENVIRONMENTALLY BENIGN POROUS
POLYMER MEMBRANES FOR SUSTAINABLE
AGRICULTURAL PRACTICES**

Submitted to University of Calicut
in partial fulfilment of the requirements
for the award of the Degree of
Doctor of Philosophy in
Chemistry

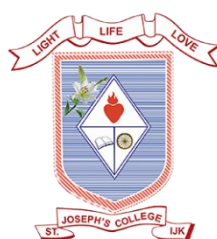
By

NONU DAVIS CHAKKALAKKAL

Registration No: 10016/2014/Admn

Under the guidance of

Dr. Pearly Sebastian Chittilappilly



RESEARCH AND PG DEPARTMENT OF CHEMISTRY

ST. JOSEPH'S COLLEGE (AUTONOMOUS)

THRISSUR, KERALA – 680121

JUNE- 2023

DECLARATION

I hereby declare that the Ph. D. thesis entitled “**Development of Environmentally Benign Porous Polymer Membranes for Sustainable Agricultural Practices**” is an original work carried out by me at Research and PG Department of Chemistry, St. Joseph’s College (Autonomous), Irinjalakuda, Kerala-680121 under the supervision of Dr. Pearly Sebastian Chittilappilly and it has not been submitted elsewhere for any other degree, diploma or title.

Irinjalakuda

26-06-2023

Nonu Davis Chakkalakkal



Research & PG Department of Chemistry
St. Joseph's College (Autonomous)
Irinjalakuda, Thrissur, Kerala 680121

Tel: 0480-2825358, Mob: 8301000125

www.stjosephs.edu.in

info@stjosephs.edu.in

Certificate

This is to certify that the work incorporated in this Ph.D. thesis entitled “**Development of Environmentally Benign Porous Polymer Membranes for Sustainable Agricultural Practices**” submitted by Ms. Nonu Davis Chakkalakkal to University of Calicut in partial fulfilment of the requirements for the award of the Degree of Doctor of Philosophy, embodies original research work done under my supervision. I further certify that this work has not been submitted to any other University or Institution in part or full for the award of any degree or diploma. Any text, illustration, table *etc.* used in the thesis from other sources, have been duly cited and acknowledged.

26-06-2023

Dr. Pearly Sebastian Chittilappilly
(Supervising Teacher)
Associate Professor (Retd.)
Research and PG Department of Chemistry
St. Joseph's College
Irinjalakuda



St. Joseph's College (Autonomous), Irinjalakuda

NAAC accredited with 'A++' grade (4th cycle)

Thrissur District, Kerala, India. Pin- 680121

Telephone: 0480-2825358, Fax: 0480-2830954

E-mail: info@stjosephs.edu.in, office@stjosephs.edu.in website: www.stjosephs.edu.in

To

Date: 10-11-2023

The Director
Directorate of Research
University of Calicut

Respected Sir,

Sub: Ph.D- Adjudication of Thesis in respect of Ms. Nonu Davis Chakkalakkal., – One and the same certificate submitting


Ref : No.153040/RESEARCH-C-ASST-1/2023/Admn - dated 17-10.2023

I hereby certify that the contents included in the hard copy and the soft copy submitted by Ms. Nonu Davis Chakkalakkal.,(U.O.No.10016/2014/Admn dated 30.10.2014), Research Scholar, Research & PG Department of Chemistry, St.Joseph's College(Autonomous), Irinjalakuda are one and the same. The title of the Thesis is "DEVELOPMENT OF ENVIRONMENTALLY BENIGN POROUS POLYMER MEMBRANES FOR SUSTAINABLE AGRICULTURAL PRACTICES".

I request you to accept the thesis and do the needful.

Thanking You,

Yours Faithfully,


Dr. Pearly Sebastian Chittilappilly,
Research Guide & Associate Professor (Retd.),
St. Joseph's College, (Autonomous), Irinjalakuda.

Acknowledgments

It is hard to put into meaningful words my deep feeling of gratitude for all the people who directly or indirectly have contributed to this achievement. I take this opportunity to express my appreciation to all those who made this Ph. D thesis possible.

I would like to express my sincere gratitude to my advisor, Dr. Pearly Sebastian Chittilappilly for her continuous support, advice, and motivation throughout my Ph. D work. Her immense knowledge and guidance helped me in all the time of research and writing of this thesis.

I also wish to place on record my deep sense of gratitude to Dr. Sr. Anjana Rose for her timely assistance, encouragement and valuable suggestions throughout my work.

I record my heartfelt thanks to Dr. Sr. Blessy, Principal and all former Principals, for the academic support and providing me the necessary facilities for carrying out my research work in this institution.

I am grateful to Dr. Deena Antony C., Head, Department of Chemistry, St. Joseph's College, Irinjalakuda for her timely advice and support for the conduct of academic procedures. I also extend my sincere thanks to former Heads of Department, for all her support and guidelines. I wish to thank all other faculty members in the Department of Chemistry for constant support and motivation. I hereby express my sincere thanks to Lab Assistants for the invaluable support they offered whenever I was in need.

I would also like to thank Dr. A. Sujith for providing lab facilities at Department of Chemistry, NIT, Calicut, Kerala.

I sincerely thank my Doctoral Advisory Committee members for their insightful comments and encouragement throughout my coursework and Ph. D programme.

I profoundly express my thanks to Ms. Anjali P.D, Research Scholar, Department of Chemistry, NIT, Calicut for the assistance in experimental part. I acknowledge in a

special way the help and cooperation extended to me by my lab mates and project students especially Jasheena, Ashiba and Sweety. I would also like to thank the administrative, library and technical staff members of St. Joseph's College for the cooperation and help in their respective roles.

I would like to acknowledge Department of Science and Technology for providing me financial support under Woman Scientist Scheme- A

I gratefully acknowledge the electrospinning facilities provided at NIT Calicut. I hereby acknowledge the help rendered by the IIT Madras, STIC-CUSAT, Kerala Agricultural University, Mannuthy and NIT Calicut in analyzing the compounds.

I express my deep sense of gratitude to all my beloved teachers in the past for teaching me the fundamentals of chemistry and their inspiration.

I cannot leave my husband, Mack, our children Evana and Evelin and my entire family members from the list of people whom I must thank for their love, care and concern. Thanks for all the sacrifices they made for me and supporting me to complete my Ph. D. I would not have been able to reach this goal without them. Most importantly I wish to thank my mother, sisters Neena and Tina whose valuable prayers and blessings were what sustained me this far. No words can sum up the gratitude I owe to my sister Tina for taking care of me and my kids while I completed my work. I also recall with gratitude the support and the motivation rendered by my dear friends.

Above all, I praise God, the Almighty for giving me strength, knowledge and opportunity to undertake this research study and granting me the ability to proceed successfully. Without thy blessings, this accomplishment would not have been possible.

Nonu Davis Chakkalakkal

Dedicated to
My Husband, Mack

CONTENTS

	Page
Declaration	i
Certificate	ii
Acknowledgements	iii
Contents	v
List of Figures	xi
List of Tables	xvi
List of Abbreviations	xvii
Preface	xix
Chapter 1	1-61
Introduction	
1.1 Current Agricultural Issues and Demands	1
1.2 Nanotechnology in Agriculture	3
1.3 Importance of Seeds and Seed Treatments	6
1.4 Seed Treatment Methods	8
1.5 Seed Coating and Types	9
1.5.1 Seed Pelleting	10
1.5.2 Encrusting	11
1.5.3 Film Coating	11
1.6 Techniques for the Preparation of Porous Polymer Membranes	13
1.6.1 Electrospinning	13
1.6.1.1 Fundamental Principle of Electrospinning	14
1.6.1.2 Electrospinning Parameters	16
1.6.1.3 Applications of Electrospinning	21
1.6.2 Phase Inversion	22
1.6.2.1 Immersion Precipitation	22
1.6.2.2 Thermally Induced Phase Separation	22
1.6.2.3 Vapour Induced Phase Separation	22
1.6.2.4 Evaporation Induced Phase Separation	22
1.7 Nanofibers in Agriculture and Nanofiber Seed Coatings	23
1.8 Importance of Polymer Selection in Seed coating	26
1.8.1 Polymer Blends	27
1.8.2 Cause for Interest in Inorganic Polymers	28
1.9 Materials Used in the Present Work	30
1.9.1 Polycaprolactone (PCL)	30
1.9.2 Poly(ethylene oxide) (PEO)	32
1.9.3 MCM-41 (Mobil Composition of Matter No. 41)	33

1.9.4	Biopolymers Chosen for the Work - Cellulose from Water Hyacinth (WH)	34
1.9.5	Zinc oxide Nanoparticles (ZnO NPs)	35
1.9.6	Magnesium oxide Nanoparticles (MgO NPs)	35
1.9.7	Nanohydroxyapatite(nHAP) : The Nanofertilizer	36
1.9.8	Carbon Dots (CDs)	37
1.9.9	Biofungicide Employed in the Study: <i>Trichoderma Viride</i>	39
1.9.10	Biocatalyst for Seed Germination : α - amylase	40
1.9.11	Plant Growth Hormone : Gibberellic Acid (GA)	41
1.10	Seeds Used in Coating Studies : Corn (<i>Zea mays</i>) Seeds	41
1.11	Objectives of the Present Research Work	42
	References	44

Chapter 2 62-88
Materials and methods

2.1	Materials	62
2.2	Synthesis of Nanoparticles	62
2.2.1	Synthesis of ZnO NPs	62
2.2.2	Synthesis of Nanohydroxyapatite (nHAP)	63
2.2.3	Synthesis of Magnesium oxide Nanoparticles (MgO NPs)	63
2.2.4	Synthesis of Carbon Dots (CDs) through Hydrothermal Carbonization and Separation of CDs from HTC Process Liquid	64
2.3	Synthesis of MCM-41	65
2.3.1	Synthesis of aminopropyl functionalized MCM-41 (MCM-41/APTES)	66
2.3.2	Activation of functionalized MCM-41 (MCM-41/GU)	66
2.3.3	Synthesis of MCM-41 immobilized α - amylase (MCM-41/Amylase)	66
2.4	Cellulose Extraction from Water Hyacinth	67
2.5	Preparation of Solution for Electrospinning and Phase Inversion	68
2.5.1	Solution for PCL Electrospun Nanofibers	68
2.5.2	Solution for PCL/nHAP/ZnONPs (PHZ) Electrospun Nanofibers	68
2.5.3	Solution for PCL/nHAP/ZnONPs/ <i>T.viride</i> (PHZT) Electrospun Nanofibers	69
2.5.4	Solution for Electrospinning PCL – PEO Blend Electrospun Nanofibers	69
2.5.5	Solution for PCL/PEO/nHAP/ZnONPs/ <i>T.viride</i> (BHZT and	69

	BHZT _F) Electrospun Nanofibers and Film	
2.5.6	Solution for PCL/Amylase (PA) Electrospun Nanofibers	70
2.5.7	Solution for PCL/MCM-41-Amylase (PMA) Electrospun Nanofibers	70
2.5.8	Solution for PCL/MCM-41-Amylase/MgO NPs (PMMA) Electrospun Nanofibers	70
2.5.9	Solution for PCL/MCM-41-Amylase/GA/ MgO NPs (PMMG) Electrospun Nanofibers	70
2.5.10	Solution for PEO/Cellulose (PC _w) Electrospun Nanofibers	71
2.5.11	Solution for PEO/Cellulose/CDs (PC _w CD _w) Electrospun Nanofibers	71
2.5.12	Solution for PEO/Cellulose/nHAP (PC _w H) Electrospun Nanofibers	71
2.5.13	Solution for PEO/Cellulose/nHAP/CDs (PC _w CD _w H) Electrospun Nanofibers	71
2.6	Electrospinning Technique	72
2.6.1	Electrospinning Parameters for PCL, PHZ, PHZT, BHZT Nanofibers	73
2.6.2	Electrospinning Parameters for PCL–PEO Blend Nanofibers	73
2.6.3	Electrospinning Parameters for PA, PMA, PMMA and PMMG Nanofibers	73
2.6.4	Electrospinning Parameters for PC _w , PC _w CD _w , PC _w H, PC _w CD _w H Nanofibers	74
2.7	Preparation of Porous Polymer Film Using Phase Inversion Method	74
2.8	Coating of the Seeds	75
2.8.1	Fiber Coating	75
2.8.2	Film Coating	75
2.9	Characterization Studies	75
2.9.1	Analysis of Functional Groups and Structure	75
	2.9.1.1 FT-IR Analysis	75
	2.9.1.2 XRD Analysis	76
	2.9.1.3 UV-Visible Spectroscopy	76
	2.9.1.4 Fluorescence Spectroscopy	76
	2.9.1.5 ICP-OES Analysis	76
2.10	Thermal Analysis	77
	2.10.1 Thermo Gravimetric Analysis (TGA)	77
2.11	Studies on Morphology	77
	2.11.1 SEM Analysis and EDX Measurement	77
	2.11.2 Fiber Diameter Measurement	77
	2.11.3 TEM Analysis	77

2.11.4	Static Water Contact Angle (SWCA)	78
2.12	Physical Property Measurements	78
2.12.1	Porosity Measurement	78
2.13	Study of the Aqueous Solution of membranes	78
2.13.1	Study of Variation in pH	78
2.13.2	Study of Variation in Conductivity	79
2.13.3	Swelling Studies	79
2.13.4	Study of the Steep Water and Imbibition Studies	80
2.13.5	Metal Release Study	80
2.14	Microbiological Test and Dual Culture Tests	80
2.15	α -Amylase Enzymatic Activity Assay	81
2.15.1	Activity Assays of Immobilized α -Amylase	81
2.15.2	Effect of pH on the Immobilized α - Amylase Activity	81
2.15.3	Effect of Temperature on the Immobilized α - Amylase Activity	82
2.15.4	Reusability and Storage Stability Studies of Immobilized α -Amylase	82
2.15.5	α - Amylase Activity of Coated Seeds Using Starch Agar Method	82
2.15.6	Antioxidant Studies	83
2.16	Germination Parameters	83
2.16.1	Statistical Analysis	85
	References	86

Chapter 389-119
Incorporation of nHAP, ZnO NPs and T.viride into PCL nanofibers
and PCL/PEO blend nanofibers and its application as seed coats

3.1	XRD Analysis	90
3.2	FTIR Study	91
3.3	Study of the Morphology	93
3.3.1	SEM Analysis	93
3.3.2	EDX Spectrum of nHAP, PHZ and BHZT Nanofibers	96
3.3.3	TEM Analysis	97
3.4	Thermal Analysis	98
3.5	Porosity Measurements	99
3.6	Study of Aqueous Solution of Nanofibers and Seeds	100
3.6.1	Swelling and Stability Studies of Nanofibers in Water	100
3.6.2	pH Study	101

3.6.3	Conductance of the Aqueous Solution of Fibers and seeds	103
3.6.4	Imbibition Studies of Seeds	105
3.7	Ca, Zn and P Release Profile Study	106
3.8	Surface Wetting Properties of the Electrospun Fibers	107
3.9	Germination Studies	108
3.9.1	Fresh Seedling Biomass	111
3.9.2	Statistical Analysis	112
3.10	Microbiological Analysis and Dual culture test	114
	Conclusion	116
	References	117

Chapter 4. 120-155

PCL nanofiber loaded with free α - amylase and α - amylase immobilized on MCM-41 in presence of plant growth promoters and its application as seed coats

4.1	XRD Analysis	121
4.2	FTIR Study	123
4.3	Study of the Morphology	126
4.3.1	SEM Analysis	126
4.3.2	EDX Spectra of the Synthesized Samples	128
4.3.3	TEM Analysis	130
4.4	Thermal Analysis	131
4.5	Surface Wetting Properties of the Electrospun Fibers	132
4.6	Porosity Measurements	133
4.7	Study of Fibers and Seeds in Aqueous Medium	133
4.7.1	Swelling and Stability Studies of the Nanofibers in PBS	133
4.7.2	pH Study	135
4.7.3	Metal ion Release Study	137
4.7.4	Imbibition Studies	137
4.8	Germination Studies	138
4.8.1	Fresh Seedling Biomass	141
4.8.2	Statistical Analysis	142
4.9	Determination of α -amylase Enzymatic Activity Assay	144
4.9.1	Effect of Incubation Time on Enzymatic Activity	144
4.9.2	Effect of pH on Enzyme Activity	145
4.9.3	Effect of Temperature on Enzyme Activity	146

4.9.4	Reuse Studies	147
4.9.5	Storage Studies	148
4.10	α - Amylases Activity in Coated and Uncoated Germinating Seeds	149
	Conclusion	150
	References	152

Chapter 5 156-191

Incorporation of nanohydroxyapatite and carbon dots into

PEO/cellulose nanofibers and its application as seed coats

5.1	XRD Analysis	157
5.2	FTIR Study	159
5.3	Study of the Morphology	162
	5.3.1 SEM Analysis	162
	5.3.2 EDX Spectrum of PC _w CD _w H Nanofibers	164
	5.3.3 TEM Analysis of CDs and PC _w CD _w H Nanofibers	164
5.4	Thermal Analysis	165
5.5	Surface Wetting Properties of the Electrospun Fibers	167
5.6.	UV-Visible Spectra of Synthesized Carbon Dots	168
5.7	Photoluminescence Spectroscopy (PL Spectra)	169
5.8	Porosity Measurements	172
5.9	Study of Fibers and Seeds in Aqueous Medium	172
	5.9.1 pH Study	172
	5.9.2 Conductance of the Aqueous Solution of Fibers and Seeds	173
	5.9.3 Swelling and Stability Studies of the Nanofibers in PBS	174
	5.9.4 Imbibition Studies	176
5.10	Metal Release Studies	178
5.11	Germination Studies	179
	5.11.1 Fresh Seedling Biomass	182
	5.11.2 Statistical Analysis	183
5.12	Antioxidant Property of Developed Nanofibers	185
	Conclusion	187
	References	188
	<i>Summary and Conclusions</i>	192
	<i>List of Publications</i>	202

List of Figures

Figure No	Title	Page
Fig.I.1	The fate of fertilizers and pesticides applied to agricultural soils	2
Fig.I.2	a) Global pesticide consumption from 1990 to 2020 b) Percentage of pesticides used in countries	2
Fig.I.3	Application of nanotechnology in different agricultural field	7
Fig. I.4	a) Market share by crop type. b) The statistics on the global seed market	7
Fig.I.5	Schematic of several seed coating methods	9
Fig.I.6	Electrospinning set up	14
Fig.I.7	Schematic representation of electrospinning apparatus a) horizontal set up b) vertical setup	14
Fig.I.8	a) Beaded nanofibers b) Ribbon like nanofibers c) Twisted nanofibers d) Spray type nanofibers	16
Fig.I.9	Applications of electrospun nanofibers	20
Fig.I.10	Evaporation-induced phase separation method to make porous polymer Film	22
Fig.I.11	Structure of Polycaprolactone (PCL)	29
Fig.I.12	Structure of Poly(ethylene oxide) (PEO)	31
Fig.I.13	Structure of nanohydroxyapatite	35
Fig.II.1	a) Frothy product formed during the synthesis of ZnO NPs b) Finely powdered ZnO NPs	62
Fig.II.2	Schematic of synthesis of CDs from Water hyacinth stem	64
Fig.II.3	Schematic illustration of synthesis of MCM-41	65
Fig.II.4	a) Surface structure of MCM-41 b) Synthesis of MCM-41 immobilized α -amylase	66
Fig.II.5	Images of a) uncoated seeds b) nanofiber coated seeds c) film coated seeds	74
Fig.II.6	Photographs of experimental set up for germination studies A) Uncoated B) – E) Nanofiber coated F) Porous film coated	82
Fig.III.1	Block diagram of methodology for seed coating: 1	87
Fig.III.2	XRD diffractogram of nHAP b) ZnO NPs	88
Fig.III.3	XRD Diffractogram of nanofibers i) PCL ii) PHZ iii) PHZT iv) BHZT	89
Fig.III.4	FTIR spectra of a) i) PCL ii) nHAP iii) ZnO NPs iv) T.viride b) i) PHZ ii) PHZT iii) BHZT c) PEO	89
Fig.III.5	SEM images of a) ZnO NPs b) nHAP Histogram bar chart of c) ZnO NPs d) nHAP	91
Fig.III.6	SEM image of PCL/PEO nanofiber with different blend ratio a) B1 (PCL/PEO: 75/25) b) B2 (PCL/PEO: 50/50) c) B3 (PCL/PEO: 30/70)	92

Fig.III.7	(ia-iva) SEM images of nanofibers ia) PCL iia) PHZ iiia) PHZT iva) BHZT (ib-ivb) Histogram bar chart of ib) PCL iib) PHZ iiib) PHZT ivb) BHZT	93
Fig.III.8	SEM images of BHZT _F	93
Fig.III.9	EDX spectrum of i) nHAP ii) PHZ iii) Elemental mapping of PHZ	94
Fig.III.10	EDX spectrum of BHZT nanofiber	95
Fig.III.11	TEM images of PHZ nanofiber	95
Fig.III.12	TGA thermogram of i) PCL ii) PHZ iii) PEO iv) PHZT v) BHZT	96
Fig.III.13	a) Swelling and b) Stability studies of nanofibers i) PCL ii) PHZ iii) PHZT iv) BHZT v) BHZT _F	98
Fig.III.14	a. pH of aqueous solutions of nanofibers and film i) PCL ii) PHZ iii) PHZT iv) BHZT v) BHZT _F b. pH of i) uncoated seeds ii-vi) seeds coated with ii) PCL iii) PHZ iv) PHZT v) BHZT vi) BHZT _F	100
Fig.III.15	a. Electrical conductance of aqueous solutions of i) PCL ii) PHZ iii) PHZT iv) BHZT v) BHZT _F b. Electrical conductance of nanofibers and film i) uncoated seeds ii-vi) seeds coated with ii) PCL iii) PHZ iv) PHZT v) BHZT vi) BHZT _F	100
Fig.III.16	Water absorption rate of i) uncoated seeds ii-vi) seeds coated with nanofibers and film ii) PCL iii) PHZ iv) PHZT v) BHZT vi) BHZT _F	103
Fig.III.17	Metal release profile of nanofibers a) Ca release pattern b) P release pattern c) Zn release pattern from i) PHZ ii) PHZT iii) BHZT iv) BHZT _F	104
Fig.III.18	Static Water Contact angle measurements of nanofibers a) PCL b) PHZ c) PHZT d) BHZT	105
Fig.III.19	Germination of corn seeds a) uncoated seeds b-f) seeds coated with nanofibers and film b) PCL c) PHZ d) PHZT e) BHZT f) BHZT _F after 1) 24 h 2) 48 h 3) 72 h 4) 96 h 5) 120 h	106
Fig.III.20	a) Radicle length and b) plumule length of seeds i) uncoated ii-vi) coated with ii) PCL iii) PHZ iv) PHZT v) BHZT vi) BHZT _F	107
Fig.III.21	Total fresh biomass of corn seedlings grown from seeds coated with developed membranes after 15 days of germination	108
Fig.III.22	Estimated marginal mean for germination parameters	110
Fig.III.23	a) The growth of <i>T. viride</i> spores alone b) <i>Aspergillus</i> alone c) The growth of <i>Aspergillus</i> in presence of BHZT d) The growth of <i>Aspergillus</i> in presence of PHZ after 5 days inoculation	111
Fig.IV.1	Block diagram of the methodology for seed coating: 2	116

Fig.IV.2	XRD Diffractogram of a) MCM-41 b) MCM-41/Amylase	117
Fig.IV.3	XRD Diffractogram of MgO NPs	118
Fig.IV.4	XRD Diffractogram of i) PA ii) PMA iii) PMMA iv) PMMG	119
Fig.IV.5	FT-IR spectra of a) MgO NPs b) MCM-41 and successive covalent grafting steps of α -amylase i) MCM-41 ii) MCM-41/APTES iii) MCM-41/GU iv) MCM-41/Amylase	119
Fig.IV.6	The FTIR spectrum of i) PA ii) PMA iii) PMMA iv) PMMG nanofibers	121
Fig.IV.7	SEM images of a) MgO NPs b) MCM-41 c) MCM-41/Amylase	122
Fig.IV.8	SEM images of ia) PA iia) PMA iiia) PMMA iva) PMMG Histogram bar chart of ib) PA iib) PMA iiib) PMMA ivb) PMMG	123
Fig.IV.9	EDX spectrum of i) MCM-41 ii) MCM-41/Amylase	125
Fig.IV.10	EDX spectrum of PMMG nanofiber	125
Fig.IV.11	HR-TEM image of a) MCM-41 b) MCM-41/Amylase c) PMA nanofiber d) PMMG nanofiber	126
Fig.IV.12	TGA thermogram of i) PA ii) PMA iii) PMMA iv) PMMG	127
Fig.IV.13	Static water contact angle measurements of nanofibers a) PA b) PMA c) PMMA d) PMMG	128
Fig.IV.14	Swelling studies of i) PA ii) PMA iii) PMMA iv) PMMG	130
Fig.IV.15	Stability studies of i) PA ii) PMA iii) PMMA iv) PMMG	130
Fig.IV.16	pH of aqueous solutions of fibers i) PA ii) PMA iii) PMMA iv) PMMG	132
Fig.IV.17	Magnesium ion release profile from nanofibers	133
Fig.IV.18	Imbibition studies of i) uncoated seeds ii-v) seeds coated with nanofibers ii) PA iii) PMA iv) PMMA v) PMMG	133
Fig.IV.19	The optical photographs of corn seed germination A) uncoated seeds B-E) Seeds coated with nanofibers B) PA C) PMA D) PMMA E) PMMG	136
Fig.IV.20	a) Radicle length b) Plumule length Uncoated seeds ii-v) Seeds coated with nanofibers ii) PA iii) PMA iv) PMMA v) PMMG	137
Fig.IV.21	Total fresh biomass of corn seedlings grown from seeds coated with developed membranes after 15 days of germination	137
Fig.IV.22	Estimated marginal mean for a) germination percentage b) germination index c) seed vigour index	139
Fig.IV.23	α -Amylase activity in i) PA ii) PMA iii) PMMA iv) PMMG	141
Fig.IV.24	Effect of pH on enzyme activity i) PA ii) PMA iii) PMMA iv) PMMG	141

Fig.IV.25	Effect of temperature on enzyme activity i) PA ii) PMA iii) PMMA iv) PMMG	142
Fig.IV.26	Reusability studies of enzymatic activity i) PA ii) PMA iii) PMMA iv) PMMG	144
Fig.IV.27	Storage studies on enzymatic activity i) PA ii) PMA iii) PMMA iv) PMMG	144
Fig.IV.28	α -Amylase activity after 7 days of germination in a) Uncoated seeds b – d) Seeds coated with nanofiber b) PA c) PMMA d) PMMG	145
Fig.V.1	Block diagram of methodology for seed coating: 3	151
Fig.V.2	XRD Diffractogram of synthesized a) nHAP b) CDs	152
Fig.V.3	XRD diffractogram of cellulose extracted from water hyacinth	153
Fig.V.4	XRD diffractogram of i) PC _w ii) PC _w CD _w iii) PC _w H iv) PC _w CD _w H	153
Fig.V.5	The FTIR Spectrum of i) pure cellulose ii) cellulose extracted from water hyacinth	154
Fig.V.6	The FTIR spectrum of synthesized carbon dots	156
Fig.V.7	The FTIR Spectrum of a) PEO b) developed nanofibers i) PC _w ii) PC _w CD _w iii) PC _w H iv) PC _w CD _w H	156
Fig.V.8	(ia - iva) The morphology of different electrospun nanofibers ia) PC _w iia) PC _w CD _w iiia) PC _w H iva) PC _w CD _w H (ib - iv) Histogram bar chart of ib) PC _w iib) PC _w CD _w iiib) PC _w H ivb) PC _w CD _w H	158
Fig.V.9	EDX spectrum of PC _w CD _w H nanofiber	159
Fig.V.10	TEM image of a) CDs b) PC _w CD _w H nanofiber	160
Fig.V.11	TG curve of isolated cellulose	161
Fig.V.12	TG curves of the nanofibers i) PC _w ii) PC _w CD _w iii) PC _w H iv) PC _w CD _w	162
Fig.V.13	Static water contact angle measurements of nanofibers a) PEO b) PC _w c) PC _w CD _w d) PC _w H e) PC _w CD _w H	163
Fig.V.14	UV–Visible spectra of CDs	164
Fig.V.15	The PL emission spectra of CDs at two excitation wavelength i) $\lambda_{ex} = 290\text{nm}$ ii) $\lambda_{ex} = 360\text{nm}$	165
Fig.V.16	The PL emission spectra of CDs and PC _w CD _w nanofiber	166
Fig.V.17	Aqueous solution of carbon dots under a) day and b) UV light.	166
Fig.V.18	a) pH of aqueous solutions of fibers i) PC _w ii) PC _w CD _w iii) PC _w H iv) PC _w CD _w H b) pH of i) uncoated seeds ii – v) seeds coated with nanofibers ii) PC _w iii) PC _w CD _w iv) PC _w H v) PC _w CD _w H	168
Fig.V.19	a) Electrical conductance of aqueous solutions of fibers i) PC _w ii) PC _w CD _w iii) PC _w H iv) PC _w CD _w H b) Electrical conductance of i) uncoated seeds ii-v) seeds coated	169

	with nanofibers ii) PC _w iii) PC _w CD _w iv) PC _w H v) PC _w CD _w H	
Fig.V.20	Swelling studies of i) PC _w ii) PC _w CD _w iii) PC _w H iv) PC _w CD _w H	170
Fig.V.21	Stability studies of i) PC _w ii) PC _w CD _w iii) PC _w H iv) PC _w CD _w H	171
Fig.V.22	Water absorption rate of i) uncoated seeds ii – v) seeds coated with nanofibers ii) PC _w iii) PC _w CD _w iv) PC _w H v) PC _w CD _w H	173
Fig.V.23	a) Ca release from PC _w H and PC _w CD _w H b) P release from PC _w H and PC _w CD _w H	173
Fig.V.24	The optical photographs of corn seed germination of A) uncoated seeds B-E) seeds coated with nanofibers B) PC _w C) PC _w H D) PC _w CD _w E) PC _w CD _w H	176
Fig.V.25	The optical photographs of germinated corn seeds coated with developed nanofibers after 5days	177
Fig.V.26	a) Radicle and b) Plumule length of seedlings i) Uncoated seeds ii – v) seeds coated with nanofibers ii) PC _w iii) PC _w H iv) PC _w CD _w v) PC _w CD _w H	177
Fig.V.27	Fresh seedling biomass after 15 days of germination	178
Fig.V.28	Estimated marginal mean of a) Germination percentage b) Germination Index c) Seed Vigour Index	180
Fig.V.29	Antioxidant activity of developed nanofibers using DPPH assay	181

List of Tables

Table No.	Title	Page
Table II.1	Solution preparation for PCL-PEO blend nanofibers	69
Table II.2	Solution preparation for PCL, PHZ, PHZT, BHZT nanofibers and BHZT _F film	70
Table II.3	Solution Preparation for PA, PMA, PMMA and PMMG nanofibers	71
Table II.4	Solution preparation for nanofibers for PC _w , PC _w CD _w , PC _w H, PC _w CD _w H	72
Table II.5	Common electrospinning parameters employed	72
Table II.6	Optimised electrospinning parameters	73
Table II.7	Optimised electrospinning parameters	73
Table II.8	Optimised electrospinning parameters	74
Table II.9	Optimised electrospinning parameters	74
Table II.10	Equations of germination parameters	84
Table III.1.	Porosity values of developed membranes	99
TableIII.2	Germination parameters of coated and uncoated seeds	113
Table IV.1	Porosity values of developed membranes	133
Table IV.2	Estimated marginal mean of germination parameters	142
Table V.1	Porosity values of developed membranes	172
Table V.2	Estimated marginal mean of germination parameters	184
Table V.3	Antioxidant activity of nanofibers	186

List of Abbreviations

FAO	: Food and Agriculture Organization of the United Nations
ISO	: International Organization for Standardization
NPs	: Nanoparticles
ZnO NPs	: Zinc oxide nanoparticles
AIs	: Active ingredients
PEO	: Poly(ethylene oxide)
PVA	: Polyvinyl alcohol
PVP	: Polyvinyl pyrrolidone
PVC	: Polyvinyl chloride
PMMA	: Poly(methylmethacrylate)
PVF	: Poly(vinylidene fluoride)
PVB	: Poly(benzimidazole)
EIP	: Evaporation Induced Phase Separation
CLSD	: Carbon dioxide Laser Supersonic Drawing
PPZ	: Poly(diethoxy) phosphazene
PCL	: Poly (ϵ -caprolactone)
nHAP	: Nanohydroxyapatite
<i>T.viride</i>	: <i>Trichoderma viride</i>
GA	: Gibberellic Acid
MgO NPs	: Magnesium oxide nanoparticles
WH	: Water hyacinth
CDs	: Carbon dots
ROP	: Ring-opening polymerization
FDA	: Food and Drug Administration
PLA	: Polylactic acid
HA NPs	: Hydroxyapatite nanoparticles
CQDs	: Carbon Quantum Dots
HTC	: Hydro Thermal Carbonization

CTAB	: Cetyltrimethylammonium bromide
TEOS	: Tetraethyl orthosilicate
APTES	: (3-aminopropyl)triethoxysilane
GU	: Glutaraldehyde
DNS	: 3,5-dinitrosalicylic acid
PBS	: Phosphate Buffer Solution
DPPH	: 2,2-diphenyl-1-picrylhydrazyl
GI	: Germination Index
SVI	: Seed Vigour Index
HSD	: Honestly Significant Difference
MCM-41	: Mobil Composition of Matter No. 41
SD	: Standard Deviation
PGPM	: Plant Growth Promoting Microbes

PREFACE

Agriculture is one of the essential sectors where nanotechnology needs to be applied as it directly affects the availability of food. Agriculture is becoming increasingly challenging to feed the growing global population, which is expected to exceed 10 billion by 2050. Over several cycles of intense farming, the soil quality deteriorates owing to nutrient depletion, making all agricultural methods completely dependent on fertilizers to increase the output from the soil. For the control of plant diseases and to prevent crops from suffering substantial losses, modern agriculture heavily relies on the use of pesticides, but many of the most crucial tools for disease control are rapidly losing their effectiveness as a result of the emergence of resistance. The usage of pesticides can have side effects that could be harmful to human health and environment. To promote agricultural production, more sustainable techniques are required to prevent crop loss, plant diseases and deterioration of arable lands. The industry is actively pursuing conventional polymer film seed coatings employing fluidized bed, rotary coater or rotating pan techniques. However, these contemporary coating techniques produce thick, nonporous coatings that may restrict gas and water exchange and have detrimental impacts on seed germination and seedling growth. Majority of the coating materials used in conventional approaches is typically dissolved in water, causing the active ingredients to be quickly and uncontrollably released. The unsustainable aspect of existing conventional agricultural techniques as well as future climatic scenarios, demand for alternatives that can maximize agricultural productivity which may ensure environmental and economic sustainability.

The goal of this research is to increase food security by creating cutting-edge agricultural practices using nanotechnology. The introduction of innovative nano-enabled seed coating platforms for precise and targeted agrichemical delivery is an emerging research topic in this field. This investigation is an attempt to increase the effectiveness of nutrient utilization and to reduce fertilizer leaching, which would reduce agricultural production systems' nonpoint sources of pollution and lower fertilizer costs. The agrichemicals are encapsulated inside the polymer and applied to the seed as seed coats. The application of developed nanofiber seed coats in seed germination and controlled release of fertilizers are analyzed. Ultrathin

nanofibers fabricated using the electrospinning technique is the polymer morphology selected for the application. For convenience and better understanding, the entire work has been presented in this thesis as five chapters.

CHAPTER 1

This chapter is an introduction to nanotechnology in agriculture to solve current agricultural issues and demands. Literature review reveals the importance of seeds, different seed treatment methods, types of seed coatings and advantages of electrospun nanofibers in seed coating. A thorough review of published work on electrospun nanofibers in seed coating and agriculture is included. The method of electrospinning and the parameters affecting the fabrication of nanofibers, the importance of selected components in the present investigation are also explained in this part. This chapter is concluded by giving the scope and aim of the present investigation.

CHAPTER 2

The methods and reagents used for the preparation of nanoparticles, nanofibers, porous film, seed coats and various characterization methods employed in the investigation are included in this chapter. The various studies of nanofibers in aqueous solution for the controlled release of agrichemicals are discussed. It also includes the methods used for germination studies, antifungal and antioxidant studies of developed nanofibers.

CHAPTER 3

This chapter discusses the application of fabricated poly(ϵ -caprolactone) and poly(ϵ -caprolactone)/poly(ethylene oxide) blend nanofibers incorporated with nanohydroxyapatite, zinc oxide nanoparticles and *Trichoderma viride* as seed coats. The nanofibers are applied as seed coats on Zea mays seeds to enable tunable agrichemical release and to analyze the germination parameters in greenhouse studies. Porous films of aforementioned materials were also developed for comparison. The synthesized samples were successfully characterized by X-ray diffraction studies (XRD), Fourier transform infrared spectroscopy (FTIR), Thermogravimetric analysis (TGA), Scanning electron microscopy (SEM), EDAX, Transmission electron microscopy (TEM), static water contact angle measurement (SWCA) and porosity measurements. The study of aqueous solution of nanofibers for the controlled release

of agrichemicals includes variation in pH and conductance, swelling studies, stability studies, imbibition studies and metal release study using ICP-OES. Germination studies are explained by germination parameters, fresh seedling biomass of coated and uncoated seeds and statistical analysis. A discussion on the antagonistic activity of immobilized *T.viride* spores in nanofibers against *Aspergillus* pathogenic fungi is included at the end. A summary of the investigation and bibliography is given at the end of each chapter.

CHAPTER 4

This chapter describes the application of nanofiber immobilized α -amylase for seed germination. PCL nanofibers with immobilized alpha-amylase in presence of essential micronutrient, magnesium oxide nanoparticles and plant growth regulator, gibberellic acid are applied as seed coats. The two methods of immobilization of α -amylase is employed in this section. The synthesized MgO NPs, inorganic support MCM-41 and nanofibers were successfully characterized by different analytical techniques as mentioned above. Further studies for the controlled release of agrichemicals and germination studies are done as discussed in the previous section. Efficiency of immobilized enzyme was studied from the optimization of pH, temperature and incubation time. The stability of immobilized enzyme was analyzed from reusability and storage studies.

CHAPTER 5

This chapter mainly focused on the incorporation of biopolymers and biofertilizers from biomass for controlled release of fertilizers. This chapter discusses the application of fabricated PEO/Cellulose nanofibers incorporated with nanohydroxyapatite, carbon dots as seed coats. The nanofibers are applied as seed coats on *Zea mays* seeds to enable tunable agrichemical release and to analyze the germination parameters in greenhouse studies. Characterization of cellulose extracted from water hyacinth, carbon dots synthesized from water hyacinth and fabricated nanofibers were done using FT-IR, XRD, TGA, SEM, EDAX, TEM, UV-Visible spectroscopy and Photoluminescence spectroscopy (PL), static water contact angle measure and porosity measurements. As mentioned in the previous section, further investigation is being done on controlled release of agrichemicals and

germination studies. A discussion on the antioxidant properties of nanofibers using DPPH assay is included.

Chapter 1

Introduction

1.1 Current Agricultural Issues and Demands

"Zero Hunger" is one of the sustainable development goals set by the United Nations which demands sustainability in agriculture. Agriculture is becoming increasingly challenging to feed the growing global population, which is expected to exceed 10 billion by 2050^{1,2}. The "green revolution" of 1970's used considerable irrigation and the application of agrochemicals to improve agricultural productivity³. As agricultural production reached a plateau now, such a boom in agriculture is the need of the time. Growing biotic and abiotic stressors such as climate change, newly developing plant pest species, lack of clean water and lack of arable land affect crop productivity and quality. Without the use of agrochemicals like pesticides, fertilizers *etc.*, sustainable production and efficiency in modern agriculture is impossible. In order to meet the ever-increasing demand for crop production, synthetic pesticides have been used excessively. This increased resistance in pests, resulting in significant ecotoxicity, which has an impact on all forms of life on earth both directly and indirectly. Chemical fertilizers are delivered inefficiently in agri-food systems, threatening the quality, safety and security of the food supply resulting in significant environmental risks such as wastage of energy, water and eutrophication of aquatic habitats. Particularly, it has been reported that 50–80% of fertilizer and insecticides used are lost as a result of photodegradation, wind, hydrolysis, evaporation, environmental runoff to water bodies, draining into the soil and microbiological activity. Hence only a small portion is biologically available for the target organisms as depicted in Fig.I.1.

Food and Agriculture Organization of the United Nations (FAO) reports show that plant diseases contribute nearly \$220 billion to annual global economic loss while plant pests reduce crop productivity to 20-40%⁴. The Global pesticide consumption from 1990 to 2020 by top ten pesticide-consuming countries⁵ is shown in Fig.I.2a. (FAO data replotted)

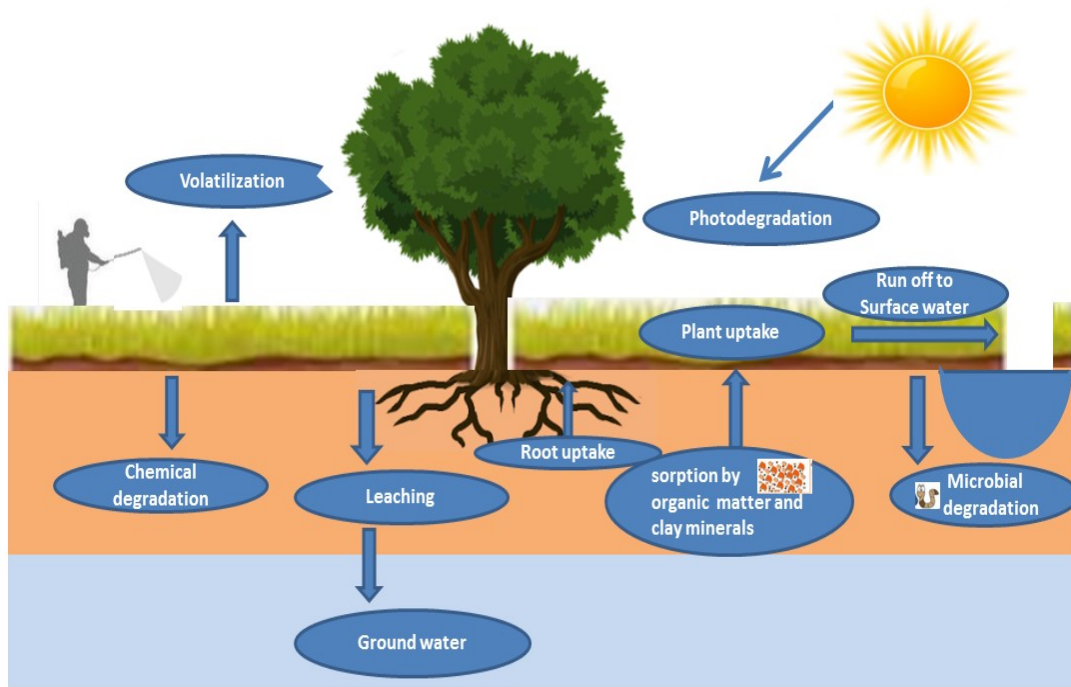
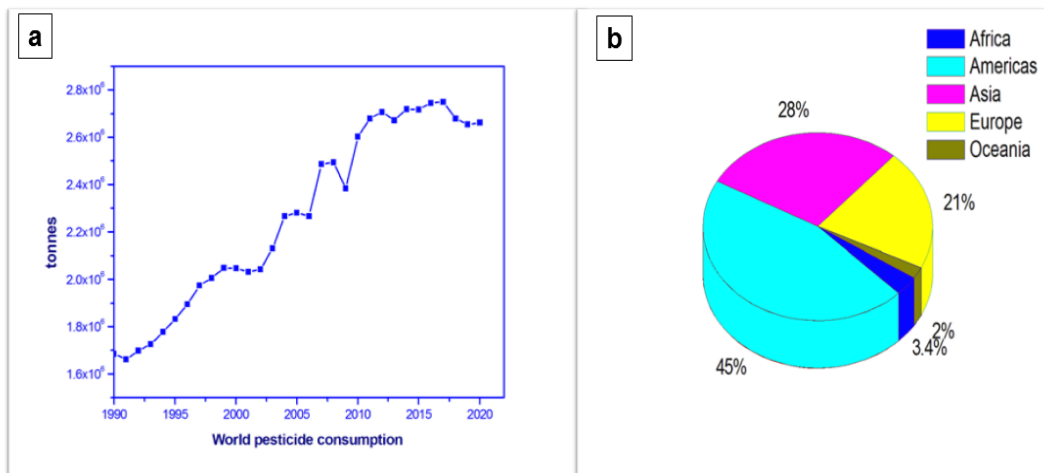


Fig.I.1 The fate of fertilizers and pesticides applied to agricultural soils



**Fig. I.2 a) Global pesticide consumption from 1990 to 2020
b) Percentage of pesticides used in countries**

America stands as the largest consumer, Asia being the second (Fig.Ib). Since the need for pesticides is not expected to decline any time soon, the growing health

dangers and environmental issues associated with their excessive use should be addressed.

Considering these constraints, in order to improve global food security and to support the sustainable development goals, present agricultural sector must strive to adopt technological advancements that offer healthy cost effective solutions for production of crops and environmental sustainability⁶. Efforts to create alternative strategies for the minimal and targeted use of pesticides have been made in response to growing environmental issues and health dangers caused by excessive pesticide usage⁷. The best strategies for fertilizer management aim to balance nutrient delivery with crop requirements to maximise output and reduce nutrient losses to the environment. Controlled and tailored pesticide release can help to increase bioavailability for prolonged crop protection, preventing the emergence of pest resistance, reducing pesticide residues in food and fields, reducing airborne pesticides and pollution. The four dimensions of nutrient management- source, rate, time and place - form the corner stone to utilise plant nutrients in an effective and efficient manner.

Nanotechnology can provide unique solutions to tackle the restrictions and challenges faced by today's agricultural systems and seed management. Significant innovations and advancements in this area have been recorded, particularly in water retention gels, nutrient sensors, soil binders, soil management, nutrient absorption enhancers, nanofertilizers, insecticide and pesticide delivery methods. Despite the fact that agricultural nanotechnology has a lot of potential, it is still in its infancy and the commercialization of the research is not yet complete.

1.2 Nanotechnology in Agriculture

Nanotechnology refers to the use of nanomaterials, whose measurements are on a nanometric scale. The International Organization for Standardisation (ISO) defines a nanomaterial as one that must have any of its dimensions on a nanometric scale, either in its internal or surface structure, despite the lack of a formal definition⁸. According to the international measurement system, a nanometer equals 10^{-9} meters, hence the term "nanoscale" refers to measures between 1 and 100 nm. At this scale,

matter attains unique physical and magnetic properties that make novel applications possible. The evolution of the engineered smart technology using nanotools in the high-tech agricultural system could bring about a revolution in farming methods and thereby minimize or even eradicate the environmental impact of modern agriculture in addition to increase the quality and quantity of crops⁹. The use of nanotechnology in agriculture aids in enhancing soil fertility, maintaining balanced nutrition, controlling weeds effectively, enhancing seed emergence and using biosensors to identify nutrients and pollutants¹⁰. Applications of nanotubes, fullerenes, biosensors, controlled delivery systems, nanofiltration *etc.* have been employed in the agri-food sectors¹¹⁻¹³. This method has been shown to be effective in managing agricultural field resources, delivering drugs to plants and preserving the fertility of the soil. Consideration of the nano-nano interaction to eliminate the toxic component of agricultural soil and make it sustainable is an interesting phenomenon¹⁴.

Nanosensors are widely utilised in agriculture due to their efficiency and reliability in environmental monitoring of contamination in soils and water¹¹. The sensitivity and performance of biosensors could be greatly increased in their applications due to the unique features of nanomaterials¹⁵. In addition, numerous new signal transduction technologies are now able to be implemented in biosensors¹⁶. Furthermore, the utilisation of nanomaterials allowed the miniaturisation of several sensors into small, lightweight and intelligent devices including nanosensors and other nanosystems that are crucial for biochemical analysis¹⁷. However, due to their extremely high surface-to-volume ratio, nanoparticles (NPs) show excellent properties that make them more appealing for use in agricultural product analysis compared to conventional methods¹⁸. Nanofertilizers have been widely accessible on the market for the past ten years. Nanofertilizers may include nanoscale amounts of titanium dioxide, silica, iron and other materials. By replacing traditional fertilizers with nanofertilizers eutrophication and water pollution caused by the build-up of nutrients in soils may be prevented¹⁹⁻²¹.

The idea of applying nano-agroparticles is a potential method, which may help to stimulate uptake of applied fertilizers in the soil. The root is the final pathway for nutrient absorption. As a result, the prolonged release of fertilizers and other nutrients to the roots and leaves in accordance with plant requirement is made possible by the

co-application of agro-nanoparticles²². Application of ZnO, Ag and Co NPs *etc.* have been used to increase plant growth and control of plant diseases^{23,24}. Application of nanoparticles are done to improve growth parameters, germination rate, chlorophyll concentrations, microbial growth, nutrient uptake, chemical release, cell elongation and crop productivity. The size range of less than 100 nm is a transitional size between the size of individual atoms and related bulk materials, resulting in biological effects on living plant cells²⁵. These outcomes have been investigated and understood in a variety of seeds. *Vigna radiata* and *Cicer arietinum* seedlings grew more quickly in the presence of nano zinc oxide (ZnO)²⁶. According to reports, exposing seeds to silver nanoparticles enhances germination and crop output in plants like maize and watermelon. When compared to untreated plants, it was discovered that Ag NPs treated plants demonstrated improved development²⁷. Although the germination and growth of plants are positively impacted by nanoparticles, there is an underground concern that the features of nanomaterials and their use could be harmful to human health and the environment. Therefore, it is important to employ these nanomaterials properly to meet society's requirements in a sustainable manner.

Studies of numerous metal oxides, including Al₂O₃, TiO₂, CeO₂, FeO and ZnO NPs, were conducted to determine their absorption, biological destiny and toxicity. Due to the alkaline character of the soils, a zinc deficit has been identified as one of the major issues restricting agricultural productivity²⁸. Since nutrient transport in soil-plant systems depends on ion exchange, adsorption-desorption, aggregation-dispersion and solubility-dissolution, nutrient management using nanotechnology must take into account two key factors. Ions must be present in the soil system in plant-available forms. Nanomaterials need to enable procedures that would make sure that nutrients are available to plants at the rate and in the form they require. Aqueous suspension and hydrogel forms of nanofabricated materials containing plant nutrients can be used for risk-free application, simple storage and a practical delivery mechanism. Based on an understanding of the nanodynamics of interacting nanostructures, it may be possible to synthesize nanoparticles for use in farming by combining the top-down and bottom-up methodologies. The methods of nanosynthesis have given a long way to what Zubarev has termed "any way you want it." This should also be the cornerstone of nanofabrication²⁹. For the reasons

mentioned above, nanofabrication for agricultural purposes may necessitate a different path than that of manufacturing industrial nanomaterials. Fig.I.3 shows the application of nanotechnology in different agricultural sectors.

The virtually uncontrollable fate and behaviour of nanoparticles is another interesting aspect of the farm production system. When sprayed to soils, plants or during irrigation, nanomaterials would never stay at source application, but would instead disperse throughout the land. They cannot be disposed of in the same way as the majority of consumer goods. The diffusion issues can be reduced by encapsulation of active ingredients (AIs) in matrices. Since it is generally known that insect pests predominate in agricultural fields, NPs may play a critical role in the management of insect pests and host infections³⁰. A new pesticide formulation with nanoencapsulation offers improved solubility, specificity, permeability and stability with gradual release characteristics³¹. These advantages are primarily attained by either preventing the encapsulated active components from premature deterioration or lengthening the duration of their pest control efficiency. Pesticide dose and human exposure have decreased as a result of the development of nanoencapsulated pesticides, which is environmentally friendly for crop protection³². Therefore, development of non-toxic and promising pesticide delivery technologies to boost global food production while minimising adverse environmental effects on ecosystems is necessary³³.

1.3 Importance of Seeds and Seed Treatments

Food security is a major issue in India and in many other emerging nations since agricultural productivity is substantially lower than population growth³⁴. Food security is based on seed security because majority of the food crops are grown from seed³⁵. Seed is the most vital and crucial input for crop production and the key to agriculture progress. The significance of seeds in the agricultural sector is crucial in developing nations like India, where the agricultural sector strongly affects both the population and economy³⁶. Fig.I.4a shows market share by crop type, maize, soybeans and vegetables being the three most important crops (Data replotted from report published by IHS markit). Maize contributes about 42% of the market. The world seed market's estimated value is shown in Fig.I.4b³⁷. The seed

used for sowing affects the crop's health in a significant way. The response of other agricultural production inputs is controlled by the seed used. Inadequate nutrient delivery during the germination phases, seed-borne infections and other factors can have disastrous effects if they are not promptly controlled. Due to ageing, dangerous chemicals including volatile aldehydes are released during seed storage. Therefore, judgments regarding seed storage can be made by identifying these gases and removing the damaged seeds. In modern agriculture, the focus is on producing more with less land, water and labour. It is advisable to prioritize crop management improvements on safeguarding and storing seeds. The traditional and chemical seed management techniques have already lost their acceptability because of its limitations such as cost, selectivity, effect on target organisms, development of pest resistance, resurgence of pests, pollution of food and feed, health hazards, toxicity towards plants and animals *etc*³⁸.

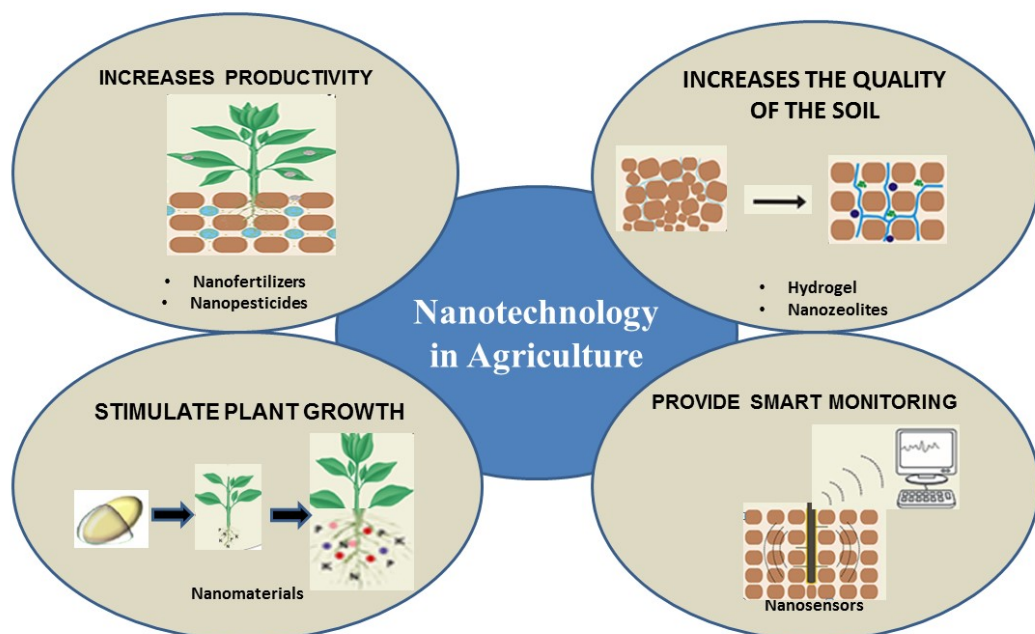
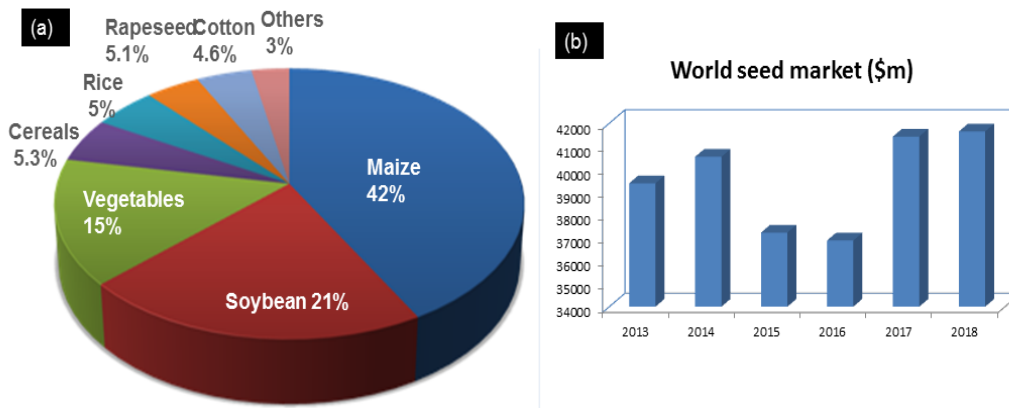


Fig.I.3 Application of nanotechnology in different agricultural field

It was discovered that cowpea seeds primed with fertilizers and microdosed or applied fertilizer in the seed hole, resulted in a 26% improvement in stand establishment³⁹. Ageing of seeds is an expected and irreversible process that can be attributed to both biotic and abiotic influences. This issue needs to be resolved in order to achieve good

germination. This can be done by regulating the storage conditions or via seed coating.



**Fig. I.4 a) Market share by crop type.
b) The statistics on the global seed market**

To increase seed germination and seedling growth, the post-harvest treatment of the seed may involve hydrating it before planting or seed priming, coating and conditioning^{40,41}. Seed enhancements are the combined name for these procedures.

1.4 Seed Treatment Methods

Seed treatment can range from a simple dressing to coating and pelleting⁴². Seed treatment refers to the exposure of the seeds to specific physical, chemical, or biological agents. These are not employed to make the seeds, pest or disease free but treated to provide the possibility of pest and disease control⁴³. With the use of highly successful technologies, seed treatments offer a cost-efficient agricultural input. Different methods have occasionally been offered for use and more sophisticated methods are needed to control plant diseases while having the least negative impact on seed health. Seed treatment provides several benefits compared to other pest control or crop enhancement techniques⁴⁴. This helps to preserve the seed from pre- and post-soil planting. More effective chemical alternatives are available in seed treatments. A significantly smaller initial inoculum is required. Seed treatments can limit the exposure to non-target organisms, eliminate drift issues and reduce the

amount of land exposed to active chemicals while maintaining maximum efficacy. Also helps to reduce the rate of application per hectare to achieve excellent control of foliar, soil-borne and seed-borne diseases while lowering the cost of disease control per hectare. Seed vigour, which is essential for a successful field's emergence, establishment and breaking seed dormancy can be boosted by seed treatments. This ensures a uniform stand across a wide variety of soil types, cultural methods and environmental circumstances.

1.5 Seed Coating and Types

The act of applying materials to the surface of seeds in order to create a continuous layer on the surface is known as seed coating⁴⁵. Seed coating alters the physical properties of seeds to produce uniform seed sizes, which makes handling seeds and precise sowing easier. Aside from acting as a channel for agricultural active ingredients (AIs), seed coatings can also promote seed germination, growth, and pest protection before and after germination^{46,47}. The precise application of the AI on the seed through coatings reduces off target exposure and minimises the need to apply the AI throughout the entire field. Thus the limitation associated with aerial spraying can be overcome and make the AI treatment process more ecologically friendly and sustainable⁴⁸.

Seed coating entails creating a film coating with polymers and other materials such that it also serves as a delivery mechanism. Coating the seeds with polymers is one method for preserving seed quality. Surface film⁴⁹, colouring⁵⁰, pelleting⁵¹ and nano range polymer coating are among the suitable techniques that are currently available⁵². A polymer coating can regulate both moisture and temperature variations that cause poor stand establishment.

Depending on the size and weight of the coat, three types of seed coatings usually employed are coating with polymer films, seed encrusting and pelletization⁵³. Fig.I.5a-d (partially adapted from the studies by Pedrini *et al.*⁴⁷ and by Farias *et al.*⁵⁴ (Copyright American Chemical Society, 2019 and Elsevier, 2017) displays a schematic diagram of various recent seed coating approaches. The movement direction of the movable parts is indicated by green arrows. To increase the pellet

size, rotating drums use a moderate rotating motion and progressive material addition. Liquids are administered with a spray nozzle, fillers are added manually or through a hopper to the seeds already in the pan.

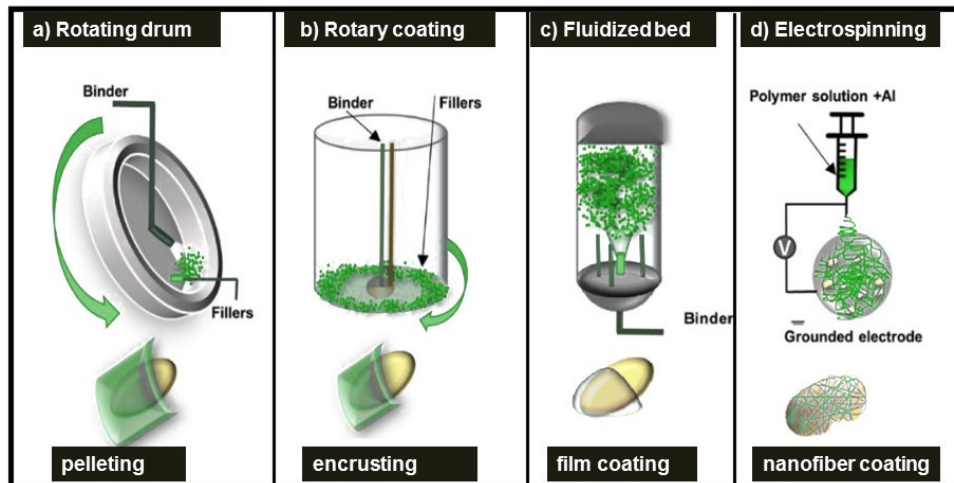


Fig.I.5 Schematic of several seed coating methods

Pelleting and film coating are also possible with rotary coating. Fluidized beds are utilised to coat the seeds with a film that holds the seeds air buoyant in the cylinder while they are exposed to subfloor air flow. In each of these methods, the seeds are coated with the AIs, either singly or in combination with filler or binder. A polymer solution containing the AI is electrospun directly onto the seeds while being driven by an electric field.

1.5.1 Seed Pelleting

Seed pelleting is the most comprehensive seed treatment technology, which alters a seed's physical form to improve pelletability and handling. To produce an overall globular form, seeds are covered with an exterior substance. Seed pellets were first prepared to obtain uniform seed dimensions for precise sowing but they can also be used to protect seeds and improve germination. The seeds are first stamped with an adhesive during the pelleting process and then the pelleting material is sprayed on top of the seeds to adhere it. The coated seeds are then rolled to create an even layering on the seeds' top. Common fillers used in seed pellets include ingredients like peat, sand

and chalk⁵⁵. Fillers like peat, serve as transporters for beneficial bacteria in seed pellets because of their high porosity and water holding capacity. Pelleting offers the chance to increase material loading surrounding the seeds and allows for variable spatial orientation of the active component within the pellet. Seed pelleting can carry any chemical in a reasonable amount with no phytotoxic effect on seeds. Pelleting is one of the most expensive applications which call for specific equipment and application methods⁵⁶.

1.5.2 Encrusting

During seed encrusting or intermediate pelleting, exterior material is accumulated on the seed surface without appreciably altering the original seed morphology. The seed weight may increase by 30–180% after encrusting. Encrusting is used to achieve consistent seed dimensions and to load the seeds with the appropriate AI, much like pelleting.

1.5.3 Film Coating

Film coating involves coating the seed with a thin layer (less than 10% of seed weight), whereas encrusting and pelleting produce coatings that are significantly thicker (~ 100- 500% and >500% of seed weight, respectively). It is hard to identify the initial seed shape because of the heavy coating during pelleting. A mixture of binders, fillers and AIs is used as seed coating mixture. The binders are polymeric solutions that adhere to the seed and carry active ingredients. To improve seed shape and size, fillers- mostly inert powdered materials like talc, sand or clays are often added. The AIs must be compatible with both binders and fillers. According to a recent investigation, covering the seeds improves the plant's ability to withstand stress during seed germination and seedling development⁵⁷.

Over the past 20 years, biodegradable polymers have been employed in seed coating in an effort to replace fossil fuel-based polymers. This is due to their biodegradable properties, accessibility and relatively inexpensive price of the precursor materials. Biopolymers such as gums, gelatin⁵⁸, chitosan⁵⁹, starch⁶⁰, cellulose and its derivatives⁶¹ and alginates⁶² are utilised either independently or in conjunction with other materials as seed coatings for better and targeted AI delivery,

improved growth and protection of plants. Majority of biopolymers require application of additional materials, namely surfactants and film formers. The hydrophilic property of the seed coat is one of the primary shortcomings of biopolymers, particularly polysaccharide-based seed coats⁶³. In order to preserve the integrity of seed coats for extended periods of time, more recent research has concentrated on the development of hybrid coatings that exhibit lower water solubility. However these methods have some limitations including time requirements, combinations of limited material ranges, cost and manufacturing rates.

Even though now a days polymer films with strong adhesion to seeds are available abrasion which causes the loss of material in film coated seeds, still remains as a challenge⁶⁴. The field of biobased plastics has undergone significant progress over the past ten years. These materials are made of organic carbon-based polymers generated from biobased materials (plant biomass, algae and fungi)^{65,66}. Bioplastics are utilised in many industries, including construction, transportation and agriculture⁶⁷. Although mulching is the primary application for bioplastics in agriculture, they are also thought to be a viable choice for covering seeds⁶⁶. The application of film coating of maize and canola seeds by bioplastic incorporated with starch was assessed. The biodegradable nature of the coat contributes to faster disintegration of bioplastic components, which speeds up the release of AIs. All bioplastics are not fully biodegradable, even though primarily made from biobased precursors (corn, sugarcane and waste fats/oils), which ultimately lead to the inclusion of undesired elements in the soil. Recent years have seen a rise in interest in creating bioplastics from lignocellulosics developed from biomass and agricultural products to solve this issue⁶⁸. The main obstacles to the widespread use of bioplastic-based seed coatings, however, are the time-consuming processing steps (such as pre-treatment, liquid detoxification, fermentation, conversion, separation and purification) as well as the use of high-cost solvents (ionic liquids) or microemulsions for fractionation. Primary challenges to the strategy include a reduction in water permeability and a reduction in gas exchange due to the film-based nature of the coatings⁶⁹.

Recent agricultural research has seen the development of novel seed coatings by employing nanotechnology principles in seed treatment processes to promote crop yields. This can be accomplished by increasing the agrochemical's efficacy by

targeted distribution and gradual release. Along with increasing productivity, it benefits the economy and the environment. Such very inventive nanoagrochemicals reduce the need for fossil fuel-based chemicals. For this purpose, research on "sustainable nano-enabled seed treatments" has recently attracted substantial attention in order to minimize the inefficiencies of pesticides and fertilizers to provide novel crop protection solutions⁷⁰⁻⁷³.

A high surface area would assist effective coating because the polymer surface area is crucial in determining the even distribution of polymer on the surface of the seed. Therefore, porous polymer membranes such as nano-fibers using electrospinning and porous polymer films using dipcoating has been used to improve agricultural production through development of efficient seed coats. Such coatings aid in the efficient and even application of chemicals and fertilizers⁷⁴.

1.6 Techniques for the Preparation of Porous Polymer Membranes

1.6.1 Electrospinning

Electrospinning is a simple, promising, low-cost and a top-down micro and nanoscale technique to produce continuous nanoscale fibers from various polymer materials with the aid of a high-voltage electric field⁷⁵. The "top-down" manufacturing approach of fiber production was more efficient and less expensive than the difficult "bottom-up" techniques. By using this technique, fibers between 100 nm and 1 μ m are fabricated⁷⁶. Electrospinning offers the most potential properties because of its reproducibility, control of fiber morphology, fineness and resemblance to the extracellular matrix *etc.* The rapidly expanding field of electrospinning includes the creation of membranes more water-repellent than lotus leaves, scaffolds that mimic tissue to enable tissue growth and threads finer than spider webs. This method can be applied to synthetic and natural polymers as well as polymers loaded with nanoparticles, drugs, vitamins, antioxidants, ionic liquids, metals and other substances. The procedure has been planned so that the polymeric substance will not suffer any chemical reactions, temperature fluctuations or decomposition, making it appropriate for producing nanofibers.

Both organic and inorganic materials can be employed to create the nanofibers as there was no heating involved in the process, chemical and physical properties are not affected much. This method can be used to incorporate changes in the polymer such as chemical modifications, incorporation of materials from the macro range such as complex enzymes, polymer, bacteria and materials from the nano range such as carbon nanotubes and metal nanoparticles. By altering the electrospinning conditions, the macroscopic characteristics of the fiber system, such as chemical, physical, biological *etc.*, that are observed in the nonwoven mats, can be improved at the molecular level. The process appears to be a straightforward application of electrostatic forces, but it is actually controlled by a complex interplay of physical, chemical, technological and molecular characteristics. The next section gives a description of these variables (section 1.6.1.2). Regarding the quantity of polymer utilised, the electrospinning method also provides an advantage. Using the electrospinning approach, nanofibers can be created using extremely small amounts (50 mg) as contrast to conventional techniques, which need huge amounts of polymer.

The first continuous nanofibers made from electrospun polymers were created and patented by Anton Formhals in 1934⁷⁷. Taylor investigated the cone shape of electrically generated jets at the needle tip in great detail and gave it the name "Taylor Cone" in 1960⁷⁸.

1.6.1.1 Fundamental Principle of Electrospinning

A glass syringe with the polymer solution, a metallic needle, a power supply, and a metallic collector make up the basic electrospinning setup (with a variable morphology). The electrospinning procedure is carried out in an air environment at ambient temperature. Fig.I.6 depicts the electrospinning setup employed in this study. Using this method, polymers are dissolved in a solvent to create a solution that is then drawn into a syringe by applying an electric field to the polymer solution, which is being held at its own surface tension at the tip of the needle. A charge is induced on the surface of a polymer liquid droplet when a suitably high voltage is applied to it. The liquid's surface tension is reduced by electrostatic repulsion, which also causes the liquid droplet to elongate and take on the Taylor cone shape. A stream of charged

liquid erupts from the tip of the Taylor cone when the electric field's strength reaches a critical level.



Fig. I.6 Electrospinning set up

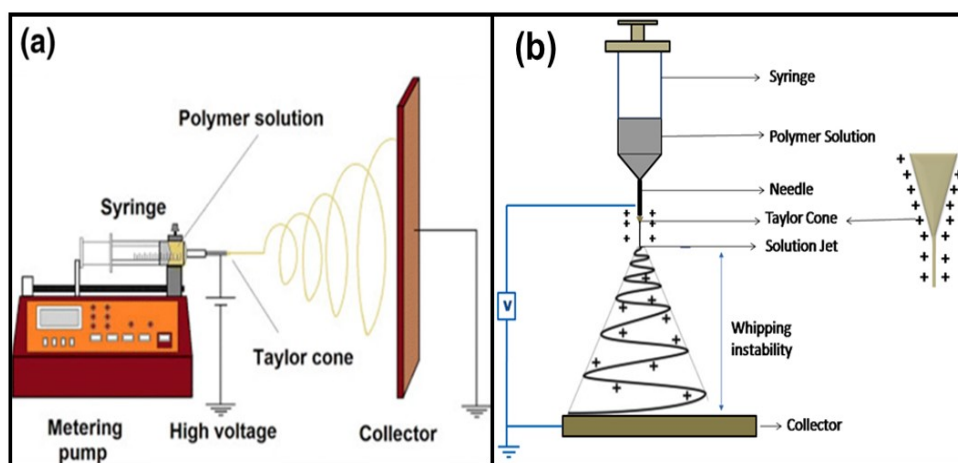


Fig. I.7 Schematic representation of electrospinning apparatus
a) horizontal set up b) vertical setup

The discharged polymer solution jet is subsequently stretched out by a whipping process brought on by electrostatic repulsion that begins at tiny bends in the fiber, as shown in Fig. I.7^{79,80}. As the jet moves through the air, the solvent evaporates and a thin, long, uniform nanofiber with a diameter of a few nanometers is formed as a result of bending instability and elongation⁸¹.

1.6.1.2 Electrospinning Parameters

The electrospinning variables determine the characteristics of nanofibers. Despite having drawbacks including flammability, toxicity and corrosiveness, electrospinning from organic solvents offers the convenience of a wide range of solvent properties. Melt electrospinning has advantages in terms of productivity and the environment, but it has the drawback of having larger fiber diameter.

Different types of fibers can be produced depending on the polymer selected and the electrospinning settings used. Fig.I.8 displays the various types of fibers developed. The formation of beads during spinning is possible (Fig.1.8a), these beads may have deformities because they decrease the surface area, mechanical strength and uniformity of the fiber's dimensions. These are flaws that must be fixed through spinning parameter optimization. These beaded fibers can exhibit particular characteristics, making them suitable in some applications. Ribbon-like fibers, which reduce surface area, can occasionally occur as in Fig.I.8b. It is also known that the production of twisted fibers Fig.I.8c. necessitates optimising the voltage parameter. Electrospaying would result from a low polymer concentration or low polymer molecular weight (Fig.I.8d).

The effectiveness of an electrospinning process depends on interrelated variables, thus it is essential to strike a delicate balance between the processing parameters, solution parameters and ambient characteristics. In order to understand how the electrospinning process might be optimised, these factors have been examined. The results of the electrospinning procedure are determined by these parameters. The following is a summary of how various parameters affect electrospinning.

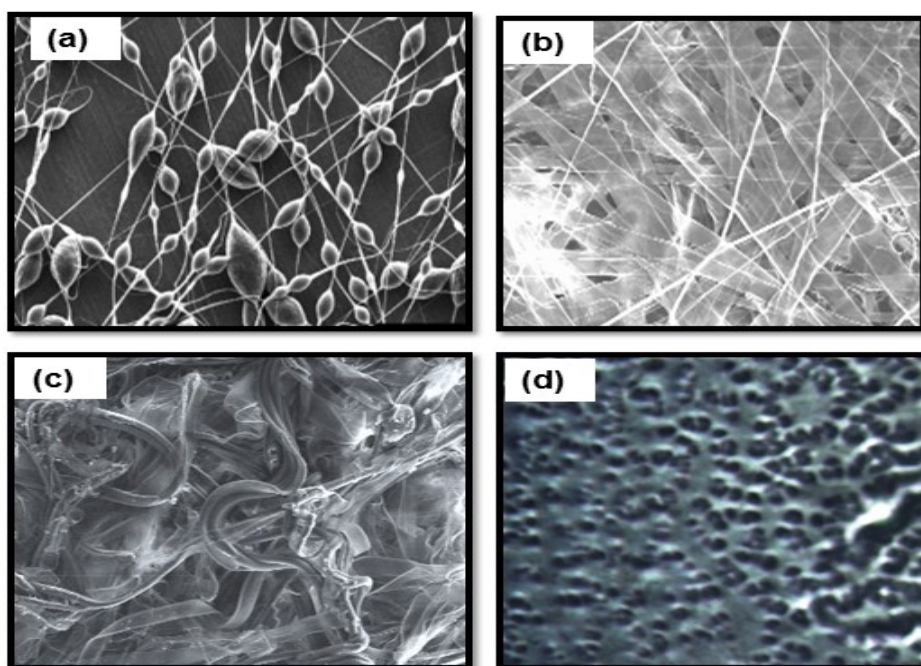


Fig. I.8 a) Beaded nanofibers b) Ribbon like nanofibers
c) Twisted nanofibers d) Spray type nanofibers

1. Choice of Polymer

Based on the qualities and intended uses of the fiber, the polymer material should first be optimised for electrospinning. Typically, nanofibers with important qualities can be easily formed from polymers with high molecular weight. Chitosan, cellulose, gelatine, collagen, silk fibroin/chitin and agarose/PVA are examples of biopolymers and blends of biopolymers with synthetic polymers that have been electrospun.

Electrospinning has been used to turn variety of polymers into nanofibers, including water-soluble polymers like poly(ethylene oxide) (PEO), polyvinyl alcohol (PVA) and polyvinyl pyrrolidone (PVP) as well as organosoluble polymers like polyimides (PI), Polyvinyl chloride (PVC), Poly(methylmethacrylate) (PMMA), Poly(vinylidene fluoride) (PVF) and poly(benzimidazole) (PVB). Electrospinning has been used to transform bioerodible polymers (polyanhydrides, polyphosphazenes, and aliphatic polyesters) into nanofibers⁸¹.

2. Solution Parameters

➤ **Concentration**

The viscosity and surface tension of the utilised polymer solution determine the polymer concentration. Surface tension takes over at very low concentrations and viscosities of the polymer, causing droplets to form rather than fibers. The result will be a mixture of beads and fibers if the concentration is a bit high. The shape of the beads shifts from spherical to spindle-like as the concentration rises and eventually uniform fibers with larger diameters are produced. This is due to the fact that an increase in the concentration of the polymeric solution causes a rise in chain entanglement between the polymer chains, which reduces surface tension and produces homogeneous beadless nanofibers. Because it is very challenging to force the polymer solution through the syringe needle at very high concentrations, continuous fiber production is prohibited. Consequently, it is necessary to maintain an ideal solution concentration to produce smooth and uniform fibers⁸².

➤ **Surface tension**

In the electrospinning process, surface tension is the main force that opposes the applied voltage. A jet of charged polymer solution is ejected from the needle's tip. When the surface tension caused by the applied voltage is overcome, the beadless nanofibers are formed. Surface tension is a solvent-related characteristic and different solvents may contribute to the surface tension in different ways. The ratio of the utilised solvent mixture affects the surface tension⁸³.

➤ **Viscosity**

Molecular weight, polymer concentration and viscosity are all connected. While a highly viscous polymer solution hinders the ejection of the polymer jet from the needle tip, a low viscosity polymer solution produces droplets of polymer (electrospray). Optimizing the polymer solution's viscosity will produce fibers that are uniformly smooth and bead-free⁸⁴. The differences in fiber shape are caused by variations in viscosity.

➤ **Conductivity**

The quantity of electric charges that can be discovered on the surface of the electrospun polymer solution is implied by conductivity. It has been shown that the polymer solution's jet radius is inversely proportional to the cube root of electrical conductivity⁸⁴. If the solution's conductivity is extremely poor, there won't be any charge on the droplet's surface, making the electrospinning process impossible. The fiber diameter decreases when the conductivity of the solution is raised to a critical level.

➤ **Molecular weight**

One of the solution parameters that has the biggest impact on the shape of the electrospun nanofibers is molecular weight. Chain entanglement in polymer solutions during the creation of nanofibers is influenced by the polymer's molecular weight⁸⁵. Changes in the polymer's molecular weight while maintaining a constant concentration have a significant impact on its fiber structure. An increase in the solution's molecular weight results in the development of micro-ribbon structure. Instead of fibers, a lower molecular weight solution typically forms beads or drops. Additionally, smooth fibers would result from a molecular weight solution that was optimal.

➤ **Selection of solvent**

The production of smooth and beadless nanofibers is significantly influenced by the solvent choice. For efficient electrospinning, the solvent must have the following properties: (i) the polymers must be entirely soluble in the chosen solvent (ii) the solvent must have a moderate boiling point and volatility and (iii) the solvent must have a good dielectric constant. While electrospinning creates nanofibers from a solvent with optimum volatility, a solvent with excessive volatility will stop electrospinning by drying the jet at the needle tip. Beaded nanofibers may occur as a result of the deposition of nanofibers with solvent on the collector⁸⁶. High dielectric constant solvents are helpful for successful polymer spinning. The electrostatic field strength increases along with the solvent's dielectric constant, creating the steady polymer jet needed for efficient electrospinning⁸⁷.

3. Processing Parameters

➤ Voltage

Since the threshold voltage must be exceeded for the charged jet to be ejected from the Taylor cone, the applied voltage across the needle and the collector is a crucial component in electrospinning. Electrospinning begins when the threshold voltage is reached. An increase in voltage leads the polymer solution to stretch and produce smooth nanofibers with a small diameter by increasing the electrostatic repulsion force on the jet. Beads or beaded nanofibers form when the applied voltage is raised above the critical level. This occurs as a result of the increase in jet velocity as the applied voltage is increased while maintaining the same flow rate⁸⁶.

➤ Distance between the collector and the needle tip

The morphology of the electrospun nanofibers is influenced by the distance between the collector and the needle tip. In order for the fibers to have enough time to dry completely before reaching the collector, a crucial distance must be maintained. The formation of beaded and large-diameter nanofibers depends on the distance. As the distance increases, the fiber diameter decreases⁸⁶.

➤ Flow rate

The jet velocity and the rate of material transfer are influenced by the flow rate of polymer solution from the syringe. In order to allow sufficient solvent evaporation and the production of smooth fibers, a minimal flow rate was preferred. If the flow rate is raised over the ideal level, beaded fibers, ribbon-like fibers, droplets *etc.* will form. These flaws were mostly related to the solvent's slow rate of evaporation and the solution's minimal stretching during its passage between the needle and the collection⁸⁵.

➤ Collectors

Nanofibers are collected using collectors as a conducting substrate. The productivity, alignment and ultimate structure of the nanofibers are influenced by the various types of collectors that are utilised. Frequently, aluminium foil is utilised as the collector. Additional materials include wire mesh, rotating rods, conductive paper or cloth and parallel or gridded bars.

4. Ambient Parameters

➤ Moisture content and temperature

The diameter and shape of nanofibers are altered by humidity. The rate of solvent evaporation reduces as humidity rises. Porous or beaded nanofibers develop from an increase in humidity. Low humidity causes nanofibers with a small diameter to develop and dries the solvent. Temperature affects the viscosity of the solution, the rate of solvent evaporation, and the diameter of the fiber. A higher temperature accelerates the solvent's evaporation rate and reduces the solution's viscosity, producing nanofibers with a smaller diameter⁸⁶. Even though the electrospinning process appears simple, parameter optimization makes it more complex. By managing these parameters, it is possible to generate nanofibers with the necessary diameters and morphologies for targeted applications.

1.6.1.3 Applications of Electrospinning

Several applications of electrospinning technology are depicted in Fig I.9.

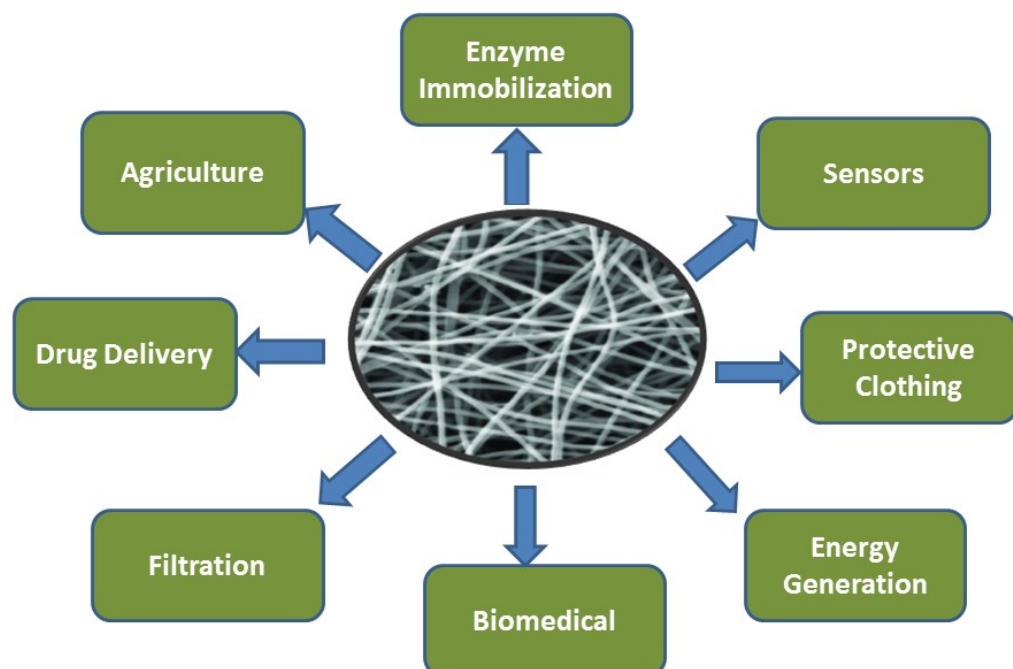


Fig. I.9 Applications of electrospun nanofibers

1.6.2 Phase Inversion

The most flexible way for creating porous polymer membranes is phase inversion. In this procedure, a homogenous polymer solution is changed from a liquid to a solid state. Immersion precipitation, thermally induced phase separation, evaporation-driven phase separation, and vapour-induced phase separation are the four primary fundamental methods for creating phase inversion membranes⁸⁸. Immersion precipitation is one of these methods that are frequently used to create porous membranes with various morphologies. The Loeb-Sourirajan technique is another name for this technique⁸⁹.

1.6.2.1 Immersion Precipitation

This method involves dissolving the polymer in a suitable solvent, casting the homogeneous polymer solution onto a glass sheet and then soaking the glass sheet in a non-solvent solution. Exchange of solvents and non-solvents causes precipitation, phase separation and mass transfer determine membrane shape.

1.6.2.2 Thermally Induced Phase Separation

This process makes use of a polymer that can be dissolved in a particular solvent only above a certain temperature and then cast on a glass sheet to form a film. The homogeneous solution is then cooled down below the dissolving temperature which leads to a phase separation. A polymer rich phase and a solvent rich phase is observed and finally the polymer rich phase solidifies to form a membrane.

1.6.2.3 Vapour Induced Phase Separation

In this method of separation, the chosen polymer is dissolved in a specific solvent and formed into a film. Then, this film was introduced to a vapour environment that included non-solvent. A porous membrane forms without a top layer as the non-solvent penetrates the cast film.

1.6.2.4 Evaporation Induced Phase Separation

A relatively easy method for creating polymer films with controlled porosity and both symmetric (pores spread evenly throughout the film) and asymmetric

(non-porous top layer supported by porous layer) morphologies is the evaporation induced phase separation (EIP) process. This method involves dissolving a polymer in a combination of solvent and non-solvent, with the solvent being more volatile than the non-solvent. The polymer solution splits into two phases when the solvent evaporates, the non-solvent richer droplets increase⁹⁰. By evaporating the solvent, the polymer rich phase solidifies to form a solid membrane, while the polymer lean phase, which is rich in non-solvent, permeates the solid membrane and creates pores in it⁸⁸. Fig. I.10 depicts a schematic design of an evaporation-induced phase separation method.

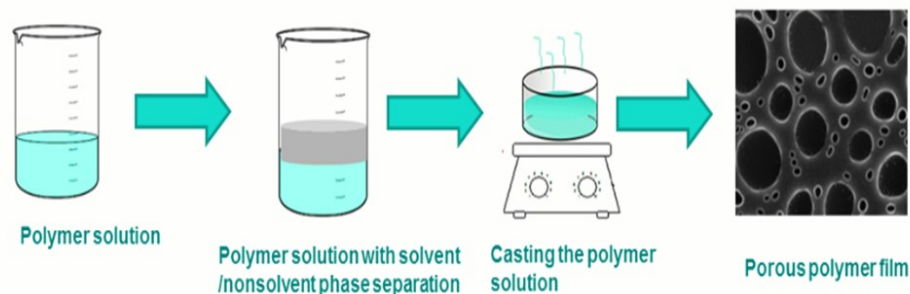


Fig.I.10 Evaporation-induced phase separation method to make porous polymer film

1.7 Nanofibers in Agriculture and Nanofiber Seed Coatings

Currently, nanofibers are considered as the nanostructured material that is being investigated and used for a variety of applications in various sectors, including tissue engineering, filtration, health, materials science, bioengineering, catalysis, energy, water and soil remediation, sensors, textile and food industry and agriculture⁹¹⁻⁹⁵. Drugs, semiconductors, catalysts and nanoparticles can be added to the developed fibers to functionalize them. Overall porosity, pore size and specific surface area are factors that aid in gas and active ingredient diffusion, resist airflow and serve as efficient filters and carriers in tissue engineering. Numerous methods for creating polymeric fibers, particularly those in the nanometer range, have been developed. These methods include drawing, template synthesis, self-assembly, phase separation, melt blowing, spun-bonding, fibrillation, carbon dioxide (CO₂) laser supersonic drawing (CLSD) and electrospinning⁹⁶⁻¹⁰⁰. The following are some

advantages of electrospun nanofibers: i) High surface-to-volume ratio ii) high porosity iii) ease of functionalization for various applications iv) superior mechanical property v) simple process vi) relatively low start-up cost vii) capability of mass production; viii) Ease of material combination and ix) small amount of required materials.

Even though electrospinning is still a process that has not fully developed in agriculture, its applications in the fields of medical, food, textiles and agriculture have been growing in recent years. The application of electrospun nanofibers in agriculture is still relatively new and still in infancy. Agriculture has advanced greatly as a result of the nanotechnology breakthrough in fertilizers. Various nanomaterials including silver, iron, zinc, titanium, carbon nanotubes, molybdenum and silica have been produced and used in crops. Depending on the concentrations used, these compounds have a significant impact on floor biomass, root and shoot elongation and seed germination. Due to the tailoring qualities of nanofibers such as high surface area, porosity, ease of adding active ingredients (such as fungicides, insecticides, herbicides, pesticides, hormones and pheromones), flexibility, biocompatibility and biodegradability, numerous researchers have recently examined the major applications of nanofibers in agriculture¹⁰¹. The major applications of nanofibers in the agricultural sector may include seed coating^{102,54}, nanofiber-based irrigation system filters¹⁰³, nanofibers for plant protection¹⁰⁴ by encapsulation of fungicides¹⁰⁵ or detecting trace amounts of pesticides in water¹⁰⁶, nano-silica grafted fiber¹⁰⁷, smart nanotextiles for sustainable agriculture¹⁰⁸, nanofibers for encapsulating agrochemicals such as fertilizers¹⁰⁹ and phytohormones¹¹⁰. For enhanced germination and seedling growth in rice^{111,112} cowpea¹⁰², groundnut¹¹³ and sesame¹¹⁴ nanofibers can be used as an efficient and sustained delivery system for agricultural inputs through seeds. The functionalization (i.e., adsorption, filtration and sterilisation) of nanofibrous filters by bioactive compounds may be required for their use in irrigation systems. This functionalization may be accomplished through interfacial polymerization, doping nanoparticles, self-assembly and layer-by-layer cross-linking or grafting of surface coatings¹¹⁵.

The most popular fertilizers on the market are those containing nitrogen, phosphorous and potassium since they deliver plants nutrition. However, because these ingredients are very soluble in water, they have a short shelf life. After

electrospinning, the fertilizers can be encapsulated in nanofibers without affecting their structure and morphology. Polyvinylpyrrolidone (PVP) and poly(diethoxy) phosphazene (PPZ), which are rich in nitrogen and phosphorus, have been utilised as encapsulants for phosphates and urea, which also deliver nutrients to the plant. The best candidate for agriculture has been compared after being analysed at various concentrations¹¹⁶.

Encapsulation of urea is advantageous in agriculture as it is toxic to farmers' health when inhaled or in touch with the skin. Urea forms a homogeneous solution with PEO because of its bonding interactions¹¹⁷. In addition to providing water resistance, coatings in plants and fruits must also have the desired wettability for a uniform coverage on the fruit surface and sufficient flexibility to permit the continuing growth of fruit prior to harvest. To prevent the usage of pesticides, which are mostly environmental pollutants, biocontrol agents like *Trichoderma* and *Bacillus subtilis* are utilised. These agents serve to extend storage period and provide protection from external influences. Chitosan, polyacrylamide, and polyethylene oxide (PEO) polymers are employed for this purpose and have been shown to have a high level of protection against phytopathogenic agents¹¹⁹. There have also been reports of nanofibrous membranes that can immobilise enzymes¹²⁰.

In order to immobilise enzymes, a variety of nanostructured support materials have been utilised, including nanoparticles, nanofilms, nanofibers, nanotubes, nanosheets and mesoporous/nanoporous silica¹²¹. Due to their interconnectivity and high porosity, nanofibers have demonstrated numerous benefits among the support materials, including self-assembling performance, surface area, enzyme binding and homogenous dispersion¹²². The main purpose of enzyme immobilization is to make it easier to handle the enzyme and allow for its on-going or repeated use. Enzyme immobilization typically involves the option of altering enzyme parameters including activity, stability, selectivity, *etc.* in addition to these technical benefits.

In seed coating research, a variety of seeds have been coated with nanofibers that have been loaded with the necessary active ingredients. The two different ways that seeds can be coated with nanofibers: (a) directly by electrospinning the solution on top of the seeds (b) indirectly by first preparing fiber mats and then wrapping them

around the seeds. Various research teams have recently conducted experiments to investigate the potential of electrospun nanofibers for the controlled distribution of agrichemicals¹²³. It was seen that the seed germination was not hindered by the coatings, at the same time the localized release of active ingredients are ensured. Based on the experiments mentioned above, it is clear that the hydrophobicity of the coating is crucial in regulating the rate at which certain AIs are released. To transport AIs effectively while preventing germination inhibition, there may be an optimal level of hydrophobicity, although this information is not currently available in the literature. The porosity of nanofibers and the extent of interactions between the polymer used in the nanofiber and AI will determine how effectively the AIs are delivered. Comparing electrospun nanofibers to the frequently applied film coatings, electrospun nanofibers appear to be a promising method with several benefits. They have a larger surface area, a porous surface and no residual solvents. When compared to dip-coated film coatings, fiber-based coatings function better because nanofibers help to overcome limited gas permeability across the coating and seed pore clogging.

1.8 Importance of Polymer Selection in Seed coating

The polymer should be affordable, have good coating properties, biocompatible and biodegradable¹²⁴. Such coatings permit the soil's nutrients to be retained, making it possible to supply the plant without incurring any losses. In addition to the aforementioned characteristics, the acceptance of the polymer coating also depends on how the polymer and the nutrients interact physically and chemically¹²⁵. Better loading and regulated release are produced when weak intermolecular forces of attraction, such as hydrogen bonds that exist between the polymer and the additional active ingredients¹²⁶.

Biodegradable polymers are intriguing biomaterials because they have a regulated rate of deterioration and are hydrolytically sensitive. They degrade into non-toxic compounds that can be reabsorbed into or expelled from the system in use. Such polymers can be made into scaffolds and used in a variety of industries, including agriculture, medicine and energy storage. The degradation of polymers is also influenced by environmental parameters, which promote polymer degradation and have an impact on the activity of microorganisms. Numerous variables, including pH, humidity, temperature, salinity and oxygen level, influence the breakdown by

microorganisms. The structure and chemical makeup of the used polymer have an impact on how quickly it degrades. Additionally, these depend on factors like crystallinity, morphology, crosslinking, additives *etc.*, which can vary over time.

1.8.1 Polymer Blends

Polymer blends are bound by weak chemical intermolecular forces between two or more polymers. Polymers have special qualities that have made them indispensable and are employed in a wide variety of applications. To achieve all the requirements, these polymer properties must be further improved. In order to reach commercial viability, costs must be reduced, certain properties must be improved, degradability must be increased and reuse or recycling must be made easier. Thus, polymer blending has emerged as a useful method whereby two polymers with desired features can be mixed in a way that overcome the drawbacks of each polymer alone. The intermolecular attraction between the two polymers, such as hydrogen bonds, ionic attraction, and others, decide whether they are completely immiscible, partially miscible, or miscible. These forces of attraction, which are adhesive forces, function to control the phase separation and outweigh the resulting entropy of mixing. Therefore, the issue is to incorporate hydrogen bonding networks effectively while maintaining other qualities such as mechanical strength¹²⁷. Blends of both poly(ϵ -caprolactone) (PCL) and poly(ethylene oxide) (PEO) have been extensively fabricated and studied. The superior rheological and viscoelastic characteristics of PCL over many of its aliphatic polyester competitors make PCL simple to manufacture and manipulate into a wide variety of applications. However, its hydrophobic nature restricts the use in delivery and agricultural applications that is primarily hydrophilic. As a result, its modification via surface potential¹²⁸ or the use of hydrophilic synthetic and biopolymers opens up new possibilities for agricultural applications¹²⁹.

Both amphiphilic blends, such as those with gelatin or PEO, or grafting hydrophilic moieties onto PCL¹³⁰ can be used to make the changes. An intriguing class of biomaterials that can be customised for certain systems in terms of morphological, mechanical and degrading features are biodegradable polymer blends. Due to a number of technical applications, PCL/PEO blends attracted interest from

both academic and industry sectors. In particular, PCL/PEO blends have been studied for the creation of biodegradable membranes¹³¹, controlled drug delivery¹³², scaffolds for tissue engineering¹³³. Literature survey reveals that PCL/PEO blends has not explored in agricultural applications so far.

1.8.2 Cause for Interest in Inorganic Polymers

One of the main fields of molecular and material sciences, polymer chemistry and technology covers many facets of contemporary life, including electronics, medicine and agriculture. Although there is a wide range and variability of organic polymers, the application of inorganic polymers finds much attention. The reaction between the organic polymer backbone and oxygen and ozone causes them to lose their beneficial features. They can emit poisonous smoke sometimes and degrade when exposed to gamma and UV rays. The availability of these organic polymers would be constrained as a result of the predicted scarcity of petroleum. The bonds created in inorganic polymers are stronger for longer periods of time and provide diverse combinations of features. As a result the bond angle, bond torsional mobility and ultimately the polymer's property are altered. The C-C backbone found in the synthetic polymers makes them resistant to degradation. The chance of degradation from hydrolysis or microbial attack is increased by the presence of a heteroatom or a heteroatomic functional group in the chain. Today, polyphosphazenes, polysiloxanes and polysilanes - all inorganic polymers made from silicon and phosphorus are well-known.

With the aforementioned considerations in mind, it was proposed to use nanotechnology in agriculture by focusing on the fabrication of nano fibrous polymer seed coatings using electrospinning technique. This research is aimed at a potent strategy to develop a biocompatible seed coat that may aid in germination and would preserve the seed against a wide range of diseases and infections and so increase crop yield. A facile approach is developed using electrospun nanofibers and porous polymer membranes loaded with essential nutrients and fungicides and applied as a combined delivery system via seed coat. Most of the coating materials used in conventional approaches, such as starches, alginate, poly(vinyl alcohol) and polyethylene glycol are typically dissolved in water. As a result, the active

ingredients, such as pesticides, antimicrobials, fertilizers and micronutrients are uncontrollably released⁴⁷. A large portion of the active substances flow out into the field, resulting in poor delivery effectiveness and perhaps serious adverse environmental effects. Therefore hydrophobic polymer, PCL was employed aiming at controlled release of agrichemicals for a prolonged time and protection of seed. However during the course of the investigation, blends of PEO were added. The nanohydroxyapatite (nHAP) as a nontoxic fertilizer, which may act as a rich source of calcium and phosphorous and the micronutrient zinc in the form of zinc oxide nanoparticles (ZnO NPs) were added to these polymer coatings. The Zea mays (corn) seed was employed in the investigation. Studies are conducted by incorporating the biofungicide *Trichoderma viride* within the nanofibrous matrix to analyse the effect of immobilized plant beneficial microbes under pathogen infected conditions.

The hydrolysis of endosperm starch into metabolizable sugars during cereal seed germination by the enzyme α -amylase in the aleurone layer is crucial for the formation of roots and shoots¹³⁴. 90% of the amylolytic activity in maize seeds is attributed to the α - amylase enzyme, which is vital for starch hydrolysis. The embryo creates and secretes natural gibberellins to the endosperm during the germination of maize seeds. These hormones promote the growth of hydrolytic enzymes like α -amylase and beta amylase in the aleurone layer, which are in charge of breaking down the endosperm reserves. In dried seeds, α - amylase enzymes are typically absent since they are produced and secreted by the aleurone layer. With this view, it is further sought to assess the activity of α -amylase immobilized on the PCL nanofiber in presence of plant growth promoting hormones such as gibberellic acid and magnesium oxide nanoparticles as a seed coat in the germination of maize seeds.

The characteristics of being stable and reusable inorganic carriers are more acceptable than their organic supporters and in some cases this can lower the actual cost of the immobilization support. The enzyme immobilised on inorganic support is less prone to degradation, aggregation, or denaturation than organic carriers - which are more easily degraded by the presence of microbes and various environmental factors. For these reasons, herein an attempt was carried out to immobilize the α -amylase on MCM-41, one member of the M41S family of silicate or aluminosilicate mesoporous materials through surface functionalization and covalent grafting.

In order to accurately transport agrichemicals to the proper location and in the right dose to promote seed germination and seedling growth, the adaptable biopolymer-based nanofibers can be employed as seed coating. With this view the present investigation is focused on the development of nanofibrous seed coating platform made from natural biopolymer cellulose, extracted from water hyacinth (*Eichhornia crassipes*). The aquatic habitat can be harmed by this plant growth rate and consider as a weed¹³⁵. The nanofibers loaded with active ingredients applied as seed coat and analysed for improved germination and seedling growth of maize seeds. Towards the end of the work, carbon dots are prepared using water hyacinth and encapsulated as nanofertilizer within nanofiber matrix. This would be advantageous because it would decrease production time, chemical costs and also reduce the aquatic pollution. The fabricated nano enabled seed coat direct sowing technology would be a novel platform to meet sustainable development goals and provide stand establishment of various crops under erratic rainfall and drought stress.

For a thorough understanding, each of the aforementioned elements has been explained in detail

1.9 Materials Used in the Present Work

1.9.1 Polycaprolactone (PCL)

PCL was chosen for this study due to its biodegradable and biocompatible qualities. It may be an ideal polymer for agricultural mulch films, controlled or slow release agrochemicals as it is a super absorbent material^{136,137}. Very few studies are done on the use of electrospun polycaprolactone (PCL) nanofibers as a base for a synthetic soilless medium for seed germination¹³⁸. The majority of the coating materials used in conventional approaches are typically dissolved in water, causing the active ingredients to be quickly and uncontrollably released. As a result, a large portion of the active substances flow out into the field, resulting in poor delivery effectiveness and perhaps serious adverse environmental effects. Poly(ϵ -caprolactone) (PCL) is an aliphatic, semicrystalline, thermoplastic polyester that is malleable at room temperature. Ring-opening polymerization (ROP) of a ϵ -caprolactone (ϵ -CL) and polycondensation of the 6-hydroxyhexanoic acid¹³⁹ are two popular processes for producing PCL that have been discussed in many references.

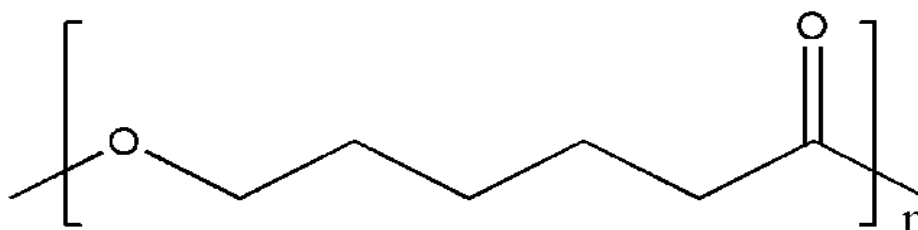


Fig. I.11 Structure of Polycaprolactone (PCL)

The Food and Drug Administration (FDA) has certified PCL as a polymer that has undergone significant research in diverse areas such as biomedical applications, as well as for environmentally sustainable packaging. Because it is soluble in a variety of organic solvents, PCL is very processable. It also has good rheological characteristics and a low melting point (glass transition (T_g) $\approx 60^\circ\text{C}$ and melting temperature (T_m) $\approx 60^\circ\text{C}$). It has ability to form miscible mixtures with a variety of polymers. The number average molecular weight of PCL samples may generally vary from 3000 to 80,000 g/mol.

The chemical structure of PCL is shown in Fig I.11, The molecular weight and end group chemistry, all have a role in its rapid and exceptional thermal breakdown at temperatures above 170°C . It is well suited to melt processing methods as injection moulding, melt extrusion, 3D printing, and electrospinning due to its low melting temperature, variable viscosity, and broad versatility^{140,141}. Additionally, the ester group on PCL is capable of hydrolysis via enzymatic and chemical pathways¹⁴². As compared to other polymer materials like PLA and poly(glycolic acid), PCL is nontoxic and its degradation products do not result in a drop in the pH of the areas around the scaffold and not producing a local acid environment^{143,144}. Through the activity of living organisms, biodegradation of polymers results in material fragmentation to total disintegration into CO_2 and H_2O . Microorganisms participate in the enzymatic breakdown that occurs on the PCL's surface. Due to PCL's hydrophobic properties, hydrolytic breakdown occurs very slowly^{145,146}. In addition to its other well-known features, PCL is attractive for the development of chemical delivery systems because of its slow degradation and hydrophobicity¹⁴⁷.

1.9.2 Poly(ethylene oxide) (PEO)

Polyethylene oxide (PEO) is a polymer with the subunit C–O–C as shown in Fig.I.12. PEOs have an average molecular weight that ranges from 200 to 5×10^6 . This average molecular weight is given by the formula $(\text{OCH}_2\text{CH}_2)_n$, where n is the typical number of oxyethylene groups. However, PEO compounds are classified as poly ethylene glycols since they are available as waxy solids or viscous liquids with molecular weights under 25,000.

The polymer polyethylene oxide (PEO), which is water-soluble, biodegradable, biocompatible and chemically stable, may be spun into nano- and microfibers by electrospinning^{148,149}. PEO may be more stable when covalent and hydrogen bonds function together. Furthermore, PEO nanofibers can encourage the attachment and development of organic cells due to their low toxicity and high surface area to volume ratio¹⁵⁰. Nonwoven PEO fibers have been used in numerous applications including biomedical, tissue engineering, electronics, energy storage, hemostatic agents and antibacterial agents^{151,152}.

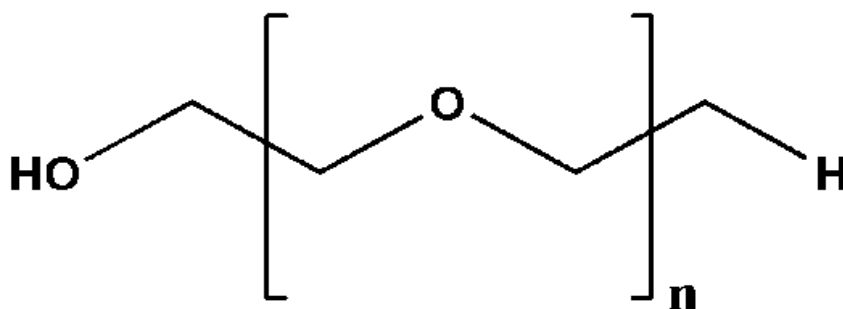


Fig. I.12 Structure of Poly(ethylene oxide) (PEO)

Poly(ethylene oxide) (PEO) is a porous material that is an excellent candidate for enzymes as chemical catalysts¹⁵³ and scaffolding¹⁵⁴. PEOs are known for their distinctive qualities like thickening, flocculent, dispersing, lubricating, binding, prolonged release and water-holding capabilities. PEO nanofibers are particularly advantageous as a potent and natural antibacterial agent against bacteria with no side effects. However lack of hydrophobicity and mechanical strength can be improved by blending with different polymers.

1.9.3 MCM-41 (Mobil Composition of Matter No. 41)

Researchers at Mobil Corporation discovered MCM-41, a member of the M41S family of silicate/aluminosilicate mesoporous materials, in 1992^{155,156}. These silica particles have disordered arrangement at the atomic scale and ordered porosity at the nanoscale.

Due to its desirable characteristics, including its stable honeycomb mesoporous structure, huge surface area (typically $>1000 \text{ m}^2/\text{g}$), narrow tunable pore size, large pore volume and well-defined surface properties, MCM-41 has received much exploration¹⁵⁷. Over the past several years, MCM-41 finds application in catalysis, adsorption/separation, sensing, optically active materials, molecular sieves and so on. The presence of large pores and the siliceous character of the MCM-41 pore walls created several possibilities for the host-guest system to be modified by bonding organosilanes with desirable structural and functional properties to the MCM-41 surface^{158,159}. Even though these alterations have the potential to significantly reduce pore size, different molecules can still be loaded into the pores. MCM-41's structural features are suitable for the immobilization of enzymes.

The method of immobilization permits the enzyme to maintain its catalytic activity while reducing unfavorable processes like autolysis. Large amounts of enzyme may be immobilised with good enzyme-substrate interaction on the support, which offer a stable physical and chemical environment. These mesoporous materials' larger pore dimensions allow for the potential accommodation of smaller enzymes within the channels, which can reach lengths of several hundred nanometers^{160,161}. This method of immobilising enzymes would address some of the drawbacks of current physical entrapment procedures, including the leaching of adsorbed molecules, the chemical degradation of the anchoring bond of covalently attached enzymes and the obstructions to substrate and product diffusion that are present for large polymeric substrates in sol-gel preparations¹⁶². Contrary to most amorphous materials, which have a substantial pore size distribution, the MCM-41 hexagonal phase are useful for the evaluation of theoretical models of enzyme immobilization that assume a uniform pore size for the model supports.

1.9.4 Biopolymers Chosen for the Work : Cellulose from Water Hyacinth

As environmental awareness grows, eco-friendly and sustainable bio-based products are being researched. Cellulose being easily accessible, non-toxic, biodegradable, biocompatible, hydrophilic and having good mechanical strength is considered to be the potential candidate for the production of bio-based nanofibers¹⁶³. The natural polymer, cellulose is present in all plants, although it is particularly abundant in cotton, linen, wood, bamboo, sugarcane, corncobs, banana plants, aquatic weeds and water hyacinth. The primary potential use of natural cellulose is the creation of biodegradable filters, membranes, adsorbent *etc.*¹⁶⁴ Cellulose contains β -1,4-glucosidic bond which are lignocellulosic fibers formed by lignin, hemicellulose and cellulose¹⁶⁵. Wood and nonwood biomass can be converted into cellulose biomass via physical or chemical extraction procedure which dissolves the intricate lignocellulosic link without destroying the cellulose fibrils¹⁶⁶. Having three -OH groups in each of its D-anhydroglucopyranose units make cellulose an active biopolymer that can be chemically modified. The primary -OH at C-6 and two more ones at C-2 and C-3 may take part in conventional reactions such as oxidation, esterification, and etherification. Despite having features that could make them useful as carriers for fertilizers and soil conditioners, the high expense of making bio-based biomaterials utilising cellulose derivatives prevents them from being widely used.

However, the most prevalent and sustainable biopolymer, cellulose, may be produced from a variety of biomass, including the water hyacinth. WH is one of the natural sources that have high cellulose content (10% lignin, 33% hemicellulose, and 25% cellulose). Hyacinths are widely available and provide a nearly free source of cellulose¹⁶⁷. The lignin content of water hyacinth is less than 10 weight percent¹⁶⁸ compared to 25–35 wt% for wood and agricultural residues. WH is a kind of aquatic weed, grows quickly and forms a thick covering on the entire water surface. Its rapid development has specific negative effects on water bodies, such as obstructing irrigation and hydropower systems, restricting animal access to water and blocking rivers, destroying native aquatic plants in rivers, canals and lakes, altering the water's pH, oxygen level and temperature and lowering sunlight infiltration¹⁶⁹. Controlling the hyacinth's invasion and proliferation has been quite difficult because of its rapid development. Herbicides work well to get rid of this weed, but their effects are

harmful to the environment. Water hyacinth has been used for a variety of things, including compost manure, animal and fish feed, papermaking, crafts (ropes, baskets, chairs and fiber boards), waste water treatment, the creation of biogas and ethanol, and charcoal briquettes. However water hyacinth is a great prospect for cellulose-based natural polymers due to its high cellulose content and ease of chemical conversion into valuable derivative products. Utilization of WH cellulose in the production of electrospun nanofibers for seed coating has not been explored.

1.9.5 Zinc oxide Nanoparticles (ZnO NPs)

Zinc (Zn) is a vital micronutrient for plant development and production, and it is taken in the form of divalent cations. It is required for various metabolic activities in the plants however it is needed in very little amounts in plants. The results show that zinc plays a critical role in the control of reactive oxygen species and in the defense of plant cells against oxidative stress. A deficiency of zinc can have an impact on the quality and yield of the produced crops¹⁷⁰. Zinc also helps in the activation of enzymes such as dehydrogenases, phosphor hydrolases, peptidases, and proteases¹⁷¹. As the pH in soil increases zinc availability is reduced¹⁷² causing zinc deficiency in both soils and plants. Zinc sulphate fertilizer is used as an alternative to alleviate this. Zn can be administered to soils in a variety of ways, such as ZnO, Zn-EDTA and Zn-oxysulfate¹⁷³. Due to their small size and large surface area, zinc oxide nanoparticles are the ideal solution to treat zinc shortage since they are quickly absorbed by plants than conventional ZnO¹⁷⁴. These nanoparticles can be a cheap, sustainable and environment friendly solution to various problems of plants such as zinc deficiency, pathogenic attacks *etc.*

1.9.6 Magnesium oxide Nanoparticles (MgO NPs)

Magnesium (Mg) is a non-toxic mineral that is a necessary component for plants. Magnesium is crucial to the process of photosynthesis and it is the structural element of chlorophyll and polysaccharides. Mg serves as an enzyme activator. Magnesium oxide nanoparticles are structural materials in biological implants due to its high strength to weight ratio, low density, good functionality, recycling activity, nontoxic and hygroscopic nature. MgO NPs have received approval from the US Food and Drug Administration as safe materials (21CFR184.1431). MgO NPs cause

systemic resistance against *R. solanacearum* by triggering the signalling pathways for salicylic acid, jasmonic acid and ethylene in tomato plants¹⁷⁵. These facts demonstrate the potential for MgO NPs to serve as an effective substitute for chemical pesticides in crop protection. MgO nanoparticles boosted plant root exudation and the delivery of carbon skeleton compounds to phosphorus-mobilizing microbes while also increasing energy supply. This strategy would permit the removal of obstacles to the use of local P and lessen reliance on imported P fertilizers¹⁷⁶.

1.9.7 Nanohydroxyapatite(nHAP) : The Nanofertilizer

Global phosphorous (P) reserves are being quickly drained, and based on current assessments, probably won't be any soil P resource left by the year 2050¹⁷⁷. In order to produce a high yield in agriculture, phosphorous (P) fertilizer must be used in sufficient quantities in agriculture fields to address nutritional deficiency. The development of smart solutions is required to address the increasing P demand on a worldwide scale in a sustainable manner. In order to avoid run-off problems, less soluble forms of P- fertilizers, such as those generated from synthetic apatite forms, $\text{Ca}_5(\text{PO}_4)_3\text{X}$, (X=F, Cl, Br, or OH), have been tried¹⁷⁸. The main disadvantage of such solid forms of P fertilizer is that decrease in uptake by plants. Although naturally occurring rock-phosphate has been utilised as a phosphorus fertilizer in the past, it has a low solubility. It is possible to increase the solubility of P by using nanoformulation. Hydroxyapatite (HAP) has also been suggested as a good source of P-fertilizer. Due to the importance of hydroxyapatite $[(\text{Ca}_{10}(\text{PO}_4)_6(\text{OH})_2)]$ nanoparticles (HA NPs) and their hybrids in material science, biology, and medicine, substantial research has been done on these materials. The majority of the literature on HA NPs is on its usage in biological applications^{179,180} whereas little research has been done on their potential uses in agriculture¹⁸¹. The structure of HAP is shown in Fig.I.13. Nanohydroxyapatite (nHAP), a nanoformulation of HAP, has previously been identified as a good fertilizer at the lab scale¹⁸². Crop plants have been reported to receive sufficient P nutrients via nHAP. nHAP has a lower mobility to adjacent agricultural and aqua-cultural areas than soluble phosphate salts and solid phosphates. Hence it has a significant potential to improve agronomical production and reduce the risk of water eutrophication.

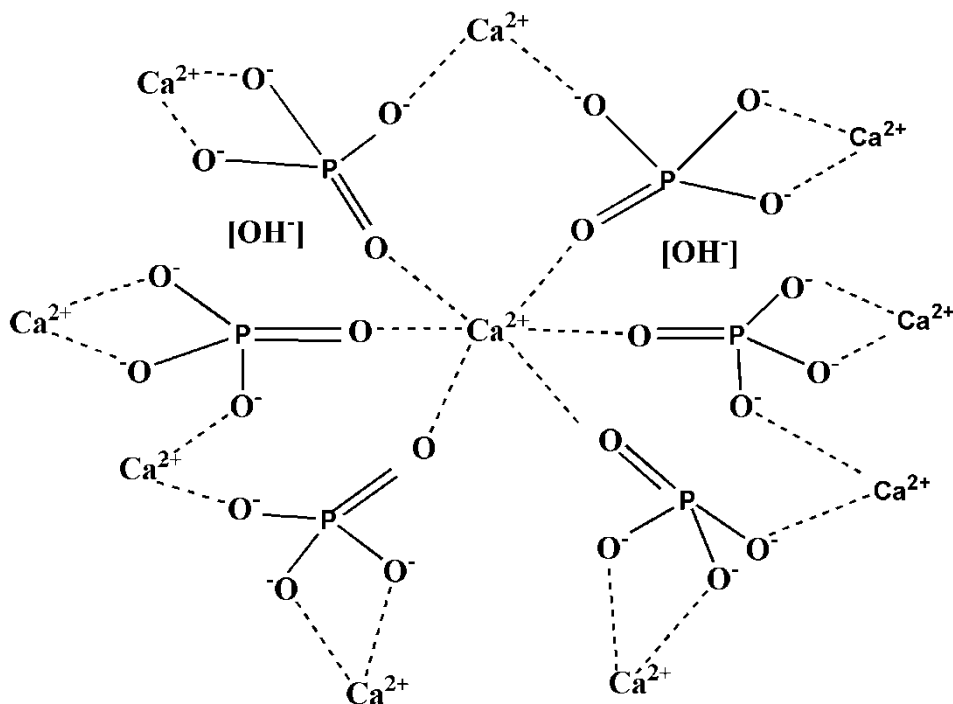


Fig. I.13 Structure of nanohydroxyapatite

The reactive surface functional groups on the HA NPs present a variety of opportunities for surface modification through the immobilization of strategic chemicals for the development of nanohybrids with multifunctional capabilities. The present investigation is focused at improving phosphorous utilization for maximum crop yield in the form of nHAP.

1.9.8 Carbon Dots (CDs)

As a new member of the nanocarbon family, carbon dots have emerged as a key player in the scientific world attributed to their amazing uses and features. These primarily have sp^3 -bonded carbon backbones that are less than 10 nm^{183,184}. Carbon dots (CDs) are zero-dimensional nanoparticles that are nearly spherical in shape. CDs have distinct benefits over inorganic, metallic and oxide-based nanomaterials, including optical stability, small size, biocompatibility, water solubility, low cost and outstanding luminescence performance¹⁸⁵. These characteristics make them ideal for applications such as bio-imaging, biosensors, drug administration and photocatalysis^{186,187}. A nano CD combines the properties of the nano effect, surface functional groups and carbon components. It has a variety of uses and applications and demonstrates three fundamental functions of optics, chemistry and biology^{188,189}.

The two basic methods used to synthesise carbon quantum dots (CQDs) are top-down and bottom-up. The bottom-up method creates CQDs from molecular precursors through microwave synthesis, thermal decomposition and hydrothermal treatment, whereas the top-down method refers to the breakdown of larger carbon particles by laser ablation, electrochemical oxidation, chemical oxidation and ultrasonic synthesis¹⁹⁰. Hydrothermal carbonization (HTC) has been regarded as the most promising synthesis technique due to its high quantum efficiency, low cost, non-toxicity and ecologically benign nature^{191,192}. CDs have been used in agriculture, particularly in the field of crops. CDs produce blue or red light that plants require, allowing them to be used as supplemental lights or sprayed on leaves to increase crop development and output¹⁹³. As a result of their small size and hydrophilic surface groups that can penetrate the plant cell wall, CDs can help in seed germination and absorb nutrients to support growth. It has the potential to function as a nano-carbon fertilizer due to the high carbon content (>60%). CDs demonstrate considerable advantages in improving photosynthesis, promoting crop development and reducing stress. The effect of CDs' on crops at various stages of their life cycle is investigated. In a study of CDs' impacts on the complete rice growth cycle, it was reported that CDs encouraged plant growth by encouraging seed germination, root growth and carbohydrate accumulation¹⁹⁴. Eventually CDs broke down into carbon dioxide and analogues of plant hormones that stimulated plant growth (which was converted to carbohydrates through the Calvin cycle). Crop stress resistance is greatly enhanced by CDs' antioxidant capabilities. Using crop waste to make CDs has advantages in terms of raw material costs and environmental advantages, which is beneficial for the long-term sustainability of agriculture. Recent reviews have examined the conception, synthesis, properties and applications of multifunctional CDs made from biomass waste¹⁹⁵. The pre-harvest phase (seed germination, nano-fertilizer, plant growth regulator, targeted delivery of fertilizers, pesticides and biomolecules, photosynthesis and stress tolerance) and post-harvest process are the two key aspects of the involvement of CDs in the entire crop life cycle (anti-bacterial preservation of harvested fruits, intelligent anti-counterfeit packaging). Crop wastes, which are good biomass materials that can be used to make CDs and re-enter the crop life cycle, create a closed loop¹⁹⁶. Here, waste water hyacinth leaves are used as a precursor for

carbon dots. It is a waste bio-material occurring naturally hence prepared CDs are cheap and biocompatible.

1.9.9 Biofungicide Employed in the Study: *Trichoderma Viride*

Currently, large-scale disease control techniques are implemented using agrochemicals such as chemical fungicides. These are costly, raise the danger of environmental pollution, human and animal health¹⁹⁷. Due to the natural decomposition of chemicals, the fungicide's effectiveness does not last very long after the seedling stage¹⁹⁸. An alternative strategy is to use natural antagonists that can inhibit the pathogenic and mycotoxigenic capabilities of naturally occurring pathogenic populations rather than working on their saprophytic phase or that can activate the host plant's built-in defense mechanisms¹⁹⁹. *Trichoderma* spp. have been thoroughly investigated as biocontrol agents since they suppress the growth of pathogens through a variety of mechanisms including the production of antibiotics, mycoparasitism, the production of cell wall degrading enzymes and competition for nutrients or space^{200,201}.

In addition, they are known to cause broad range systemic resistance responses in leaves, plant defense responses, growth hormone production, antibiosis chemical production and cell wall disintegrating enzyme production¹⁹⁸. *Trichoderma* species have attracted significant economic and industrial attention, leading to the development of regulated and marketed products for agricultural application²⁰². As an essential part of agricultural practise in the seed-plant-soil system that can replace chemical seed treatments, seed coating is employed with *Trichoderma viride*, a beneficial microbe. *T.viride* spores are capable of colonising the rhizosphere at the crucial "early germination" stage, which promotes early, healthy and rapid development while enhancing nutrient intake and stress tolerance²⁰³. Encapsulation is a cutting-edge technique that allows the loading of solids, liquids or gases into a carrier matrix protecting biocontrol agents from the environment, enhancing their viability and enabling controlled release at the appropriate time and location. Immobilization of the biocontrol agent in a suitable polymer carrier is one way to improve its efficiency. Degradable polymers are particularly well suited to the production of effective and environmentally friendly phytopharmaceuticals.

1.9.10 Biocatalyst for Seed Germination : α - amylase

α -Amylase (α -1,4-glucan-4-glucanohydrolases) is an enzyme that speeds up the breakdown of carbohydrates. In plants, amylase is responsible for decomposition of starch. Usually, during seed germination, starches are converted into sugars in this manner. The plant then uses these sugars as its primary source of energy during its early development. The production of sugars by plants allow them to store solar energy. Before a plant can utilise energy from photosynthesis, amylase aids in its early development. As the plant's seed starts to sprout and grow, the amylase enzymes start to play a part in the growth of the plant.

A cluster of hydrolases known as amylases can break the O-glycosidic bond in starch²⁰⁴. The second-largest category of enzymes utilised globally is the amylase family. According to their functions and properties, glucoamylase, α -amylase and β -amylase are the three major categories of amylases. α -amylases are used in a variety of industrial processes, from food preparation to pharmaceutical and drug development. They are frequently employed in starch saccharification processes in biotechnology-related industries, including the textile industry, food and animal feed, detergents, fermented drinks and distilleries. They could also be used in the bakery, pharmaceutical and refined chemical sectors²⁰⁵. Glucose, maltose and dextrin are produced as a result of the hydrolysis of starch by α - and β -amylases. In industrial applications, α -amylases are regarded as economically significant enzymes for the catalytic hydrolysis of a-1,4-glycosidic bonds in starch. This enzyme starts the mobilization of starch in seed germination. In a study involving the relative significance of amylase in determining germination ability, showed that amylase is more significant in the early stages of germination in some plants²⁰⁶.

Numerous studies have examined the significance of α -amylase function in seed germination under various environmental stresses, including heat stress, drought stress and others^{207,208}. The amylase in the seed becomes more active as the ground warms. High temperature will often cause the enzymes to stop working. Amylase in plants serves as a food storage reserve as the plant matures. Immobilization of amylase in the nanofibrous membrane would provide thermal stability to amylase to aid in seed germination under drought stress and varying pH conditions of soil.

1.9.11 Plant Growth Hormone: Gibberellic Acid (GA)

Gibberellic acid (GA), a crucial hormone for plants, regulates their growth and development. It is frequently utilised in horticulture, gardening, agriculture and other fields. Auxins, cytokinins, gibberellins and other growth regulators have been used successfully to break seed dormancy²⁰⁹. Gibberellins regulate several phases of plant growth, including seed germination, seedling development, stem elongation, root development, leaf area and shape, flower and fruit development and pollination²¹⁰. In order to break seed dormancy and manage the hydrolysis of reserves, GA is required. The presence of sufficient levels of this acid in the seeds stimulates the synthesis, activation and secretion of hydrolytic enzymes, primarily α -amylase, releasing reducing sugars and aminoacids that are crucial for embryo growth. Water received during the first stage of seed germination activates enzymes²¹¹. Exogenous supply of gibberellic acid in controlled manner helps to solve the issues related to different environmental conditions and also helps in the α - amylase activity.

1.10 Seeds Used in Coating Studies: Corn (*Zea mays*) Seeds

Corn (*Zea mays*), often known as maize or field corn is an edible grain produced by a cereal plant in the Poaceae (grass) family. The yearly global production demand of corn exceeds that of wheat and rice. About 42% of the world's total grain production was made up of corn. The staple grain crop maize is grown all over the world in a variety of soil types and climatic regions. Stresses as salinity, dryness and temperature can make maize relatively sensitive²¹². It has the largest genetic yield potential of all the cereals, maize is referred to as the "queen of cereals" internationally. It is grown on a diverse range of soil types, climates, diversity and management techniques, contributing 36% to the world's grain supply. Thousands of industrial products, including those in the starch, oil, protein, alcoholic beverages, food sweeteners, pharmaceutical, cosmetic, film, textile, gum, package and paper industries, among others, use maize as a basic raw material. However, soils with high water holding capacity, neutral pH and good organic matter content are thought to be good for increased productivity. It is preferable to stay away from low-lying fields with poor drainage and fields with higher salinity since this crop is vulnerable to moisture stress, especially excess soil moisture and salinity strains. Therefore, the

fields with adequate drainage should be chosen for maize growing. Corn seedlings and stands can become infected by soil borne and seed borne diseases, which reduces seedling vigour and stands. The fungi *Fusarium moniliforme*, *Penicillium oxalicum*, and many species of *Rhizopus* are examples of seedborne diseases. *Pythium ultimum*, *Rhizoctonia solani* and a number of *Fusarium* species are examples of soilborne pathogens. Pre- or post-emergence damping off is frequently the outcome of these diseases' infection. Cool, moist conditions that hinder seed germination and seedling growth increase damping-off. Early season problems with corn establishment are caused by a variety of additional causes as well. It can also be brought by insect damage, nutritional imbalances, herbicide damage, soil conditions and environmental factors, particularly saturated soil conditions and oxygen deprivation. Wet soils, low lying fields and soils that are wet for a long time all contribute to the severity of corn seedling blights. The planting depth, soil type, seed quality, mechanical damage to the seed, soil crusting, herbicide damage or other factors that delay corn germination and emergence can also have an impact on disease severity. Almost all field corn seeds are treated with a fungicide before planting. Keeping all these constraints in corn seed germination and farming, herein, this research is focused on corn seed coating using nanofibrous membranes and porous polymer films with an aim to avoid the hazards of chemical seed treatments. This also provide a better seedling vigour and germination parameters under different climatic condition.

1.11 Objectives of the Present Research Work

The main objectives of the present study can be briefed as follows;

1. To fabricate and assess the efficiency of seed coating system as a delivery strategy for controlled release of agrichemicals and microbial formulations and its impact on agricultural crops
2. To synthesize ZnO NPs, nHAP, MgO NPs, MCM-41. Carbon dots and cellulose are synthesized from water hyacinth. Characterization method include FTIR, UV, TG, XRD, SEM, EDX, TEM and PL
3. To develop PCL electrospun nanofibers incorporated with nHAP and ZnO NPs and recognise the suitable morphology
4. To improve the applicability of PCL nanofibers for controlled release by blending it with PEO which increases wettability and release behaviour

5. To fabricate nHAP, ZnO NPs and *Trichoderma viride* incorporated PCL-PEO blended nanofibers and analogous porous polymer film
6. To synthesize and characterise covalently grafted α -amylase on MCM-41 and further incorporation of MCM-41 immobilized α -amylase in PCL nanofibers
7. To extract cellulose from water hyacinth and further fabrication of nanofibers from cellulose and PEO to replace PCL
8. To develop Cellulose/PEO electrospun nanofibers loaded with carbon dots as biomarker nanofertilizer
9. To develop Cellulose/PEO electrospun nanofibers loaded with nontoxic nHAP in presence and absence of carbon dots
10. To characterise the developed nanofibers and films by XRD, FTIR, TGA, SEM, TEM, EDX, EDX mapping and Static Water Contact Angle
11. To analyse the behaviour of the fiber, film, respective fiber and film coated corn seeds in aqueous solution, the variation of pH, conductivity, swelling and stability and imbibition rate
12. To understand the nutrient release behaviour through ICP-OES analysis
13. To test the antagonistic activity of loaded beneficial biofungicide, *Trichoderma viride* spores against *Aspergillus* fungal pathogen and to prove the ability of developed seed coating approach in pathogen infested soil conditions to increase production yields
14. To quantify and compare the enzymatic activity, thermal stability, reusability, optimum pH conditions and storage stability of α -amylase directly incorporated in PCL nanofiber with PCL incorporated with α -amylase covalently grafted on MCM-41
15. To compare the nanofiber coated and porous polymer film coated corn seeds with uncoated seeds with respect to germination potential and fresh biomass of seedling
16. To investigate the antioxidant nature of nanofibers against crop oxidative stress tolerance

References

1. Zhang, X., Davidson, E. A., Mauzerall, D. L., Searchinger, T. D., Dumas, P., & Shen, Y. (2015). Managing nitrogen for sustainable development. *Nature*, 528(7580), 51-59.
2. Foley, J., Ramankutty, N., Brauman, K. *et al.* (2011). Solutions for a cultivated planet. *Nature* 478, 337–342
3. Swaminathan, M. S., & Kesavan, P. C. (2017). The transition from green to evergreen revolution. In *Sustainable Development of Organic Agriculture*, 91-100. Apple Academic Press.
4. FAO. (2019). New standards to curb the global spread of plant pests and diseases. *Web page of the Food and Agriculture Organization of the United Nations*
5. FAOSTAT. <http://www.fao.org/faostat/en/#data/RP/visualize> (accessed January 13, 2020). Graphs and corresponding data are presented to visualize global pesticides use from 1990-2020. Data has been collected through the auspices of the Food and Agriculture Organization of the United Nations
6. Jeremić, V., & Sachs, J. D. (2014). The United Nations in the age of sustainable development. *The Economic and social review*, 45(2, Summer), 161-188.
7. Kumaraswamy, R. V., Kumari, S., Choudhary, R. C., Pal, A., Raliya, R., Biswas, P., & Saharan, V. (2018). Engineered chitosan based nanomaterials: Bioactivities, mechanisms and perspectives in plant protection and growth. *International journal of biological macromolecules*, 113, 494-506.
8. Boverhof, D. R., Bramante, C. M., Butala, J. H., Clancy, S. F., Lafranconi, M., West, J., & Gordon, S. C. (2015). Comparative assessment of nanomaterial definitions and safety evaluation considerations. *Regulatory Toxicology and Pharmacology*, 73(1), 137-150.
9. Liu, R., & Lal, R. (2015). Potentials of engineered nanoparticles as fertilizers for increasing agronomic productions. *Science of the total environment*, 514, 131-139.
10. Manjunatha, S. B., Biradar, D. P., & Aladakatti, Y. R. (2016). Nanotechnology and its applications in agriculture: A review. *J farm Sci*, 29(1), 1-13.
11. Ion, A. C., Ion, I., and Culetu, A. (2010). Carbon-based nanomaterials: Environmental applications. *Univ. Politehn. Bucharest*, 38, 129–132
12. Sabir, S., Arshad, M., & Chaudhari, S. K. (2014). Zinc oxide nanoparticles for revolutionizing agriculture: synthesis and applications. *The Scientific World Journal*.
13. Floros, J. D., Newsome, R., Fisher, W., Barbosa-Cánovas, G. V., Chen, H., Dunne, C. P., & Ziegler, G. R. (2010). Feeding the world today and tomorrow: the importance of food

- science and technology: an IFT scientific review. *Comprehensive Reviews in Food Science and Food Safety*, 9(5), 572-599.
14. Dixit, R., Malaviya, D., Pandiyan, K., Singh, U. B., Sahu, A., Shukla, R., & Paul, D. (2015). Bioremediation of heavy metals from soil and aquatic environment: an overview of principles and criteria of fundamental processes. *Sustainability*, 7(2), 2189-2212.
 15. Fraceto, L. F., Grillo, R., & Gerson, A. de Medeiros, Viviana Scognamiglio, Giuseppina Rea, and Cecilia Bartolucci. (2016) "Nanotechnology in agriculture: Which innovation potential does it have?" *Frontiers in Environmental Science*, 4 (March). *Frontiers in Environmental Science*, 4.
 16. Sertova, N. M. (2015). Application of nanotechnology in detection of mycotoxins and in agricultural sector. *J Cent Eur Agric* 16: 117–130.
 17. Viswanathan, S., and Radecki, J. (2008). Nanomaterials in electrochemical biosensors for food analysis- a review. *Pol. J. Food Nutr. Sci.* 58, 157–164.
 18. Kandasamy, S., & Prema, R. S. (2015). Methods of synthesis of nano particles and its applications. *J Chem Pharm Res*, 7(3), 278-285.
 19. DeRosa, M. C., Monreal, C., Schnitzer, M., Walsh, R., & Sultan, Y. (2010). Nanotechnology in fertilizers. *Nature nanotechnology*, 5(2), 91-91.
 20. Bhalla, D., & Mukhopadhyay, S. S. (2010). Eutrophication: Can nanophosphorous control this menace?-A preview. *J Crop Weed*, 6, 13-16.
 21. Mukhopadhyay, S. S., & Sharma, S. (2013). Nanoscience and nanotechnology: cracking prodigal farming. *Journal of Bionanoscience*, 7(5), 497-502.
 22. Kottegoda, N., Munaweera, I., Madusanka, N., & Karunaratne, V. (2011). A green slow-release fertilizer composition based on urea-modified hydroxyapatite nanoparticles encapsulated wood. *Current science*, 73-78.
 23. Zheng, L., Hong, F., Lu, S., & Liu, C. (2005). Effect of nano-TiO₂ on strength of naturally aged seeds and growth of spinach. *Biological trace element research*, 104, 83-91.
 24. Shah, V., & Belozeroval, I. (2009). Influence of metal nanoparticles on the soil microbial community and germination of lettuce seeds. *Water, air, and soil pollution*, 197, 143-148.
 25. Nel, A, Xia, T, Madler, L & Li, N (2006). Toxic potential of materials at the nanolevel, *Science*, 311, 5761, 622-627.

-
26. Mahajan, P., Dhoke, S.K. & Khanna, A.S. (2011). Effect of nano-ZnO particle suspension on growth of mung (*Vigna radiata*) and gram (*Cicer arietinum*) seedlings using plant agar method, *Journal of Nanotechnology*, 2011, 1-7
 27. Almutairi, Z.M., & Alharbi, A. (2015), Effect of silver nanoparticles on seed germination of crop plants, *Journal of Advances in Agriculture*, 4, 1, 283-288.
 28. Sadeghzadeh, B. (2013). A review of zinc nutrition and plant breeding. *Journal of soil science and plant nutrition*, 13(4), 905-927.
 29. Zubarev, E. R. (2013). Any way you want it. *Nature nanotechnology*, 8(6), 396-397.
 30. Khot, L. R., Sankaran, S., Maja, J. M., Ehsani, R., & Schuster, E. W. (2012). Applications of nanomaterials in agricultural production and crop protection: a review. *Crop protection*, 35, 64-70.
 31. Bhattacharyya, A., Duraisamy, P., Govindarajan, M., Buhroo, A. A., & Prasad, R. (2016). Nano-biofungicides: emerging trend in insect pest control. *Advances and applications through fungal nanobiotechnology*, 307-319.
 32. Nuruzzaman, M. D., Rahman, M. M., Liu, Y., & Naidu, R. (2016). Nanoencapsulation, nano-guard for pesticides: a new window for safe application. *Journal of agricultural and food chemistry*, 64(7), 1447-1483.
 33. Goin, S. (2004). Microencapsulation: industrial appraisal of existing technologies. *Food Sci. Technol.*, 15, 330-347.
 34. Behera, M., & Ram, S. (2013). Spectroscopy-based study on the interaction between gold nanoparticle and poly (vinylpyrrolidone) molecules in a non-hydrocolloid. *International Nano Letters*, 3, 1-7.
 35. Schwinn, F. J. (1994). Seed treatment-a panacea for plant protection?
 36. Tyagi, V. (2012). India's agriculture: challenges for growth & development in present scenario. *International Journal of Physical and social sciences*, 2(5), 116-128.
 37. Graph I. M. Phillips McDougall, (2019) Analysis on sales and profitability within the seed sector: Independent report by IHS Markit (Phillips McDougall) for the co-chairs of the adhoc open-ended working group to enhance the functioning of the multilateral system of FAO'S International Treaty on Plant Genetic Resources for Food and Agriculture
 38. Reddy, P. P. (2012). Recent advances in crop protection.
 39. Abdalla, E. A., Osman, A. K., Maki, M. A., Nur, F. M., Ali, S. B., & Aune, J. B. (2015). The response of sorghum, groundnut, sesame, and cowpea to seed priming and fertilizer micro-dosing in South Kordofan State, Sudan. *Agronomy*, 5(4), 476-490.

-
40. Singh, A., Dahiru, R., Musa, M., & Sani Haliru, B. (2014). Effect of Osmopriming duration on germination, emergence, and early growth of Cowpea (*Vigna unguiculata* (L.) Walp.) in the Sudan Savanna of Nigeria. *International Journal of Agronomy*.
 41. Eskandari, H., & Kazemi, K. (2011). Effect of seed priming on germination properties and seedling establishment of cowpea (*Vigna sinensis*). *Notulae Scientia Biologicae*, 3(4), 113-116.
 42. ASF (2010). National code of practice for the use of seed treatments. Australian Seed Federation Limited, pp.1-7. Retrieved: September 4, 2014 from <http://www.asf.asn.au/userfiles>
 43. Forsberg, G., Kristensen, L., Eibel, P., Titone, P., & Hartl, W. (2003). Sensitivity of cereal seeds to short duration treatment with hot, humid air/Empfindlichkeit von Getreidesaatgut gegen kurzzeitige Behandlung mit heißer, feuchter Luft. *Zeitschrift für Pflanzenkrankheiten und Pflanzenschutz/Journal of Plant Diseases and Protection*, 1-16.
 44. DPPQS (Department of Plant Protection Quarantine and Storage) (2007). Campaign for Seed Treatment: Campaign for 100% Seed Treatment during Rabi, 2007. Retrieved: August 31, 2014 from <http://ppqs.gov.in/Seedtreatment.html>
 45. Rocha, I., Ma, Y., Souza-Alonso, P., Vosátka, M., Freitas, H., & Oliveira, R. S. (2019). Seed coating: a tool for delivering beneficial microbes to agricultural crops. *Frontiers in Plant Science*, 10, 1357.
 46. Martinez, A. (Ed.). (2004). Challenges and Opportunities for Organic Agriculture and the Seed Industry.
 47. Pedrini, S., Merritt, D. J., Stevens, J., & Dixon, K. (2017). Seed coating: science or marketing spin? *Trends in plant science*, 22(2), 106-116.
 48. CropLife Foundation, (2013) The Role of Seed Treatment in Modern U.S. Crop Production.
 49. Almeida, C. D., Rocha, S. C. D. S., & Razera, L. F. (2005). Polymer coating, germination and vigor of broccoli seeds. *Scientia Agricola*, 62, 221-226.
 50. Tonapi, V. A., Babu, P. H., Ansari, N. A., Varanavasiappan, S., Ravinder Reddy, C., Navi, S. S., & Seetharama, N. (2006). Studies on seed coloring in soybean and tomato. *International Journal of Agriculture Sciences*, 2(1), 219-224.
 51. Grellier, P., Riviere, L. M., & Renault, P. (1999). Transfer and water-retention properties of seed-pelleting materials. *European Journal of Agronomy*, 10(1), 57-65.

-
52. Adak, T., Kumar, J., Shakil, N. A., & Pandey, S. (2016). Role of nano-range amphiphilic polymers in seed quality enhancement of soybean and imidacloprid retention capacity on seed coatings. *Journal of the Science of Food and Agriculture*, 96(13), 4351-4357.
 53. Taylor, A. G. (2020). Seed storage, germination, quality, and enhancements. In *The physiology of vegetable crops*, 1-30, Wallingford UK: CABI.
 54. Farias, B. V., Pirzada, T., Mathew, R., Sit, T. L., Opperman, C., & Khan, S. A. (2019). Electrospun polymer nanofibers as seed coatings for crop protection. *ACS Sustainable Chemistry & Engineering*, 7(24), 19848-19856.
 55. Hartley, E., Gemell, L. G., & Herridge, D. F. (2004). Lime pelleting inoculated serradella (*Ornithopus* spp.) increases nodulation and yield. *Soil Biology and Biochemistry*, 36(8), 1289-1294.
 56. Khanna, R., Nath, A., Pal, K., & Ojha, P. K. (2022). A Review on Seed Pelleting in Increasing the Production Potential of Pulses.
 57. Ren, X. X., Chen, C., Ye, Z. H., Su, X. Y., Xiao, J. J., Liao, M., & Cao, H. Q. (2019). Development and application of seed coating agent for the control of major soil-borne diseases infecting wheat. *Agronomy*, 9(8), 413.
 58. Girardi, N. S., Passone, M. A., García, D., Nesci, A., & Etcheverry, M. (2018). Microencapsulation of *Peumus boldus* essential oil and its impact on peanut seed quality preservation. *Industrial Crops and Products*, 114, 108-114.
 59. Ziani, K., Ursúa, B., & Maté, J. I. (2010). Application of bioactive coatings based on chitosan for artichoke seed protection. *Crop Protection*, 29(8), 853-859.
 60. Vercelheze, A. E. S., Marim, B. M., Oliveira, A. L., & Mali, S. (2019). Development of biodegradable coatings for maize seeds and their application for *Azospirillum brasilense* immobilization. *Applied microbiology and biotechnology*, 103, 2193-2203.
 61. Amirkhani, M., Netravali, A. N., Huang, W., & Taylor, A. G. (2016). Investigation of soy protein-based biostimulant seed coating for broccoli seedling and plant growth enhancement. *HortScience*, 51(9), 1121-1126.
 62. Berninger, T., Mitter, B., & Preininger, C. (2016). The smaller, the better? The size effect of alginate beads carrying plant growth-promoting bacteria for seed coating. *Journal of microencapsulation*, 33(2), 127-136.
 63. Campos, E. V. R., de Oliveira, J. L., Fraceto, L. F., & Singh, B. (2015). Polysaccharides as safer release systems for agrochemicals. *Agronomy for sustainable development*, 35, 47-66.

-
64. Accinelli, C., Abbas, H. K., Shier, W. T., Vicari, A., Little, N. S., Aloise, M. R., & Giacomini, S. (2019). Degradation of microplastic seed film-coating fragments in soil. *Chemosphere*, 226, 645-650.
 65. Iles, A., & Martin, A. N. (2013). Expanding bioplastics production: sustainable business innovation in the chemical industry. *Journal of Cleaner Production*, 45, 38-49.
 66. Malinconico, M. (Ed.). (2017). *Soil degradable bioplastics for a sustainable modern agriculture*. Springer.
 67. Rosseto, M., Rigueto, C. V., Krein, D. D., Balbé, N. P., Massuda, L. A., & Dettmer, A. (2019). Biodegradable polymers: opportunities and challenges. *Organic Polymers*, 110-119.
 68. Brodin, M., Vallejos, M., Opedal, M. T., Area, M. C., & Chinga-Carrasco, G. (2017). Lignocellulosics as sustainable resources for production of bioplastics—A review. *Journal of Cleaner Production*, 162, 646-664.
 69. Krishnamoorthy, V., & Rajiv, S. (2018). Tailoring electrospun polymer blend carriers for nutrient delivery in seed coating for sustainable agriculture. *Journal of Cleaner Production*, 177, 69-78.
 70. Lowry, G. V., Avellan, A., & Gilbertson, L. M. (2019). Opportunities and challenges for nanotechnology in the agri-tech revolution. *Nature nanotechnology*, 14(6), 517-522.
 71. Kah, M., Tufenkji, N., & White, J. C. (2019). Nano-enabled strategies to enhance crop nutrition and protection. *Nature nanotechnology*, 14(6), 532-540.
 72. Achari, G. A., & Kowshik, M. (2018). Recent developments on nanotechnology in agriculture: plant mineral nutrition, health, and interactions with soil microflora. *Journal of agricultural and food chemistry*, 66(33), 8647-8661.
 73. Camara, M. C., Campos, E. V. R., Monteiro, R. A., do Espirito Santo Pereira, A., de Freitas Proença, P. L., & Fraceto, L. F. (2019). Development of stimuli-responsive nano-based pesticides: emerging opportunities for agriculture. *Journal of nanobiotechnology*, 17(1), 1-19.
 74. Greiner, A., & Wendorff, J. H. (2007). Electrospinning: a fascinating method for the preparation of ultrathin fibers. *Angewandte Chemie International Edition*, 46(30), 5670-5703.
 75. Hoseyni, S. Z., Jafari, S. M., Tabarestani, H. S., Ghorbani, M., Assadpour, E., & Sabaghi, M. (2020). Production and characterization of catechin-loaded electrospun nanofibers from Azivash gum-polyvinyl alcohol. *Carbohydrate polymers*, 235, 115979.

-
76. MacDiarmid, A. G., Jones Jr, W. E., Norris, I. D., Gao, J., Johnson Jr, A. T., Pinto, N. J., & Llaguno, M. (2001). Electrostatically-generated nanofibers of electronic polymers. *Synthetic metals*, 119(1-3), 27-30.
 77. Formhals, A (1934), Process and apparatus for preparing artificial threads, US patent 1975504.
 78. Taylor, G. I. (1969). Electrically driven jets. *Proceedings of the Royal Society of London. A. Mathematical and Physical Sciences*, 313(1515), 453-475.
 79. Riazi, K., Kübel, J., Abbasi, M., Bachtin, K., Indris, S., Ehrenberg, H., & Wilhelm, M. (2016). Polystyrene comb architectures as model systems for the optimized solution electrospinning of branched polymers. *Polymer*, 104, 240-250.
 80. Zhang, C. L., & Yu, S. H. (2014). Nanoparticles meet electrospinning: recent advances and future prospects. *Chemical Society Reviews*, 43(13), 4423-4448.
 81. Greiner, A., & Wendorff, J. H. (2007). Electrospinning: a fascinating method for the preparation of ultrathin fibers. *Angewandte Chemie International Edition*, 46(30), 5670-5703.
 82. Tarus, B., Fadel, N., Al-Oufy, A., & El-Messiry, M. (2016). Effect of polymer concentration on the morphology and mechanical characteristics of electrospun cellulose acetate and poly (vinyl chloride) nanofiber mats. *Alexandria Engineering Journal*, 55(3), 2975-2984.
 83. Doshi, J., & Reneker, D. H. (1995). Electrospinning process and applications of electrospun fibers. *Journal of electrostatics*, 35(2-3), 151-160.
 84. Hasan, M., Yousuf, A., Azim, A. Y. M., & Shamim, M. (2014). Effect of Electrospinning Parameters on Fiber Morphology of Tissue Engineering Scaffolds: A Review. *Journal of Fashion Technology & Textile Engineering*, 2.
 85. Koski, A., Yim, K., & Shivkumar, S. J. M. L. (2004). Effect of molecular weight on fibrous PVA produced by electrospinning. *Materials Letters*, 58(3-4), 493-497.
 86. Haider, A. (2015). S. Haider. IK Kang, A comprehensive review summarizing the effect of electrospinning parameters and potential applications of nanofibers in biomedical and biotechnology. *Arabian J. Chem.* 12,1878-5352.
 87. Luo, C. J., Stride, E., & Edirisinghe, M. (2012). Mapping the influence of solubility and dielectric constant on electrospinning polycaprolactone solutions. *Macromolecules*, 45(11), 4669-4680.
 88. Pervin, R., Ghosh, P., & Basavaraj, M. G. (2019). Tailoring pore distribution in polymer films via evaporation induced phase separation. *RSC advances*, 9(27), 15593-15605.

-
89. So, M. T., Eirich, F. R., Strathmann, H., & Baker, R. W. (1973). Preparation of asymmetric loeb-sourirajan membranes. *Journal of Polymer Science: Polymer Letters Edition*, 11(3), 201-205.
 90. Zhao, J., Luo, G., Wu, J., & Xia, H. (2013). Preparation of microporous silicone rubber membrane with tunable pore size via solvent evaporation-induced phase separation. *ACS applied materials & interfaces*, 5(6), 2040-2046.
 91. Babitha, S., Rachita, L., Karthikeyan, K., Shoba, E., Janani, I., Poornima, B., & Sai, K. P. (2017). Electrospun protein nanofibers in healthcare: A review. *International journal of pharmaceutics*, 523(1), 52-90.
 92. Stojanov, S., & Berlec, A. (2020). Electrospun nanofibers as carriers of microorganisms stem cells, proteins, and nucleic acids in therapeutic and other applications. *Frontiers in bioengineering and biotechnology*, 8, 130.
 93. Zander, N. E., Gillan, M., & Sweetser, D. (2016). Recycled PET nanofibers for water filtration applications. *Materials*, 9(4), 247.
 94. Mercante, L. A., Scagion, V. P., Migliorini, F. L., Mattoso, L. H., & Correa, D. S. (2017). Electrospinning-based (bio) sensors for food and agricultural applications: A review. *TrAC Trends in Analytical Chemistry*, 91, 91-103.
 95. Macagnano, A., Zampetti, E., & Kny, E. (Eds.). (2015). *Electrospinning for high performance sensors* (Vol. 1). Cham, Switzerland: Springer International Publishing.
 96. Abbas, J. A., Said, I. A., Mohamed, M. A., Yasin, S. A., Ali, Z. A., & Ahmed, I. H. (2018). Electrospinning of polyethylene terephthalate (PET) nanofibers: Optimization study using taguchi design of experiment. In *IOP conference series: materials science and engineering*, 454, 1, 012130. IOP Publishing.
 97. Khude, P. (2017). Nanofibers for high efficiency filtration. *J. Mater. Sci. Eng*, 6(6), 1-10.
 98. Tarrés, Q., Oliver-Ortega, H., Boufi, S., Pèlach, M. À., Delgado-Aguilar, M., & Mutje P. (2020). Evaluation of the fibrillation method on lignocellulosic nanofibers production from eucalyptus sawdust: A comparative study between high-pressure homogenization and grinding. *International journal of biological macromolecules*, 145, 1199-1207.
 99. Suzuki, A., Mikuni, T., & Hasegawa, T. (2014). Nylon 66 nanofibers prepared by CO₂ laser supersonic drawing. *Journal of Applied Polymer Science*, 131(6).
 100. Suzuki, A., & Hayashi, H. (2013). Ethylene tetrafluoroethylene nanofibers prepared by CO₂ laser supersonic drawing. *eXPRESS Polymer Letters*, 7(6).

-
101. Asmatulu, R., & Khan, W. S. (2019). Electrospun nanofibers for agriculture and food industries. *Synthesis and Applications of Electrospun Nanofibers. Synth. Appl. Electrospun Nanofibers*, 89-109.
 102. Krishnamoorthy, V., Elumalai, G., & Rajiv, S. (2016). Environment friendly synthesis of polyvinylpyrrolidone nanofibers and their potential use as seed coats. *New Journal of Chemistry*, 40(4), 3268-3276.
 103. Espinoza Márquez, E., Soto Zarazúa, G. M., & Pérez Bueno, J. D. J. (2020). Prospects for the use of electrooxidation and electrocoagulation techniques for membrane filtration of irrigation water. *Environmental Processes*, 7, 391-420.
 104. Meraz-Dávila, S., Pérez-García, C. E., & Feregrino-Perez, A. A. (2021). Challenges and advantages of electrospun nanofibers in agriculture: a review. *Materials Research Express*, 8(4), 042001.
 105. Latha, M., Raja, K., Subramanian, K., Karthikeyan, M., & Lakshmanan, A. (2019). Fabrication and characterization of tebuconazole loaded PVA nanofiber. *Int. J. Agric. Sci*, 10, 8514-8517.
 106. Osanloo, M., Arish, J., & Sereshti, H. (2020). Developed methods for the preparation of electrospun nanofibers containing plant-derived oil or essential oil: a systematic review. *Polymer Bulletin*, 77, 6085-6104.
 107. Dilfi, A. K., Che, Z. J., & Xian, G. J. (2019). Grafting of nano-silica onto ramie fiber for enhanced mechanical and interfacial properties of ramie/epoxy composite. *Journal of Zhejiang University-SCIENCE A*, 20(9), 660-674.
 108. De Jorge, B. C., & Gross, J. (2021). Smart nanotextiles for application in sustainable agriculture. In *Nanosensors and Nanodevices for Smart Multifunctional Textiles*, 203- 227, Elsevier.
 109. Nooeaid, P., Chuysinuan, P., Pitakdantham, W., Aryuwananon, D., Techasakul, S., & Dechtrirat, D. (2021). Eco-friendly polyvinyl alcohol/polylactic acid core/shell structured fibers as controlled-release fertilizers for sustainable agriculture. *Journal of Polymers and the Environment*, 29, 552-564.
 110. Liu, S., Wu, Q., Sun, X., Yue, Y., Tubana, B., Yang, R., & Cheng, H. N. (2021). Novel alginate-cellulose nanofiber-poly (vinyl alcohol) hydrogels for carrying and delivering nitrogen, phosphorus and potassium chemicals. *International Journal of Biological Macromolecules*, 172, 330-340.

-
111. Itrotwar, P. D., Govindaraju, K., Tamilselvan, S., Kannan, M., Raja, K., & Subramanian, K. S. (2020). Seaweed-based biogenic ZnO nanoparticles for improving agro-morphological characteristics of rice (*Oryza sativa* L.). *Journal of plant growth regulation*, 39, 717-728.
112. Castaneda, L. M. F., Genro, C., Roggia, I., Bender, S. S., Bender, R. J., & Pereira, C. N. (2014). Innovative rice seed coating (*Oryza sativa*) with polymer nanofibres and microparticles using the electrospinning method. *J. Res. Updates Polym. Sci*, 3(1), 33-39.
113. Raja, K., Prabhu, C., Subramanian, K. S., & Govindaraju, K. (2021). Electrospun polyvinyl alcohol (PVA) nanofibers as carriers for hormones (IAA and GA 3) delivery in seed invigoration for enhancing germination and seedling vigor of agricultural crops (groundnut and black gram). *Polymer Bulletin*, 78, 6429-6440.
114. Sivalingam, S., Kunhilintakath, A., Nagamony, P., & Paspulathi Parthasarathy, V. (2021). Fabrication, toxicity and biocompatibility of *Sesamum indicum* infused graphene oxide nanofiber-a novel green composite method. *Applied Nanoscience*, 11, 679-686.
115. Badgar, K., Prokisch, J., & El-Ramady, H. (2021). Nanofibers for sustainable agriculture: A short communication. *Egyptian Journal of Soil Science*, 61(3), 373-380.
116. Krishnamoorthy, V., & Rajiv, S. (2017). Potential seed coatings fabricated from electrospinning hexaaminocyclotriphosphazene and cobalt nanoparticles incorporated polyvinylpyrrolidone for sustainable agriculture. *ACS Sustainable Chemistry & Engineering*, 5(1), 146-152.
117. Hassounah, I., Shehata, N., Hudson, A., Orlor, B., & Meehan, K. (2014). Characteristics and 3D formation of PVA and PEO electrospun nanofibers with embedded urea. *Journal of Applied Polymer Science*, 131(3).
118. Krishnamoorthy, V., & Rajiv, S. (2017). An eco-friendly top down approach to nutrient incorporated electrospun seed coating for superior germination potential. *Journal of Advanced Applied Scientific Research*, 1(7).
119. Noruzi, M. (2016). Electrospun nanofibres in agriculture and the food industry: a review. *Journal of the Science of Food and Agriculture*, 96(14), 4663-4678.
120. Kamaci, U. D., & Peksel, A. (2020). Fabrication of PVA-chitosan-based nanofibers for phytase immobilization to enhance enzymatic activity. *International Journal of Biological Macromolecules*, 164, 3315-3322.
121. Wang, Z. G., Wan, L. S., Liu, Z. M., Huang, X. J., & Xu, Z. K. (2009). Enzyme immobilization on electrospun polymer nanofibers: An overview. *Journal of Molecular Catalysis B: Enzymatic*, 56(4), 189-195.

-
122. Bilal, M., & Iqbal, H. M. (2019). Chemical, physical, and biological coordination: An Interplay between materials and enzymes as potential platforms for immobilization. *Coordination Chemistry Reviews*, 388, 1-23.
123. Campana, J. M., & Arias, M. (2020). Nanofibers as a delivery system for arbuscular mycorrhizal fungi. *ACS Applied Polymer Materials*, 2(11), 5033-5038.
124. Naseri, N., Algan, C., Jacobs, V., John, M., Oksman, K., & Mathew, A. P. (2014). Electrospun chitosan-based nanocomposite mats reinforced with chitin nanocrystals for wound dressing. *Carbohydrate polymers*, 109, 7-15.
125. Avella, M., Martuscelli, E., & Raimo, M. (2000). Review Properties of blends and composites based on poly (3-hydroxy) butyrate (PHB) and poly (3-hydroxybutyrate-hydroxyvalerate)(PHBV) copolymers. *Journal of materials science*, 35(3), 523-545.
126. Shan, D., Huang, Z., Zhao, Y., Cai, Q., & Yang, X. (2014). Improving the miscibility of Biodegradable polyester/polyphosphazene blends using cross-linkable polyphosphazene. *Biomedical Materials*, 9(6), 061001.
127. Krogman, N. R., Weikel, A. L., Nguyen, N. Q., Kristhart, K. A., Nukavarapu, S. P., Nair, L. S., & Allcock, H. R. (2010). Hydrogen bonding in blends of polyesters with dipeptide-containing polyphosphazenes. *Journal of applied polymer science*, 115(1), 431-437.
128. Metwally, S., Karbowniczek, J. E., Szewczyk, P. K., Marzec, M. M., Gruszczyński, A., Bernasik, A., & Stachewicz, U. (2019). Single-step approach to tailor surface chemistry and potential on electrospun PCL fibers for tissue engineering application. *Advanced Materials Interfaces*, 6(2), 1801211.
129. Ghasemi-Mobarakeh, L., Prabhakaran, M. P., Morshed, M., Nasr-Esfahani, M. H., & Ramakrishna, S. (2008). Electrospun poly (ϵ -caprolactone)/gelatin nanofibrous scaffolds for nerve tissue engineering. *Biomaterials*, 29(34), 4532-4539.
130. Ma, Z., He, W., Yong, T., & Ramakrishna, S. (2005). Grafting of gelatin on electrospun poly (caprolactone) nanofibers to improve endothelial cell spreading and proliferation and to control cell orientation. *Tissue engineering*, 11(7-8), 1149-1158.
131. Tiwari, A. P., Joshi, M. K., Lee, J., Maharjan, B., Ko, S. W., Park, C. H., & Kim, C. S. (2017). Heterogeneous electrospun polycaprolactone/polyethylene glycol membranes with improved wettability, biocompatibility, and mineralization. *Colloids and Surfaces A: Physicochemical and Engineering Aspects*, 520, 105-113.

-
132. Grossen, P., Witzigmann, D., Sieber, S., & Huwyler, J. (2017). PEG-PCL-based nanomedicines: A biodegradable drug delivery system and its application. *Journal of Controlled Release*, 260, 46-60.
133. Scaffaro, R., Lopresti, F., Catania, V., Santisi, S., Cappello, S., Botta, L., & Quatrini, P. (2017). Polycaprolactone-based scaffold for oil-selective sorption and improvement of bacteria activity for bioremediation of polluted water: Porous PCL system obtained by leaching melt mixed PCL/PEG/NaCl composites: Oil uptake performance and bioremediation efficiency. *European Polymer Journal*, 91, 260-273.
134. Akazawa, T., & Hara-Nishimura, I. (1985). Topographic aspects of biosynthesis, extracellular secretion, and intracellular storage of proteins in plant cells. *Annual review of plant physiology*, 36(1), 441-472.
135. Patel, S. (2012). Threats, management and envisaged utilizations of aquatic weed *Eichhornia crassipes*: an overview. *Reviews in Environmental Science and Bio/Technology*, 11, 249-259.
136. Cesari, A., Loureiro, M. V., Vale, M., Yslas, E. I., Dardanelli, M., & Marques, A. C. (2020). Polycaprolactone microcapsules containing citric acid and naringin for plant growth and sustainable agriculture: physico-chemical properties and release behavior. *Science of the Total Environment*, 703, 135548.
137. Milani, P., França, D., Balieiro, A. G., & Faez, R. (2017). Polymers and its applications in agriculture. *Polímeros*, 27, 256-266.
138. Fadil F, Affandi ND, Ibrahim NA, Misnon MI, Harun AM, Alam MK. (2021) Advanced application of electrospun polycaprolactone fibers for seed germination activity. *Advances in Polymer Technology*. 1-0.
139. Guarino, V., Gentile, G., Sorrentino, L., & Ambrosio, L. (2017). *Encyclopedia of Polymer Science and Technology*.
140. Correlo, V. M., Boesel, L. F., Bhattacharya, M., Mano, J. F., Neves, N. M., & Reis, R. L. (2005). Hydroxyapatite reinforced chitosan and polyester blends for biomedical applications. *Macromolecular materials and Engineering*, 290(12), 1157-1165.
141. Eshraghi, S., & Das, S. (2010). Mechanical and microstructural properties of polycaprolactone scaffolds with one-dimensional, two-dimensional, and three-dimensional orthogonally oriented porous architectures produced by selective laser sintering. *Acta biomaterialia*, 6(7), 2467-2476.
142. Ali SAM, Zhong SP, Doherty PJ, Williams DF. (1993)Mechanisms of polymer degradation

- in implantable devices: I. Poly(caprolactone). *Biomater* 14,648-56
143. Ceonzo, K., Gaynor, A., Shaffer, L., Kojima, K., Vacanti, C. A., & Stahl, G. L. (2006). Polyglycolic acid-induced inflammation: role of hydrolysis and resulting complement activation. *Tissue engineering*, 12(2), 301-308.
144. Dulnik, J., Denis, P., Sajkiewicz, P., Kołbuk, D., & Choińska, E. (2016). Biodegradation of bicomponent PCL/gelatin and PCL/collagen nanofibers electrospun from alternative solvent system. *Polymer Degradation and Stability*, 130, 10-21.
145. Banerjee, A., Chatterjee, K., & Madras, G. (2014). Enzymatic degradation of polymers: a brief review. *Materials Science and Technology*, 30(5), 567-573.
146. Haponiuk, J., & Karlsson, S. (2002). Biodegradation of modified poly (ϵ -caprolactone) in different environments. *Polish Journal of Environmental Studies*, 11(4), 413-420.
147. Woodruff, M. A., & Hutmacher, D. W. (2010). The return of a forgotten polymer- Polycaprolactone in the 21st century. *Progress in polymer science*, 35(10), 1217-1256.
148. Wang, Y., Li, M., Rong, J., Nie, G., Qiao, J., Wang, H., & Huang, Y. (2013). Enhanced orientation of PEO polymer chains induced by nanoclays in electrospun PEO/clay composite nanofibers. *Colloid and Polymer Science*, 291, 1541-1546.
149. Lumley, J. L. (1969). Drag reduction by additives. *Annual review of fluid mechanics*, 1(1), 367-384.
150. Nair, S., Natarajan, S., & Kim, S. H. (2005). Fabrication of electrically conducting polypyrrole-poly (ethylene oxide) composite nanofibers. *Macromolecular rapid communications*, 26(20), 1599-1603.
151. Ma, G., Fang, D., Liu, Y., Zhu, X., & Nie, J. (2012). Electrospun sodium alginate/poly (ethylene oxide) core-shell nanofibers scaffold potential for tissue engineering applications. *Carbohydrate polymers*, 87(1), 737-743.
152. Savaş, H., & Güven, O. (2001). Investigation of active substance release from poly (ethylene oxide) hydrogels. *International journal of pharmaceutics*, 224(1-2), 151-158.
153. Xie, J., & Hsieh, Y. L. (2003). Ultra-high surface fibrous membranes from electrospinning of natural proteins: casein and lipase enzyme. *Journal of Materials Science*, 38, 2125-2133.
154. Subramanian, A., Vu, D., Larsen, G. F., & Lin, H. Y. (2005). Preparation and evaluation of the electrospun chitosan/PEO fibers for potential applications in cartilage tissue engineering. *Journal of Biomaterials Science, Polymer Edition*, 16(7), 861-873.
155. Zhao, D., Wan, Y., & Zhou, W. (2012). *Ordered mesoporous materials*. John Wiley & Sons.

-
156. Vallet-Regí, M., Garcia, M. M., & Colilla, M. (2012). *Biomedical applications of mesoporous ceramics: drug delivery, smart materials and bone tissue engineering*. CRC Press.
157. Martínez-Edo, G., Balmori, A., Pontón, I., Martí del Rio, A., & Sánchez-García, D. (2018). Functionalized ordered mesoporous silicas (MCM-41): Synthesis and applications in catalysis. *Catalysts*, 8(12), 617.
158. Feng, X., Fryxell, G. E., Wang, L. Q., Kim, A. Y., Liu, J., & Kemner, K. M. (1997). Functionalized monolayers on ordered mesoporous supports. *Science*, 276(5314), 923- 926.
159. Jaroniec, C. P., Kruk, M., Jaroniec, M., & Sayari, A. (1998). Tailoring surface and structural properties of MCM-41 silicas by bonding organosilanes. *The Journal of Physical Chemistry B*, 102(28), 5503-5510.
160. Chen, C. Y., Xiao, S. Q., & Davis, M. E. (1995). Studies on ordered mesoporous materials III. Comparison of MCM-41 to mesoporous materials derived from kanemite. *Microporous Materials*, 4(1), 1-20.
161. Papat, A., Hartono, S. B., Stahr, F., Liu, J., Qiao, S. Z., & Lu, G. Q. M. (2011). Mesoporous silica nanoparticles for bioadsorption, enzyme immobilisation, and delivery carriers. *Nanoscale*, 3(7), 2801-2818
162. Avnir, D., Braun, S., Lev, O. & Ottolenghi, M. (1994). *Chem. Mater*, 6(1605), 1.
163. Dai, H., Ou, S., Liu, Z. & Huang, H. (2017). *Carbohydrate Polymers* 169 504-514
164. Sundari, M. T., & Ramesh, A. (2012). Isolation and characterization of cellulose nanofibers from the aquatic weed water hyacinth—*Eichhornia crassipes*. *Carbohydrate Polymers*, 87(2), 1701-1705.
165. de Oliveira, J. P., Bruni, G. P., Lima, K. O., El Halal, S. L. M., da Rosa, G. S., Dias, A. R.G., & da Rosa Zavareze, E. (2017). Cellulose fibers extracted from rice and oat husks and their application in hydrogel. *Food chemistry*, 221, 153-160.
166. Brasileiro, L. B., Colodette, J. L., & Piló-Veloso, D. (2001). The use of peracids in delignification and cellulose pulp bleaching. *Quimica Nova*, 24, 819-829.
167. Kaur, M., Kumar, M., Sachdeva, S., & Puri, S. K. (2018). Aquatic weeds as the next generation feedstock for sustainable bioenergy production. *Bioresource Technology*, 251, 390-402.
168. Singh, A., & Bishnoi, N. R. (2013). Comparative study of various pretreatment techniques for ethanol production from water hyacinth. *Industrial Crops and Products*, 44, 283-289.

-
169. Istirokhatun, T., Rokhati, N., Rachmawaty, R., Meriyani, M., Priyanto, S., & Susanto, H. (2015). Cellulose isolation from tropical water hyacinth for membrane preparation. *Procedia Environmental Sciences*, 23, 274-281.
170. Mansour, M. M. (2014). Response of soybean plants to exogenously applied with ascorbic acid, zinc sulphate and paclobutrazol. *Rep Opin*, 6(11), 17-25.
171. Alloway, B. J. (2009). Soil factors associated with zinc deficiency in crops and humans. *Environmental geochemistry and health*, 31(5), 537-548.
172. Wassel, A. H., El-Hameed, M. A., Gobara, A., & Attia, M. (2007). Effect of some micronutrients, gibberellic acid and ascorbic acid on growth, yield and quality of white Banaty seedless grapevines. In *8th African Crop Science Society Conference, El-Minia, Egypt*, 547-553, African Crop Science Society.
173. Cakmak, I. (2008). Enrichment of cereal grains with zinc: agronomic or genetic biofortification?. *Plant and soil*, 302, 1-17.
174. Xie, Y., He, Y., Irwin, P. L., Jin, T., & Shi, X. (2011). Antibacterial activity and mechanism of action of zinc oxide nanoparticles against *Campylobacter jejuni*. *Applied and environmental microbiology*, 77(7), 2325-2331.
175. Imada, K., Sakai, S., Kajihara, H., Tanaka, S., & Ito, S. (2016). Magnesium oxide nanoparticles induce systemic resistance in tomato against bacterial wilt disease. *Plant Pathology*, 65(4), 551-560.
176. Tapan Adhikari (2019). Magnesium Oxide Nano Particles Effects on utilization of soil Phosphorus by Maize (*Zea mays* L.) *Plant.Int.J.Curr.Microbiol.App.Sci.* 8(10): 410-419.
177. Dey, P., Santhi, R., Maragatham, S., & Sellamuthu, K. M. (2017). Status of phosphorus and potassium in the Indian soils vis-à-vis world soils. *Indian Journal of Fertilizers*, 13(4), 44-59.
178. Fageria, N. K. (2016). *The use of nutrients in crop plants*. CRC press.
179. Katti, K. S., Katti, D. R., & Dash, R. (2008). Synthesis and characterization of a novel chitosan/montmorillonite/hydroxyapatite nanocomposite for bone tissue engineering. *Biomedical Materials*, 3(3), 034122.
180. Teng, S. H., Lee, E. J., Wang, P., Jun, S. H., Han, C. M., & Kim, H. E. (2009). Functionally gradient chitosan/hydroxyapatite composite scaffolds for controlled drug release. *Journal of Biomedical Materials Research Part B: Applied Biomaterials*, 90(1), 275-282.

-
181. Giroto, A. S., Fidélis, S. C., & Ribeiro, C. (2015). Controlled release from hydroxyapatite nanoparticles incorporated into biodegradable, soluble host matrixes. *RSC advances*, 5(126), 104179-104186.
182. Liu, R., & Lal, R. (2014). Synthetic apatite nanoparticles as a phosphorus fertilizer for soybean (*Glycine max*). *Scientific reports*, 4(1), 5686.
183. Georgakilas, V., Perman, J. A., Tucek, J., & Zboril, R. (2015). Broad family of carbon nanoallotropes: classification, chemistry and applications of fullerenes, carbon dots, nanotubes, graphene, nanodiamonds and combined superstructures. *Chemical reviews*, 115(11), 4744-4822.
184. Choi, Y., Choi, Y., Kwon, O. H., & Kim, B. S. (2018). Carbon dots: bottom-up synthesis, properties and light-harvesting applications. *Chemistry—An Asian Journal*, 13(6), 586-598.
185. Xu, X., Ray, R., Gu, Y., Ploehn, H. J., Gearheart, L., Raker, K., & Scrivens, W. A. (2004). Electrophoretic analysis and purification of fluorescent single-walled carbon nanotube fragments. *Journal of the American Chemical Society*, 126(40), 12736-12737.
186. Peng, Z., Han, X., Li, S., Al-Youbi, A. O., Bashammakh, A. S., El-Shahawi, M. S., & Leblanc, R. M. (2017). Carbon dots: biomacromolecule interaction, bioimaging and nanomedicine. *Coordination chemistry reviews*, 343, 256-277.
187. Choudhary, R., Patra, S., Madhuri, R., & Sharma, P. K. (2016). Equipment-free, single-step, rapid, “on-site” kit for visual detection of lead ions in soil, water, bacteria, live cells, and solid fruits using fluorescent cube-shaped nitrogen-doped carbon dots. *ACS Sustainable Chemistry & Engineering*, 4(10), 5606-5617.
188. Gao, X., Lu, Y., Zhang, R., He, S., Ju, J., Liu, M., & Chen, W. (2015). One-pot synthesis of carbon nanodots for fluorescence turn-on detection of Ag⁺ based on the Ag⁺-induced enhancement of fluorescence. *Journal of Materials Chemistry C*, 3(10), 2302-2309.
189. Wang, B., & Lu, S. (2022). The light of carbon dots: From mechanism to applications. *Matter*, 5(1), 110-149.
190. Li, H., He, X., Kang, Z., Huang, H., Liu, Y., Liu, J., & Lee, S. T. (2010). Water-soluble fluorescent carbon quantum dots and photocatalyst design. *Angewandte Chemie International Edition*, 49(26), 4430-4434.
191. Zhou, J., Booker, C., Li, R., Zhou, X., Sham, T. K., Sun, X., & Ding, Z. (2007). An electrochemical avenue to blue luminescent nanocrystals from multiwalled carbon nanotubes (MWCNTs). *Journal of the American Chemical Society*, 129(4), 744-745.

-
192. Wang, W., Ni, Y., & Xu, Z. (2015). One-step uniformly hybrid carbon quantum dots with high-reactive TiO₂ for photocatalytic application. *Journal of Alloys and Compounds*, 622, 303-308.
193. Bian, J., Huang, C., Wang, L., Hung, T., Daoud, W. A., & Zhang, R. (2014). Carbon dot loading and TiO₂ nanorod length dependence of photoelectrochemical properties in carbon dot/TiO₂ nanorod array nanocomposites. *ACS applied materials & interfaces*, 6(7), 4883-4890.
194. Guo, B., Liu, G., Wei, H., Qiu, J., Zhuang, J., Zhang, X., & Liu, Y. (2022). The role of fluorescent carbon dots in crops: Mechanism and applications. *SmartMat*, 3(2), 208-225.
195. Li, Y., Xu, X., Wu, Y., Zhuang, J., Zhang, X., Zhang, H., & Liu, Y. (2020). A review on the effects of carbon dots in plant systems. *Materials Chemistry Frontiers*, 4(2), 437- 448.
196. Khairol Anuar, N. K., Tan, H. L., Lim, Y. P., So'aib, M. S., & Abu Bakar, N. F. (2021). A review on multifunctional carbon-dots synthesized from biomass waste: Design/fabrication , characterization and applications. *Frontiers in Energy Research*, 9, 626549
197. El-Sobky, M. A., Fahmi, A. I., Eissa, R. A., & El-Zanaty, A. M. (2019). Genetic characterization of *Trichoderma* spp. isolated from different locations of Menoufia, Egypt and assessment of their antagonistic ability. *J Microb Biochem Technol*, 11(1).
198. Li, Y., Sun, R., Yu, J., Saravanakumar, K., & Chen, J. (2016). Antagonistic and biocontrol potential of *Trichoderma asperellum* ZJSX5003 against the maize stalk rot pathogen *Fusarium graminearum*. *Indian journal of microbiology*, 56, 318-327.
199. Liu, C., & Ogbonnaya, F. C. (2015). Resistance to *F usarium* crown rot in wheat and barley: a review. *Plant Breeding*, 134(4), 365-372.
200. GUO, R. F., LIU, X. G., GAO, K. X., GAO, B. J., SHI, B. S., & ZHEN, Z. X. (2002). Progress in biocontrol research with *Trichoderma*. *Chinese Journal of Biological Control*, 18(4), 180.
201. Whipps, J. M., Lumsden, R. D., Butt, T. M., Jackson, C., & Magan, N. (2001). Fungi as biocontrol agents—progress, problems and potential. *Commercial Use of Fungi as Plant Disease Biological Control Agents—Status and Prospects*, 9-22.
202. Filizola, P. R. B., Luna, M. A. C., de Souza, A. F., Coelho, I. L., Laranjeira, D., & Campos-Takaki, G. M. (2019). Biodiversity and phylogeny of novel *Trichoderma* isolates from mangrove sediments and potential of biocontrol against *Fusarium* strains. *Microbial cell factories*, 18(1), 1-14.

-
203. Nagaraju, A., Sudisha, J., Murthy, S. M., & Ito, S. I. (2012). Seed priming with *Trichoderma harzianum* isolates enhances plant growth and induces resistance against *Plasmopara halstedii*, an incitant of sunflower downy mildew disease. *Australasian Plant Pathology*, 41, 609-620.
204. Sunita, S. (2014). A comparative study on immobilization of alpha amylase enzyme on different matrices. *International Journal of Plant, Animal and Environmental Sciences*, 4(3), 192-198.
205. Gurung, N., Ray, S., Bose, S., & Rai, V. (2013). A broader view: microbial enzymes and their relevance in industries, medicine, and beyond. *BioMed research international*, 2013.
206. Gupta, R., Gigras, P., Mohapatra, H., Goswami, V. K., & Chauhan, B. (2003). Microbial α -amylases: a biotechnological perspective. *Process biochemistry*, 38(11), 1599-1616.
207. Sidhu, G. S., Sharma, P., Chakrabarti, T., & Gupta, J. K. (1997). Strain improvement for the production of a thermostable α -amylase. *Enzyme and Microbial Technology*, 21(7), 525-530.
208. DAS, G., & Sen-Mandi, S. W. A. T. I. (1992). Scutellar amylase activity in naturally aged and accelerated aged wheat seeds. *Annals of Botany*, 69(6), 497-501.
209. Han, C., & Yang, P. (2015). Studies on the molecular mechanisms of seed germination. *Proteomics*, 15(10), 1671-1679.
210. Hedden, P., & Thomas, S. G. (2012). Gibberellin biosynthesis and its regulation. *Biochemical Journal*, 444(1), 11-25.
211. Miransari, M., & Smith, D. L. (2014). Plant hormones and seed germination. *Environmental and experimental botany*, 99, 110-121.
212. Lobell, D. B., Roberts, M. J., Schlenker, W., Braun, N., Little, B. B., Rejesus, R. M., & Hammer, G. L. (2014). Greater sensitivity to drought accompanies maize yield increase in the US Midwest. *Science*, 344(6183), 516-519.

Chapter 2

Materials and Methods

This chapter provides details of general reagents and synthetic methods employed in the present study. A brief account of the various analytical and physicochemical techniques employed in the characterization is discussed. The studies of developed membranes towards controlled release of agrichemicals and germination studies are also explained.

2.1 Materials

Poly(ϵ -caprolactone) (PCL), (average $M_w=80,000$ g/mol), Polyethylene oxide (PEO), (average $M_w = 2,00000$ g/mol), Cetyltrimethylammonium bromide (CTAB, purity 99%), Tetraethyl orthosilicate (TEOS) and (3-aminopropyl)triethoxysilane (APTES), alpha-amylase from *Bacillus subtilis* used in the present investigation were purchased from Sigma-Aldrich Co.Ltd. Glutaraldehyde (GU) (25%), Gibberellic acid (GA) procured from HiMedia. Di-ammonium hydrogen phosphate, Calcium nitrate tetrahydrate, Zinc nitrate hexahydrate, Urea, Magnesium nitrate hexahydrate, Sodium hydroxide, Sodium hypochlorite (10%) and the solvents Chloroform (99.7% AR grade) and N,N-Dimethylformamide (DMF 99.5% AR grade) were procured from Merck. Deionized water was used throughout the experiments. Water Hyacinth was collected from nearby ponds in the locality. Chemicals and solvents employed in the study were used as obtained. Zea mays seeds were purchased from local agrifarm. *Trichoderma viride* spores were obtained from the collection at the Department of Microbiology, Kerala Agricultural University, Mannuthy. All the chemicals were kept at room temperature.

2.2 Synthesis of Nanoparticles

2.2.1 Synthesis of ZnO NPs

High purity ZnO nanoparticles were synthesized by fuel approach in solution combustion method¹. Zinc nitrate hexahydrate (5g) and urea (3g) were dissolved in deionised water (10mL) and vigorously stirred to obtain a clear solution, then placed into a preheated muffle furnace at 600°C. The mixture burned with a flame in a short

time, with the rapid evolution of large volumes of gases resulted in a frothy product as shown (Fig. II.1). The powder obtained was finely ground using a pestle and mortar without any extra heat treatment. The Chemical reaction in combustion synthesis² of ZnO is given in Equation 2.1

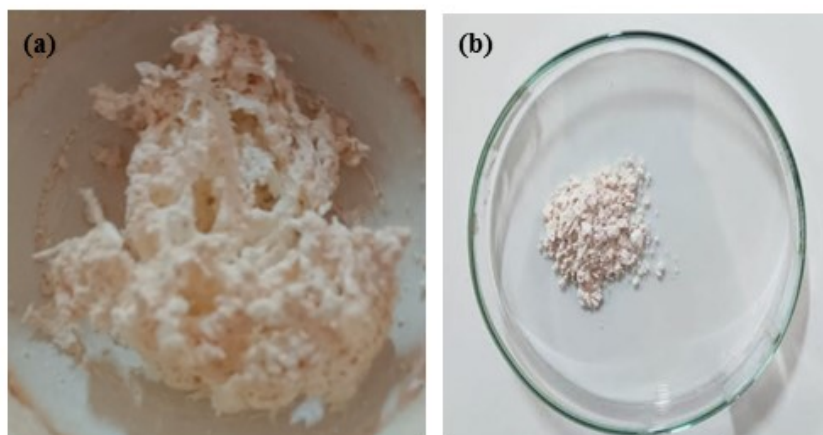
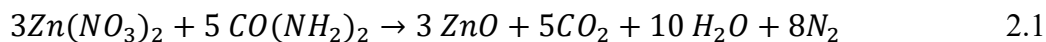
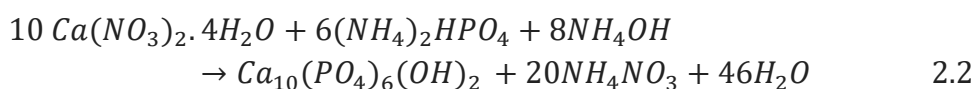


Fig.II.1 a) Frothy product formed during the synthesis of ZnO NPs
b) Finely powdered ZnO NPs

2.2.2 Synthesis of Nanohydroxyapatite (nHAP)

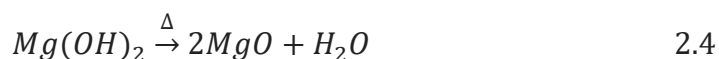
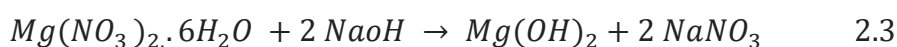
The wet chemical method was used to synthesize hydroxyapatite nanoparticles³. 0.15M diammonium hydrogen phosphate (250 mL) was vigorously stirred at room temperature, 0.25M calcium nitrate tetrahydrate (250mL) was added drop-wise at a rate of 10mL/min. Ammonium hydroxide solution was used to keep the pH of the system at 10.5 during the stirring procedure. The mixture was stirred for 12 h. It resulted in the formation of a white precipitate. The precipitate was filtered, washed four times with distilled water and ethanol and dried at 120°C for 12 h. The chemical precipitation reaction for the synthesis of nHAP⁴ is shown in Equation 2.2.



2.2.3 Synthesis of Magnesium oxide Nanoparticles (MgO NPs)

Sol-gel technology was used to synthesize magnesium oxide nanoparticles⁵. Magnesium nitrate ($\text{Mg}(\text{NO}_3)_2 \cdot 6\text{H}_2\text{O}$) was used as a precursor in the synthesis. De-

ionized water (100mL) was combined with 0.2 M magnesium nitrate. 0.5M sodium hydroxide solution was added drop by drop to the previously prepared magnesium nitrate solution for 30 min with stirring. A white precipitate of magnesium hydroxide was formed in the beaker as indicated in the Equation 2.3. Stirring was continued for 30 min. The pH of the solution as determined by the digital pH meter was found to be 12.5. To get rid of ionic impurities, the precipitate was filtered, washed with methanol three to four times and then dried at ambient temperature after being centrifuged for 5 min at 5000 rpm. The samples of dried white powder were annealed in the air for 2 h at 500°C to get MgO NPs according to Equation 2.4.



2.2.4 Synthesis of Carbon Dots (CDs) through Hydrothermal Carbonization and Separation of CDs from HTC Process Liquid

Carbon dots (CDs) are prepared from water hyacinth (WH). Stem of Water hyacinth (WH) was treated hydrothermally to create CDs. The WH was collected, washed with water and then dried in the sunlight for 3 days. Prior to being finely ground into powder, the WH stems were first dried in the oven over night to remove any moisture. To make the mixture homogenous, prepared stem powder (5g) was mixed with Milli-Q water (120 mL). The mixture was then put into a 150 mL Teflon-lined stainless steel autoclave and subjected to hydrothermal treatment process at 200°C for 4 h⁶. The reactor was sealed and heated at a steady rate of 10°C/min until it reached the desired temperature. It was then kept at that temperature for 10 h under isothermal conditions. The reactor was quickly cooled down to ambient temperature 30°C by submerging in ice water. Then the reactor's lid was opened and HTC process liquid was filtered using Whatman 41 filter paper. Samples of the dark-brown HTC process liquid were gathered in centrifuge tubes and kept in the refrigerator for further procedure.

To separate the larger particles from the liquid phase, the dark brown HTC process liquid was centrifuged at 5000 rpm for 15 min by R-8M plus laboratory centrifuge. The liquid phase containing the fluorescent CD was next filtered using a

typical syringe filter (0.22 μm)⁷. After filtering, vacuum distillation was used to evaporate the CD-containing solution. To produce powdered CDs, the concentrated product from vacuum distillation was placed in a high vacuum freeze dryer for 24 h. Schematic diagram for the synthesis of CDs is shown in Fig. II.2

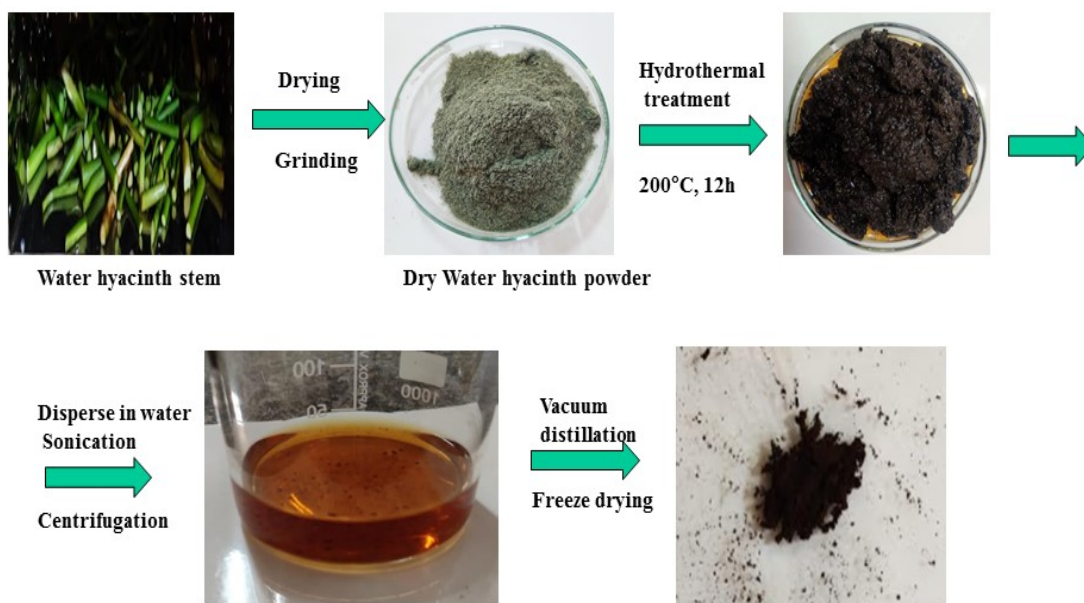


Fig.II.2 Schematic of synthesis of CDs from Water hyacinth stem

2.3 Synthesis of MCM-41

Hydrothermal techniques were used to prepare MCM-41 samples⁸. To create a homogenous solution, cetyltrimethylammonium bromide (CTAB) was dissolved in water and agitated for 30 min. Ammonia was added to the homogenous solution, which was adjusted to have a pH between 11-12. Tetraethyl orthosilicate (TEOS) was added to the mixture and again agitated for 8 h. The solution was filtered and rinsed with Millipore water. The white homogenous suspension produced after 8 h of stirring was hydrothermally treated in an autoclave reactor for 24 h at 110°C. The precipitate was filtered, washed and dried under vacuum, prior to calcination. Calcination was carried out in a muffle furnace at 550°C to remove the organic template for 5 h. The calcination temperature of 550°C was attained at a heating rate of 1°C/min. Fig.II.3 illustrates the hydrolysis and condensation reactions that take place during the synthesis of MCM-41. The surface structure of MCM-41⁹ is shown in Fig.II.4a.

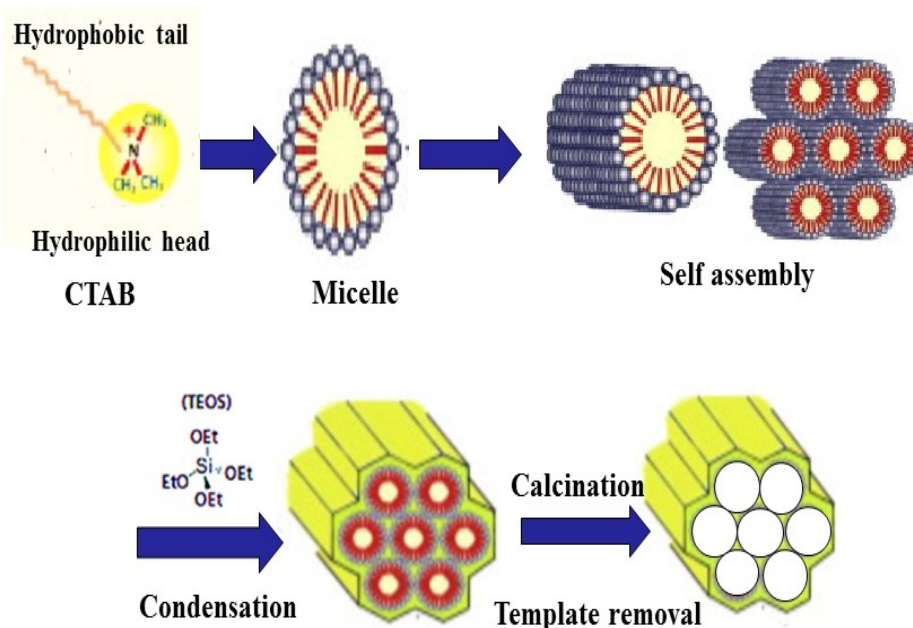


Fig.II.3 Schematic illustration of synthesis of MCM-41

2.3.1 Synthesis of aminopropyl functionalized MCM-41(MCM-41/APTES)

The amino modified MCM-41 was prepared by grafting technology¹⁰. The pure siliceous MCM-41(3g) was suspended in dry toluene (100mL) and (3-aminopropyl)triethoxysilane (APTES) (3 g) was added to it. The suspension was stirred and refluxed for 24 h. The product MCM-41/APTES was filtered, washed with toluene, then washed with dichloromethane and dried at 100°C for 5h.

2.3.2 Activation of functionalized MCM-41 (MCM-41/GU)

To bind the carrier to aldehyde groups, MCM-4/APTES (2g) was added to 25 mL of 100% ethanol with 25% glutaraldehyde (MCM-41/GU). The carrier was centrifuged at 1800 rpm for 3 min at ambient temperature (25°C), followed by four separate washes in 100% ethanol and deionized water¹¹.

2.3.3 Synthesis of MCM-41 immobilized α - amylase (MCM-41/Amylase)

The enzyme α -amylase was immobilized on functionalized MCM-41 by reacting MCM-41/GU (2g) with 0.1% α -amylase (100mL) at room temperature for 6 h with occasional shaking of the mixture¹². The immobilized enzyme on MCM-41 was separated by filtration and washed thoroughly with phosphate buffer. Schematic

pathway for the surface modification of MCM-41 and enzyme immobilization is shown in Fig.II.4b¹³.

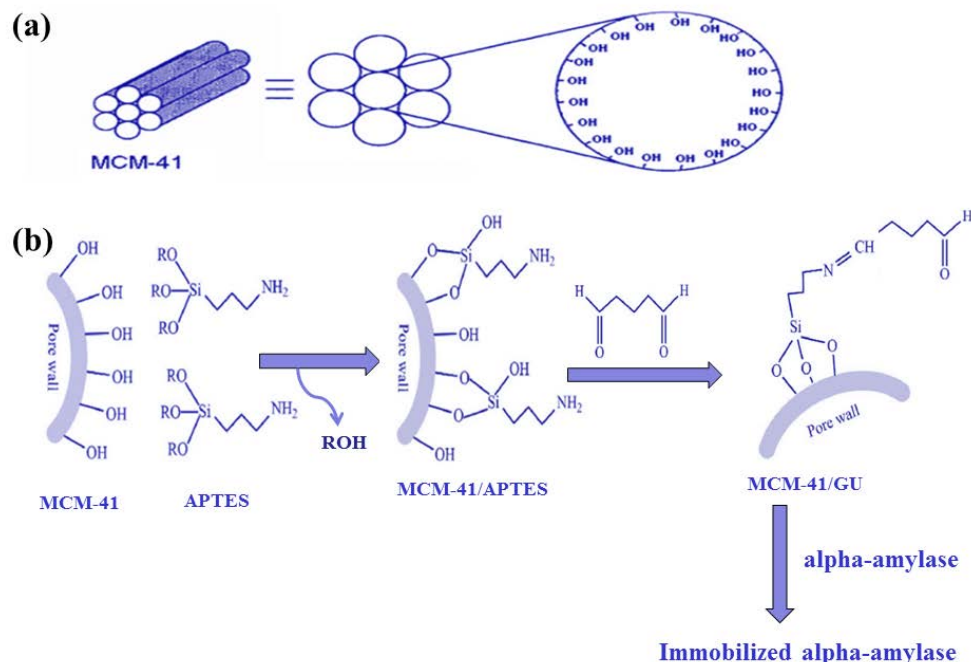


**Fig.II.4 a) Surface structure of MCM-41
b) Synthesis of MCM-41 immobilized α -amylase**

2.4 Cellulose Extraction from Water Hyacinth

Fresh water hyacinth (WH) plants were cleansed with water to get rid of any surface dirt. Water hyacinth was subjected to chemical processes such as dewaxing, alkaline bleaching and alkaline hydrolysis to isolate cellulose. The water hyacinth stem was first washed, dried for three days, ground then sieved through a 40 mesh sieve. Dewaxing procedure was done by mixing dried water hyacinth (25 g) with ethanol and toluene for 6 h, at 75°C. Wax, oils, resin, organic compounds, pigments and extractive chemicals can be eliminated during the dewaxing process from the water hyacinth stem, retaining lignin, hemicellulose and cellulose in the product¹⁴.

The dewaxed product was brown, indicating that additional contaminants like lignin and hemicellulose were present in water hyacinth fibers. After dewaxing, the sample was bleached using 10% sodium hypochlorite (NaOCl). The bleaching

procedure was carried out for 4 h while stirring at a speed of 590 rpm at a heating temperature of 75°C to 80°C. The dispersion of the bleached samples was washed with distilled water until the pH was 7. To separate the sample from the filtrate, it was decanted and filtered. By breaking the ether linkages during the bleaching process, lignin was completely eliminated, which enhanced the whiteness level of the bleached sample¹⁵.

The bleached sample was neutralized and refluxed with 2% NaOH (150mL) with stirring at a rate of 500rpm for 3 h at a heating temperature of 45°C. Hemicellulose can be separated from the main chain or cellulose, using NaOH. Furthermore, the dissolution of the complex lignin-carbohydrate network occurs as a result of the breakdown of ester bonds connecting lignin and hemicellulose in the interaction with NaOH¹⁶. The residue, which had the consistency of white powder, was once more treated with distilled water until the pH reached 7. It was then allowed to air dry for two to three days.

2.5 Preparation of Solution for Electrospinning and Phase Inversion

2.5.1 Solution for PCL Electrospun Nanofibers

The 10% (w/v) PCL solution was prepared by dissolving PCL (0.5 g) in chloroform/DMF (5 mL) (4:1 v/v) at room temperature (30°C). This was allowed to stir for 4 h till a homogenous clear solution was obtained.

For the preparation of solution for composite nanofibers and film, the percentage of nHAP, ZnO NPs and *T.viride* added were wt % of each component with respect to the weight of PCL taken.

2.5.2 Solution for PCL/nHAP/ZnONPs (PHZ) Electrospun Nanofibers

The similar procedure as in section 2.5.1 was followed. The PHZ solution was made by dispersing nHAP (0.1g, 20% by weight of PCL) and ZnO NPs (0.05g 10% by weight of PCL) in PCL solution using ultrasound (Ultronique QR500, frequency 20kHz). All the prepared solutions were stirred continuously for 4 h at room temperature to obtain a homogeneous solution.

2.5.3 Solution for PCL/nHAP/ZnONPs/*T.viride* (PHZT) Electrospun Nanofibers

To the prepared PHZ solution as in section 2.5.2, *T.viride* (0.05g, 10% by weight of PCL) was added to obtain a homogeneous solution of PHZT.

2.5.4 Solution for Electrospinning PCL – PEO Blend Electrospun Nanofibers

The polymer PCL being hydrophobic was blended with hydrophilic, electrospun PEO to increase the water wettability of PCL. The concentration of 10% (w/v) of PCL in a 4:1 chloroform: DMF solution produced smooth fibers. The concentration of PCL and the ratio of solvent used were determined by optimisation to get good fibers. Optimization of composition of blended polymer solution was conducted as follows. PCL (0.5g) was taken in a solvent mixture of chloroform and DMF (5 mL) in the ratio of 4:1 and stirred for 4h using a magnetic stirrer. To this solution PEO was added to get PCL: PEO ratios of 75:25, 50:50 and 30:70. The weights of the polymers taken are given in Table II.1. The stirring was carried out under ambient temperature ($30 \pm 2^\circ\text{C}$)

Table II.1 Solution preparation for PCL-PEO blend nanofibers

Solution PCL:PEO	Blend name	Polymer quantity (g)		Solvent (mL)	
		PCL	PEO	CHCl ₃	DMF
75:25	B1	0.5	0.167	4	1
50:50	B2	0.5	0.500	4	1
30:70	B3	0.5	0.750	4	1

2.5.5 Solution for PCL/PEO/nHAP/ZnONPs/*T.viride* (BHZT and BHZT_F) Electrospun Nanofibers and Film

The blend solution B3 was selected for the further study was prepared as explained in section 2.5.4. To this 20% nHAP, 10% ZnONPs and 10% *T.viride* (by weight of PCL) were added to get a blended polymer solution (BHZT). The solution was stirred for 4 h at ambient temperature to form a homogeneous solution. The prepared solutions were utilized to make both the film (BHZT_F) and the fibers. Table II.2 shows the concentrations used for making the solution.

Table II.2 Solution preparation for PCL, PHZ, PHZT, BHZT nanofibers and BHZT_F

Solution	Polymer and agrichemicals					Solvent (mL)	
	(g)						
	PCL	PEO	nHAP	ZnO NPs	<i>T.viride</i>	CHCl ₃	DMF (CH ₃) ₂ NCH
PCL	0.5	-	-	-	-	4	1
PHZ	0.5	-	0.1	0.05	-	4	1
PHZT	0.5	-	0.1	0.05	0.05	4	1
BHZT	0.5	0.750	0.1	0.05	0.05	4	1
BHZT _F	0.5	0.750	0.1	0.05	0.05	4	1

2.5.6 Solution for PCL/Amylase (PA) Electrospun Nanofibers

Encapsulation of α -amylase in PCL nanofibers (PA) was done by adding α -amylase (0.1g, 20% by weight of PCL) to the solution of PCL (0.5 g) in chloroform (5 mL) under stirring. The resulting solution (PA) was sonicated for 30 min at the ultrasonic bath.

2.5.7 Solution for PCL/MCM-41-Amylase (PMA) Electrospun Nanofibers

10% PCL (w/v) solution was prepared by dissolving PCL (0.5g) in chloroform (5mL). To this solution, MCM-41 immobilized α -amylase (0.25g) was added and sonicated for 10 min. The solution (PMA) thus obtained was further stirred for 4 h at room temperature.

2.5.8 Solution for PCL/MCM-41-Amylase/ MgO NPs (PMMA) Electrospun Nanofibers

To prepare PMMA solution, MgO NPs (0.05g, 10% by weight of PCL) was dispersed through sonication in PMA solution. A homogeneous clear solution (PMMA) was obtained after 4 h of stirring.

2.5.9 Solution for PCL/MCM-41-Amylase/ GA/ MgO NPs (PMMG) Electrospun Nanofibers

MgO NPs (0.05g), GA (0.05g) and MCM-41immobilized α -amylase (0.25g) were dispersed in chloroform (5 mL) using ultrasound sonicator. To this PCL (0.5 g) was added and the solution was further stirred for 4h at room temperature to obtain PMMG solution. Table II.3 shows the concentrations used for making the solutions of enzyme immobilized nanofibers.

Table II.3 Solution Preparation for PA, PMA, PMMA and PMMG nanofibers

Solution	Weight of polymer, Immobilized enzyme and agrichemicals (g)					Solvent (mL)
	PCL	Free/ α -Amylase	MCM-41/ α -Amylase	MgO NPs	GA	CHCl ₃
PA	0.5	0.1	-	-	-	5
PMA	0.5	-	0.1	-	-	5
PMMA	0.5	-	0.1	0.05	-	5
PMMG	0.5	-	0.1	0.05	0.05	5

2.5.10 Solution for PEO/Cellulose (PC_w) Electrospun Nanofibers

A homogeneous solution of PEO and cellulose in the ratio 50:50 was prepared by blending PEO (0.5 g) and cellulose (0.5 g) extracted from WH in 5 mL of chloroform /DMF (4:1 v/v). It was stirred for 6 h till a homogenous solution (PC_w) was obtained. The solutions were prepared at room temperature (30°C).

2.5.11 Solution for PEO/Cellulose/CDs (PC_wCD_w) Electrospun Nanofibers

To the PC_w solution, carbon dots (CDs) was added (PC_wCD_w). This was optimised to 20% by weight of PEO (0.1g). This was allowed to stir for 6 h till a homogenous solution was obtained.

2.5.12 Solution for PEO/Cellulose/nHAP (PC_wH) Electrospun Nanofibers

To the PC_w solution, nHAP (0.1g, 20% by weight of PEO) was added. A homogeneous solution PC_wH was obtained after 6 h of stirring.

2.5.13 Solution for PEO/Cellulose/nHAP/CDs (PC_wCD_wH) Electrospun Nanofibers

The PC_w solution containing both CDs and nHAP was prepared by dispersing CDs (0.1g) and nHAP (0.1g) in 5 mL of chloroform/DMF (4:1 v/v) using ultrasound (Ultronique QR500, frequency 20kHz). The PC_wCD_wH solution was allowed to stir for 6 h till a homogenous solution was obtained. Table II.4 shows the concentrations used for making the solution.

Table II.4 Solution preparation for nanofibers for PC_w, PC_wCD_w, PC_wH, PC_wCD_wH

Solution	Polymer and agrichemicals (g)				Solvent (mL)	
	PEO	Cellulose	CDs	nHAP	CHCl ₃	DMF
PC _w	0.5	0.5	-	-	4	1
PC _w CD _w	0.5	0.5	0.1	-	4	1
PC _w H	0.5	0.5	-	0.1	4	1
PC _w CD _w H	0.5	0.5	0.1	0.1	4	1

2.6 Electrospinning Technique

Fig.I.7 depicts the electrospinning apparatus used in the present study. The electrospun nanofibers were prepared by electrospinning the solutions prepared as discussed earlier in the Department of Chemistry, National Institute of Technology, Calicut. The produced polymer solution was dispensed into a syringe (10 mL) fitted with a stainless steel needle (0.3 mm). The solution flow rate was modified using a syringe pump. Aluminium foil rolled over the rotating drum was used as collector. A high voltage power supply was applied in between needle and collector. The polymer nanofibers were collected as fiber mat on collector which was later peeled off. Table II.5 lists the standard variables that were applied to the electrospinning of all solutions. Each solution's specific parameters are described in a separate section.

Table II.5 Common electrospinning parameters employed

Parameters	Ideal Values
Needle Volume	10 mL
Needle Diameter	0.3 mm
Collector Type	Static- Aluminium Foil
Solvent	Chloroform/ DMF
Temperature	28 ± 1°C
Humidity	62 ± 5 %

2.6.1 Electrospinning Parameters for PCL, PHZ, PHZT, BHZT

Nanofibers

Table II.6 shows the electrospinning parameters for the formation of fibers of PCL, PHZ, PHZT and BHZT.

Table II.6 Optimised electrospinning parameters

Polymer solution	Tip-target Distance (cm)	Applied Voltage (kV)	Flow Rate (mL/h)
PCL	15	20	0.5
PHZ	15	20	1
PHZT	15	20	1
BHZT	15	20	1

Solvent : Chloroform + DMF in the ratio 4:1

2.6.2 Electrospinning Parameters for PCL– PEO Blend Nanofibers

Table II.7 shows the electrospinning parameters for the formation of fibers of PCL and PEO blends.

Table II.7 Optimised electrospinning parameters

Polymer solution	Tip-target Distance (cm)	Applied Voltage (kV)	Flow Rate (mL/h)
B1	15	20	2
B2	15	20	2
B3	15	20	2

Solvent : Chloroform + DMF in the ratio 4:1

2.6.3 Electrospinning Parameters for PA, PMA, PMMA and PMMG

Nanofibers

Table II.8 shows the parameters of electrospinning for the polymer solutions of PA, PMA, PMMA and PMMG nanofibers.

Table II.8 Optimised electrospinning parameters

Polymer solution	Tip-target Distance (cm)	Applied Voltage (kV)	Flow Rate (mL/h)
PA	14	22	1
PMA	13	26	1
PMMA	13	26	1
PMMG	13	26	1

Solvent : Chloroform +DMF in the ratio 4:1

2.6.4 Electrospinning Parameters for PC_w, PC_wCD_w, PC_wH, PC_wCD_wH Nanofibers

Table II.9 shows the parameters of electrospinning for the polymer solutions of PC_w, PC_wCD_w, PC_wH, PC_wCD_wH nanofibers

Table II.9 Optimised electrospinning parameters

Polymer solution	Tip-target Distance (cm)	Applied Voltage (kV)	Flow Rate (mL/h)
PC _w	14	21	1.5
PC _w CD _w	14	21	1.5
PC _w H	14	21	1.5
PC _w CD _w H	14	21	1.5

Solvent : Chloroform +DMF in the ratio 4:1

2.7 Preparation of Porous Polymer Film Using Phase Inversion Method

The homogeneously mixed solution of nHAP/ZnONPs/*T.viride* –PCL/PEO (BHZT) was used for the preparation of porous polymer film. For phase separation, deionised water was added to the homogeneous solution of BHZT as a non-solvent and stirred constantly. From the resultant solution the aqueous portion was removed and dried on a petri dish at 80°C. The films were labelled as BHZT_F

2.8 Coating of the Seeds

2.8.1 Fiber Coating

A layer-by-layer electrospinning coating method was used to embed seeds into the nanofiber membrane. A nanofiber layer was first electrospun on the aluminium foil for 2 h, then the corn seeds were spread on top of this layer. To obtain uniform coating on both sides, another nanofiber layer was electrospun for 2 h on the seeds. The nanofiber coated seeds was cut by a circular punch. The prepared solutions from section 2.5 were loaded into the syringe one by one to develop different nanofibrous seed coating.

2.8.2 Film Coating

Seeds were covered using the dip coating technique. Prepared solution of BHZT was ingested in a bottle that had a secure cap. 25 seeds were added to the solution bottle and shaken vigorously for 5 min. They were emptied into a petri dish and left to dry¹⁷. Fig.II.5 shows the images of coated and untreated seeds.

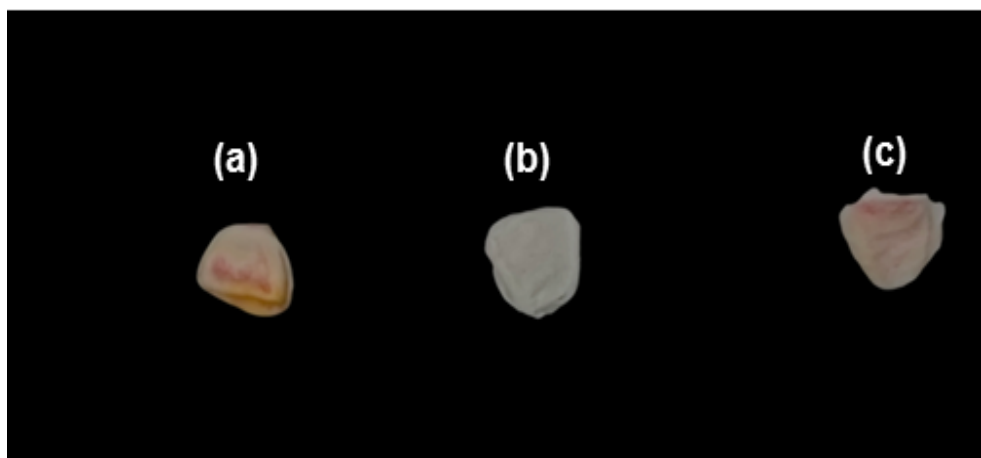


**Fig.II.5 Images of a) uncoated seeds b) nanofiber coated seeds
c) film coated seeds**

2.9 Characterization Studies

2.9.1 Analysis of Functional Groups and Structure

2.9.1.1 FT-IR Analysis

Fourier transform infrared studies were conducted using a BRUKER Alpha FT-IR spectrometer in the range of 4000 cm^{-1} to 400 cm^{-1} to determine the functional

groups of the samples. The liquid and powder samples, as well as the dried sample membranes, were all deposited directly to the sample holder.

2.9.1.2 XRD Analysis

The crystallinity of the polymer nanofibers and nanoparticles were examined by XRD (Panalytical, Aeris Research) using Cu K α radiation (wavelength = 1.540598 Å) produced at 40 kV and 30 mA. The XRD spectrum was recorded from 20° to 80° at 295 K. The XRD study helped in understanding the blends' miscibility to some extent. The crystallite size was calculated from the Scherrer equation.

$$D_p = \frac{0.94\lambda}{\beta \cos\theta} \quad 2.5$$

where D_p = average crystallite size, β = line broadening in radians, θ = Bragg angle, and λ = X-ray wavelength¹⁸

2.9.1.3 UV-Visible Spectroscopy

A Shimadzu UV-1800 UV-visible absorption spectrometer was used to observe the absorption behaviour of the synthesized nanoparticles and immobilized enzyme. The syringe-filtered CD solution was used in this analysis.

2.9.1.4 Fluorescence Spectroscopy

To check the fluorescence intensity of CDs broadband 450-W xenon arc lamp from UV to near-IR was used. Fluorescence spectra were recorded on a Fluorolog 3 TCSPC, between 280 nm to the 400nm excitation wavelength.

2.9.1.5 ICP-OES Analysis

The release patterns of metals and nanoparticles from the developed nanofibers into the soils was assessed using inductively coupled plasma optical emission spectroscopy (ICP-OES, Perkin 221 Elmer Optima 5300DV)

2.10 Thermal Analysis

2.10.1 Thermo Gravimetric Analysis (TGA)

The thermal stability and decomposition temperature of samples were evaluated using TGA with a heating rate of 20°C/min under nitrogen atmosphere using a TGAQ50. Alumina was used as the reference material on platinum pans and calcium sulphate was used as standard.

2.11 Studies on Morphology

2.11.1 SEM Analysis and EDX Measurement

A FEIQuanta FEG 200 High Resolution Scanning Electron Microscope (HR-SEM) provided with Energy Dispersive X-ray spectroscopy (EDX) was used to study the surface morphology. This was observed with a FEG assembly with Schottky emitter(-200V to 30kV) Secondary electrons thus produced gives rise to surface morphological images and tracked using Everhart Thornley detector. Presence of elements such as nanoparticles, metals on the polymer nanofibers were detected through EDX attached to SEM. Before doing the SEM study, the samples were sputtered with gold to make them conductive.

2.11.2 Fiber Diameter Measurement

The UTHSCSA image J tool software was used to calculate the fiber diameter of SEM images of electrospun nanofibers membrane. The average diameter of nanofibers was calculated based on 50 random nanofibers.

2.11.3 TEM Analysis

Transmission electron microscopy (TEM) studies were conducted to analyse the presence of agrichemicals loaded in the PCL/PEO nanofiber matrix and synthesized MCM-41 structure using JEOL instrument with a voltage of 200 kV. This instrument uses high energy electron beam for material characterization and gives the information of nanoparticles dispersion inside or on the surface of the fiber. The TEM images display the details of the internal structure of the fibers.

2.11.4 Static Water Contact Angle (SWCA)

With the use of a Euromex Optical Microscope and a CCD camera, the hydrophilicity of the polymer was investigated by measuring the water contact angle. A contact angle of less than 90° suggests hydrophilic wettability and more than 90° implies hydrophobic wettability.

2.12 Physical Property Measurements

2.12.1 Porosity Measurement

The porosity (P) of the electrospun nanofibers was evaluated by the n-butanol uptake method. In this method, the electrospun nanofibrous membrane was dipped in n-butanol for 2 h. The weights of the membranes before and after immersion were measured. The porosities (P%) of the membranes were investigated using Equation 2.6¹⁹.

$$P(\%) = \frac{\frac{m_a}{\rho_b}}{\frac{m_a}{\rho_b} + \frac{m_i}{\rho_s}} \times 100 \quad (2.6)$$

where 'm_i' and 'm_a' were the weights of the electrospun nanofibrous membranes before and after soaking in n-butanol and 'ρ_b' and 'ρ_s' are the densities of the n-butanol and dried electrospun membranes respectively. The ratio of the weight of the dried electrospun nanofibers (m) to volume (v) [length (0.7 cm), breadth (0.7 cm), thickness (30 mm)] was used to find the density of the electrospun membranes (ρ_s).

2.13 Study of the Aqueous Solution of Membranes

Each of the samples (0.1 g) was soaked in 20 mL of water. The analysis of the samples was done at regular intervals up to 5 days. The solutions were covered with aluminium foil to avoid evaporation of water and contamination and kept at room temperature. Similar procedure was done for uncoated seeds and seeds coated with nanofibers and film.

2.13.1 Study of Variation in pH

Synthesized fibers and film (0.1 g) was dissolved in distilled water (20 mL) and the change in pH and conductivity was recorded for a period of 5 days. The

change in pH and conductivity of the steep waters obtained on dissolution of the fiber and film coated seeds in water and fibers and film in water were studied at room temperature ($30 \pm 1^\circ\text{C}$). The Scientific tech ST2002M pH meter was used to study the pH change.

2.13.2 Study of Variation in Conductivity

The conductivity measurements were done using Systronics MK-509 conductivity meter. The variation in conductivity values was investigated to analyze the release of nutrients. Uncoated, fiber and film coated Zea Mays seeds (1g) were steeped in distilled water (20 mL) for 5 days at ambient temperature ($30 \pm 1^\circ\text{C}$) in a beaker. Conductivity of solution is expressed in Siemens per metre (S/m). A 0.01M solution of KCl was used to calibrate the apparatus. Conductivity testing, which is widely used in environmental and industrial applications is a quick, affordable and reliable technique, mostly for testing water samples. Using conductivity measurements from the literature, this work investigates how fibers containing nutrients dissolve in water²⁰.

2.13.3 Swelling Studies

1x1 cm square pieces of fiber mats and film were cut and dried at 60°C to remove moisture and weighed (W_1). It is placed on aluminium foil. The samples were immersed in water (2 mL). After every 2, 4, 6, 8, 10, 12, 24 and 36 h the foils were removed, wiped and weighed (W_2). In the case of enzyme immobilized nanofibers swelling studies were done in PBS at a pH of 6.5. The samples completely dried in a preheated oven at 60°C . The dried sample's weight is recorded (W_3). The percentage swelling and stability were calculated^{21,22} using Equation 2.7 and 2.8.

$$\% \text{ Swelling } (\%Sw) = \frac{W_2 - W_1}{W_1} \times 100 \quad 2.7$$

$$\% \text{ Stability } (\%S) = \frac{W_3 - W_1}{W_1} \times 100 \quad 2.8$$

An analytical balance with a 0.0001g precision, the Citizen Cx120, was used to measure the weights.

2.13.4 Study of the Steep Water and Imbibition Studies

The rate of imbibition and water uptake of uncoated, fiber and film coated seeds were tested and compared. Seeds (1 g) were placed between two wet tissue papers, and the weight gained owing to water absorption was calculated by subtracting the weight of dry seed from the imbibed seed. The surface moisture of imbibed seeds was wiped out before weighing. The measurements were repeated three times and the average value was reported.

2.13.5 Metal Release Study

The release patterns of metals from the developed nanofibers into the soils was assessed using inductively coupled plasma optical emission spectroscopy (ICP-OES, Perkin Elmer Optima 5300DV) analysis of the soils over a 7 day period. The nanofibers and film (100 mg) were put into various vials, each containing soil (1 g) and Milli-Q water (10 mL)²³. The vials were incubated at room temperature for 7 days. The soil samples were dried at 100°C after being incubated. The soil samples (100 mg) were placed in various vials with HNO₃ (5 mL) and digested at 100°C for 48 h over a hot plate. The digested samples were combined with HNO₃ (2 mL) and the samples were incubated at room temperature for 24 h. Milli-Q water (10 ml) and the digested samples (0.2 mL) were combined, then the mixture was filtered using syringe filters. The process was repeated for the samples taken from the vials at various times. For the ICP-OES analysis, the filtered samples (5 mL) were combined with Milli-Q water (5 mL). To ensure analytical accuracy, appropriate blank and standard runs were conducted.

2.14 Microbiological Test and Dual Culture Tests

By inoculating the surface of the agar with the fibrous mats that were put on the aluminium foil at 28°C, it was possible to determine the viability of the spores of the soil bacterium *T. viride* in the fibers. The diameter of colonies was measured on alternate days after inoculation up to 7 days.

Through double culture on the solid medium in Petri dishes, the interaction between the pathogenic fungus *Aspergillus* and the fungal antagonist *T. viride* was studied. The plate was covered with a disc (7 mm) of the pathogen's 5-day agar

culture. At the other end of the dish, a *T. viride* spore-infused, fibrous BHZT mat was positioned. The ability of the spores of the soil microorganism *T. viride* in the fibers was assessed after incubation for 7 days at 28°C. The growth of the colonies of the phytopathogen and antagonist fungi was examined.

2.15 α -Amylase Enzymatic Activity Assay

2.15.1 Activity Assays of Immobilized α -Amylase

α -Amylase enzyme activity was assessed using the Bernfeld method for both free and immobilised forms²⁴. By measuring the amount of maltose released from starch, the activity of amylase was evaluated. 1cm² section of enzyme immobilized nanofiber was used to determine the activity. In a test tube the immobilised enzyme were combined with 1% starch solution (1 mL) prepared in phosphate buffer (pH = 6.5). This mixture was then incubated at 37°C for 30 min. Before adding 3,5-dinitrosalicylic acid (DNS) reagent, the immobilised enzyme was taken out of the reaction mixture and rinsed with distilled water. After this, DNS (1mL) was added as terminator of the reaction and the mixture was heated for 5 min at 100°C. The amount of released maltose in the reaction mixture was calculated using the absorbance at 540 nm. The calibration curve was obtained with maltose solutions at different concentrations. The amount of the enzyme producing 1 μ mol of reducing sugars per minute under the assay conditions was used to define one unit of enzyme activity (U). The whole procedure was repeated with other fabricated nanofibers PMA, PMMA and PMMG.

2.15.2 Effect of pH on the Immobilized α - Amylase Activity

In general, enzymes are sensitive to changes in pH and they have an optimum pH range over which their activity decreases. The pH level at which the enzyme activity reaches its peak is known as the optimum pH value. Using 0.1 M phosphate buffer solutions (PBS) with pH ranges between 4.0 and 9.0 in steps of one pH unit, the effect of pH changes on the α -amylase activity of the extract was investigated. Each of the five identical test tubes, labelled 1-5, was set up to indicate a specific pH value. The similar procedure was followed as in the enzyme assay procedure (Section 2.15.1) using different pH solutions.

2.15.3 Effect of Temperature on the Immobilized α -Amylase Activity

The effect of varying temperature on the activity of enzyme was investigated to determine the optimum temperature of immobilised enzyme samples. The process for determining how temperature variation affected enzyme activity was the same as that used to determine how pH variation affected amylase activity; however, in this case, a buffer solution with a pH of 5.6 (0.1 M phosphate buffer) was used, and the reaction was monitored at various temperatures (20°C, 30°C, 40°C, 50°C, 60°C and 70°C).

2.15.4 Reusability and Storage Stability Studies of Immobilized α -Amylase

The residual activity of the immobilised enzyme under ideal circumstances after five reuses was used to analyse the reusability of α -amylase. 1mL of the prepared starch solution was added to the reaction mixture containing the immobilised enzyme in each cycle of the reaction. Following each cycle, the immobilised enzyme was removed from the reaction mixture and rinsed with deionised water and PBS (50 mM; pH 6) and then a new enzymatic reaction cycle was initiated using the freshly prepared substrate solution. The enzyme activity was assessed after the enzyme had reacted for 30 mins with 1% soluble starch in order to ascertain whether the immobilised amylase was reusable. As previously said, the activity was measured. The enzyme's initial activity was taken as 100%.

By monitoring the residual activity after storage at 4°C in 20 mM phosphate buffer, at pH 6.5 in every 10 days for a period of 8 weeks, the storage stability of immobilised α -amylase was examined. The reaction medium's pH and temperature were optimum. The initial activity was compared to the activities at various times. Each result was determined by averaging the results of three replicates.

2.15.5 α - Amylase Activity of Coated Seeds Using Starch Agar Method

The starch agar medium was made with distilled water, 2% bacteriological agar and 1% soluble starch. Using an autoclave, the medium was sterilised at 121°C. The germinated seeds after 5 days were then detached from the root and shoot. The remaining scutella was placed on the starch agar medium for 24 h. Uncoated and

prepared coated seeds were spread on starch agar plates. After 24 h, the treated plates were drained with iodine solution. The digested starch area stayed transparent while the undigested area turned blue²⁵. The diameter of the digested zone surrounding the treated seed was measured and the amylase activity was taken into account. The process is repeated three times.

2.15.6 Antioxidant Studies

The radical scavenging experiment was used to determine the developed electrospun nanofibers' antioxidant activity. According to the reported method, the radical scavenging activity was assessed using the diphenylpicrylhydrazyl radical (DPPH)²⁶. Developed nanofibers (100mg) were dipped in methanol solution of DPPH (1 mL, 0.1 mM). As a control, a blank was prepared without the addition of the sample. The solutions were gently mixed and their absorbance was measured at 517 nm after 30 min incubation in the dark. The DPPH scavenging activity (%) was calculated using the Equation 2.9.

$$\text{DPPH scavenging activity} = \frac{\text{Absorbance of Control} - \text{Absorbance of Sample}}{\text{Absorbance of Control}} \times 100 \quad 2.9$$

2.16 Germination Parameters

Approximately uniform sized Zea mays seeds were selected for the experiment. The greenhouse studies were conducted to assess the efficacy of this seed coating approach. The germination assays were done at room temperature, with the seeds being placed on wet filter paper on a petridish²⁷. The experiment was conducted using synthesized electrospun fibers and film as seed coat. The seeds were divided into sub samples of 25 seeds each as shown in the Fig.II.6. One of the sets was uncoated seeds and other sets were coated with nanofibers and porous polymer film respectively. The sprouting studies were carried out using the "in between paper" method. The tissue paper is kept wet by spraying water regularly. They were permitted to remain in the dark for 24 h before being investigated. Decayed seeds were removed. The root and shoot length were measured after every 24 h. To assure data consistency, the study used a completely randomised experimental design with three replicates of 10 seeds each.

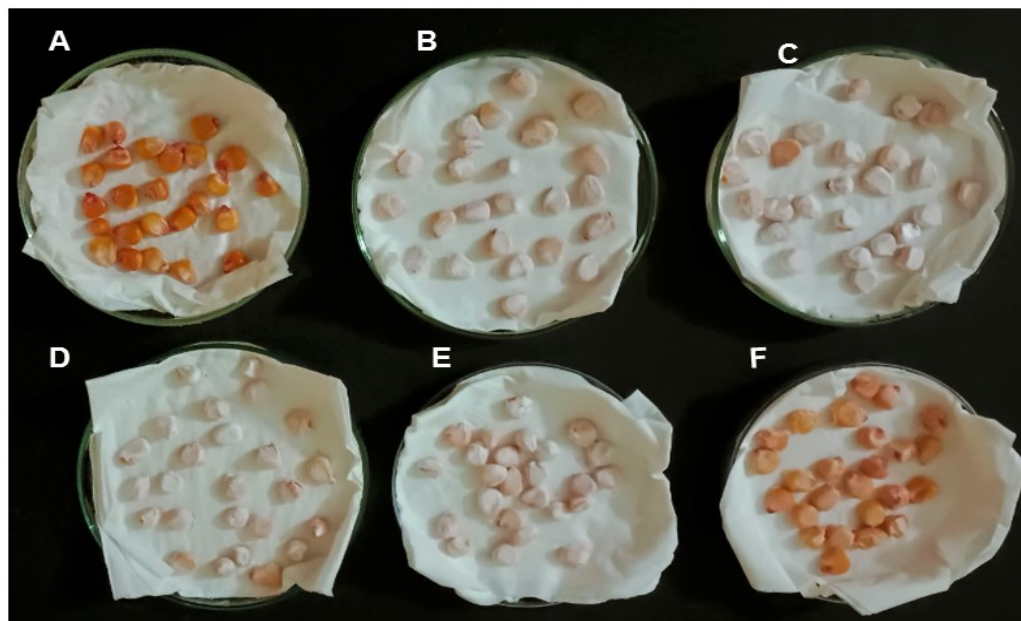


Fig.II.6 Photographs of experimental set up for germination studies
A) Uncoated B – E) Nanofiber coated F) Porous film coated

The number of seeds germinated was counted after every 24 h. Six good seedlings were chosen from each treatment at random. The root and shoot length were measured with a thread and ruler. When the radicle protruded from the seed coat, a seed was said to have germinated. The status of seed germination was observed between 0 h and 120 h. The formulas listed in Table II.10 were used to compute the germination parameters, including germination percentage, germination index and seed vigour index. G_0 , G , L and L_0 represent the number of seeds in the sample, the number of seeds that germinated, shoot length of the seed and the shoot length of the control, respectively²⁸. Additionally, the wet biomass of the shoots and roots was calculated after 15 days of germination.

Table II.10 Equations of germination parameters

Germination Parameter	Formula
Germination Percentage (% G)	$= G/G_0 * 100$
Germination Index (GI)	$= G/G_0 \times L/L_0 \times 100$
Seed Vigour Index (SVI)	$= \%G \times L(cm)$

2.16.1 Statistical Analysis

To analyse the effect of developed seed coat on germination, one way ANOVA was used to examine the data for germination percentage, germination index, and seed vigour index. This test was carried out using Statistical Package for Social Sciences - SPSS 24.0 software (IBM). All data were tested for homogeneity using Levene's test before conducting the one way ANOVA. Treatment effects were declared significant at $p < 0.05$ for all analyses. Tukey's HSD test was used to test post hoc for difference among means.

References

1. De Sousa, V. C., Morelli, M. R., & Kiminami, R. H. (2000). Combustion process in the synthesis of ZnO–Bi₂O₃. *Ceramics International*, 26(5), 561-564.
2. Pathak, T. K., Kumar, A., Swart, C. W., Swart, H. C., & Kroon, R. E. (2016). Effect of fuel content on luminescence and antibacterial properties of zinc oxide nanocrystalline powders synthesized by the combustion method. *RSC advances*, 6(100), 97770-97782.
3. Bouyer, E., Gitzhofer, F., Boulos, M.I. (2000). Morphological study of hydroxyapatite nanocrystal suspension. *J. Mater. Sci. Mater. Med.* 11, 523–531.
4. Abidi, S. S. A., & Murtaza, Q. (2014). Synthesis and characterization of nano-hydroxyapatite powder using wet chemical precipitation reaction. *Journal of Materials Science & Technology*, 30(4), 307-310.
5. Wahab, R., Ansari, S. G., Dar, M. A., Kim, Y. S., & Shin, H. S. (2007). Synthesis of magnesium oxide nanoparticles by sol-gel process. *Materials Science Forum*, 558,983-986, Trans Tech Publications Ltd.
6. Sachdev, A., & Gopinath, P. (2015) Green synthesis of multifunctional carbon dots from coriander leaves and their potential application as antioxidants, sensors and bioimaging agents. *Analyst* 140, 4260–4269.
7. Deka, M. J., Dutta, P., Sarma, S., Medhi, O. K., Talukdar, N. C., & Chowdhury, D. (2019). Carbon dots derived from water hyacinth and their application as a sensor for pretilachlor. *Heliyon*, 5(6), e01985.
8. Araujo, J. A., Cruz, F. T., Cruz, I. H., & Cardoso, D. (2013). Encapsulation of polymers in CTA-MCM-41 via microemulsion. *Microporous and mesoporous materials*, 180, 14-21.
9. Ojani, R., Raoof, J. B., & Fathi, S. (2009). Ferricyanide immobilized within organically modified MCM-41; application for electrocatalytic reduction of hydrogen peroxide. *Journal of Solid State Electrochemistry*, 13, 837-842.
10. Fellenz, N., Perez-Alonso, F. J., Martin, P. P., García-Fierro, J. L., Bengoa, J. F., Marchetti, S. G., & Rojas, S. (2017). Chromium (VI) removal from water by means of adsorption-reduction at the surface of amino-functionalized MCM-41 sorbents. *Microporous and Mesoporous Materials*, 239, 138-146.
11. Xie, W., & Zang, X. (2016). Immobilized lipase on core-shell structured Fe₃O₄–MCM-41 nanocomposites as a magnetically recyclable biocatalyst for interesterification of soybean oil and lard. *Food Chemistry*, 194, 1283-1292.
12. Diaz, J. F., & Balkus Jr, K. J. (1996). Enzyme immobilization in MCM-41 molecular sieve. *Journal of Molecular Catalysis B: Enzymatic*, 2(2-3), 115-126.

13. Yu, D., Zhang, X., Wang, T., Geng, H., Wang, L., Jiang, L., & Elfalleh, W. (2021). Immobilized *Candida antarctica* lipase B (CALB) on functionalized MCM-41: Stability and catalysis of transesterification of soybean oil and phytosterol. *Food Bioscience*, 40, 100906.
14. Istirokhatun, T., Rokhati, N., Rachmawaty, R., Meriyani, M., Priyanto, S., & Susanto, H. (2015). Cellulose isolation from tropical water hyacinth for membrane preparation. *Procedia Environmental Sciences*, 23, 274-281.
15. Osong, S. H., Norgren, S., & Engstrand, P. (2016). Processing of wood-based microfibrillated cellulose and nanofibrillated cellulose, and applications relating to papermaking: a review. *Cellulose*, 23, 93-123.
16. Setyaningsih, L., Satria, E., Khoironi, H., Dwisari, M., Setyowati, G., Rachmawati, N. & Anggraeni, J. (2019). Cellulose extracted from water hyacinth and the application in hydrogel. In *IOP Conference Series: Materials Science and Engineering*, 673, 1, 012017).
17. Corlett, F. M., de A Rufino, C., Vieira, J. F., Tavares, L. C., de Tunes, L. M., & Barros, A. C. (2014). The influence of seed coating on the vigor and early seedling growth of barley. *Ciencia e investigación agraria: revista latinoamericana de ciencias de la agricultura*, 41(1), 129-136.
18. Raj, J., & Viswanathan, B. (2011). Synthesis of cobalt nanoparticles with vegetable oil as the stabilizing agent. *Bulletin of the Catalysis Society of Indias*, 9, 6-12.
19. Lobregas, M. O. S., & Camacho, D. H. (2019). Gel polymer electrolyte system based on starch grafted with ionic liquid: Synthesis, characterization and its application in dye-sensitized solar cell. *Electrochimica Acta*, 298, 219-228.
20. Corwin, D. L., & Lesch, S. M. (2005). Apparent soil electrical conductivity measurements in agriculture. *Computers and electronics in agriculture*, 46(1-3), 11-43.
21. Liu, S., Kang, M., Hussain, I., Li, K., Yao, F., & Fu, G. (2016). High mechanical strength and stability of alginate hydrogel induced by neodymium ions coordination. *Polymer Degradation and Stability*, 133, 1-7.
22. Kim, S. H., Seong, J. H., & Oh, K. W. (2002). Effect of dopant mixture on the conductivity and thermal stability of polyaniline/Nomex conductive fabric. *Journal of applied polymer science*, 83(10), 2245-2254.
23. Kumar, R., Ashfaq, M., & Verma, N. (2018). Synthesis of novel PVA–starch formulation-supported Cu–Zn nanoparticle carrying carbon nanofibers as a nanofertilizer: controlled release of micronutrients. *Journal of Materials Science*, 53(10), 7150-7164
24. Bernfield, P. (1955). Amilase α and β . Dalam Colowick, SP and ND Kaplan (eds). New York: Methode in Enzimology and Related of Biochemistry.

25. Bhatti, G. & Ujjan, A. (2018). Determination of amylase activity in germinating seeds of wheat (*Triticum Aestivum* L.) varieties and its correlation with seedling growth and yield. 10.13140/RG.2.2.29126.32326/1.
26. Liu, J., Wang, C., Wang, Z., Zhang, C., Lu, S., & Liu, J. (2011). The antioxidant and free-radical scavenging activities of extract and fractions from corn silk (*Zea mays* L.) and related flavone glycosides. *Food Chemistry*, 126(1), 261-269.
27. McNair, J. N., Sunkara, A., & Frobish, D. (2012). How to analyse seed germination data using statistical time-to-event analysis: non-parametric and semi-parametric methods. *Seed Science Research*, 22(2), 77-95.
28. Pradeep, P. (2018). Seed quality parameters (Germination percentage and seedling vigor index) of rabi sorghum seeds influenced by rice weevil infestation. *MOJ Toxicol*, 4, 391-396.

Incorporation of nHAP, ZnO NPs and T.viride into PCL nanofibers and PCL/PEO blend nanofibers and its application as seed coats

This chapter deals with the characterization of synthesized ZnO NPs and nHAP followed by the optimisation and characterisation of the fabricated PCL, PHZ, PHZT and BHZT nanofibers. The analogous porous polymer film of BHZT_F was prepared. The developed porous membranes were used as *Zea mays* seed coats. The efficiency of seed coats towards controlled release of nutrients was monitored for nanofiber and film coated seeds. The germination studies of coated seeds were performed to evaluate the germination parameters. The antagonistic activity of immobilized biofungicide *T.viride* was studied against pathogenic fungi. Block diagram for seed coating for the study is shown in Fig.III.1.

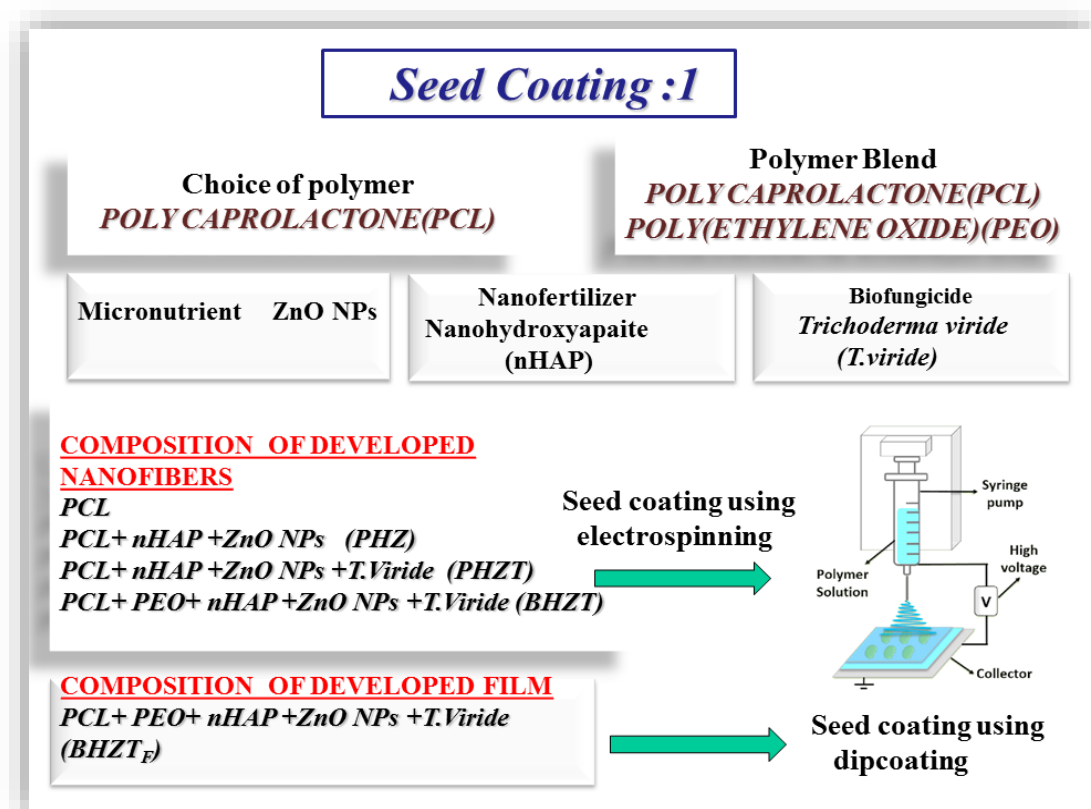


Fig.III.1 Block diagram of methodology for seed coating: 1

3.1 XRD Analysis

The developed nanofibers and all the precursors used in the synthesis of the electrospun membranes ie, nHAP and ZnO NPs were characterized by X-ray diffraction. XRD patterns of ZnO NPs (Fig.III.2a) has characteristic crystalline Bragg reflections at 31.6° , 34.3° , 36.11° , 47.44° , 56.73° , 62.8° , 67.8° , 68.8° , 46.72° and 76.98° (JCPDS 36-1451). Fig.III.2b shows the XRD pattern of the nHAP. The Bragg diffraction peaks closely matched those of conventional nano-HAP² at 25.9° , 31.7° , 32.9° , 39.6° , 49.4° and 53.1° which are the 2θ values, and have the following indices: (002), (210), (211), (112), (300) and (220) (JCPDS File No. 89-6440)

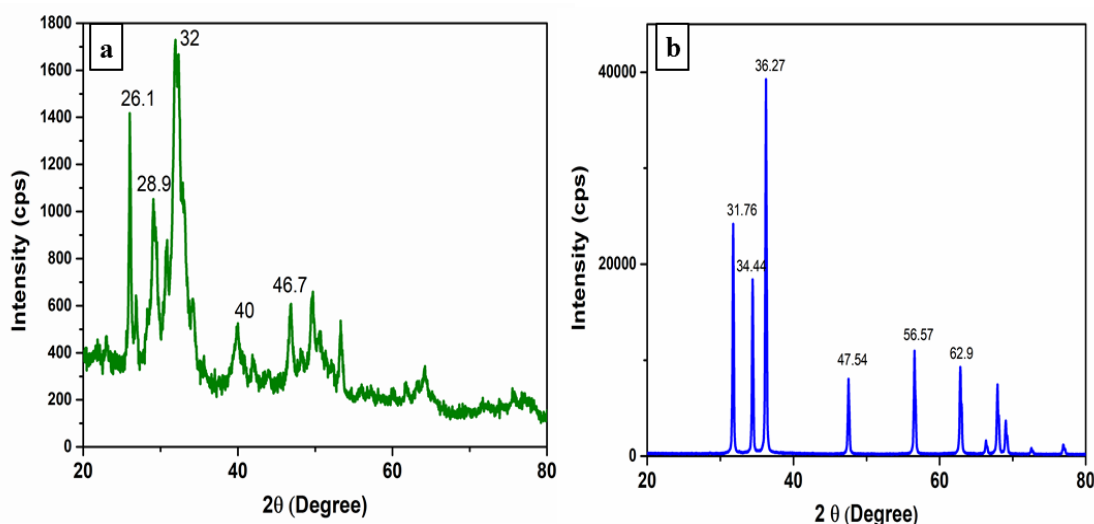
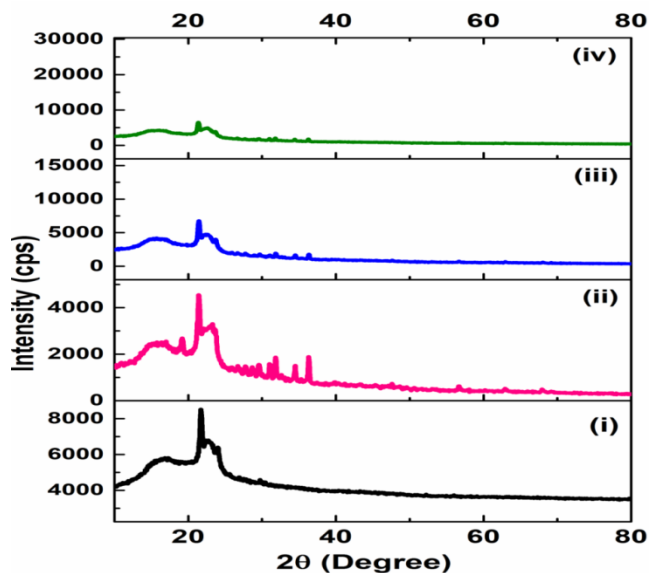


Fig.III.2 XRD diffractogram of a) nHAP b) ZnO NPs

In the case of PCL nanofibers (Fig.III.3i), two major peaks appeared at $2\theta = 21.3^\circ$ and 23.8° , attributed to the diffraction of (110) and (200) lattice planes indicate semi-crystalline nature³. The nanofibers PHZ, PHZT and BHZT showed (Fig.III.3 ii-iv) three new peaks at diffraction angles at 26.1° (002), 31.7° (211) and 32.4° (112), which may be attributed to the characteristic diffraction angles of crystalline nHAP and ZnO NPs. This clearly indicates the successful incorporation of nHAP and ZnO NPs within the nanofiber. These XRD patterns of nanofibers showed that there was no formation of a new crystal phase. The crystalline diffraction peaks of neat PCL nanofiber showed a broadening and a decrease in intensity in agricultural loaded nanofibers, indicating an amorphous behaviour, which is attributed to the degradation of the ordered structure during the preparation of electrospinning solution. Moreover, the fillers hindered the crystallization and facilitated the

formation of an amorphous structure of PCL. The XRD data show that the crystallinity of PCL is more sensitive to the addition of PEO. The unassigned peaks in the spectrum of BHZT suggest the presence of organic materials from fungal cells.



**Fig.III.3 XRD Diffractogram of nanofibers i) PCL ii) PHZ iii) PHZT
iv) BHZT**

3.2 FTIR Study

Fig.III.4 displays FTIR spectra of the synthesized ZnO NPs, nHAP, *T.viride* and the prepared membranes. In the case of PCL (Fig.III.4a(i)) the peaks at 2945 cm^{-1} and 2869 cm^{-1} indicates asymmetric and symmetric CH_2 stretching vibrations respectively. Carbonyl stretching vibration is observed at 1721 cm^{-1} . C–C stretching in the crystalline phase is observed at 1250 cm^{-1} . In nHAP (Fig.III.4a(ii)) the peaks at 1461 cm^{-1} and 1025 cm^{-1} are due to the asymmetric stretching vibrations of CO_3^{2-} and PO_4^{3-} respectively. The out of plane bending mode of CO_3^{2-} is observed at 948 cm^{-1} . The peak at 555 cm^{-1} is due to asymmetric bending vibration of PO_4^{3-} . The functional groups of the nHAP observed from FTIR spectra analyses are compared to literature and confirmed the successful synthesis of nHAP⁴. The spectrum of ZnO NPs in Fig.III.4a(iii) showed a peak at 421 cm^{-1} attributing to Zn–O stretching vibrations^{5,6}. As shown in Fig.III.4a(iv), *T.viride* had a broad band around 3335 cm^{-1} which was assigned to the overlapping of O–H and N–H stretching vibrations⁷. The peaks at 2927 cm^{-1} , 2260 cm^{-1} , 1641 cm^{-1} and 1018 cm^{-1} were

attributed to stretching vibrations from C-H of alkane, $C\equiv N$ of amide and bending vibrations of C=O of amide and C-O of ester or ether respectively.

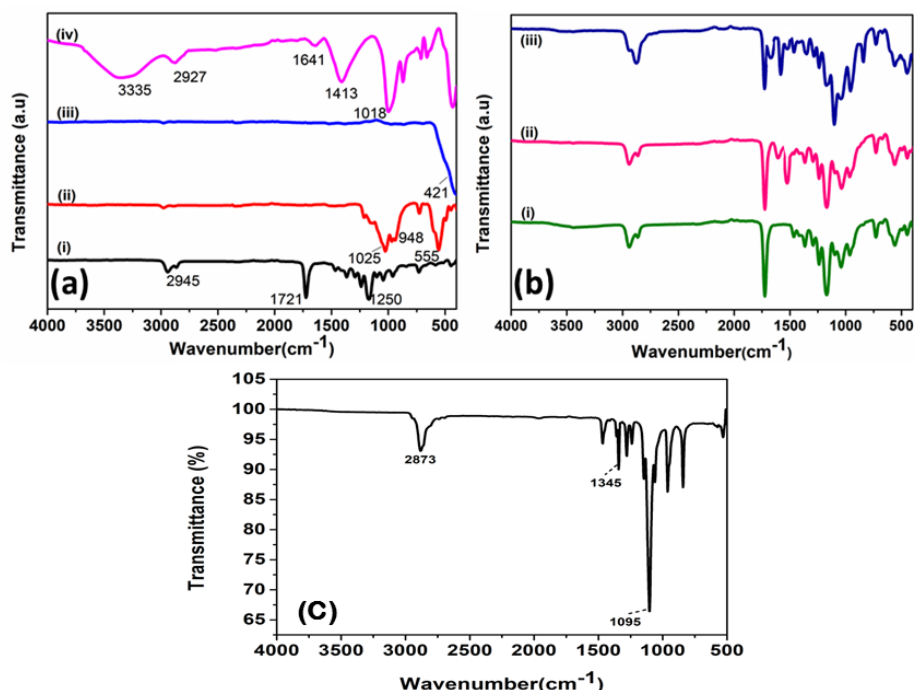


Fig.III.4 FTIR spectra of a) i) PCL ii) nHAP iii) ZnO NPs iv) *T.viride* b) i) PHZ ii) PHZT iii)BHZT c) PEO

FTIR spectrum of PEO is shown in Fig.III.4c. The strong peak at 1095 cm^{-1} represents C-O-C stretching vibration. The peak at 1345 cm^{-1} is assigned to CH_2 bending and the peak at 2873 cm^{-1} corresponds to C-H symmetric stretching vibration⁸.

The IR bands of PHZ, PHZT and BHZT was observed in Fig.III.4b(i- iii) respectively. The peak appeared around 420 cm^{-1} in all the samples revealed the presence of Zn-O absorption bands and confirms the incorporation of ZnO NPs. The peaks around 2257 cm^{-1} , 1645 cm^{-1} and 1000 cm^{-1} exhibited in PHZT (Fig.III.4(b(ii))) and BHZT (Fig.III.4b(iii)) specifies the stretching vibrations from $C\equiv N$ of amide and bending vibrations of C=O of amide and C-O of ester or ether groups of *T.viride*. For BHZT nanofibers, all characteristic peaks corresponding to PCL, PEO, nHAP, ZnO NPs and *T.viride* were observed. This shows successful unification of fillers into BHZT nanofibrous membrane.

3.3 Study of the Morphology

3.3.1 SEM Analysis

The SEM images of ZnO NPs and nHAP are depicted in Fig.III.5a and b. The morphology of synthetic ZnO nanostructures is spherical nanoparticles (SNPs) with an average size of 98.72 nm. Fig.III.5b displays the SEM images of the prepared hydroxyapatite nanoparticles. The hydroxyapatite nanoparticles have a mean diameter of 95.36 nm and a spherical shape with more aggregation.

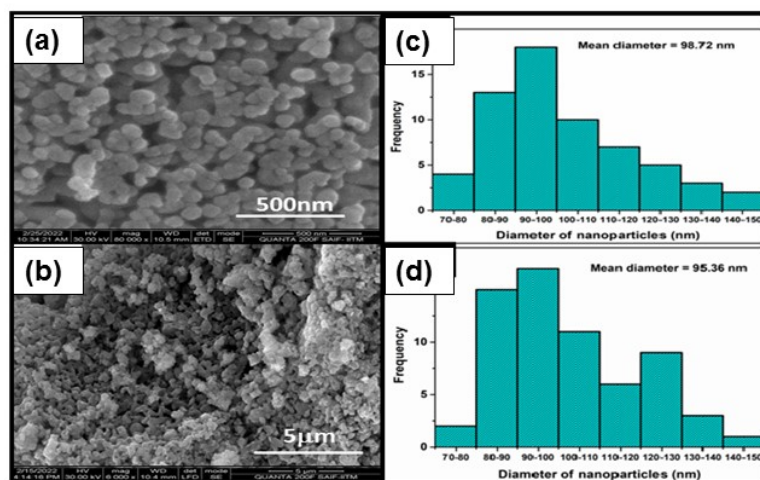


Fig.III.5 SEM images of a) ZnO NPs b) nHAP Histogram bar chart of c) ZnO NPs d) nHAP

The electrospinning solution preparation of PCL/PEO based blended nanofibers was done using the optimal process parameters that produced homogeneous, bead-free PCL nanofibers. Three different PCL/PEO blending ratios (75/25, 50/50 and 30/70 w/w) were used to make nanofibers. The smooth, uniform and bead-free fibers were observed in blend B3.

The variations in average diameter and beading morphologies were seen, as shown in Fig.III.6. However, in PCL/PEO blended nanofibers (PCL/PEO: 75/25 and 50/50 w/w), bead defects increased with PCL concentration. This is explained by the fact that PCL-based electrospinning solutions in chloroform and DMF have lower solution viscosities than PEO, which is caused by a big difference in their average molecular weights. The beaded morphologies and average diameter variations were

observed as shown in Fig.III.6. However, bead defects were observed to increase with PCL content amongst PCL/PEO blended nanofibers (PCL/PEO: 75/25 and 50/50 w/w). As a result, for solutions containing a high concentration of PCL, electrostatic forces produced by the application of high voltages have an impact on the continuity of the jet, which leads to the production of beaded morphologies⁹. Conversely, for PEO rich blends (PCL/PEO: 30/70 w/w), an increase in average electrospun fiber diameter and a subsequent decrease in beaded morphologies are attributable to their greater solution viscosities, which boost their capacity to achieve a continuous stable jet with Taylor cone formation. Thus the morphology and fiber diameter of the blended fibers are significantly influenced by the concentration and composition of the polymer solution used for spinning.

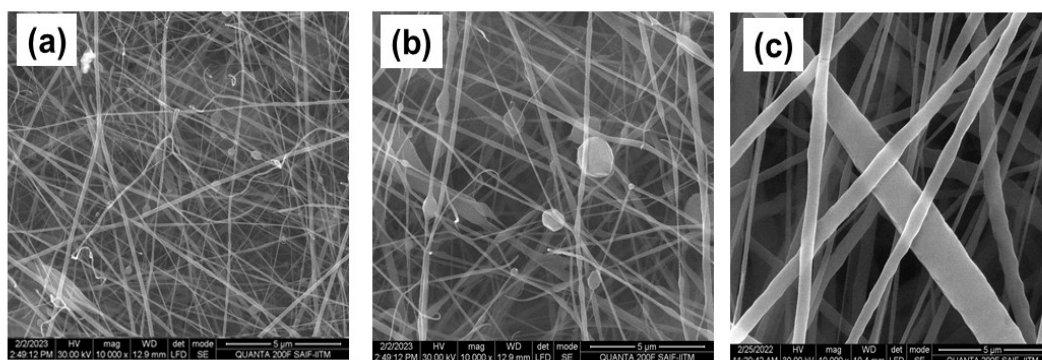


Fig.III.6 SEM image of PCL/PEO nanofiber with different blend ratio

**a) B1 (PCL/PEO: 75/25) b) B2 (PCL/PEO: 50/50)
c) B3 (PCL/PEO: 30/70)**

The SEM micrographs of PCL, PHZ, PHZT and BHZT indicates the formation of ultrafine continuous fibers as shown in Fig.III.7(ia-iva) respectively. The SEM analysis shows (Fig. III.7ia) diameter of electrospun pristine PCL nanofibers is 276nm. The nutrient incorporated PHZ, PHZT and BHZT nanofibers (Fig.III.7(ia – iva)) showed a decrease in diameter from 119.5nm to 98nm. Higher reduction in diameter observed for *T.viride* incorporated nanofibers which might be caused by the colonization of spores of *T.viride* within the fibers. It is assumed that the addition of nHAP and zinc increased the solution's conductivity and the surface charge density of the solution jet. It is well known that a solution's conductivity will decrease with increase in fiber diameter. This can be explained by the fillers acting as a plasticizer and the polymeric solution becoming less viscous. A polymer solution with a higher

viscosity resists elongation during the electrospinning process. In other words, by reducing the viscosity of the polymer solution, the injected jet can be stretched and elongated further, producing finer fibers. Thus the fiber diameter and structure of the fibers are significantly influenced by the content of the polymer solution used for spinning¹⁰. The homogeneous dispersion of the polymer coating on the seed surface is ensured by the high surface area of the PCL nanofibers.

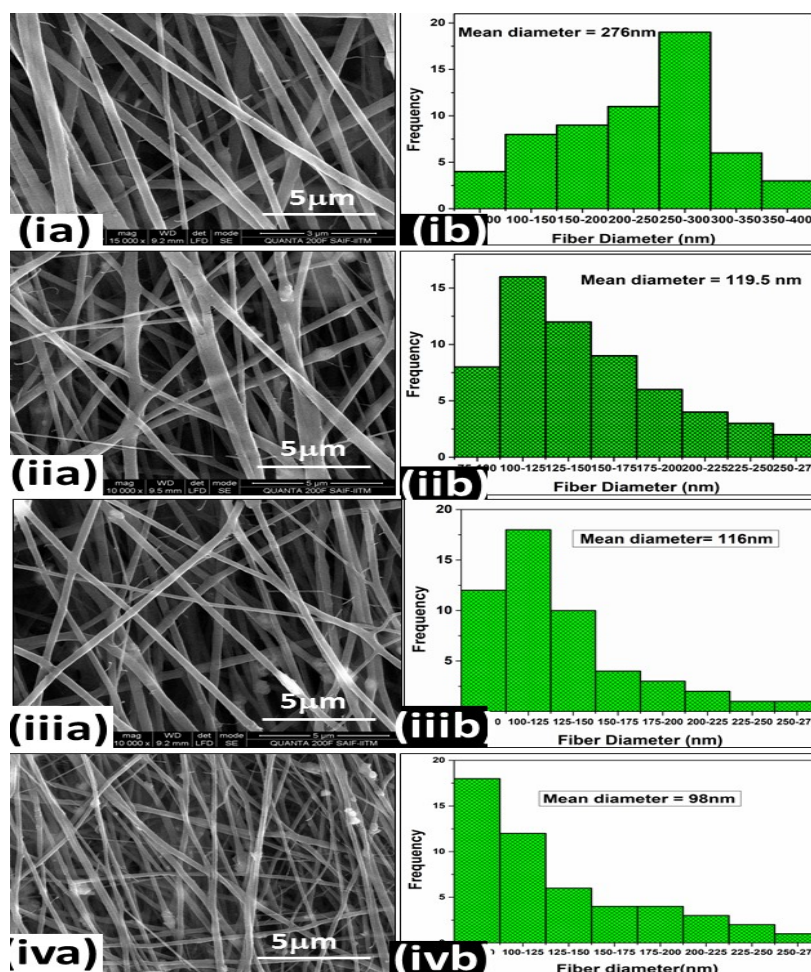


Fig.III.7 (ia-iva) SEM images of nanofibers ia) PCL iia) PHZ iiia) PHZT iva) BHZT (ib-ivb) Histogram bar chart of ib) PCL iib) PHZ iiib) PHZT ivb) BHZT

SEM image of BHZT_F (nHAP, ZNO NPs and *T.viride* incorporated PCL/PEO films), shows that the nanoparticles are spread unevenly on the surface (Fig.III.8). The morphology of film shows low degree of porosity. By incorporating ZnO NPs into PCL nanofibers, nitrogen fixing in leguminous plants is enhanced due to increased nitrogenase enzyme activity during germination¹¹. The diameter of PCL, PHZ, PHZT

and BHZT fibers taking 50 fibers at random plotted in the histogram bar chart as shown in Fig.III.7(ib-ivb). The nutrient loaded PHZ, PHZT and BHZT are found to have more fibers with lesser diameters than the pristine PCL.

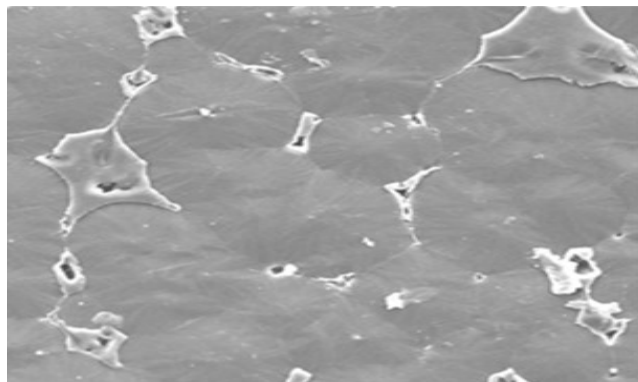


Fig.III.8 SEM images of BHZT_F

3.3.2 EDX Spectrum of nHAP, PHZ and BHZT Nanofibers

The EDX spectrum of synthesized nHAP is depicted in Fig.III.9(i). The EDX of nHAP shows the presence of Ca and P in stoichiometric ratio as in hydroxyapatite. This reveals the successful formation of hydroxyapatite. EDX (Fig. III.9(ii)) and elemental mapping of the PHZ nanofibers (Fig.III.9(iii)) also confirmed the presence of carbon, calcium, phosphorus, oxygen and zinc in the PHZ membrane indicating that nHAP and ZnO nanoparticles are successfully incorporated in the PHZ fiber.

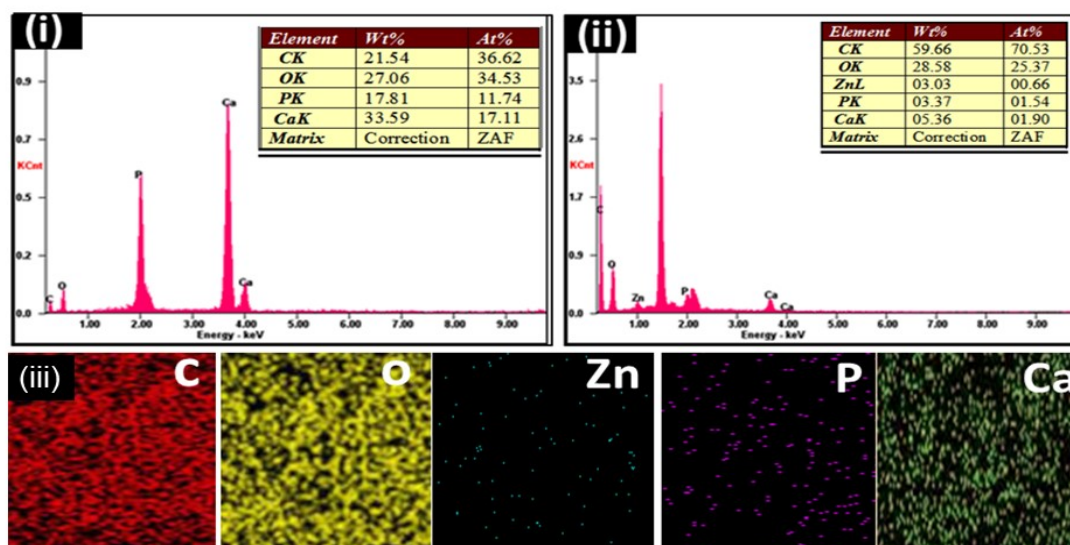


Fig.III.9 EDX spectrum of i) nHAP ii) PHZ iii) Elemental mapping of PHZ

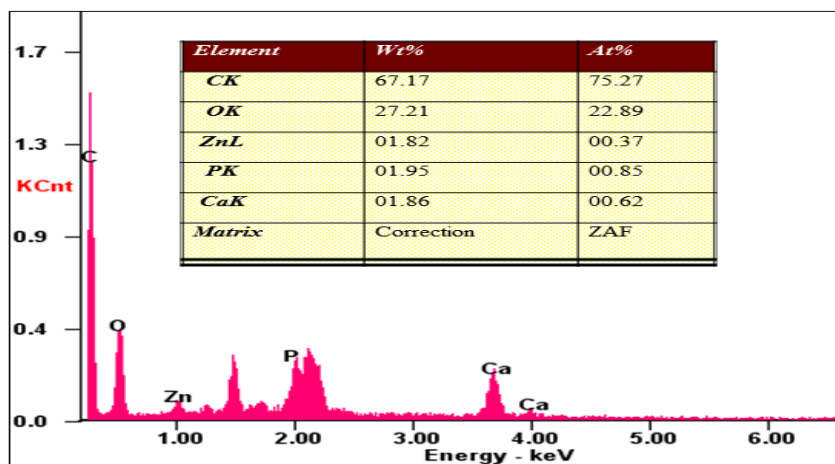


Fig.III.10 EDX spectrum of BHZT nanofiber

The EDX spectrum of BHZT nanofibers shown in Fig.III.10 also confirmed the presence of carbon, calcium, phosphorus, oxygen and zinc in the BHZT membrane. This indicates that nHAP and ZnO nanoparticles are successfully incorporated in the BHZT fiber.

3.3.3 TEM Analysis

TEM analysis of PHZ (Fig.III.11) revealed the presence of nanoparticles inside the fiber but they were not uniformly distributed, NPs were agglomerated along the fiber direction. These results supported the grafting of nHAP and ZnO NPs in the polymer matrix.

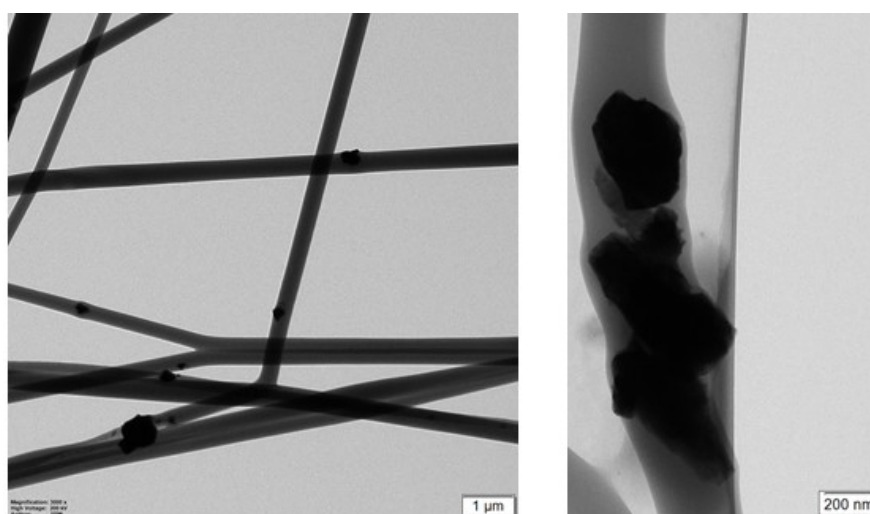


Fig.III.11 TEM images of PHZ nanofiber

3.4 Thermal Analysis

The thermal stability of prepared membranes were analysed by thermogravimetric analysis (TGA) (Fig.III.12). According to TGA curve (Fig.III.12i), PCL has a degradation temperature in the range from 290°C to 430°C, with a maximum decomposition at 363°C. For PHZ, the transition region shifted to 381°C showing better thermal stability due to incorporation of nHAP and ZnO NPs on the PCL matrix as plotted in Fig.III.12ii. TGA curve of pure PEO (Fig.III.12iii) showed major weight loss at about 268°C and decomposes completely at 341°C. The decomposition of the PEO matrix may be due to thermal degradation or random chain scission of C-O bonds in PEO. It can be observed that degradation temperature of PHZT (Fig.III.12iv) starts at 271°C and completes at 350°C by the addition of *T.viride*. In TGA analysis of BHZT, weight loss occurred at 215°C–321°C is related to the C-O bond breaking of polymers in the blend and decomposition of organic *T.viride* spores (Fig.III.12v). The blend nanofiber also shows a second stage degradation starts at 334°C and completes at 406°C. This corresponds to the depolymerisation of the polymer into monomer occurred most frequently during the thermal degradation of the polymer. Due to the addition of *T.viride* which caused plasticity in the sample, there was a slight decrease in the decomposition temperature of PHZT and BHZT compared to PHZ. The addition of nanoparticles increases the char yield of composite nanofibers. These variations in the degradation temperature of the electrospun nanofibers could be due to interactions between the filler material and the electrospun fiber matrix, which in turn depends on the dopants specific surface area and its distribution in the polymer matrix¹². From the results, all the prepared materials possess good thermal stability, which make them suitable for seed coating applications.

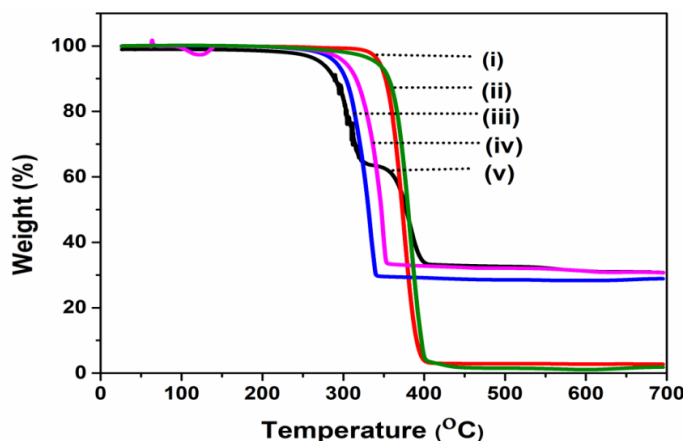


Fig.III.12 TGA thermogram of i) PCL ii) PHZ iii) PEO iv) PHZT v) BHZT

3.5 Porosity Measurements

Table III.1 shows the porosity measurements of synthesized polymer membranes as calculated from Equation 2.6.

Table III.1 Porosity values of developed membranes

Polymer membrane	PCL	PHZ	PHZT	BHZT	BHZT _F
P(%)	80	87	93	98	25

The maximum porosity of 98% was observed for BHZT. The developed polymer film shows very low degree of porosity. The early germination rate is aided by factors like porosity, pore size and specific surface area which facilitate gas and active component diffusion. Despite the fact that both fiber and film have the same components, morphological difference and high porosity makes the fiber a superior seed coat over conventional polymer films. This is in consistent with germination data. Polymer film having low porosity inhibits the movement of gases between the internal structure and the external environment. Polymer films with low porosity prevent the flow of gases between the internal structure of seed and environment.

3.6 Study of Aqueous Solution of Nanofibers and Seeds

3.6.1 Swelling and Stability Studies of Nanofibers in Water

The developed fibers and films were soaked in water for 36 h and weights were monitored at regular time intervals. The swelling percentage is calculated by substituting the weights in Equation 2.7. The degree of swelling is one of the important factors in controlling the release rate of ingredients loaded in the fibers. Swelling properties depend on the hydrophilic/hydrophobic nature of nanofibers. Fig.III.13a shows the swelling studies of the prepared nanofibers and films. As PCL is a hydrophobic polymer the swelling percentage increased very slowly in the first 10h (Fig.III.13a(i)). The swelling of PCL in water is attributed to the porous structure of nanofibers. The swelling percentage of PHZ, PHZT and BHZT increased in the first 5 h and then showed a sustained patterns in Fig.III.13a(ii-iv). This is due to the added hydrophilic components in these fibers. The BHZT_F film swells at lower rate owing to less porous nature of prepared film (Fig.III.13a(v)).

The stability of the samples were studied using Equation 2.8 and are shown (Fig.III.13b). The weight loss in an aqueous solution typically corresponds to the polymer's index of instability. The weight loss is inversely correlated with the stability of the polymer in aqueous solution. PCL is water insoluble hence it is expected to remain after 36 h. Hydrophobic nature of PCL is reduced by the addition of nHAP and ZnO NPs.

The stability of film is very lower than nanofibers because of the dissolution of ions or particles on the surface which results in immediate weight loss. Blending of water soluble polymer PEO with PCL makes it a suitable matrix for seed germination by allowing a sustained release of nutrients. Coating the seeds with nanofibers maintains controlled water absorption. The close proximity of nanofibers around seed surface can ensure the protection of seed. The slow swellability of PCL allows the fertilizers stay on seed surface for a prolonged time during the seedling development stages than the hydrophilic polymers which dissolved easily. PHZ nanofibers show swelling percentages about 250% to 300%, which is due to the high porosity of PHZ electrospun nanofibrous mats. This could be explained as the addition of fillers like nHAP with sufficient hydrophilicity increases the porosity¹³. The high swelling

percentage makes the loaded nutrients in the samples to deliver to crops in a programmed manner for use as a nanofertilizer.

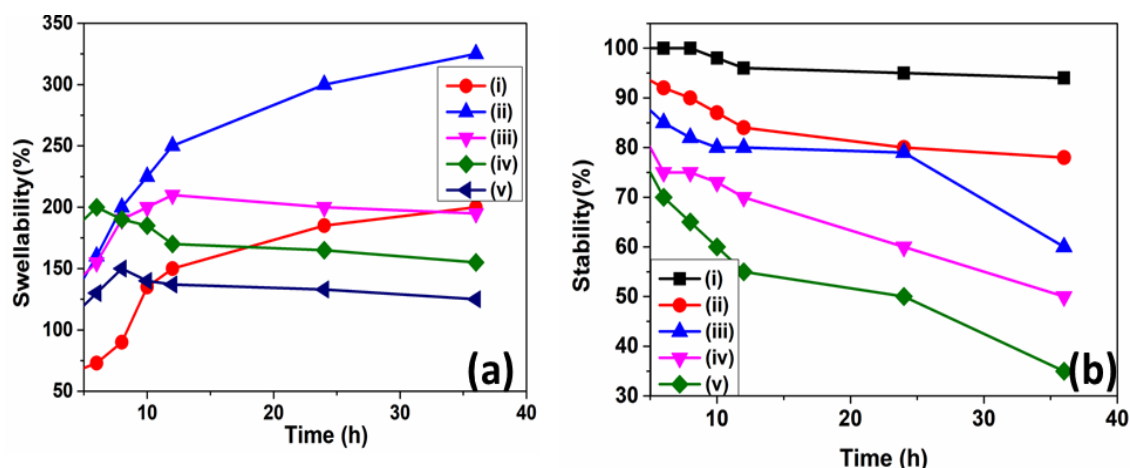


**Fig.III.13 a) Swelling and b) Stability studies of nanofibers
 i) PCL ii) PHZ iii) PHZ iv) BHZT v) BHZT_F**

3.6.2 pH Study

The pH of fabricated nanofibers, film, seeds coated with respective fibers and film were studied over a period of 5 days as the seed germination requires time. The variation of pH of the fibers and film and that of fiber and film coated seeds over a period of 5 days plotted respectively in Fig.III.14a and b. The pH of pristine PCL fibers (Fig.III.14a(i)) was found to be in the range 5 to 5.3. The nutrient incorporated PHZ, PHZT and BHZT fibers have a pH range from 5.4 and 6.5 (Fig.III.14a (ii-iv)). The change in pH is due to the release of nutrients from the fibers into water. The presence of most vital plant nutrients was in the pH range of 5.5-6.2, 5.5 which has been suggested as optimal for plant growth^{14,15}. The nHAP and ZnO NPs incorporated PHZ fibers showed a slight increase in pH within the first 24 h due to the dissolution of phosphate ions (Fig.III.14a(ii)). Both *Trichoderma viride* spores and nanoparticles seem to raise the pH to a favourable range. The gradual increase in pH after 24 h indicated controlled delivery of agrichemicals. The pH of blended fiber BHZT, shows a higher value in the early hours because the blending of PCL with PEO makes the fiber more hydrophilic. After 24 h pH of BHZT follows a sustainable trend making it a better candidate for the regulated release of loaded nutrients. The most significant environmental factor influencing the activity of *Trichoderma* strains is probably pH

dependent¹⁶. Isolates of trichoderma demonstrated optimum growth and sporulation rate at different pH values ranging from 4.6 to 6.8¹⁷. Therefore the immobilisation of *T.viride* spores within the nanofiber allowed a pH environment suitable for the increased efficacy of beneficial microorganism. The high porosity of nanofibers allows the prolonged release of agrichemicals throughout germination stages than traditional film coating. The pH changes of BHZT_F film is plotted in Fig.III.14a(v). The change in pH was found to be at a higher rate for the film compared to the nanofibers in first 3 days. This may be due to the fact that the active ingredients may be available at the surface of film but in the case of nanofibers the agrichemicals are encapsulated within the pores of fibers. The sudden changes in the pH range causes to toxicity to the plant¹⁸.

An increase in pH can be seen for the uncoated seeds in the first 24 h (Fig.III.14b(i)). This increase in pH could be due to the exudates from the seeds which easily dissolve in water indicating high deterioration tendency. Therefore coating of seeds is essential in the early stages of germination. The pH of PCL coated seeds was almost constant as can be seen in Fig.III.14b(ii) and thus protect the seed from damage due to extreme pH changing conditions. Even though the active ingredients are absent in PCL fiber, neat PCL fiber is a good matrix for the protection of seeds. PHZ, PHZT, BHZT fiber coated seeds shows a controlled change in pH (Fig.III.14b(iii-v)) which is due to the controlled release of agrochemicals. The pH range for the PHZ, PHZT and BHZT coated seeds seems to be the most suitable since optimum pH range for corn seed germination is found to be 5.8-6.5. This provides a favourable condition for the growth of *T.viride*. Also it does not show large pH variation and can deliver the essential ingredients at a controlled rate. The pH of film and film coated seeds follow a similar trend as can be seen in Fig.III.14b(vi). The polymer films would not allow easy diffusion of ions and gas exchange due to limited porosity.

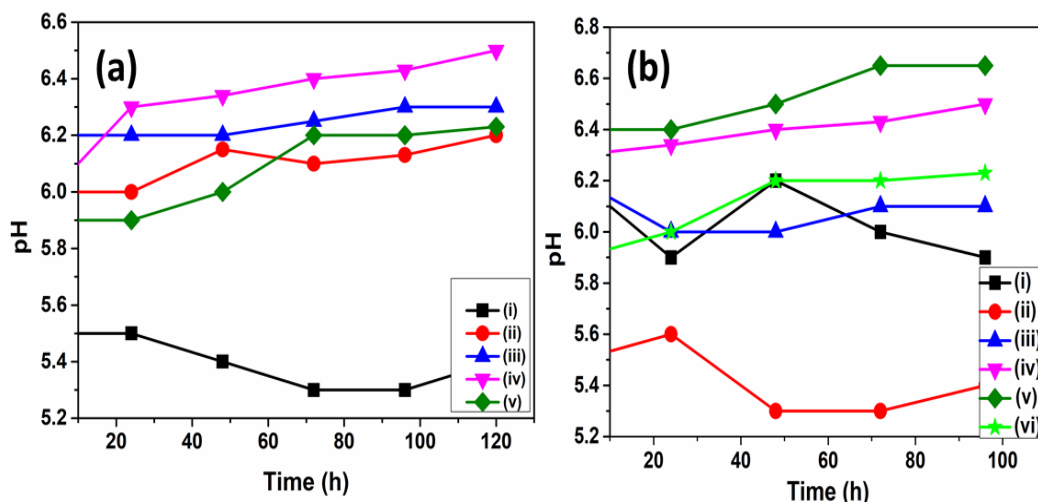


Fig.III.14 a. pH of aqueous solutions of nanofibers and film
 i) PCL ii) PHZ iii) PHZT iv) BHZT v) BHZT_F
 b. pH of i) uncoated seeds ii-vi) seeds coated with nanofibers
 ii) PCL iii) PHZ iv) PHZT v) BHZT vi)BHZT_F

3.6.3 Conductance of the Aqueous Solution of Fibers and seeds

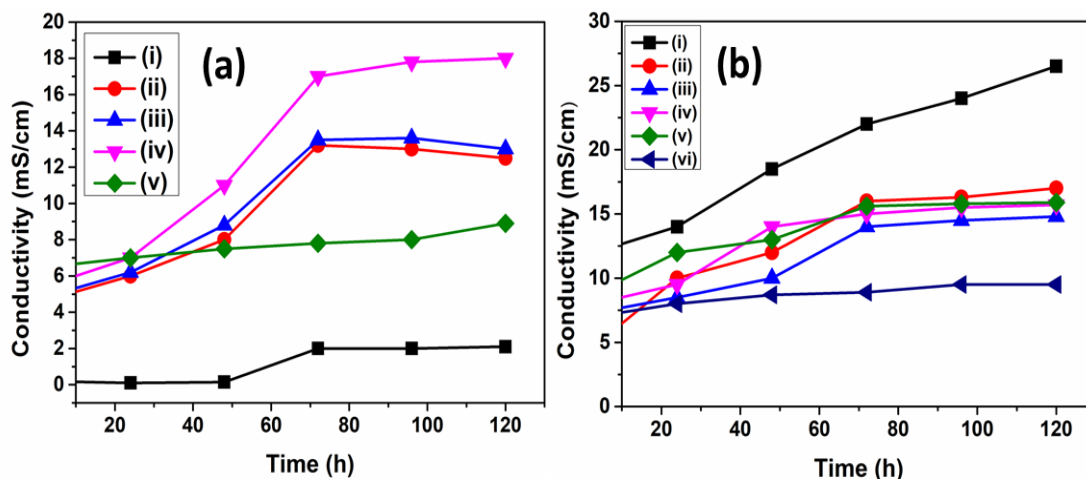


Fig.III.15 a. Electrical conductance of aqueous solutions of nanofibers and film
 i) PCL ii) PHZ iii) PHZT iv) BHZT v) BHZT_F
 b. Electrical conductance of i) uncoated seeds ii-vi) seeds coated with nanofibers
 ii) PCL iii) PHZ iv) PHZT v) BHZTvi) BHZT_F

The conductivity measurements were also determined using the same solutions made for the investigation of pH measurements and the findings are displayed in Fig.III.15a (i to v). The conductivities of the solution were determined for a period of 5 days so as to get constant value. Conductivity measurements in

agriculture were used for the assessment of soil salinity earlier¹⁹. As there are no ions in the pristine PCL fiber, the conductivity of PCL nanofibers is very low as in Fig.III.15a(i). Fig.III.15a(ii) displays the conductance of PHZ nanofiber. The conductivity increased within the first 24 h and then follows a constant pattern. According to the graph, the peak of the nutrient release occurs in the first few hours. This is indicative of the electrospun fibers which have the potential to be an effective seed coating material. Thus the increase in conductivity in nutrient loaded nanofibers could be due to dissolution of metal ions. The imbibition rate and swellability was also found to be high during the first 3 h which is in agreement with observed conductance. For the blended BHZT nanofiber, the conductance is high in first few hours as hydrophilicity of PEO allows dissolution of ions easily than from PHZ and PHZT nanofibers. The general trend line for the film is shown in Fig.III.15a(v). When compared to the corresponding fibers, the conductivity values of the film in water were found to be initially higher but eventually reached a constant value. The conductivity values of the film in water were found to be initially greater than the corresponding fibers but ultimately reached a constant value. The initial high conductivity of film is due to the dissolution of ions on the surface of film.

A reliable measure of seed vigour is the electrical conductance (EC) of seeds in steep water (seeds submerged for 24 h)²⁰. The conductance of the seed soak solution was shown to be inversely proportional to the germination potential. The primary purpose of the EC test was to quantify how much exudate ions, mostly potassium, calcium, and amino acid ions, were being released²¹. Uncoated seeds' conductivity increases rapidly over time (Fig.III.15b(i)). This may be because, as the cell membrane repair was slowed down during water uptake for germination, more exudates were released into the deep water from any damaged seeds. A coating is necessary because untreated seeds were found to have high conductivity, which could cause toxicity in the seed. Hence it is clear that the prepared seed coatings are effective. On comparison of seeds coated with PCL and PHZ (Fig.III.15b(ii) and (iii)), the conductivity was found to be the less for PCL coating. The conductivity was found to increase from PHZ, PHZT to BHZT coated seeds (Fig.III.15b(iii- v)), This is due to the release of ions from the composite fibers. Agrichemicals loaded nanofiber coated seeds exhibits a controlled increase in conductivity but not a drastic increase as in the uncoated seed. This again confirms the controlled release of nutrients and

protection of seeds in the early stages of germination. The BHZT_F film coated seeds' conductivity is low compared to fiber coated seeds because of less porous nature of film which is revealed in Fig.III.15b(vi). The low porosity of film restricts the ions and gas exchange.

3.6.4 Imbibition Studies of Seeds

The seeds were left soaked in the water and the weight change was monitored in every half an hour. Fig.III.16 reveals that the highest amount of water was absorbed during the first three hours which is in agreement with the previous reports²². This is further confirmed by electrical conductance measurements. The first and crucial stage in seed germination is imbibition of seeds in water which converts the dormant seed to a growing embryo. Water absorption via the seed coat induces germination. Corn kernels need to absorb roughly 30% of their weight in water during the initial stage of germination. Germination may be slowed down or prevented by less than optimal water absorption caused by a fast drying seed zone. The uncoated seeds shows (Fig.III.16b(i)) highest imbibition rate of 50% within first 2 h. This drastic increase in imbibition rate may lead to rotting of uncoated seeds. Seeds coated with PHZ, PHZT and BHZT exhibited a greater extent of water uptake (Fig.III.16b(iii-v)) than PCL coated seeds. The lower water uptake of PCL nanofiber is attributed to its high hydrophobic nature. The BHZT coated seeds showed a sustained absorption rate within 3 hours as required for the germination conditions of corn seeds. Additionally, the fibers' pores permit gas exchange between the interior structure and the external environment. The tiny pores in the seed coat may become clogged by the polymer solution during film coating. It is essential for germination that the seed coat's pores are distributed unevenly across the surface and the micropyle. Due to poor porosity after coating, water absorption may not be possible in a film. A controlled rate of water absorption was made possible by the polymer nanofiber coating which also minimised imbibitional damage. Corn seed germination starts in between 24 to 48 h. The controlled absorption rate of water in all nutrient loaded nanofiber coated seeds allows dissolution of fertilizers and micronutrients and can reach the seed in right amount at right time.

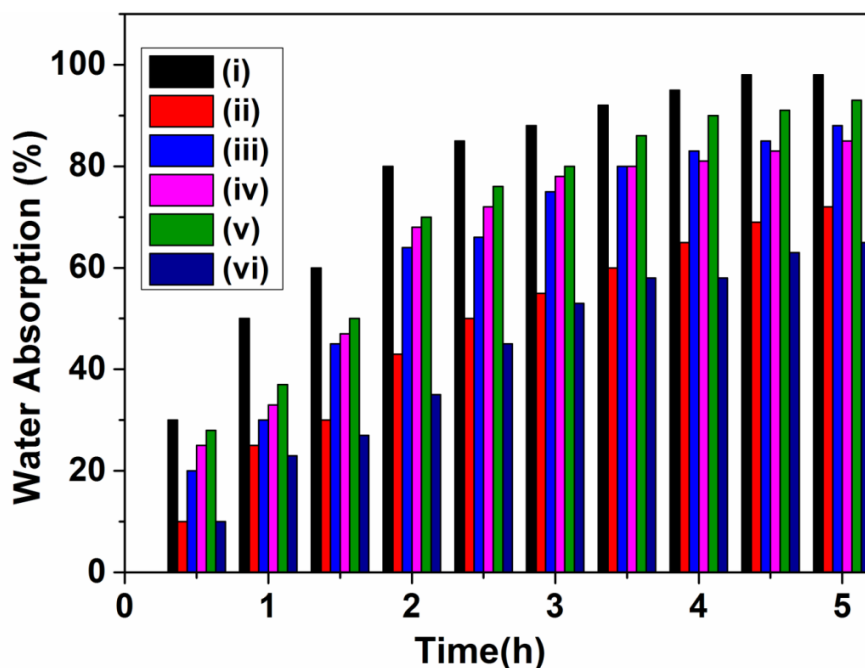


Fig.III.16 Water absorption rate of i) uncoated seeds ii-vi) seeds coated with nanofibers and film ii) PCL iii) PHZ iv) PHZT v) BHZT vi) BHZT_F

3.7 Ca, Zn and P Release Profile Study

Fig.III.17 displays the Ca, P and Zn release profiles of developed nanofibers and film in soil using ICP-OES. Release of elements from nanofibers was slow compared to film. However the release was rapid during the initial 3 days and then it is slowed down. The rate at which Ca, P and Zn released from PHZ after 3 days follows a constant pattern. The release pattern of PHZT follows similar trend as in PHZ release and a very small increase in the amount of metal indicates the slight higher hydrophilicity of PHZT. It is further confirmed by water contact angle analysis. The presence of *T.viride* does not affect the metal release. The BHZT nanofiber shows high release compared to other three owing to the high hydrophilicity of PEO in the blended polymer. After 3 days, BHZT fiber allows a controlled release of nutrients. The data clearly indicated that the polymeric formulation helped to slow the metal release. In the case of BHZT_F porous film the initial increase is due to the dissolution of surface metals. The release pattern from BHZT_F shows a continuous rise and not having a controlled release. The slow release of calcium and phosphorous from nanofibers indicates the low solubility of nanoformulation of HAP. It is important to keep in mind that various seed types may require various nutritional dosages for germination and seedling growth. It is crucial to create a flexible polymer-

based nanoplatform with controllable agrichemical release kinetics so that it can be modified for various types of seed²³. It can be seen from the results that the release of nutrient from the developed nanoplatform can be further tuned by altering the nanofiber chemical composition. Even though high quantity of elemental release is obtained in the case of film it follows an uncontrolled pattern. The results show that nanohydroxyapatite fertilizer increases phosphorus availability to plants and encapsulation of nHAP in nanofibers prevents phosphorus loss. The nanofertilizers used in this study not only provided the plant nutrients during its growth phase, but also stopped too much of these substances from leaching.

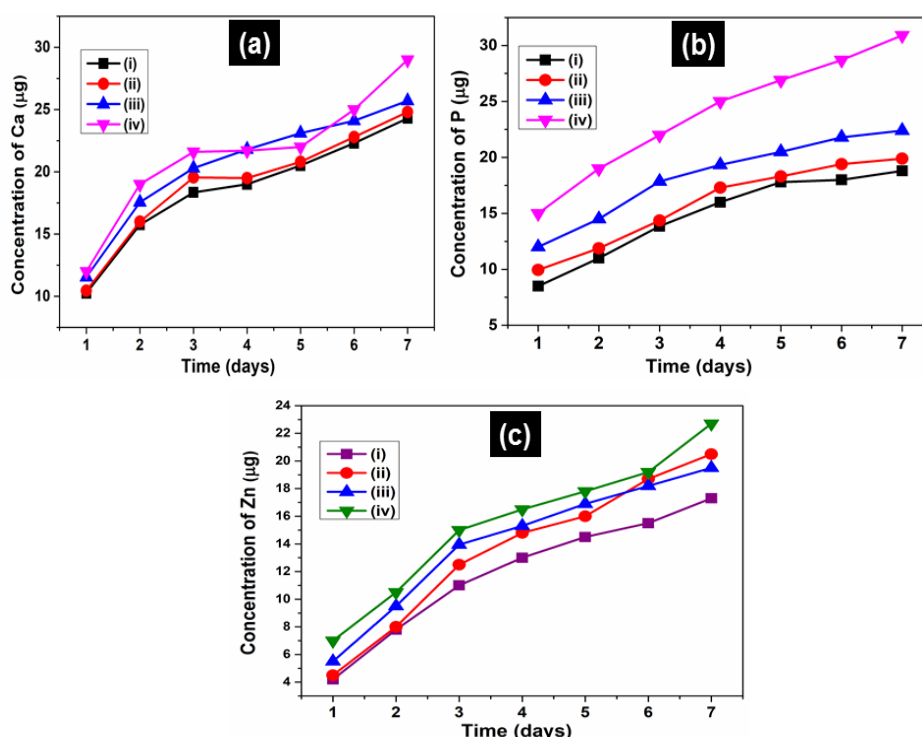


Fig.III.17 Metal release profile of nanofibers a) Ca release pattern b) P release pattern c) Zn release pattern from i) PHZ ii) PHZT iii) BHZT iv) BHZTF

3.8 Surface Wetting Properties of the Electrospun Fibers

Static water contact angle measurements on the nanofibers were used to analyse the surface wetting characteristics of the polymer nanofibrous membranes. From Fig.III.18a and b, it was clear that water contact angle reduced from 119° for pure PCL nanofibers to 90.5° for PHZ nanofibers. This indicates that the surface hydrophilicity of the PCL nanofibrous membrane is increased by the addition of

nHAP and ZnO NPs. The hydrophilic OH group in nHAP has improved the surface wettability of PHZ membrane²⁴. The addition of *T.viride* spores in the nanofiber matrix increase the water contact angle to 110.6° (Fig.III.18c) which is due to the hydrophobic nature of organic matter present in the *T.viride* spores. Blending of PCL with hydrophilic PEO increased the surface wettability and water contact angle in the blended fiber BHZT decreases to 34.6° which is shown in Fig.III.18d. It was considered to be favorable because the porous fibrous structure would allow gases to pass through while the nanofibrous seed coatings would prevent seed degradation due to water absorption during storage. As a result, these materials might be utilised as seed coatings that enable both gas and water exchange.

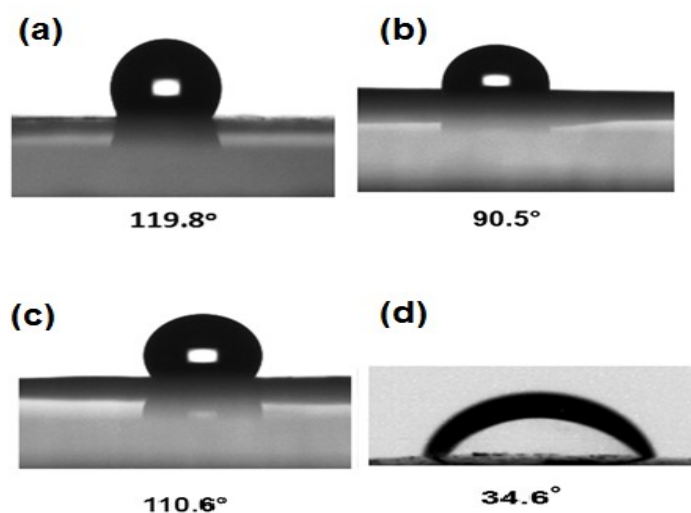


Fig.III.18 Static Water Contact angle measurements of nanofibers
a) PCL b) PHZ c) PHZT d) BHZT

3.9 Germination Studies

Fig.III.19 depicts the germination behaviour of coated and untreated seeds. Five days of germination tests were carried out. When the length of the shoot reached about 4 to 5 cm, it was planted in the soil for further growth²⁵. The germination percentage, germination index, and seed vigour index were all calculated in order to study the germination rate. From each batch, the best six seedlings were chosen for comparison. In this investigation, it was examined how sprouting corn seeds responded to seed coating. It was seen visually that the corn seeds have a substantial growth pattern and high germination features among all subsamples other

than film coated seeds. Seeds coated with BHZT nanofiber showed an enhanced growth potential. It was observed that in the seedlings treated with BHZT, root hairs and nodules had grown longer than in the treatment with PCL nanofiber without any fertilizer.

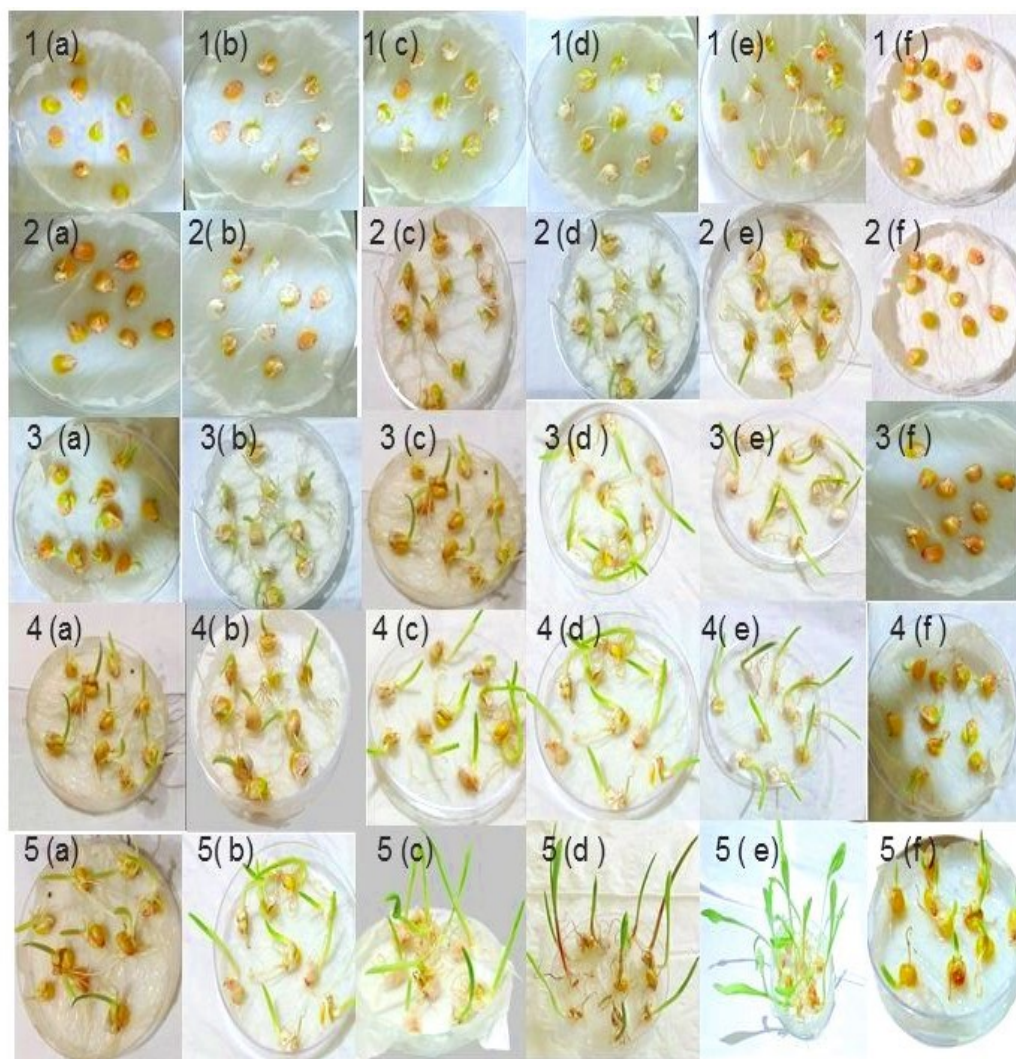


Fig.III.19 Germination of corn seeds a) uncoated seeds b-f) seeds coated with nanofibers and film b) PCL c) PHZ d) PHZT e) BHZT f)BHZT_F after 1) 24 h 2) 48 h 3) 72 h 4) 96 h 5) 120 h

The maize seeds germinated effectively in all of the petri dishes of seeds coated with fibers. Water molecules enter the seed coat during the water uptake mechanism and start to soften the tough, dry tissues inside the seed. Intake of water caused the seed to enlarge, which caused the seed coat to rupture and emerge radicles between 0 and 24 h. The principal source of nutrients for corn seeds' early development is their small life support system, similar to that of other seeds²⁶.

Additionally, water intake increased the turgor pressure within the seed's cell walls, which continually enlarged during growth²⁷. The plumule erupted after the imbibition of the seed coverings and the cotyledons gradually expanded. With time, the radicle and plumule's grew longer. The seeds coated with agricultural loaded fiber had a higher development potential, which could be observed visually. These findings make it obvious that the developed seed coats would promote better germination. The radicle length and plumule length of germinated seeds is shown in Fig.III.20a and b. Availability of calcium, phosphorous and the zinc might be the reason for improved the seedling growth. The availability of a plant growth promoting microbe in the close proximity enhances the seedling development in PHZT and BHZT coated seeds. *Trichoderma* strains are invariably connected to root ecosystems and plant roots. *Trichoderma* strains can colonise plant roots by processes resembling those of mycorrhizal fungi and produce substances that promote plant development and defensive mechanisms²⁸.

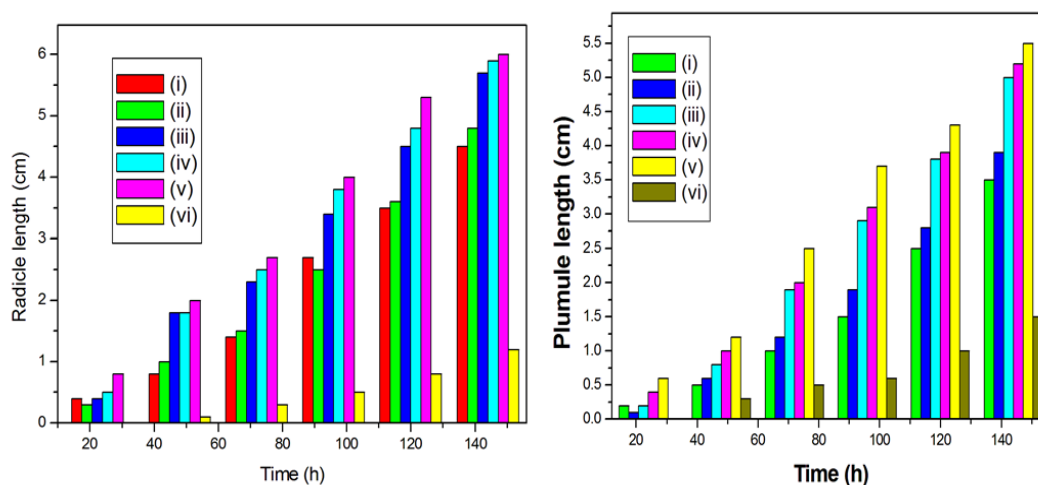


Fig.III.20 a) Radicle length b) plumule length of seeds
i)uncoated ii-vi) coated with ii) PCL iii) PHZ
iv) PHZT v) BHZT vi) BHZT_F

Trichoderma strain colonisation of roots frequently improves root growth and development, crop productivity, tolerance to abiotic stressors, uptake and utilisation of nutrients²⁹. It is worth mentioning that the beneficial trends of the *T.viride* can be seen in results of germination studies and it boost the immune system against *Aspergillus* pathogen as evidenced from microbiological test. The seeds treated with BHZT_F film showed a delayed germination or no significant improvement in growth

compared to controls. During the process of film coating the small pores in the seed may become blocked by the seed coating solution. The air and moisture exchange is restricted in film coating compared to nanofiber coating. From the graphs the germination potential of the seed coating can be graded as follows:

BHZT_F film coated < Uncoated < PCL < PHZ < PHZT < BHZT

3.9.1 Fresh Seedling Biomass

The root, shoot and overall biomass of all treated seedlings were measured after 15 days. Data were standardized to the tissue mass of the untreated control plants to make comparisons easier (Fig.III.21). Without incorporating fertilizers and nutrients in the nanofiber coating, PCL alone is not expected to boost biomass. It is interesting to notice that many of the improvements in germination mentioned above also led to improvements in seedling biomass as stated below. Furthermore BHZT nanofiber coating significantly increased total biomass by 50% possibly because of controlled delivery of nutrients and plant growth promoting microbes (PGPM) to the right place utilizing the properties of high porosity and optimum hydrophobicity of the nanofibrous membrane. The total wet mass of PHZT and BHZT do not differ significantly. The higher biomass of BHZT is due to the hydrophilicity of PEO in the blended fiber that allows diffusion of minerals and nutrients. Colonization of *T.viride* facilitated in a wet environment. Biomass of uncoated and neat PCL nanofiber coated seedlings did not significantly alter whereas total wet mass of film coatings decreased compared to untreated control. This suggests that the impacts of seed coating on plant growth depend on the composition and morphology of coating membrane and also on the loaded fertilizers and nutrients.

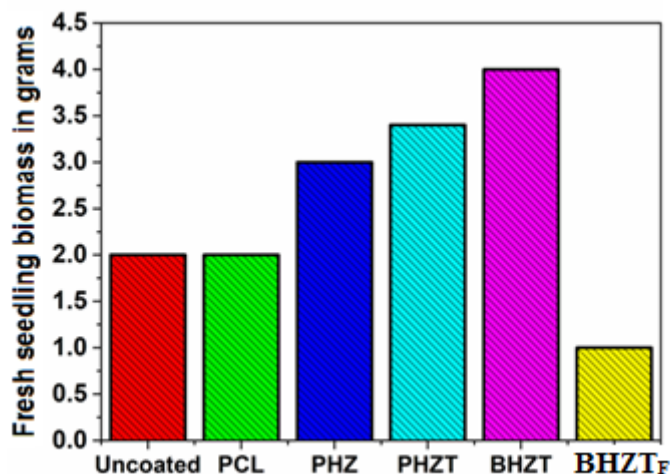


Fig.III.21 Total fresh biomass of corn seedlings grown from seeds coated with developed membranes after 15 days of germination

3.9.2 Statistical Analysis

The germination studies of the six sub samples and their five replicates was performed, and the outcomes were examined. As the results were homogeneous, one way ANOVA was applied to the data. Table III.2 provides the mean and standard deviation for each germination parameter. The Tukey's test ($p < 0.05$) revealed statistically significant differences between the estimated marginal means of germination parameters of fiber and film coated seeds. An entirely random design was used for the statistical analysis of the data using analysis of variance. When the F values were significant, the main and interaction effects were evaluated using Tukey's HSD test at 0.05 level of probability³⁰.

Levene's test revealed a homogeneous germination percentage³¹. No transformation was necessary. As a result, the null hypothesis that the germination percentage (the dependent variable) varied equally among groups was incorrect. According to statistical studies, the addition of nutrients had a substantial impact on the germination percentage and a considerable difference in germination parameters. The addition of *T.viride* and nutrients enhanced the plant growth to a significant extent. But there was no significant difference in germination percentage between the uncoated and PCL nanofiber coated seeds. The neat PCL seed coat does not appear to supply any nourishment at the seed germination stage and nutrition originates from the incorporated nutrients and PGPM only.

TableIII.2 Germination parameters of coated and uncoated seeds

Sample		%Germination (%G)	Germination Index (GI)	Seed Vigour Index (SVI)
Uncoated seeds	Mean	72.00	72.00	256.40
	(SD)	(4.472)	(4.472)	(19.321)
PCL nanofiber coated seeds	Mean	76.00	79.20	293.60
	(SD)	(5.477)	(10.40)	(26.293)
PHZ nanofiber coated seeds	Mean	96.00	134.40	472.00
	(SD)	(5.477)	(7.688)	(20.494)
PHZT nanofiber coated seeds	Mean	97.20	142.30	507.40
	(SD)	(1.304)	(4.868)	(7.403)
BHZT nanofiber coated seeds	Mean	99.40	157.20	556.60
	(SD)	(0.894)	(4.764)	(8.355)
BHZT _F film coated seeds	Mean	64.00	25.20	92.20
	(SD)	(3.082)	(2.588)	(11.234)

The BHZT nanofiber coating produced the greatest rate of germination. Fig.III.22 shows the graphical representation of statistically determined germination parameters for each of the treatments. The graph showed that the percentage of germination for seeds with nutrient-rich seed coats was significantly higher than untreated seeds. The polymer film coated seeds show significantly reduced values for all parameters.

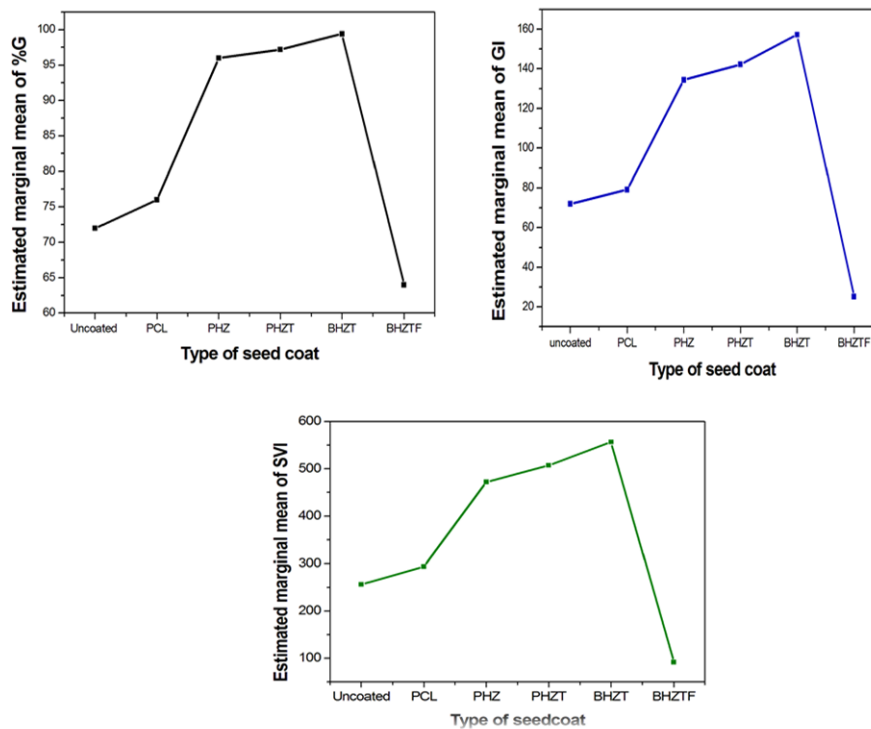


Fig.III.22 Estimated marginal mean for germination parameters

The germination index and seed vigour index investigations also revealed similar pattern. The length of the seedling was used to determine the germination index and seed vigour index. As shown by the Tukey HSD test, the growth of the seedling had been clearly significant in both cases for the treatment. The presence of nutrients and *T.viride* caused a considerable alteration.

3.10 Microbiological Analysis and Dual culture test

Trichoderma strains have been shown to have antifungal efficacy against phytopathogenic fungi^{32,33}. To determine the antagonist viability of the *T.viride* spores incorporated in the nanofibrous mats against pathogenic fungi *Aspergillus*, the biohybrid mats with and without *T.viride* were placed in agar. *T.viride* and the pathogenic fungus *Aspergillus* were grown separately in different plates for the purpose of comparison as seen in Fig.III.23a and b. In the BHZT sample, it is seen that the *T.viride* spores are incorporated in the fibers, *Trichoderma* spores are found to grow and reproduce normally.

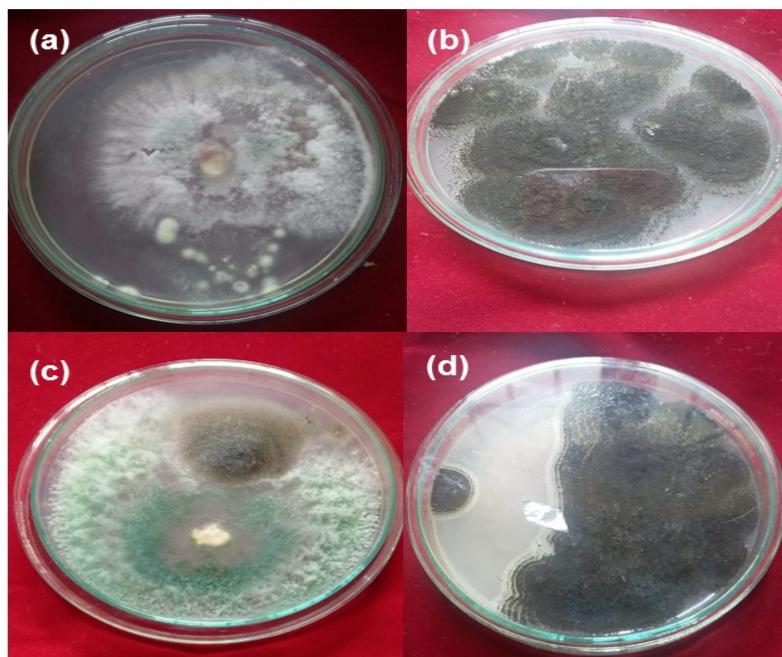


Fig.III.23 a) The growth of *T.viride* spores alone b) *Aspergillus* alone
 c) The growth of *Aspergillus* in presence of BHZT d) The growth of
Aspergillus in presence of PHZ after 5 days inoculation

As seen in Fig. III.23a and b after incubating for 5 days, all the fungi (*T.viride* and *Aspergillus*) placed in separate dishes grew normally and the fungal colonies colonized well. When the BHZT nanofiber mat containing spores of *T.viride* were placed against *Aspergillus*, clear inhibition of the growth of the phytopathogenic *Aspergillus* strains was detected (Fig.III.21c). It was observed that *T.viride* placed at the same conditions grew much faster than the pathogenic fungi did. *T.viride* has an edge over pathogenic fungus in the struggle for nutrients and space as a result of its rapid development. In addition, *T.viride* releases extracellular hydrolytic enzymes that target and destroy the pathogen's cell walls directly. The colonization of *Aspergillus* is high in PHZ due to the absence of *T.viride*. The growth of pathogen is occurred in PHZ but compared to growth of *Aspergillus* alone in Fig.III.21b the colony diameter is shorter in PHZ placed petri dish. This may be attributed to the antifungal activity of ZnO NPs. Results of dual culture test shows that the spores embedded into the fibrous mats are alive and mature *T. viride* still has the capacity to stop phytopathogen growth.

Conclusion

A sustainable, nontoxic nanoplatform was developed using electrospinning and used for seed coating. By varying the chemical composition of nanofibers, this technique provides controllable agrichemical release kinetics. This versatile nanofiber platform precisely delivered agrichemicals in the close proximity of the seed during germination stages. It is worth highlighting that the various seed coats developed from PCL nanofiber loaded with active ingredients appeared to promote seed germination of *Zea mays* seeds and provide a promising approach to protect seeds in pathogen infested soil. The high germination percentage, germination index and seed vigour index led to increased seedling biomass in the nHAP/ZnO NPs/*T.viride* incorporated PCL/PEO blended nanofiber (BHZT). Even though there is no significant difference in the germination rate of seeds coated with pristine PCL nanofiber and control, PCL coating provide a sustainable environment to developing embryo by providing optimum retention of moisture and protecting the seed directly from harmful pathogens. However the porous polymer film, BHZT_F had not shown any improvement in germination and seedling biomass. The developed nanofiber seed coating approach significantly improved seedling biomass than conventional film coating approaches utilized by the industry. This inhibited gas and water exchange which hindered radicle and plumule emergence during the germination. The antagonistic activity of immobilised *T.viride* spores, a plant beneficial microorganism against *Aspergillus* pathogenic fungi proved the use of such nanofiber seed coating protection as a powerful and versatile platform to enable plant growth in pathogen infested soils.

A further in-depth mechanistic investigation will be planned in the future because the exact processes causing the variable effects of the nanofibers depending on plant type or disease condition are still unknown. A variety of micro- and macronutrients as well as other analytes, as such growth stimulants or antimicrobial compounds that extend shelf life, can easily be delivered using this platform. This study is expected to open the door to new advancements in fertilizer administration methods, dosage and types used in sustainable agriculture.

References

1. Ramimoghadam, D., Bin Hussein, M. Z., & Taufiq-Yap, Y. H. (2013). Hydrothermal synthesis of zinc oxide nanoparticles using rice as soft biotemplate. *Chemistry Central Journal*, 7, 1-10.
2. Bouyer, E., Gitzhofer, F., & Boulos, M. I. (2000). Morphological study of hydroxyapatite nanocrystal suspension. *Journal of Materials Science: Materials in Medicine*, 11(8), 523-531.
3. Mirica, I. C., Furtos, G., Lucaciu, O., Pascuta, P., Vlassa, M., Moldovan, M., & Campian, R. S. (2021). Electrospun Membranes based on polycaprolactone, nano-hydroxyapatite and metronidazole. *Materials*, 14(4), 931.
4. Choi, D., Marra, K. G., & Kumta, P. N. (2004). Chemical synthesis of hydroxyapatite/poly (ϵ -caprolactone) composites. *Materials Research Bulletin*, 39(3), 417-432.
5. Yang, K., Lin, D., & Xing, B. (2009). Interactions of humic acid with nanosized inorganic oxides. *Langmuir*, 25(6), 3571-3576.
6. Zak, A. K., Razali, R., Majid, W. H., & Darroudi, M. (2011). Synthesis and characterization of a narrow size distribution of zinc oxide nanoparticles. *International journal of nanomedicine*, 6, 1399–1403.
7. Juric, S., Dermic, E., Topolovec-Pintaric, S., Bedek, M., & Vincekovic, M. (2019). Physicochemical properties and release characteristics of calcium alginate microspheres loaded with *Trichoderma viride* spores. *Journal of Integrative Agriculture*, 18(11), 2534-2548.
8. Luo, D., Geng, R., Wang, W., Ding, Z., Qiang, S., Liang, J., & Fan, Q. (2021). *Trichoderma viride* involvement in the sorption of Pb (II) on muscovite, biotite and phlogopite: Batch and spectroscopic studies. *Journal of Hazardous Materials*, 401, 123249.
9. Sharma, D., & Satapathy, B. K. (2022). Optimization and physical performance evaluation of electrospun nanofibrous mats of PLA, PCL and their blends. *Journal of Industrial Textiles*, 51(4_suppl), 6640S-6665S.
10. Wang, M., Fang, D., Wang, N., Jiang, S., Nie, J., Yu, Q., & Ma, G. (2014). Preparation of PVDF/PVP core-shell nanofibers mats via homogeneous electrospinning. *Polymer*, 55(9), 2188-2196.
11. Krishnamoorthy, V., & Rajiv, S. (2017). Potential seed coatings fabricated from electrospinning hexaaminocyclotriphosphazene and cobalt nanoparticles incorporated polyvinylpyrrolidone for sustainable agriculture. *ACS Sustainable Chemistry & Engineering*, 5(1), 146-152.

12. Patlolla, A., Collins, G., & Arinzeh, T. L. (2010). Solvent-dependent properties of electrospun fibrous composites for bone tissue regeneration. *Acta biomaterialia*, 6(1), 90-101.
13. Bertram, U., & Bodmeier, R. (2006). In situ gelling, bioadhesive nasal inserts for extended drug delivery: in vitro characterization of a new nasal dosage form. *European journal of pharmaceutical sciences : official journal of the European Federation for Pharmaceutical Sciences*, 27 1, 62-71 .
14. Chen, H., & Yada, R. (2011). Nanotechnologies in agriculture: new tools for sustainable development. *Trends in Food Science & Technology*, 22(11), 585-594.
15. Krishnamoorthy, V., Elumalai, G., & Rajiv, S. (2016). Environment friendly synthesis of polyvinylpyrrolidone nanofibers and their potential use as seed coats. *New Journal of Chemistry*, 40(4), 3268-3276
16. Kredics, L., Antal, Z., Szekeres, A., Hatvani, L., Manczinger, L., Vagvolgyi, C. S., & Nagy, E. (2005). Extracellular proteases of *Trichoderma* species. *Acta microbiologica et immunologica hungarica*, 52(2), 169-184.
17. Bandyopadhyay, S., Jash, S., & Dutta, S. (2003). Effect of different pH and temperature levels on growth and sporulation of *Trichoderma*. *Environment and Ecology*, 21(4), 770-773.
18. Mickelbart, M.V., Stanton, K.M., Camberato, J.M., & Lee, B.D. (2007). *Purdue extension publication*, HO-240-W, 1-4
19. Corwin, D. L., & Lesch, S. M. (2005). Apparent soil electrical conductivity measurements in agriculture. *Computers and electronics in agriculture*, 46(1-3), 11-43.
20. Matthews, S., & Powell, A. (2006). Electrical conductivity vigour test: physiological basis and use. *Seed Testing International*, 131(131), 32-35.
21. Marcos Filho, J. (2015). Seed vigor testing: an overview of the past, present and future perspective. *Scientia agricola*, 72, 363-374.
22. Rathinavel, K. (2015). Extension of shelf life of cotton (*Gossypium hirsutum* L.) seeds through polymer coating under ambient storage condition. *Indian Journal of Agricultural Research*, 49(5), 447-451.
23. Bansiwala, A. K., Rayalu, S. S., Labhasetwar, N. K., Juwarkar, A. A., & Devotta, S. (2006). Surfactant-modified zeolite as a slow release fertilizer for phosphorus. *Journal of Agricultural and Food Chemistry*, 54(13), 4773-4779.
24. Hassan, M. I., & Sultana, N. (2017). Characterization, drug loading and antibacterial activity of nanohydroxyapatite/polycaprolactone (nHA/PCL) electrospun membrane. *Biotech*, 7(4), 249.

25. Amadi, J. E., & Oso, B. A. (1996). Mycoflora of Cowpea Seeds (*Vigna unguiculata* L.) and their effects on seed nutrient content and germination. *Nigerian Journal of Science*, 30, 63-69.
26. Ali, A. S., & Elozeiri, A. A. (2017). Metabolic processes during seed germination. *Advances in seed biology*, 2017, 141-166.
27. Mo, M., Yokawa, K., Wan, Y., & Baluška, F. (2015). How and why do root apices sense light under the soil surface? *Frontiers in Plant Science*, 6,775
28. Harman,G.E.(2006). Overview of Mechanisms and Uses of *Trichoderma* spp. *Phytopathology*, 96(2), 190-194.
29. Asaduzzaman, M., Alam, M., & Islam, M. (2013). Effect of *Trichoderma* on Seed Germination and Seedling Parameters of Chili. *Journal of Science Foundation*, 8(1-2), 141–150.
30. Steel, R. G. D., & Torrie, J. H. (1980). *Principles and procedures of statistics, a biometrical approach* (No. Ed. 2). McGraw-Hill Kogakusha, Ltd..
31. Gastwirth, J. L., Gel, Y. R., & Miao, W. (2009). The impact of Levene’s test of equality of variances on statistical theory and practice. 343-360.
32. Kucuk, C., & Kivanc, M. (2004). In vitro antifungal activity of strains of *Trichoderma harzianum*. *Turkish Journal of Biology*, 28(2), 111-115.
33. Rojo, F. G., Reynoso, M. M., Ferez, M., Chulze, S. N., & Torres, A. M. (2007). Biological control by *Trichoderma* species of *Fusarium solani* causing peanut brown root rot under field conditions. *Crop protection*, 26(4), 549-555.

Chapter 4

PCL nanofiber loaded with free α -amylase and α -amylase immobilized on MCM-41 in presence of plant growth promoters and its application as seed coats

This chapter describes the immobilization of α -amylase, an enzyme of agricultural interest, in PCL nanofiber matrix via two approaches. Immobilization of α -amylase was carried out through covalent grafting on inorganic polymer MCM-41. PCL nanofibers were fabricated by loading MCM-41 immobilized amylase and by direct entrapment of free α -amylase. To study the effect of micronutrients and plant growth promoting hormones, PCL nanofibers with immobilized α -amylase were prepared in presence of MgO NPs and GA. The fabricated nanofibers were characterized and the results are discussed in this chapter. Catalytic activity of the developed nanofibers was studied in starch hydrolysis. The optimum incubation time, pH, temperature, storage stability and reusability of the immobilized α -amylase were also investigated. The application of developed nanofibers as seed coats on *Zea mays* seeds and their efficiency was monitored by germination studies. Flow chart of the work done is shown in FigIV.1.

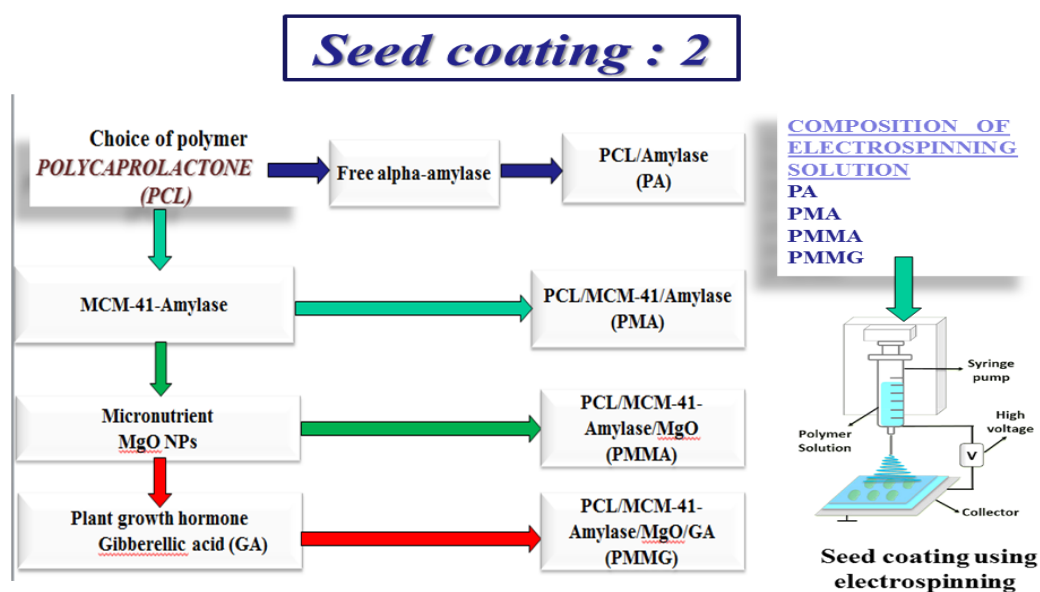


Fig.IV.1 Block diagram of the methodology for seed coating: 2

4.1 XRD analysis

Small-angle XRD patterns of the synthesized MCM-41 and MCM-41-immobilized α -amylase are shown respectively in Fig.IV.2a and b. The X-ray diffraction of both shows a strong peak at $2\theta = 2.3^\circ$ corresponding to the reflections of the (100) plane and two weak peaks at $2\theta = 3.9^\circ, 4.3^\circ$ corresponding to the reflections of the (110) and (200) plane, indicating a well-ordered two dimensional hexagonal symmetry of channels^{1,2}. This indicates the host structure of the ordered mesoporous MCM-41 is well maintained after the encapsulation of α -amylase. However, the intensity of diffraction peaks of MCM-41-immobilized amylase is less than that of pure MCM-41. The reduction of the intensity of the reflections of the plane reflections can be attributed to the fall in the ordering of the channels after covalent grafting. The intensity decrease in the (100) peak for enzyme-immobilized MCM-41 provides further evidence of functionalization occurring mainly inside pore channels³.

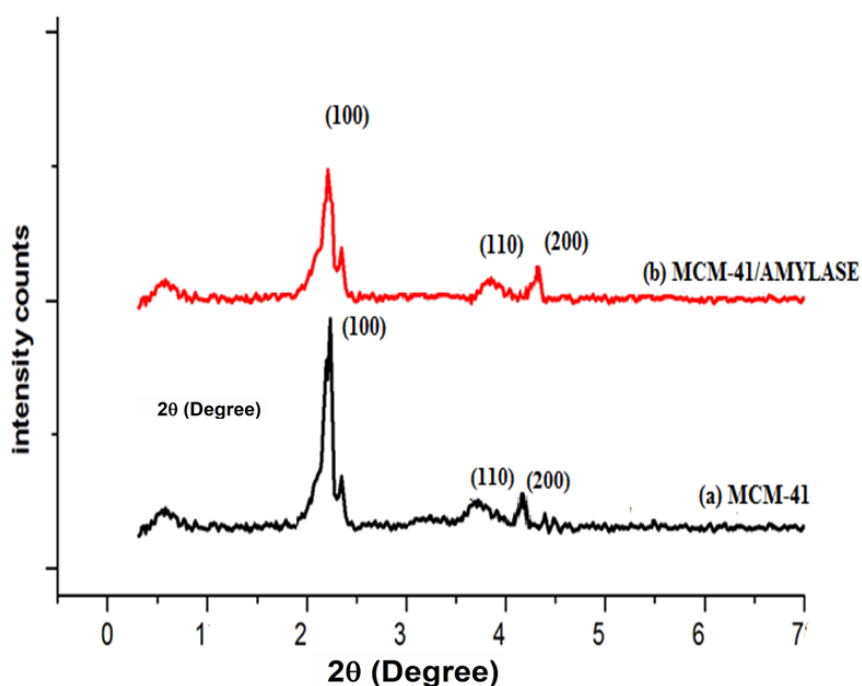


Fig.IV.2 XRD Diffractogram of a) MCM-41 b) MCM-41/Amylase

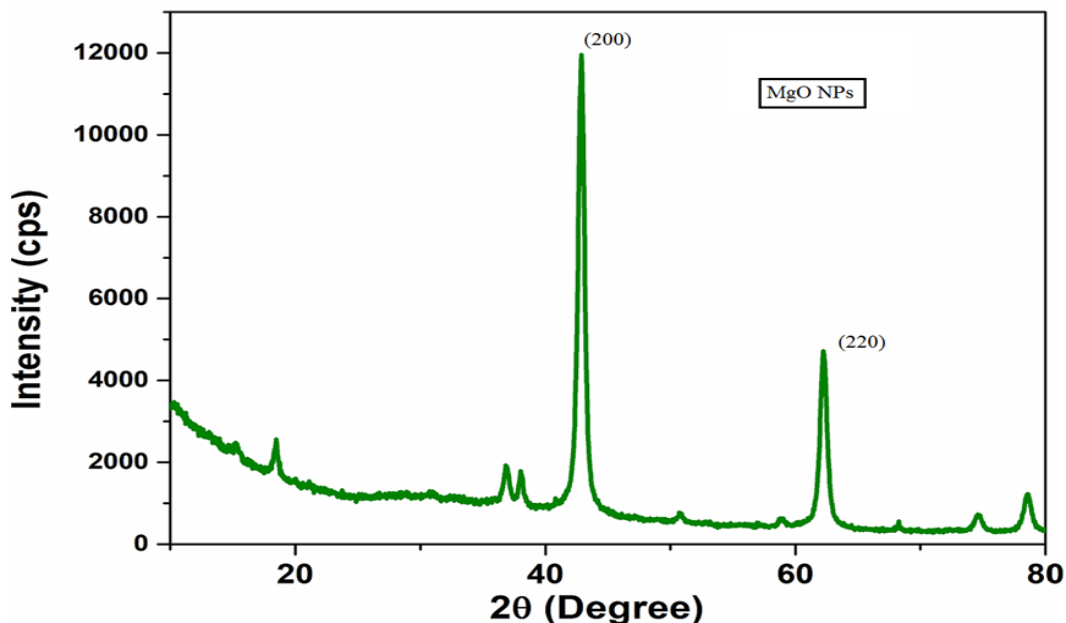


Fig.IV.3 XRD Diffractogram of MgO NPs

The diffractogram of MgO NPs (Fig.IV.3) shows characteristic crystalline peaks at 43° (200) and 62° (220). The XRD spectrum of fabricated nanofibers is depicted in Fig.IV.4. XRD pattern for PA (Fig IV.4 i) shows two intense diffraction peaks at Bragg angles $2\theta = 21.3^\circ$ and 23.8° . This might be due to the diffraction lattice planes (110) and (200) respectively, of orthorhombic crystal structure of semi-crystalline PCL⁴. When compared to PA, the three MCM-41 composite nanofibers Fig. IV.4 ii-iv showed decreased peak intensities and peak widening, which suggests decreased crystallinity. Faster nucleation of the polymer chain caused by the action of fillers leads to the production of disordered lamellae. Also it reveals higher interaction, which lowers the crystallinity of nanocomposite nanofibers⁵. Several filler-loaded PCL composite electrospun scaffolds possess elevated crystallisation temperature and decreased crystallinity⁶. This could be explained by the limited mobility of polymer chains coupled with fillers, which makes PCL difficult to crystallize. XRD spectrum of PMMA (Fig.IV.4 iii) shows a small peak at $2\theta = 45^\circ$ corresponding to MgO which reveals the incorporation of MgO in nanofiber matrix. In PMMG, upon the addition of gibberellic acid (GA) the intensity of MgO NPs decreases due to decreased crystallinity of PMMG.

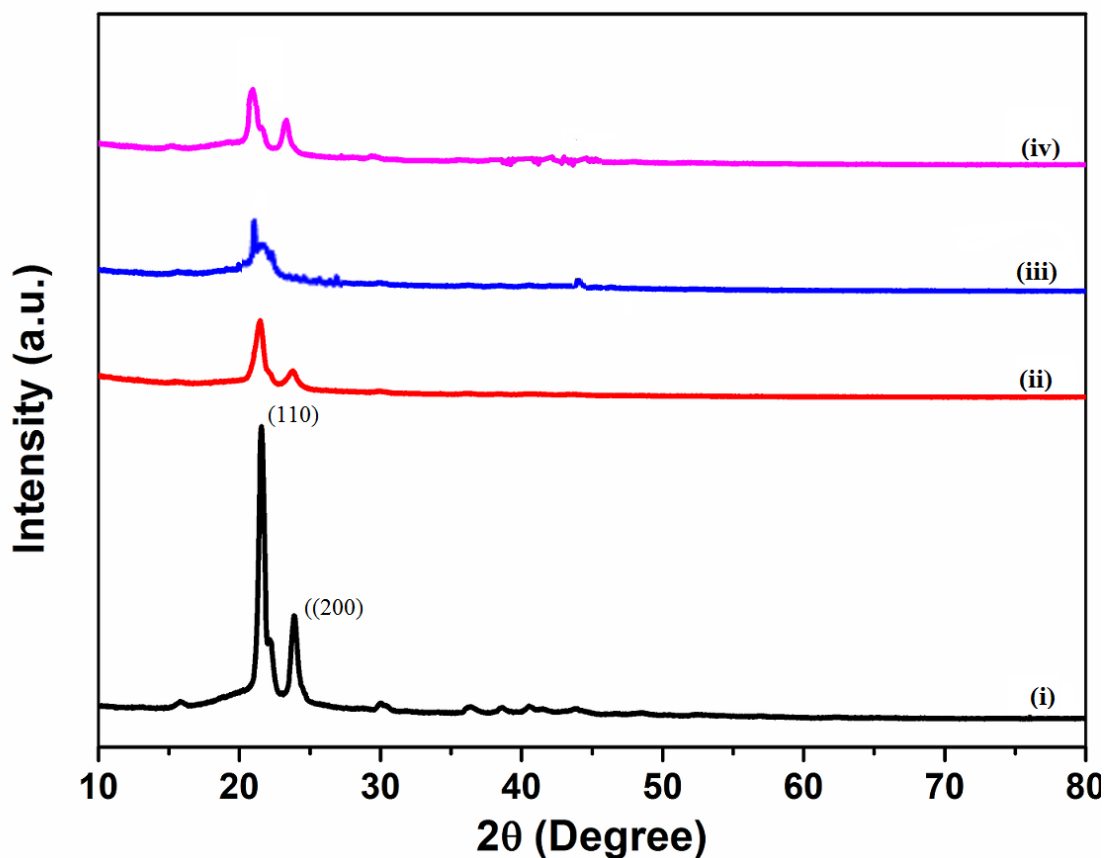


Fig.IV.4 XRD Diffractogram of i) PA ii) PMA iii) PMMA iv) PMMG

4.2 FT-IR study

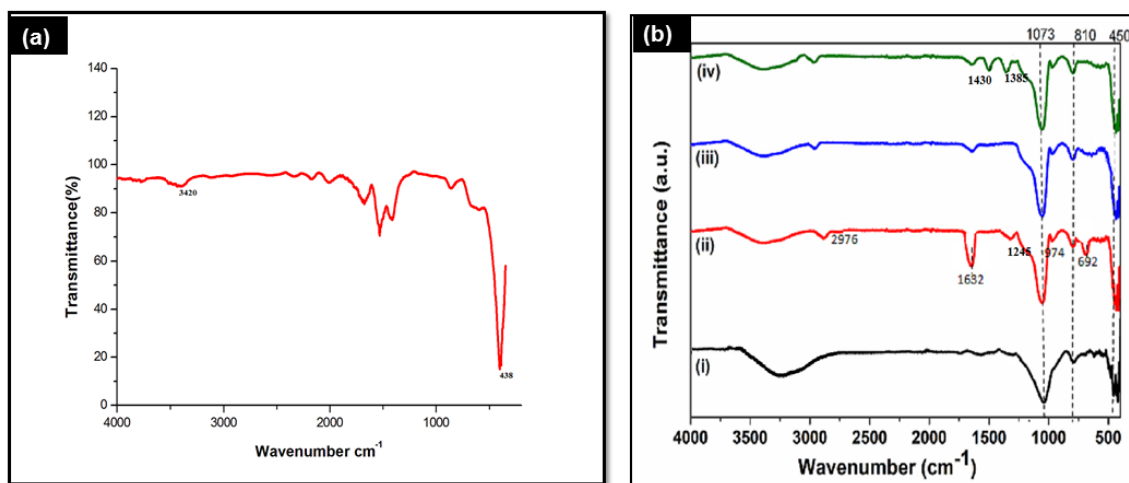


Fig.IV.5 FT-IR spectra of a) MgO NPs

b) MCM-41 and successive covalent grafting steps of α -amylase

i) MCM-41 ii) MCM-41/APTES iii) MCM-41/GU iv) MCM-41/Amylase

FT-IR spectra of MgO NPs is shown in the Fig.IV.5a. The peak at 438 cm^{-1} indicated Mg-O bond stretching, which in turn confirmed that the obtained product was MgO NPs. The peak observed at 1460 cm^{-1} and 3420 cm^{-1} was due to the presence of O-H bending and stretching, respectively, assigned to the H₂O adsorption on the surface of metal. The metal-oxygen frequencies observed for the respective metal oxides were in accordance with the literature values⁷.

The infrared spectra of synthesized MCM-41 and its successive covalently grafted groups during enzyme immobilization are shown in Fig.IV.5b. MCM-41 shows the Si-O-Si stretching band around $1240\text{-}1030\text{ cm}^{-1}$ which was assigned as the fingerprint region of MCM-41. The bands at 1073 cm^{-1} and 810 cm^{-1} corresponded to asymmetric and symmetric vibrations of Si-O-Si bond respectively⁸ (Fig.IV.5b(i)). MCM-41/APTES, MCM-41/GU and MCM-41/Amylase showed different peaks⁹ at 450 , 810 and 1073 cm^{-1} . The absorption peak at 3400 cm^{-1} was attributed to the asymmetric stretching vibration absorption of -OH, which confirmed that the surface of MCM-41 contains hydroxyl groups. The spectrum of MCM/APTES showed a strong decrease in the intensities of bands associated with hydroxyl groups (Fig.IV.5b(ii)). This might be because the silanization reaction replaced Si-OH groups with the more stable Si-C bonds¹⁰. The absorption peaks near 1632 cm^{-1} and 692 cm^{-1} were attributed to the stretching vibrations of -NH₂ and N-H respectively, indicating that APTES had successfully achieved covalent binding on MCM-41 as can be seen in Fig.IV.5b(ii). The decrease in intensity of these peaks in MCM-41/GU indicates grafting of GU through NH₂ in MCM-41/GU in Fig.IV.5b(iii). For MCM-41/APTES, the intensity of Si-OH vibration band at 972 cm^{-1} decreased due to the hydrogen bonding between silanol and -NH₂ groups. The C-N stretching vibration absorbance is normally around $1200\text{ - }1000\text{ cm}^{-1}$ but this band cannot be resolved due to its overlapping with the absorbance of Si-O-Si stretch in $1000\text{ - }1300\text{ cm}^{-1}$ range and that of Si-CH₂-R stretch in $1200\text{-}1250\text{ cm}^{-1}$. The band at 1245 cm^{-1} can be assigned to the bending vibration of N-H. This is assigned to the vibration of free amino groups on the silicon surface¹¹.

The weak bands observed at 2976 cm^{-1} and 2990 cm^{-1} in the spectrum of MCM-41/APTES and MCM-41/Amylase is due to the asymmetric vibration of the CH₂ groups of the propyl chain of the silylating agent, indicating successful grafting of organic amine on to the pore of MCM-41. This confirmed the attachment of the

aminopropyl group on the surface of MCM-41. The bands at 3400–3450 cm^{-1} in Fig.IV.5b(iv) showed the characteristic signal of the stretching vibration of amine groups. The C-N stretching vibration at 1385 cm^{-1} and the symmetric and asymmetric stretching vibrations of C-O at 1430 cm^{-1} and 1625 cm^{-1} which are the characteristic signals of amide carbonyl (CO-NH) groups, demonstrated the efficient grafting of α -amylase through glutaraldehyde on MCM-41.

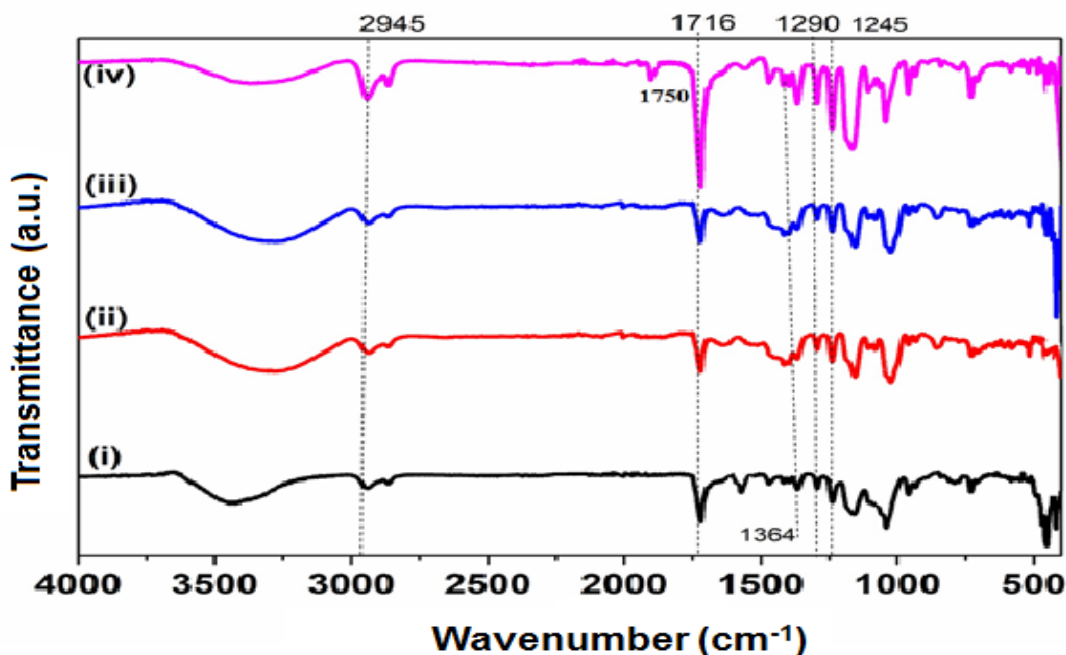


Fig.IV.6 The FTIR spectrum of i) PA ii) PMA iii) PMMA iv) PMMG nanofibers

The interactions between the functional groups in the polymeric matrix are revealed by FTIR investigations. The FTIR spectrum of PA, PMA, PMMA and PMMG nanofibers are shown in Fig.IV.6. The absorption peaks around 1245, 1290, 1716 and 2945 cm^{-1} are related to symmetric stretching of C—O—C, C=O, C—C and CH₂ bonds of PCL respectively¹². FTIR spectra of all composite fibers are dominated by the main PCL bands. FTIR spectrum of PA (Fig. IV.6 i) shows additional bands at 3450 cm^{-1} and between 1600 and 1700 cm^{-1} . This confirms the presence of amide groups of alpha amylase upon encapsulation in PCL nanofiber matrix.

The presence of MCM-41/Amylase in PCL nanofibers could be identified by observing the new bands in the composite fiber spectrum of PMA, PMMA, PMMG in

Fig.IV.6ii-iv. These bands are related to the presence of Si–O bonds, namely Si–O–Si stretching around 1100 cm^{-1} , Si–OH stretching around 1000 cm^{-1} and Si–O stretching around 800 cm^{-1} . This indicates the encapsulation of MCM-41/Amylase in the nanofibers. In PMMA and PMMG the presence of MgO NPs is indicated by less intense peak at 460 cm^{-1} . The most characteristic peaks in gibberellic acid are reported at 1177 cm^{-1} (C=C), 1747 cm^{-1} (C=O), 2965 cm^{-1} (CH₃ group), and 3449 cm^{-1} (OH group)¹³. The nanofiber PMMG loaded with Gibberellic acid (GA) shows a new peak at 1750 cm^{-1} . This proved the loading of GA in nanofiber PMMG. The intensity of band is weak due to the very low weight percentage of GA.

4.3 Study of the morphology

4.3.1 SEM analysis of developed samples

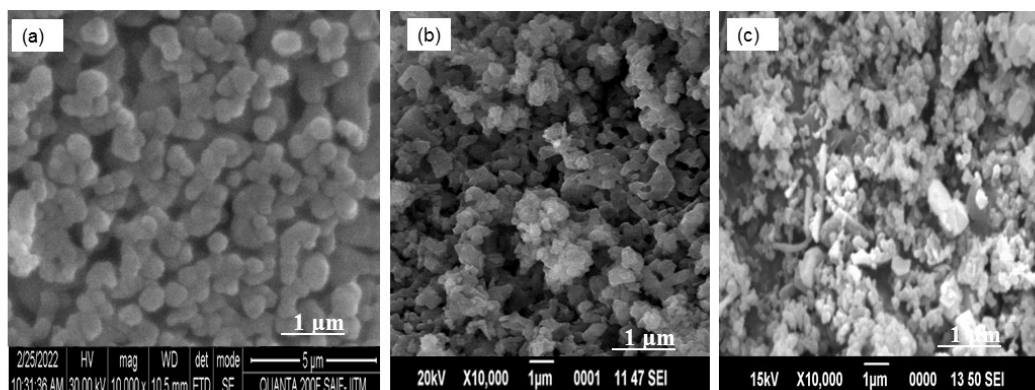


Fig.IV.7 SEM images of a) MgO NPs b) MCM-41 c) MCM-41/Amylase

The morphology of the synthesized MgO NPs is observed in Fig.IV.7a. The particle-like morphologies can be seen in SEM image. Almost every particle is well distributed, but they are all connected or closely linked. This supported the existence of nanoscale particle structure. The size of the produced particles ranges from a few nanometers to 90 nm. The smaller pieces are packed so closely that it appears as though they are embedded on the surface. The SEM image of MCM-41 is shown in Fig.IV.7b. The MCM-41 exhibits aggregated, irregular spherical particles with smooth surface and an interconnected network. SEM image of α -amylase immobilized MCM-41 is shown in Fig.IV.7c. The surface modification and covalent grafting may cause a partial collapse of the pore structure and the irregularity in this sample.

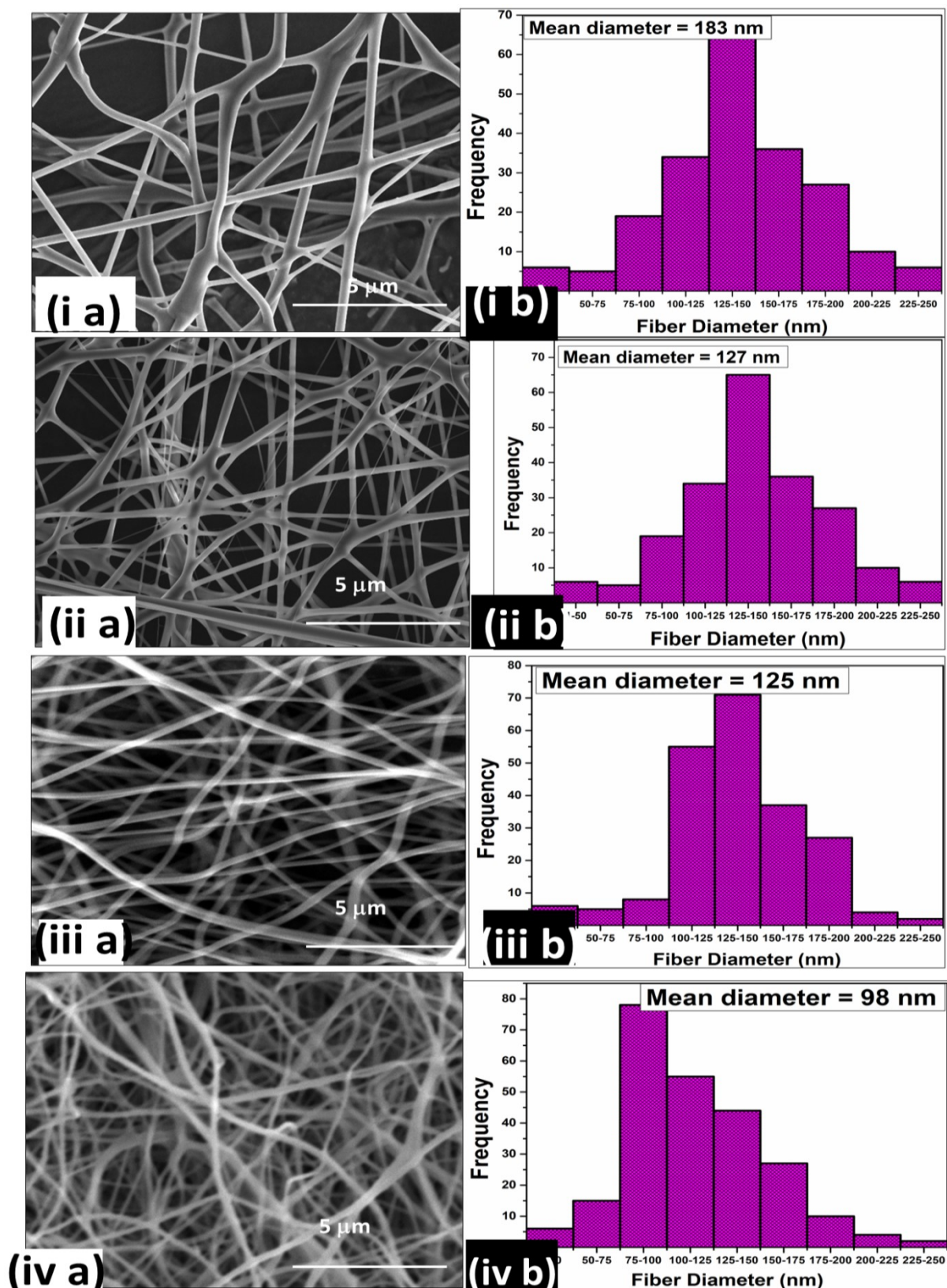


Fig.IV.8 SEM images of ia) PA iia) PMA iiii) PMMA iva) PMMG
Histogram bar chart of ib) PA iib) PMA iiib) PMMA ivb) PMMG

SEM images of PA, PMA, PMMA and PMMG are presented in Fig.IV.8(ia-iva). Fig.IV.8(ia) shows electrospun nanofiber PA has a homogenous uniform, bead free and fine morphology with an average diameter of 183 nm. The fibers produced with the MCM-41 composite nanofibers of PMA, PMMA and PMMG display a narrower diameter distribution than PA as noticed in the SEM image (Fig.IV.8(ia-iva)). For these nanofibers mean fiber diameter decreases. For PMA, PMMA and PMMG average fiber diameter is 127 nm, 125nm and 98nm respectively. Adding the agricultural chemicals and nutrients resulted in a reduced diameter and all the nanofibers showed smooth and bead-free morphology. The difference in diameter between the MCM-41 grafted enzyme loaded fiber scaffolds and PA can be related to the presence of nanoparticles in the filler-polymer solution, which causes the charge density of the solution to increase¹⁴. This could be connected to a strong polymer-solvent interaction, solution viscosity or electrical conductivity. The addition of fillers to PCL decreased the fiber diameter than neat PCL nanofiber as reported in the previous work. These differences were most apparently brought on by difference in conductivities between PCL and the fillers loaded¹⁵. The diameter of the nanofibers taking 50 fibers at random plotted in the histogram bar chart (Fig.IV.8(ib-ivb)). Majority of nanofibers are found to have lesser diameter after the addition of nutrients.

4.3.2 EDX Spectra of the Synthesized Samples

Energy dispersive X-ray analysis (EDX) was used for the analysis of the elements in the synthesized samples. MCM-41 functionalization and enzyme immobilization were validated by elemental EDX analysis. The EDX spectrum of the MCM-41 and MCM-41 immobilized α -amylase are shown in Fig.IV.9i and ii. Fig.IV.9i indicate the atomic percent (At%) and weight percent (Wt%) of Si and O existing in the MCM-41 structure. After modification of their surfaces and enzyme immobilization the weight % of C and N indicate the successful immobilization of α -amylase. EDX spectrum of composite PMMG nanofiber confirmed the presence of Mg in addition to C, O, N and Si (Fig.IV.10). This reveals the effective loading of MgO NPs. The presence of Si and N indicates the incorporation of α -amylase grafted on MCM-41 in PCL matrix. The absence of residual solvent after nanofiber formation is indicated by the absence of peaks for chlorine.

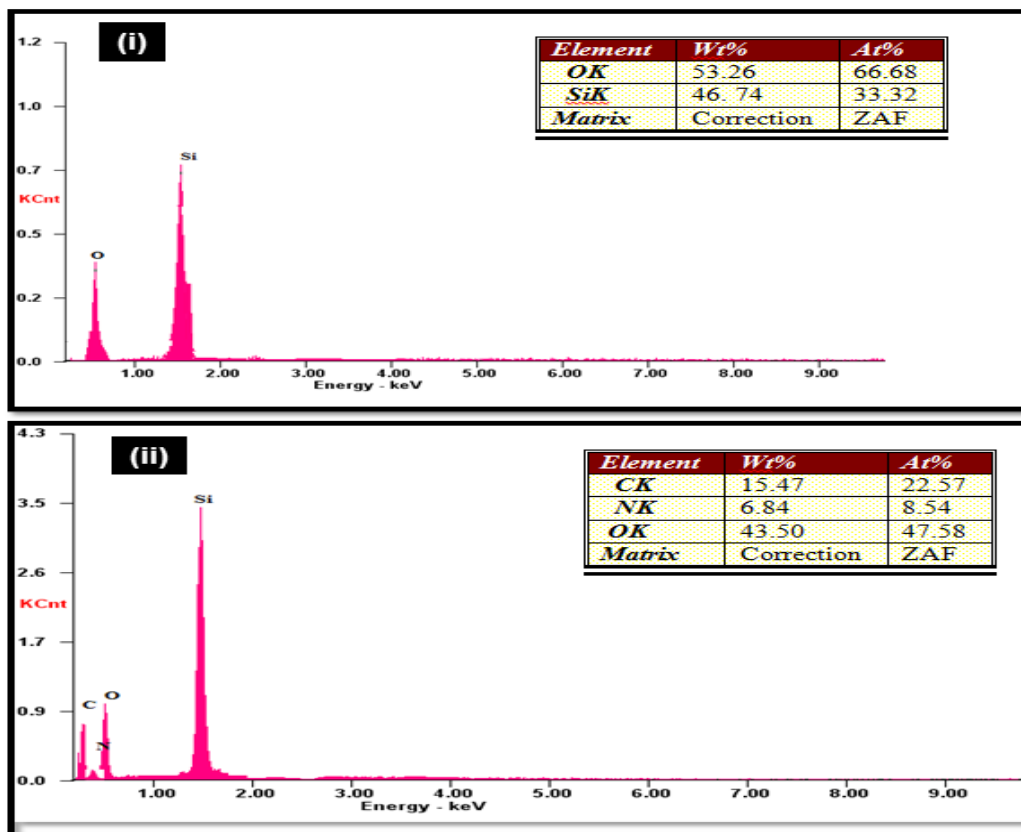


Fig.IV.9 EDX spectrum of i) MCM-41 ii) MCM-41/Amylase

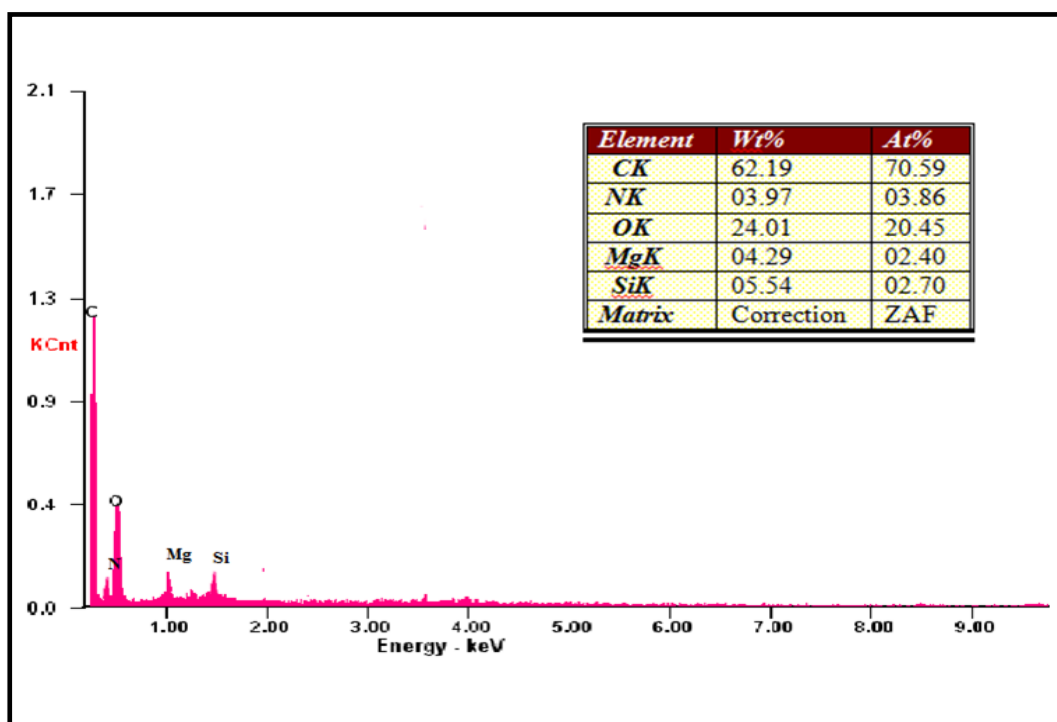


Fig.IV.10 EDX spectrum of PMMG nanofiber

4.3.3 TEM Analysis

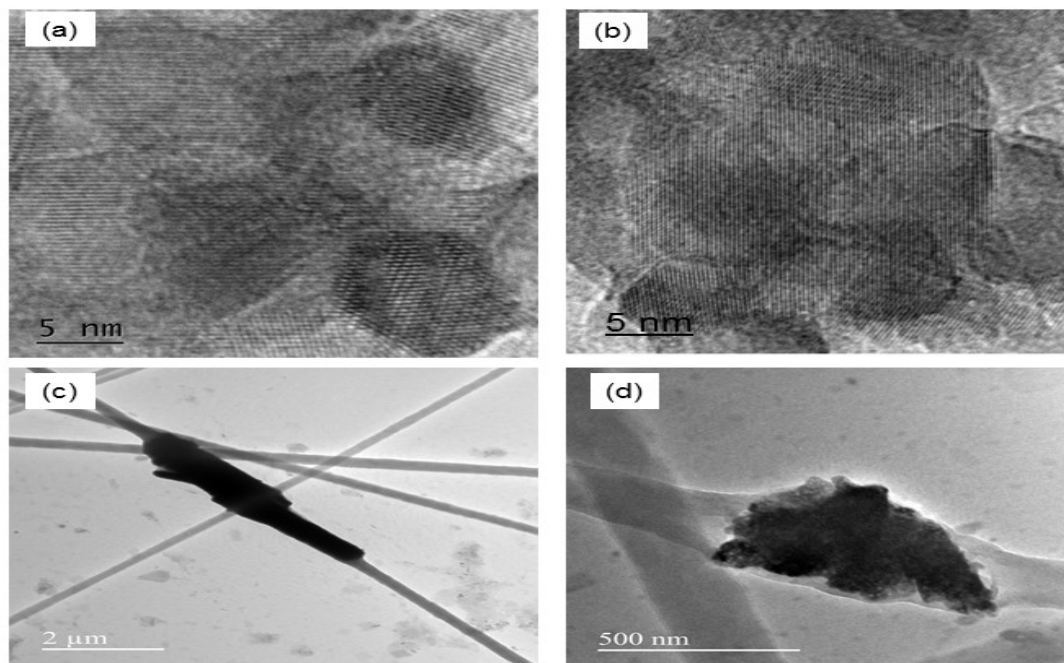


Fig.IV.11 HR-TEM image of a) MCM-41 b) MCM-41/Amylase c) PMA nanofiber d) PMMG nanofiber

TEM images of MCM-41 and α -amylase immobilized MCM-41 (MCM-41/Amylase) are shown in Fig.IV.11a and b respectively. Fig.IV.11a shows uniform lines in the vertical direction of the pore channels referring to a long-range ordered structure of the one-dimensional channels of MCM-41 structure. This matches well with the XRD results. The TEM image of MCM-41/Amylase (Fig.IV.11b) presented a similar pore shape related to the pure MCM-41 sample. However, partially irregular pore-ordering and morphological defects are observed which probably related to a partial collapse of the structure of MCM-41 due to the loading of enzyme. This is in agreement with obtained SEM results. The hexagonal array and the regularity of the pore channels are more pronounced in the TEM image of MCM-41. A distinctive hexagonal pore structure is clearly observed in MCM-41 indicating the existence of a highly ordered hexagonal array¹⁶. These structural features confirm the formation of an ordered structure at the nanoscale. The TEM image of PMA and PMMG nanofiber is shown in Fig.IV.11c and d respectively. This indicates the incorporation of fillers within nanofibers. Even though they were not uniformly distributed, the components

added were agglomerated along the fiber direction. These results supported the grafting in the polymer matrix.

4.4 Thermal analysis

The Fig.IV.12 depicts the TGA thermogram of fabricated nanofibers. The nature of TG curve of PA was not altered much from that of pristine PCL. This is due to the direct encapsulation of enzyme in PCL matrix which did not involve any strong bonding interactions compared to covalent grafting as seen in Fig.IV.12i. The TG curve of PA nanofiber shows a sudden decomposition in the range 280°C - 300°C, until weight% decreased to 25%. After that a very small weight loss is observed till 480°C then the weight remains constant. The first decomposition temperature of PMG, PMMA was raised to 313°C, 321°C and 379°C respectively (Fig.IV.12ii-iv). This could be due to the addition of thermally stable inorganic support and MgO NPs.

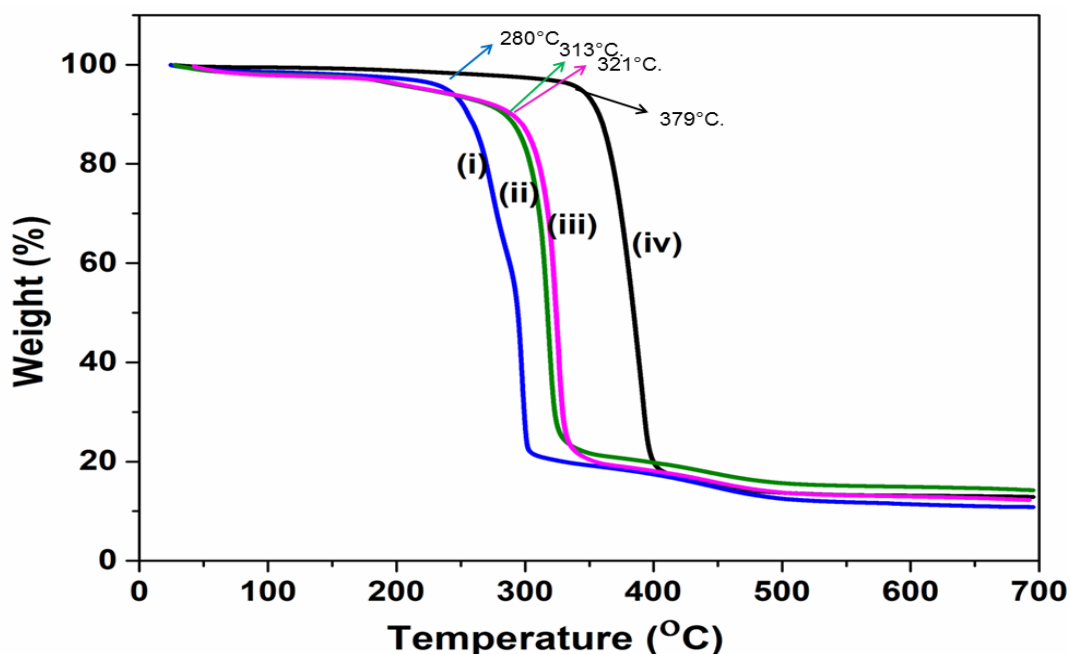


Fig.IV.12 TGA thermogram of i) PA ii) PMA iii) PMMA iv) PMMG

The char yield of PA was found to be low while on addition of MCM-41 immobilized α -amylase in PMA, PMMA and PMMG char yield increases because of the presence of non-volatile inorganic carrier. However a similar trend is observed in all cases. The interactions between the filler material and the electrospun fiber matrix, which in turn depend on the dopants specific surface area and its distribution in the

polymer matrix, may be the cause of these variations in the degradation temperature of the electrospun nanofibers¹⁷. Above 400°C the PCL matrix began to decompose as a result of the combustion of organic residues. No weight loss was noticed above 480°C, indicating that decomposition of the polymer is complete¹⁸.

4.5 Surface Wetting Properties of the Electrospun Fibers

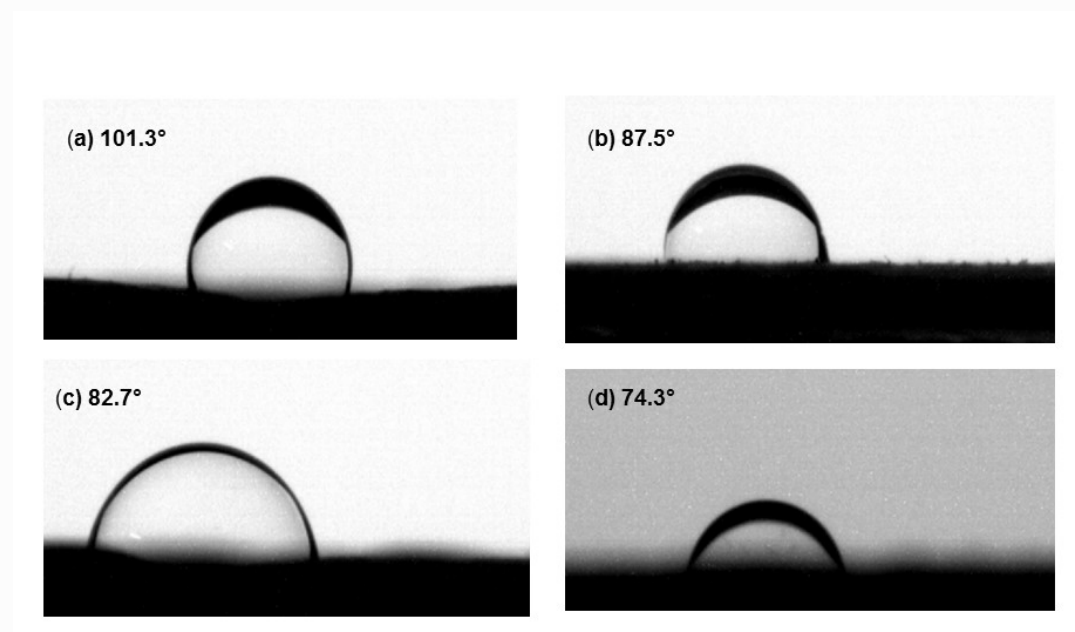


Fig.IV.13 Static water contact angle measurements of nanofibers

a) PA b) PMA c) PMMA d) PMMG

Since the fabricated PCL -based nanofibers are intended to be used in seed coating, contact with water and different soil conditions have to be taken in to account. Hence, determining the nanofibers' wettability is crucial. The water contact angle was used to evaluate the fiber's wettability. Fig.IV.13 demonstrates the contact angle of water on the surface of nanofibers produced at different composition. It was observed that the PA nanofibers showed the highest contact angle of 101.3° compared to those of PMA, PMMA and PMMG. Encapsulation of α -amylase was found to decrease the water contact angle of pristine PCL which was reported to be 119.8° in previous work. When the amount of loaded component increases, the contact angle decreased significantly. The water contact angle of PMMG in Fig.IV.13d is only 74.3°. The contact angle of α -amylase grafted MCM-41 loaded nanofibers like PMA, PMMA and PMMG showed hydrophilic property with less than 90° value. The

decrease in the water contact angle is beneficial for nanofibrous seed coating as it prevents the seed decay and seed drying by controlled water absorption.

4.6 Porosity Measurements

Table IV.1 shows the porosity measurements of synthesized polymer membranes calculated from Equation 2.2

Table IV.1 Porosity values of developed membranes

Polymer membrane	PA	PMA	PMMA	PMMG
P(%)	78	85	90	96

The maximum porosity 96% was observed for PMMG. The developed polymer fibers show high degree of porosity. The incorporation of MCM-41 grafted enzyme in PMA increases the porosity. The seedling development rate is promoted by factors like porosity, pore size and specific surface area which facilitate agricultural diffusion. This is in agreement with germination data.

4.7 Study of Fibers and Seeds in Aqueous Medium

4.7.1 Swelling and Stability Studies of the Nanofibers in PBS

Understanding the swelling capacity of the polymer nanofibers in water will help to evaluate the capacity for hydration. As a result it gives information on the nutrient release, adhesiveness and buoyancy. The swelling studies for nanofibers were done by allowing the fibers to remain in PBS medium and determine their weights at regular intervals.

The swelling percentages of developed electrospun nanofibrous membrane with time is shown in Fig.IV.14. Swelling properties depend on wettability and structure of nanofibers. According to the swelling test results, the membrane PA absorbs the solution slowly compared to other nanofibers. But slow increase in swellability of PA is due to porous structure of nanofibers. The swelling rate of PMMG membrane was found to be as high as 170% after 12 h. PMMG nanofibers have higher surface/volume ratio because of small pore size. This may be attributed to the presence of inorganic porous support MCM-41 which also helps to absorb water.

After 12 h the PMA, PMMA and PMMG swelling gradually decreases with time and reaches 130% after 36 h. The swelling rate also decreases due to the presence of hydrophilic components in the polymer matrix.

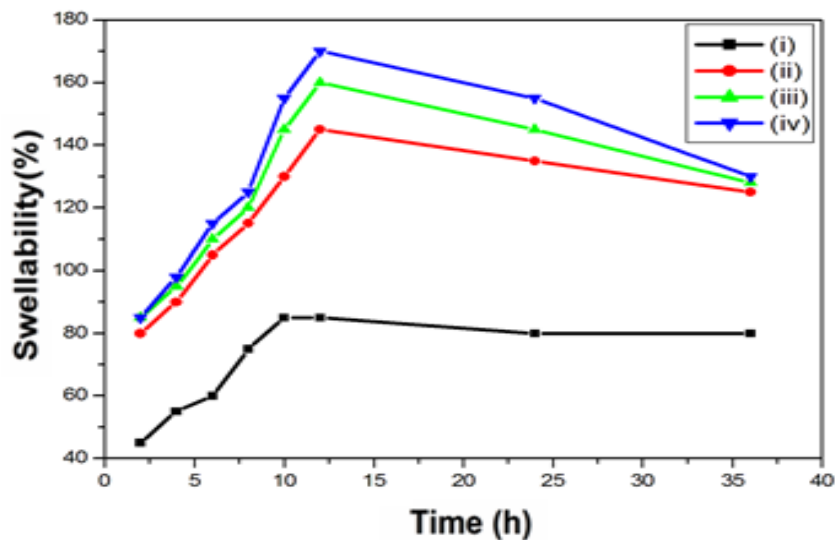


Fig.IV.14 Swelling studies of i) PA ii) PMA iii) PMMA iv) PMMG

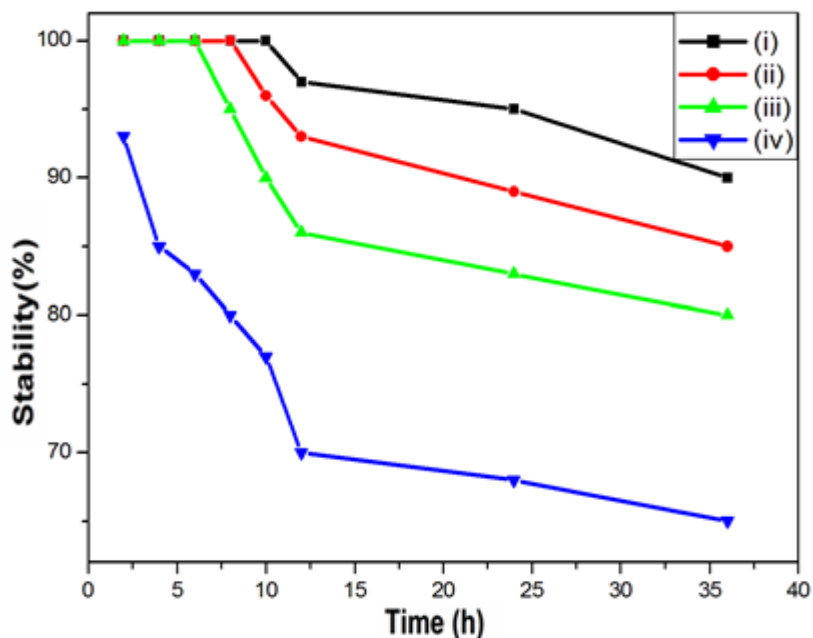


Fig.IV.15 Stability studies of i) PA ii) PMA iii) PMMA
iv) PMMG

All the three scaffolds PMA, PMMA, PMMG show comparable swelling rates. The high surface/volume ratio enabled nanofibers to interact more with solutions, positively affecting swelling. The large surface area of electrospun fibers and the porosity on the fibers favour fluid absorption. Previous reports reveal that pores and fiber diameter affect wettability and fluid absorption¹⁹. The stability of the nanofibers was studied using Equation 2.4 (Fig.IV.15). In aqueous solution the weight loss indicates the instability index of the polymer. As PCL is water insoluble, it will not dissolve and leach into water²⁰. Thus the results of PA, PMA, PMMA showed almost 100% stability even after 12 h. MCM-41 is water insoluble hence it is expected to remain for a long time.

The extremely crystalline and less hydrophilic nature of PCL nanofibrous scaffolds in comparison to its composites is strongly suggested by the results of XRD and contact angle experiments. Compared to pristine PCL, the developed nanofibers facilitate water penetration into PCL nanofibers. The weight loss of the composite fiber mats was primarily caused by the deterioration of the composite bulk, which is aided by the release of fillers and accelerated ester bond breakage. The decrease in stability of PMMG is due to dissolution of water soluble components such as GA and dispersion of MgO NPs from the matrix to water. A small weight loss was also seen in PA, PMA and PMMA. This may be due to the enzymatic degradation of PCL. The main method of breakdown is chain cleavage via hydrolysis of ester bonds, either abiotic (non-enzymatic) hydrolysis or enzyme-promoted hydrolysis. Enzymatic degradation speeds up material deterioration by a mechanism that is comparable to that of hydrolytic degradation²¹. Therefore even PCL is a hydrophobic polymer, encapsulation of enzymes and fillers increases its degradation in a controlled manner. Thus facilitates nutrient release and enzymatic activity. α -Amylase immobilized nanofibrous mat on seed's surface provide energy and nutrients during seedling growth.

4.7.2 pH Study

The pH variation for PBS buffer was found to be controlled by the PCL matrix degradation rate as well as the MgO nanoparticles' dissolution profile (Fig.IV.16). The pH values of PA nanofiber did not significantly change throughout the first three days of immersion. After three days, it began to follow a somewhat acidic trend as

seen by a steady pH decrease due to degradation of polymer PCL in presence of enzyme α -amylase in PA. This facilitates the degradation of acidic carboxyl groups²¹. This is further confirmed in the swelling and stability studies.

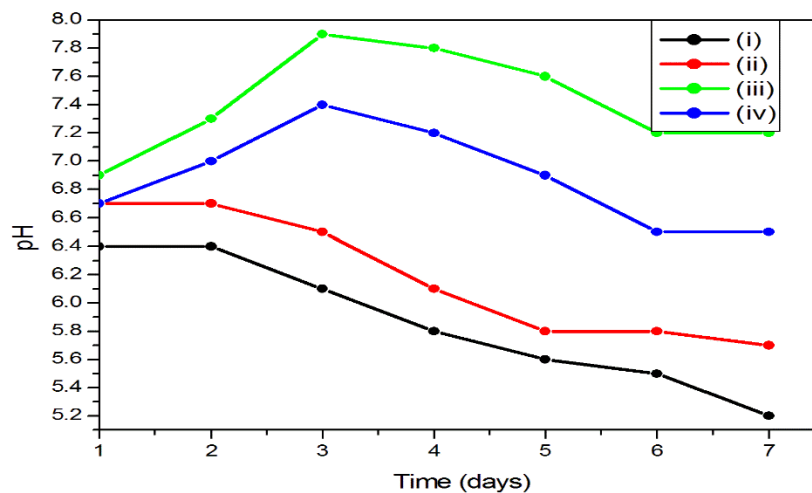


Fig.IV.16 pH of aqueous solutions of fibers i) PA ii) PMA iii) PMMA iv) PMMG

The nanofiber PMA follows almost similar trend as in PA but the extent of decrease in pH is low compared to PA, may be due to covalent grafting of α -amylase on MCM-41. Thus reduces the degradation of PCL membrane. In the case of PMMA composite fiber with MgO NPs, pH values of PBS solutions showed a sharp rise during the first three days of soaking peaking at 7.9 and then a steady decline to 7.2 by the seventh day. This phenomenon may be due to local neutralisation of acidic breakdown products of the polymer by the filler-induced alkalinity of the medium²⁰. Alkaline nanofiller's buffering properties may help to minimise any damage of seeds brought on by the acidic degradation products of polyester polymers when applied as seed coat. Similar results have also been noted in polymer composites that contain bioceramics such as forsterite, bioglass, and wollastonite²². The nanofiber PMMG also shows similar pH change as in PMMA. After three days pH reaches up to 7.4 and then decreases gradually to 6.5 on seventh day. This is attributed to the acidic nature of GA. Out of the nanofibers, the pH range for PMMG nanofiber seems to be most suitable for seed coat since optimum pH range for corn seed germination is found to be 5.8 - 6.5.

4.7.3 Metal ion Release Study

Fig.IV.17 shows analysis of Mg ion release from PMMG and PMMA composites in PBS medium for 7 days of incubation. Mg ion release is increased gradually from both nanofibers reaching a maximum of approximately 44 μg for PMMA and 32 μg for PMMG at the end of the incubation period. Thus, there was a time dependent Mg ion release from scaffold composites PMMA and PMMG. This might be one of the factors responsible for facilitating weight reduction in these as compared to PA and PMA nanofiber and for rise of medium pH at the initial stage²³. These findings are in agreement with stability data and pH change measurements of developed nanofibers.

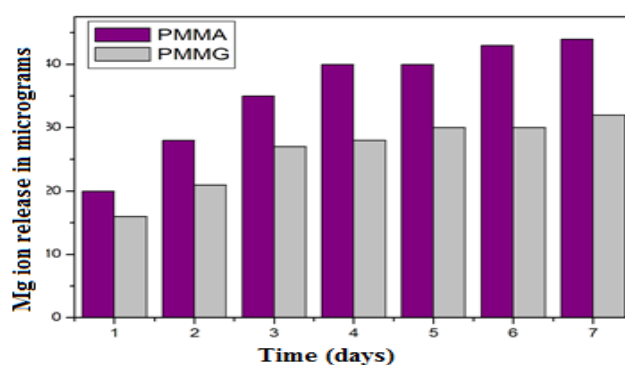


Fig.IV.17 Magnesium ion release profile from nanofibers

4.7.4 Imbibition Studies

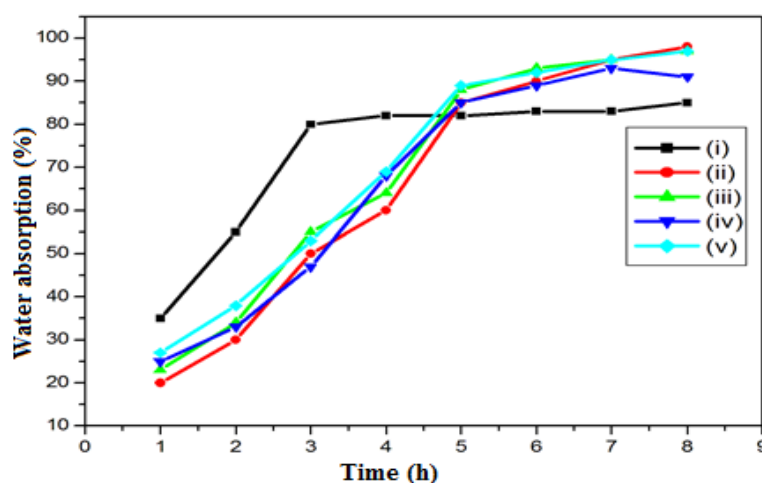


Fig.IV.18 Imbibition studies of i) uncoated seeds ii-v) seeds coated with nanofibers ii) PA iii) PMA iv) PMMA v) PMMG

The weight gain of the coated and uncoated seeds was monitored every hour while they were soaked in the water. The largest amount of water intake was seen in the first 3 h for uncoated seeds, as shown in Fig.IV.18 i. Seed hydration was most rapid at the first 3 h of imbibition and started to slow down noticeably after 6 h of imbibition for uncoated seeds. But coated seeds imbibition rate increases slowly in a sustainable manner. However, coated seeds showed a higher rate of water uptake than uncoated ones in the later hours of germination (Fig.IV.18ii-v). During seed germination, rapid seed hydration may result in cellular damage and coating eliminates this situation. The high and controlled water uptake caused seeds' proteins to be completely hydrated. This facilitated the restoration of enzymatic activity, promoting seed germination and growth. Therefore nanofibrous seed coating allows controlled hydration which may help in seed dormancy break, even when an unfavourable environment exists. The polymer covering on soybean seeds allowed for controlled water uptake and reduced imbibitional damage²⁴. It was evident that the polymer nanofiber coating controlled the rate of water absorption and reduced imbibitional damage. These outcomes were consistent with the published research. Higher germination and seedling vigour are the results of increased imbibition. Due to the high metabolic activity of the maize seed, polykote film coating on the seeds had an improved effect on seedling establishment. This was linked to the coating's nutritional content²⁵. Water is necessary to hydrate protoplasmic metabolism activities, provide dissolved O₂ to the seed embryo, soften the seed's outer coat and improve seed permeability. Water aids the rupturing of the seed and converts the insoluble endospermic-stored materials into soluble substances through enzyme activation, breakdown and translocation, reserving storage materials in the endosperm and then translocating them to the growing embryo. The large surface area of electrospun fibers and the presence of pores on the fibers favour fluid absorption.

4.8 Germination Studies

The germination percentage, germination index, and seed vigour index were all calculated in order to study the germination rate. The Fig.IV.19 shows the results of germination trials performed for a period of 5 days. The shoot length of the seedling grew about 3 to 6 cm. Planting in the soil for further growth is required. Corn seeds have a robust growth pattern and high germination qualities across all

subsamples. It was noted that root hairs and nodules had taken longer time to emerge in the nanofiber coated seedlings than in the control treatment. But after 48 h the nanofiber coated seedlings show enhanced growth than control plant. The seeds coated with PMMG demonstrated improved growth potential, which could be observed visually. The germination potential and coating efficiency follows the order

Uncoated < PA nanofiber coated seeds < PMA nanofiber coated seeds < PMMA nanofiber coated seeds < PMMG nanofiber coated seeds

The high growth rate in PMMA and PMMG is due to the presence of MgO NPs. In PMMG additional enhancement is due to the presence of GA. In cereal seeds, endosperm-stored proteins and carbohydrates are released during germination which supplies seedlings with energy and substrates. Bioactive GAs are created in the embryo during seed germination and transferred to the aleurone layer to activate the α -amylase gene and cause α -amylase production. The stored starch is then hydrolyzed by the secretion of α -amylase into the endosperm²⁶. Therefore additional GA loaded in the seed coats boost the germination parameters. 90% of the amylolytic activity in maize seeds is attributed to the α -amylase enzyme, which is crucial for starch hydrolysis. The 1,4 glycosidic bonds of starch, glycogen and other carbohydrates are hydrolyzed by the α -amylase²⁷. Saline soil reduces the seed germination which can be enhanced by the addition of GA²⁸. MgO NPs were found to be an excellent source of magnesium for plants. As a result, the MgO NPs had a dual role in boosting Mg uptake as a necessary nutrient and enables their utilisation as a cofactor to mobilise nutritional enzymes.

Salinity of the soil is an abiotic stress that has a negative impact on agricultural production all over the world. Salinity is thought to have an impact of about 6% of all land and 20% of irrigated land²⁹. According to reports salinity prevents seed germination and seedling growth, diminishes photosynthesis and as a result, lowers yield³⁰ whereas GA promotes seed germination^{31,32}. Addition of GA in the nanofiber is quite significant and suggests the implementation of the nanofiber seed coating strategy to promote germination and high crop yield even in saline soils. It is worth mentioning that the beneficial trends of the nanofiber coating for corn seeds are likely due to the loaded components. This type of seed coating would help the crop under variable climatic conditions such as drought and chilling stress. This is

further confirmed in the study of effect of temperature and pH on immobilized enzyme. Water imbibition allows water to enter the seed coat during the water uptake mechanism and start to soften the tough, dry tissues inside the seed. Intake of water enlarges the seed, which caused the seed coat to rupture leading to emergence of radicles during the germination period. The imbibition data clearly supports the germination data as imbibition is fast for uncoated seeds during initial hours and therefore uncoated seeds show seedling emergence more than nanofiber coated seeds in first day. Later coated seeds exhibit high germination potential.



Fig.IV.19 The optical photographs of corn seed germination
A) uncoated seeds B-E) Seeds coated with nanofibers
B) PA C) PMA D) PMMA E) PMMG

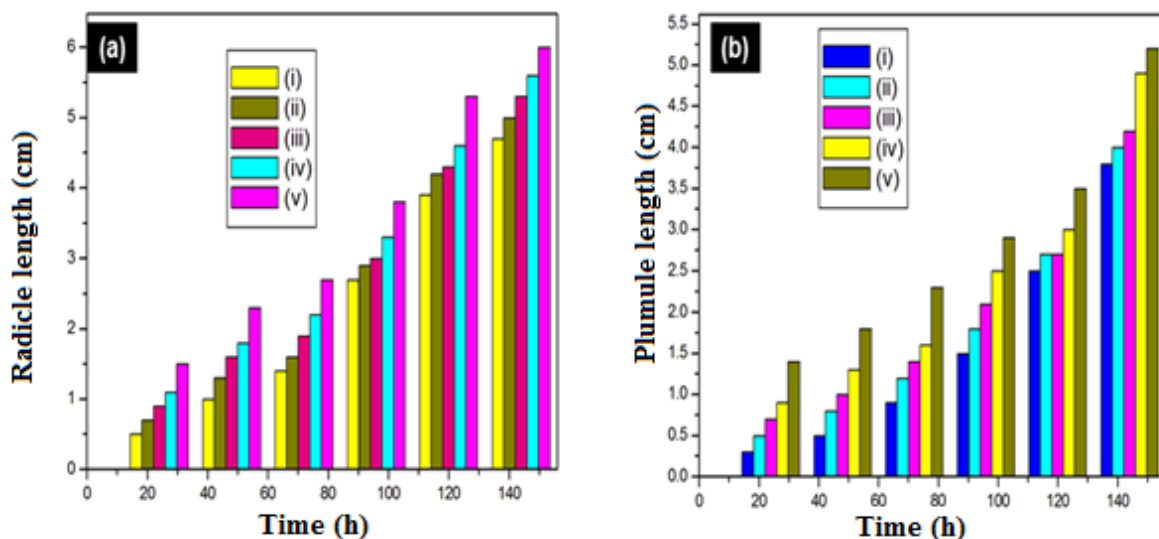


Fig.IV.20 a) Radicle length b) Plumule length
 i) Uncoated seeds ii-v) Seeds coated with nanofibers ii) PA iii) PMA iv) PMMA v) PMMG

4.8.1 Fresh Biomass of Seedling

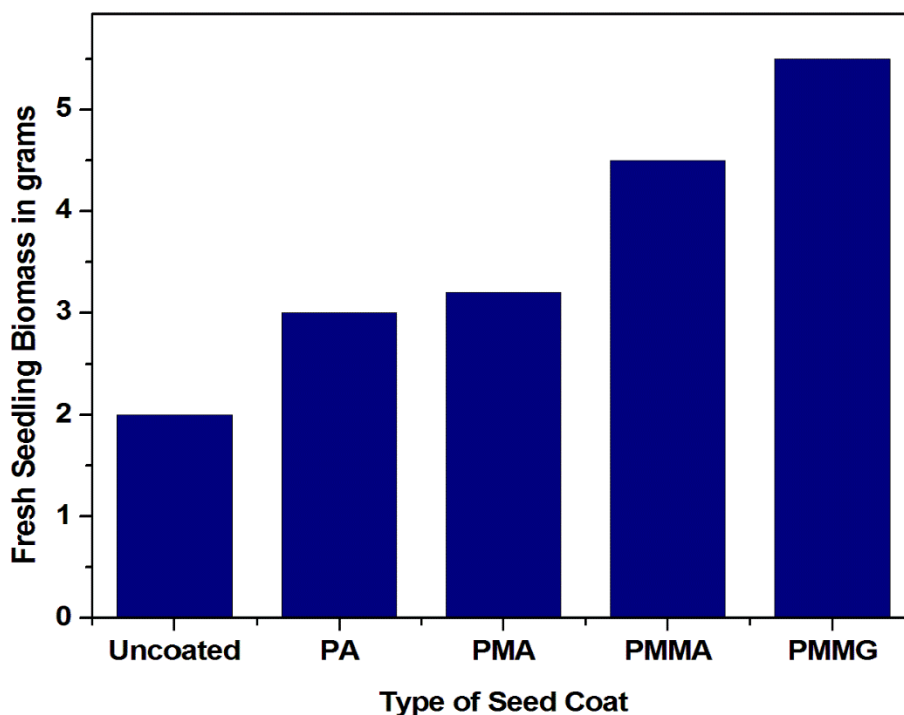


Fig.IV.21 Total fresh biomass of corn seedlings grown from seeds coated with developed membranes after 15 days of germination

Fig.IV.20a and b shows the measurements of radicle and plumule length with days of germination. The root, shoot and overall biomass of all treated seedlings were measured after 15 days (Fig.IV.21). Data were adjusted to the tissue mass of the untreated control plants to make comparisons easier. The α -amylase alone does not increase biomass without the addition of GA and MgO NPs to the nanofiber coating. It's interesting to note that many of the improvements in germination resulted in more seedling biomass.

4.8.2 Statistical Analysis

The findings of the germination of the five sub samples and their five replicates were examined. Following a homogeneity test, a one-way ANOVA was performed on the findings. The results are shown in Table IV.2. An entirely random design was used for the statistical analysis of the data using analysis of variance.

Table IV.2 Estimated marginal mean of germination parameters

Sample		% Germination (%G)	Germination Index (GI)	Seed Vigour Index (SVI)
Uncoated seed	Mean	72.00	72.00	271.00
	(SD)	(4.472)	(4.472)	(24.658)
PA nanofiber coated seeds	Mean	78.00	83.34	313.60
	(SD)	(4.472)	(5.850)	(20.707)
PMA nanofiber coated seeds	Mean	92.00	105.28	397.40
	(SD)	(8.367)	(10.281)	(37.454)
PMMA nanofiber coated seeds	Mean	96.00	123.20	464.20
	(SD)	(5.477)	(6.301)	(24.864)
PMMG nanofiber coated seeds	Mean	96.00	131.00	493.60
	(SD)	(5.477)	(5.788)	(33.982)

A 0.05 level of probability was used for the Tukey's HSD test to analyse the main and interaction effects when the F values were significant³³. A homogenous germination

percentage was found by Levene's test³⁴. According to statistical analysis, the addition of nutrients and enzyme had a substantial impact on the germination percentage. The addition of MgO NPs and Gibberellic acid resulted in considerable difference. Graphical representations of the germination parameters for each treatment are shown in Fig.IV.22. Fig.IV.22b and c show similar results for germination index and seed vigour index as for germination percentage. The length of the seedling was used to determine the germination index and seed vigour index. According to the Tukey HSD test, the growth of the seedlings for the treatment was clearly significant (Table IV.2). The alteration brought on by MgO NPs and GA was substantial.

The results of the one-way ANOVA showed that the addition of fertilizers and treatment had a significant impact on all coatings. On doing the one way ANOVA, the effectiveness of nutrient addition in each case was substantially different from the absence of agrichemicals in the fibers.

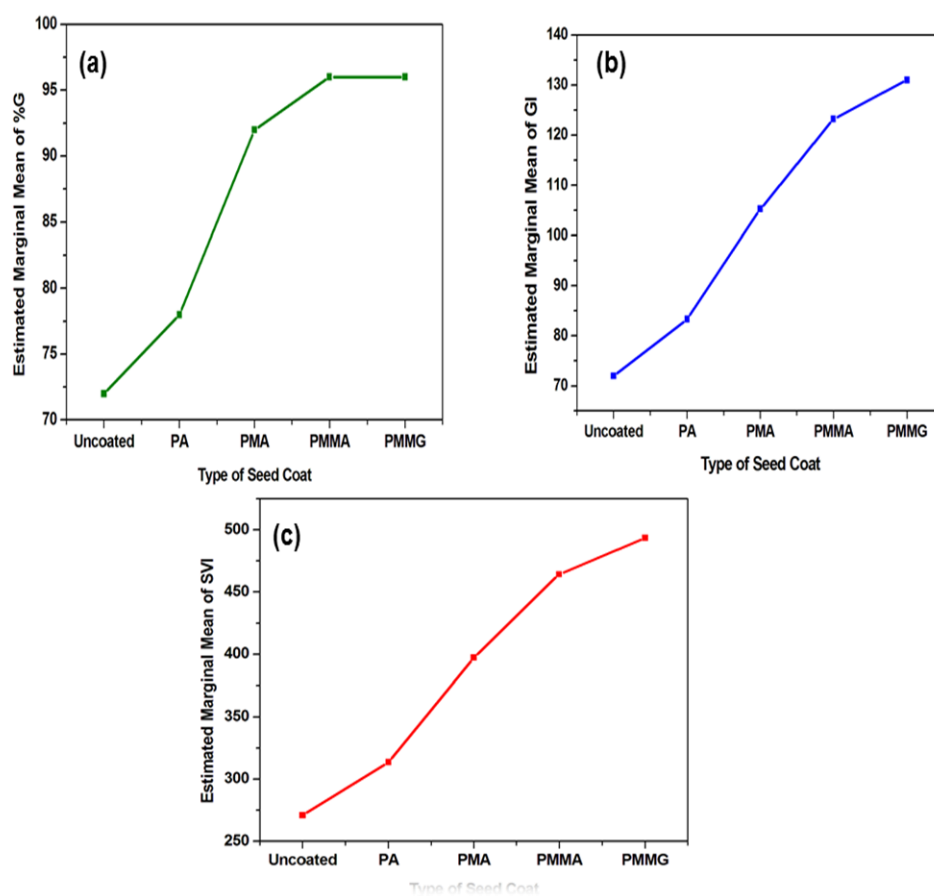


Fig.IV.22 Estimated marginal mean for a) germination percentage
b) germination index c) seed vigour index

4.9 Determination of α -amylase Enzymatic Activity Assay

4.9.1 Effect of Incubation Time on Enzymatic Activity

The enzymatic activity of developed nanofibers depicted in Fig.IV.23. This was monitored over 60 min incubation period of starch solution treated with nanofiber. The activity was measured at 10 min interval. The results showed that the enzymatic activity increased initially from 103 U/mL to 127U/mL till 30 min of incubation time for PA. The optimum incubation time for maximum enzyme activity was found to increase to 40 min in PMA, PMMA and PMMG than directly loaded enzyme for which it was 30 min. The modified enzyme was also able to maintain its activity throughout the period of incubation without significant loss in activity. There was no drastic decrease compared to the directly encapsulated enzyme in PA. The addition of MgO NPs in PMMA and both MgO NPs and GA in PMMG results in more enzymatic activity than PMA. The addition of these fillers increases the wettability and porosity of the fiber with time and therefore enzyme could catalyse the reaction easily. It may be hypothesised that the increased α -amylase activity for the higher starch breakdown is attributed to the presence of GA.

After the substrate molecules have attached to the functionalized silica surfaces, access to some of the enzyme active sites is restricted. In PA there is more freedom for enzyme molecules and substrate molecules can attach to the active sites quite easily. Therefore PA shows high activity initially due to direct encapsulation in polymer nanofibers which allows easy access for enzyme to react with the substrate without any steric hindrance. In the case of PMA, PMMA, PMMG the enzyme is covalently grafted on inorganic polymer MCM-41. Encapsulation in PCL matrix makes it more resistant to changes in conformation. Initial low activity of MCM-41 immobilized enzyme is due to the fact that the enzyme molecules need enough space for catalysing the reaction of the substrate. The presence of intra- and intermolecular cross-links results in stiffer enzyme molecules. This result is similar to that reported by³⁵ Dada *et al.* α -amylase binding through glutaraldehyde in MCM-41 immobilized enzyme increases the stability of the enzyme but decreases the enzyme catalytic activity for initial time periods. The MCM-41 grafted enzyme loaded nanofiber shows high activity which might be useful as an effective seed coat to enhance the starch

degradation ability and germination performance during entire seedling development stages.

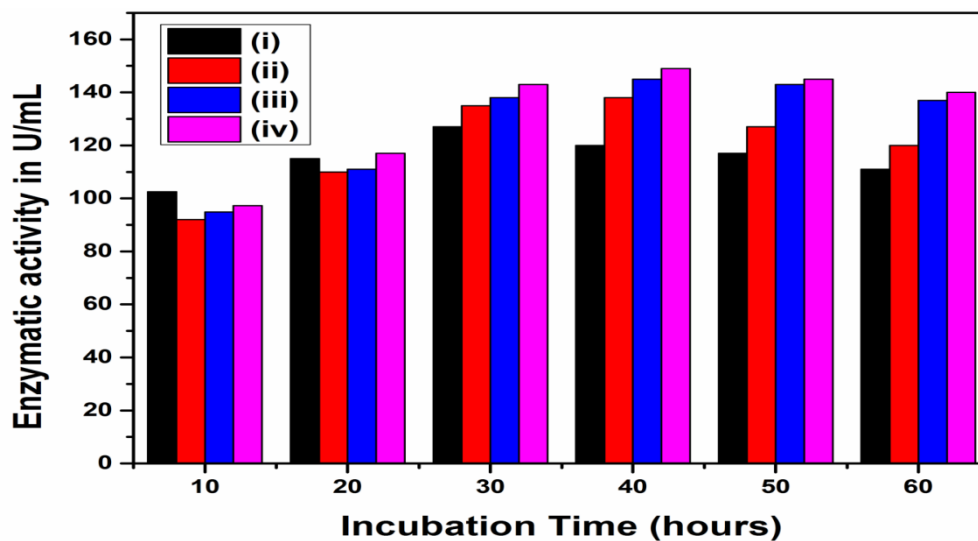


Fig.IV.23 α – Amylase activity in i) PA ii) PMA iii) PMMA iv) PMMG

4.9.2 Effect of pH on Enzyme Activity

Incubating buffers with pH levels between 4.5 and 8.5 were used to evaluate the effect of pH on the activity of covalently grafted α -amylase and directly loaded α -amylase (Fig.IV.24). At low and high pH enzyme immobilized through covalent grafting shows better performance than enzyme directly loaded in PCL matrix. The optimum pH for both nanofibers was found to be 6.5. Immobilization through covalent grafting enzyme activity maintains almost constant even at pH 7.5 without any significant decrease (Fig.IV.24 ii-iv). The high enzymatic activity at basic pH values in MCM-41 immobilized enzyme may be the result of newly established interactions between basic enzyme residues and nanocarriers. This might be the reason for the change in acidic and basic amino acid side chain in the microenvironment around the active site. According to the data, linking α -amylase with nanocarriers can increase its activity at acidic pH and demonstrate good stability of α -amylase at this pH range when compared to the free enzyme. In the covalently immobilized enzymes, the enzymes were fixed to the support material through multiple cross-linking interactions, which stabilized the structure of the overall enzyme and protected it from pH and temperature changes³⁶.

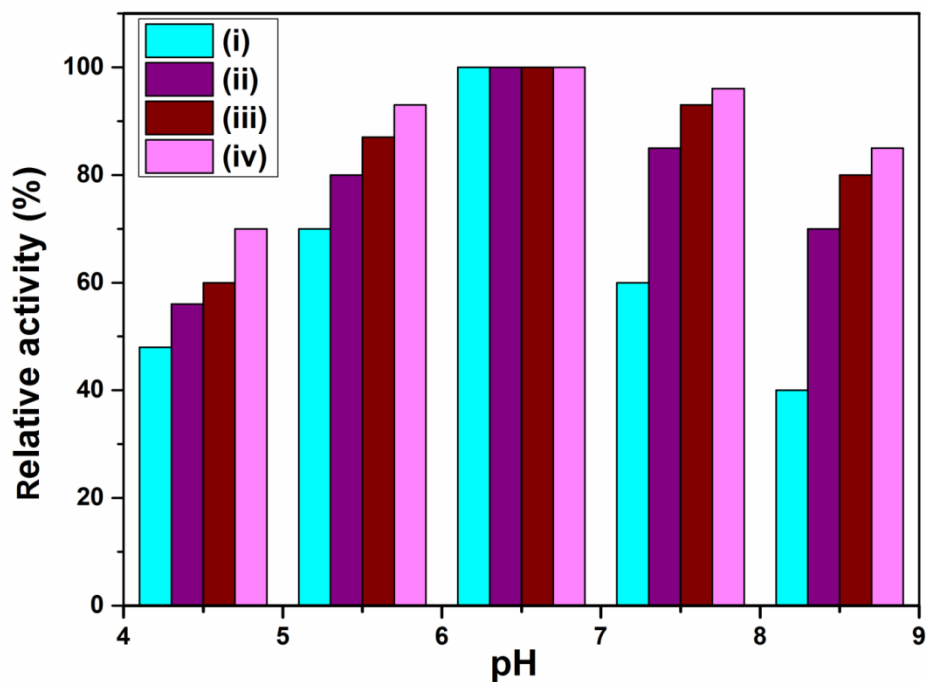


Fig.IV.24 Effect of pH on enzyme activity i) PA ii) PMA iii) PMMA iv) PMMG

4.9.3 Effect of Temperature on Enzyme Activity

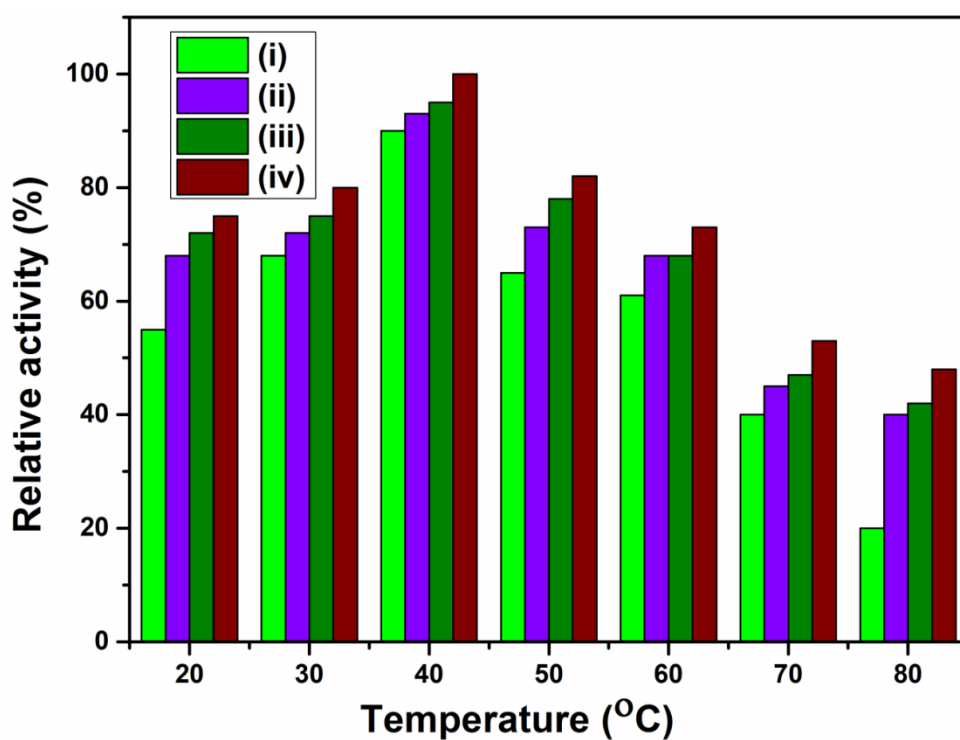


Fig.IV.25 Effect of temperature on enzyme activity
i) PA ii) PMA iii) PMMA iv) PMMG

The enzyme is very susceptible to different temperatures. The relative activity of fabricated nanofibers was examined at various temperatures and the results are presented in Fig.IV.25. As shown in this figure, the maximum activity for all nanofibers was observed at 40°C and the activity maintains high for PMMG, PMMA and PMA even at 50°C due to covalent immobilization through inorganic carrier MCM-41. It is observed from the Fig.IV.25ii-iv that the thermal stability of α -amylase is slightly enhanced because of its immobilization onto inorganic supports. Actually, the immobilization may improve the rigidity of the structure of the enzyme and decreased thermal disturbances in enzyme's structure. Therefore, by increasing the temperature from 20°C to 50°C, the activity of immobilized enzymes increased and gradually decreased at temperature more than 50°C. This might be due to conformational changes of enzyme or its denaturation at higher temperatures. Even though there is a decrease in the activity at higher temperature the MCM-41 immobilized α -amylase in PCL nanofiber matrix samples shows higher activity than PA. Although α -amylase is the most significant enzyme, the germination rate and rice seedling growth characteristics were strongly correlated with its activity^{37,38}. The α -amylase, however, was extremely sensitive to temperatures³⁹. Poor stand establishment under chilling stress was caused by the decreased α -amylase activity, which lowered the total soluble sugar content and respiration rate in rice seeds and seedlings⁴⁰. Therefore, this enzyme immobilized seed coat would be an effective solution to improve seed germination performance and starch degradation ability under cold and drought stress.

4.9.4 Reuse Studies

The sole determiner of an enzyme's cost-effective use in industrial applications is the preservation of immobilized enzyme activity after numerous repetitions of its utilisation. Immobilization on nanofibers has several benefits such as easy separation and reusability. The reuse of enzyme-loaded nanofibers was investigated for up to five runs and the impact of reuses on the retention activity of all fibers under ideal conditions was shown (Fig.IV.26). As depicted in Fig.IV.26iv, after five recycles, almost 56% of the initial activity of PMMG was retained. The main causes of the immobilized enzyme's activity decline after numerous reuses included enzyme denaturation brought on by temperature and hydrodynamic stress as well as

leaching of the enzyme from nanocarriers during incubation. Since substrate repeatedly adheres to the immobilized enzyme's active site, the binding between the matrix and the immobilized α -amylase weakens, which leads to leaching of the enzyme in recycling tests. This can be attributed to the decline in enzymatic activity during continuous use of nanofibers. The immobilized α -amylase's active site becomes distorted and loses activity as a result of repeated interaction with the substrate.

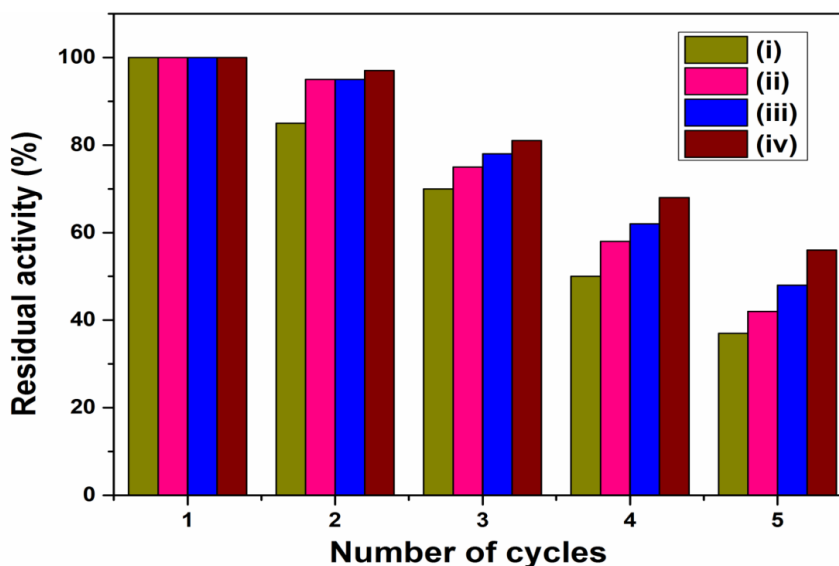


Fig.IV.26 Reusability studies of enzymatic activity
i) PA ii) PMA iii) PMMA iv) PMMG

4.9.5 Storage Studies

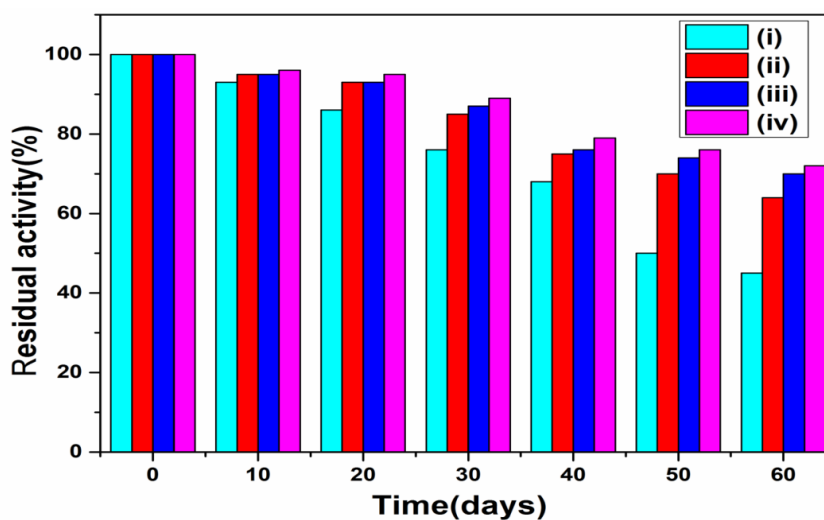


Fig.IV.27 Storage studies on enzymatic activity i) PA ii) PMA iii) PMMA
iv) PMMG

Enzymes lose their activity with time and are not stable when stored in solutions⁴¹. The enzyme immobilized nanofibers were stored at 4°C in 20 mM phosphate buffer, at pH 6.5. Enzyme activity was measured in every 10 days for a period of 8 weeks and the storage stability of immobilized α -amylase was examined. Storage studies are shown Fig.IV.27. Previous research revealed that free enzyme entirely lost its activity after 15 days⁴². The findings demonstrated unambiguously that immobilized amylase maintained its activity for a longer period of time than free amylase. The α -amylase directly encapsulated PA nanofiber shows 45% activity after 60 days where as PMMG in which enzyme incorporated through inorganic silica support lost only 28% activity even after 60 days. The enzyme's denaturation and chemical inactivation during storage studies are two potential causes of the decreased activity.

4.10 α - Amylases Activity in Coated and Uncoated Germinating Seeds

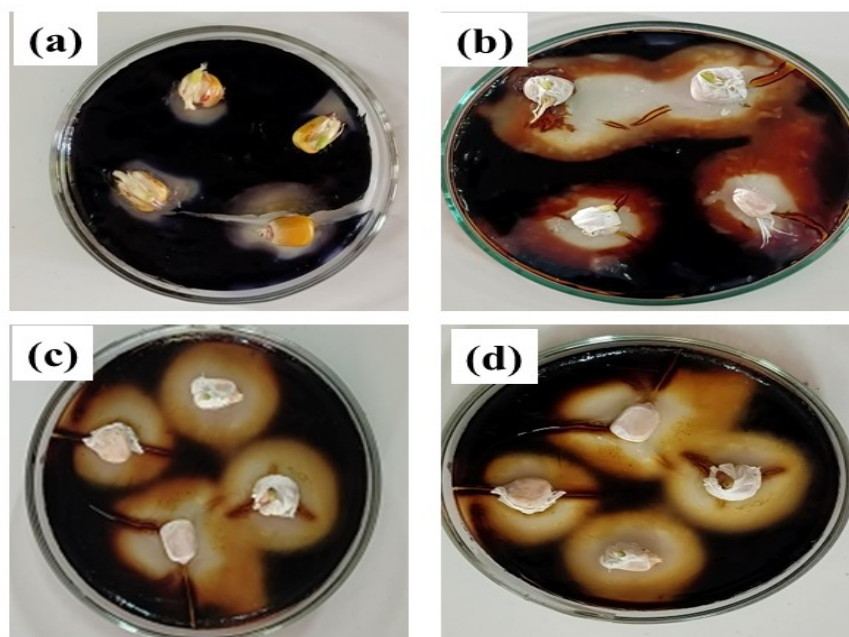


Fig.IV.28 α -Amylase activity after 7 days of germination in
a) Uncoated seeds b – d) Seeds coated with nanofibers
b) PA c) PMMA d) PMMG

α -Amylase activity in the coated and uncoated maize seeds at 144 h of germination is shown in Fig.IV.28. Enzyme activity was detected on agar plate containing 1% (w/v) starch and stained with 5% (w/v) Iodine-Potassium iodide

solution. The digested starch area stayed transparent while the undigested area turned blue. Pale areas identify intense α -amylase activity. In the picture, the width of the transparent area corresponds exactly to the degraded starch by the activity of α -amylase. The diameter of digested zone is very small in uncoated seeds than in immobilized α -amylase loaded nanofibers PA, PMMA and PMMG coated seeds. The larger diameter of pale areas suggests the additional α -amylase activity other than the enzymes within the maize seeds even after 7 days of germination. Therefore the developed seed coatings would aid in starch degradation to sugars during the early stages of germination.

Conclusion

In this study, covalent binding of α -amylase on MCM-41 was done through surface functionalization. The immobilization of α -amylase, an enzyme of agricultural interest, in PCL nanofiber matrix was done via two approaches. PCL nanofibers were successfully fabricated by loading MCM-41 immobilized amylase and by direct entrapment of free α -amylase using electrospinning. Results indicate that the PCL nanofibers with amylase immobilized on MCM-41 showed improved optimum temperature, pH, reuse and storage stability compared with direct entrapment. Immobilization on PCL nanofiber protected α -amylase from denaturation and loss of activity induced by pH and temperature variations. Although α -amylase directly encapsulated PA nanofiber shown 45% activity, PMMG and PMMA displayed amazing stability and maintained almost 72% of relative activity even after 8 weeks. As the nanobiocatalyst was able to retain more than 56% of its initial activity after 5 operational cycles, the prospective reuses of the immobilised system may be successful for five or more cycles. The findings show that PCL nanofiber is a promising choice for α -amylase immobilization as a nanocarrier. In comparison to direct entrapment, the immobilisation of enzyme in PCL nanofiber after covalent grafting in inorganic carrier provides increased stability. Therefore the role of immobilized alpha amylase loaded nanofiber seed coat would be an effective solution to improve seed germination performance and starch degradation ability under different abiotic stress conditions such as drought and salinity of crops. This study confirmed that nanofibers of PCL can serve as an excellent support for enzyme immobilization. The presence of MgO NPs and GA significantly boost the

germination parameters. The germination studies and magnesium ion release profile of nanofibers reported here suggests the potential of nanofibrous scaffold in seed coating industry to enhance crop yield and for the controlled release of nutrients.

References

1. Shu, Y., Shao, Y., Wei, X., Wang, X., Sun, Q., Zhang, Q., & Li, L. (2015). Synthesis and characterization of Ni-MCM-41 for methyl blue adsorption. *Microporous and Mesoporous Materials*, 214, 88-94.
2. Bhunia, S., Saha, D., & Koner, S. (2011). MCM-41-supported oxo-vanadium (IV) complex: a highly selective heterogeneous catalyst for the bromination of hydroxy aromatic compounds in water. *Langmuir*, 27(24), 15322-15329.
3. Hajjami, M., Ghorbani, F., & Bakhti, F. (2014). MCM-41-N-propylsulfamic acid: An efficient catalyst for one-pot synthesis of 1-amidoalkyl-2-naphthols. *Applied Catalysis A: General*, 470, 303-310.
4. Lee, K. H., Kim, H. Y., Khil, M. S., Ra, Y. M., & Lee, D. R. (2003). Characterization of nano-structured poly (ϵ -caprolactone) nonwoven mats via electrospinning. *Polymer*, 44(4), 1287-1294.
5. Gupta, K. K., Kundan, A., Mishra, P. K., Srivastava, P., Mohanty, S., Singh, N. K. & Maiti, P. (2012). Retracted Article: Polycaprolactone composites with TiO₂ for potential nanobiomaterials: tunable properties using different phases. *Physical Chemistry Chemical Physics*, 14(37), 12844-12853.
6. Guang-Mei, C., Tie-Mei, Z., Lei, C., & Yi-Ping, H. (2010). Crystallization properties of polycaprolactone induced by different hydroxyapatite nano-particles. *Asian Journal of Chemistry*, 22(8), 5902.
7. Amina, M., Al Musayeb, N. M., Alarfaj, N. A., El-Tohamy, M. F., Oraby, H. F., Al Hamoud, G. A. & Moubayed, N. M. (2020). Biogenic green synthesis of MgO nanoparticles using *Saussurea costus* biomasses for a comprehensive detection of their antimicrobial, cytotoxicity against MCF-7 breast cancer cells and photocatalysis potentials. *PLoS One*, 15(8), e0237567.
8. Gao, N., Lu, G., Lercher, M. J., & Chen, W. H. (2017). Selection for energy efficiency drives strand-biased gene distribution in prokaryotes. *Scientific reports*, 7(1), 10572.
9. Abd El Rahman, S. K., Hassan, H. M., & El-Shall, M. S. (2012). Acid catalyzed organic transformations by heteropoly tungstophosphoric acid supported on MCM-41. *Applied Catalysis A: General*, 411, 77-86.
10. Parida, S. K., Dash, S., Patel, S., & Mishra, B. K. (2006). Adsorption of organic molecules on silica surface. *Advances in colloid and interface science*, 121(1-3), 77-110.

11. Dobrowolski, R., Oszust-Cieniuch, M., Dobrzyńska, J., & Barczak, M. (2013). Amino-functionalized SBA-15 mesoporous silicas as sorbents of platinum (IV) ions. *Colloids and Surfaces A: Physicochemical and Engineering Aspects*, 435, 63-70.
12. Hamblin, M. R. (2016). Shining light on the head: photobiomodulation for brain disorders. *BBA clinical*, 6, 113-124.
13. Sleem, D. A. E. (2013). Studies on the Bio production of Gibberellic Acid from Fungi.
14. Thomas, V., Jagani, S., Johnson, K., Jose, M. V., Dean, D. R., Vohra, Y. K., & Nyairo, E. (2006). Electrospun bioactive nanocomposite scaffolds of polycaprolactone and nanohydroxyapatite for bone tissue engineering. *Journal of nanoscience and nanotechnology*, 6(2), 487-493.
15. Mahardika, I. B. P., Trisunaryanti, W., Triyono, T., Wijaya, D. P., & Dewi, K. (2017). Transesterification of used cooking oil using CaO/MCM-41 catalyst synthesized from lapindo mud by sonochemical method. *Indonesian Journal of Chemistry*, 17(3), 509-515.
16. Patlolla, A., Collins, G., & Arinze, T. L. (2010). Solvent-dependent properties of electrospun fibrous composites for bone tissue regeneration. *Acta biomaterialia*, 6(1), 90-101.
17. Sivaiah, K., Kumar, K. N., Naresh, V., & Buddhudu, S. (2011). Structural and optical properties of Li⁺: PVP & Ag⁺: PVP polymer films. *Materials Sciences and Applications*, 2(11), 1688.
18. Kwon, Y. A., & Majid Sarmadi, A. (1995). Wettability of nonwoven fabrics: effect of laundering on water absorption. *Clothing and Textiles Research Journal*, 13(1), 17-29.
19. Johari, N., Fathi, M. H., Golozar, M. A., Erfani, E., & Samadikuchaksaraei, A. (2012). Poly (ϵ -caprolactone)/nano fluoridated hydroxyapatite scaffolds for bone tissue engineering: in vitro degradation and biocompatibility study. *Journal of Materials Science: Materials in Medicine*, 23, 763-770.
20. Jenkins, M. J., & Harrison, K. L. (2008). The effect of crystalline morphology on the degradation of polycaprolactone in a solution of phosphate buffer and lipase. *polymers for Advanced Technologies*, 19(12), 1901-1906.
21. Augustine, R., Kalarikkal, N., & Thomas, S. (2016). Effect of zinc oxide nanoparticles on the in vitro degradation of electrospun polycaprolactone membranes in simulated body fluid. *International Journal of Polymeric Materials and Polymeric Biomaterials*, 65(1), 28-37.
22. Wei, J., Chen, F., Shin, J. W., Hong, H., Dai, C., Su, J., & Liu, C. (2009). Preparation and characterization of bioactive mesoporous wollastonite–polycaprolactone composite scaffold. *Biomaterials*, 30(6), 1080-1088.

23. Hosseini, Y., Emadi, R., & Kharaziha, M. (2017). Surface modification of PCL-diopside fibrous membrane via gelatin immobilization for bone tissue engineering. *Materials Chemistry and Physics*, 194, 356-366.
24. Borji, M., Ghorbanli, M., & Sarlak, M. (2007). Some seed traits and their relationships to seed germination, emergence rate electrical conductivity in common bean (*Phaseolus vulgaris* L.). *Asian Journal of Plant Sciences*, 6(5), 781-787.
25. Damasceno, R., Roggia, I., Pereira, C., & de Sá, E. (2013). Rhizobia survival in seeds coated with polyvinyl alcohol (PVA) electrospun nanofibres. *Canadian journal of microbiology*, 59(11), 716-719.
26. Kaneko, M., Itoh, H., Ueguchi-Tanaka, M., Ashikari, M., & Matsuoka, M. (2002). The α -amylase induction in endosperm during rice seed germination is caused by gibberellin synthesized in epithelium. *Plant Physiology*, 128(4), 1264-1270
27. Franco, O. L., Rigden, D. J., Melo, F. R., & Grossi-de-Sá, M. F. (2002). Plant α -amylase inhibitors and their interaction with insect α -amylases: Structure, function and potential for crop protection. *European journal of biochemistry*, 269(2), 397-412.
28. Shu, K., Qi, Y., Chen, F., Meng, Y., Luo, X., Shuai, H. & Yang, W. (2017). Salt stress represses soybean seed germination by negatively regulating GA biosynthesis while positively mediating ABA biosynthesis. *Frontiers in plant science*, 8, 1372.
29. Munns, R., & Tester, M. (2008). Mechanisms of salinity tolerance. *Annu. Rev. Plant Biol.*, 59, 651-681.
30. Tuteja, N., Sahoo, R. K., Garg, B., & Tuteja, R. (2013). OsSUV3 dual helicase functions in salinity stress tolerance by maintaining photosynthesis and antioxidant machin-R. *Ruhel et al.*
31. Meng, Y., Chen, F., Shuai, H., Luo, X., Ding, J., Tang, S. & Yang, W. (2016). Karrikins delay soybean seed germination by mediating abscisic acid and gibberellin biogenesis under shaded conditions. *Scientific reports*, 6(1), 22073.
32. Dong, T., Tong, J., Xiao, L., Cheng, H., & Song, S. (2012). Nitrate, abscisic acid and gibberellin interactions on the thermoinhibition of lettuce seed germination. *Plant Growth Regulation*, 66, 191-202.
33. Steel, R. G. D., & Torrie, J. H. (1980). *Principles and procedures of statistics, a biometrical approach* (No. Ed. 2). McGraw-Hill Kogakusha, Ltd..
34. Gastwirth, J. L., Gel, Y. R., & Miao, W. (2009). The impact of Levene's test of equality of variances on statistical theory and practice.

-
35. Daba, T., Kojima, K., & Inouye, K. (2013). Chemical modification of wheat β -amylase by trinitrobenzenesulfonic acid, methoxypolyethylene glycol, and glutaraldehyde to improve its thermal stability and activity. *Enzyme and microbial technology*, 53(6-7), 420-426.
 36. Pandya, P. H., Jasra, R. V., Newalkar, B. L., & Bhatt, P. N. (2005). Studies on the activity and stability of immobilized α -amylase in ordered mesoporous silicas. *Microporous and Mesoporous Materials*, 77(1), 67-77.
 37. Williams, J. F., & Peterson, M. L. (1973). Relations Between Alpha-amylase Activity and Growth of Rice Seedlings 1. *Crop science*, 13(6), 612-615.
 38. McCouch, S. R., Wright, M. H., Tung, C. W., Maron, L. G., McNally, K. L., Fitzgerald, M., & Mezey, J. (2016). Open access resources for genome-wide association mapping in rice. *Nature communications*, 7(1), 10532.
 39. Umemoto, T., Nakamura, Y., & Ishikura, N. (1995). Activity of starch synthase and the amylose content in rice endosperm. *Phytochemistry*, 40(6), 1613-1616.
 40. Wang, W., Chen, Q., Hussain, S., Mei, J., Dong, H., Peng, S. & Nie, L. (2016). Pre-sowing seed treatments in direct-seeded early rice: consequences for emergence, seedling growth and associated metabolic events under chilling stress. *Scientific reports*, 6(1), 19637.
 41. Oktay, B., Demir, S., & Kayaman-Apohan, N. (2015). Immobilization of α -amylase onto poly (glycidyl methacrylate) grafted electrospun fibers by ATRP. *Materials Science and Engineering: C*, 50, 386-393.
 42. Defaei, M., Taheri-Kafrani, A., Miroliaei, M., & Yaghmaei, P. (2020). Alpha-amylase immobilized on polycaprolactone-grafted magnetic nanoparticles: improving stability and reusability. *Journal of Chemical Technology & Biotechnology*, 95(8), 2243-2250.

Chapter 5

Incorporation of nanohydroxyapatite and carbon dots into PEO/cellulose nanofibers and its application as seed coats

This chapter discusses the design and the application of biopolymer based nanofibers as seed coats for precision agricultural applications. Focus of research is shifting to biopolymers in order to tackle the economic and environmental challenges. Water hyacinth was used as a source for the synthesis of carbon dots and cellulose. The present investigation discusses the application of nanofiber matrix of PEO and cellulose for the encapsulation of nontoxic nanofertilizers carbon dots and nanohydroxyapatite. The developed membranes are characterized and applied as seed coats for controlled agrichemical release and to increase germination performance. The block diagram of methodology for seed coating is shown in Fig.V.1

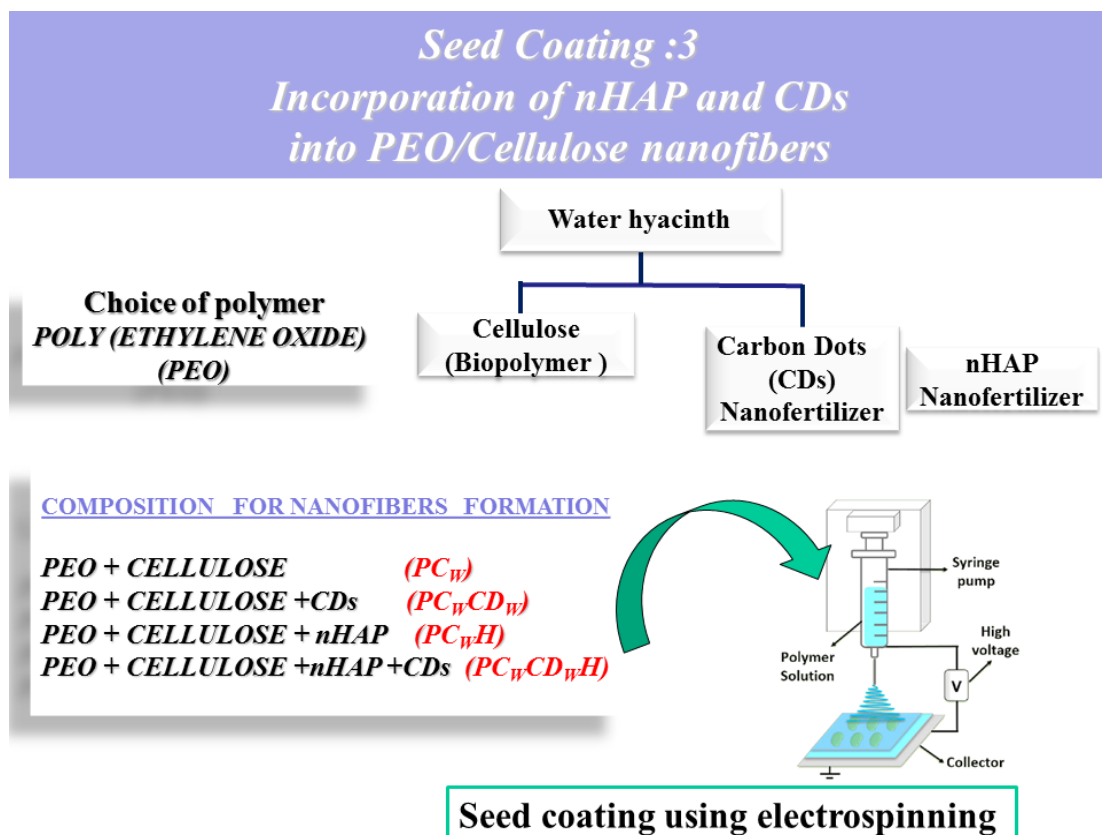


Fig.V.1 Block diagram of methodology for seed coating: 3

5.1 XRD Analysis

The XRD spectra of synthesized nHAP and CDs are investigated (Fig.V.2). The Bragg diffraction peaks of the synthesized nHAP closely matched with those of conventional nano-HAP¹. 2θ values at 25.9° , 31.7° , 32.9° , 39.6° , 49.4° and 53.1° , had the following indices: (002), (210), (211), (112),(300) and (220) (JCPDS File No. 89-6440). The XRD pattern of CDs displays a broad peak at $2\theta = 22^\circ$ corresponding to (002) hkl plane (JCPDS card no. 26-1076). In addition to the broadness feature, the interlayer spacing of the CDs is greater than that of the graphitic interlayer spacing². This demonstrates that CDs are amorphous in nature. The incorporation of CDs in to nanofibers does not produce any additional peaks corresponding to CDs and the diffraction pattern remains the same. Hence CDs can be assigned to have non-crystalline or amorphous nature.

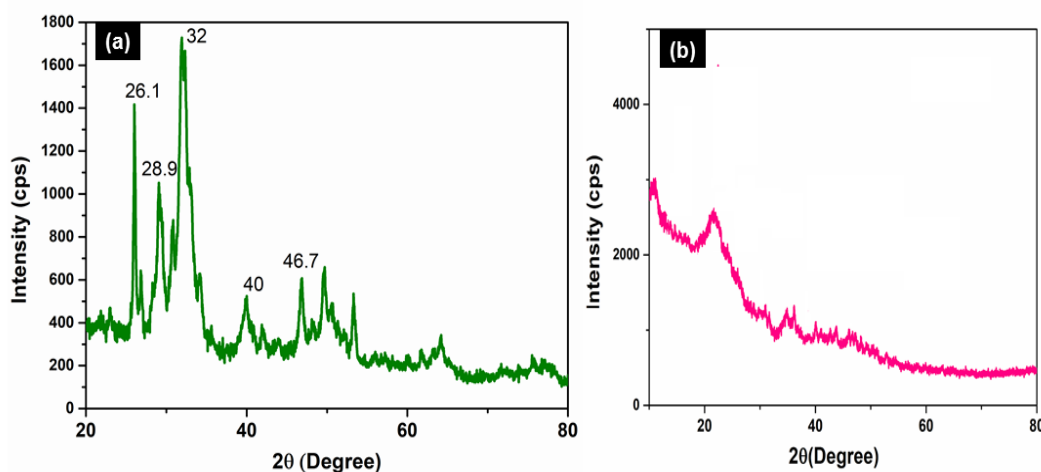


Fig.V.2 XRD Diffractogram of synthesized a) nHAP b) CDs

The XRD pattern of cellulose isolated from water hyacinth is given in Fig.V.3. It shows significant peaks around $2\theta = 16.7^\circ$, 22.3° and 35.34° which are characteristic peaks for cellulose corresponding to the lattice planes (110), (200) and (004)³. This is related to the crystalline structure of cellulose isolated from water hyacinth. Swelling properties of the nanofibers are related to the crystallinity of cellulose. A high crystallinity can decrease the water-holding capacity of a nanofiber⁴.

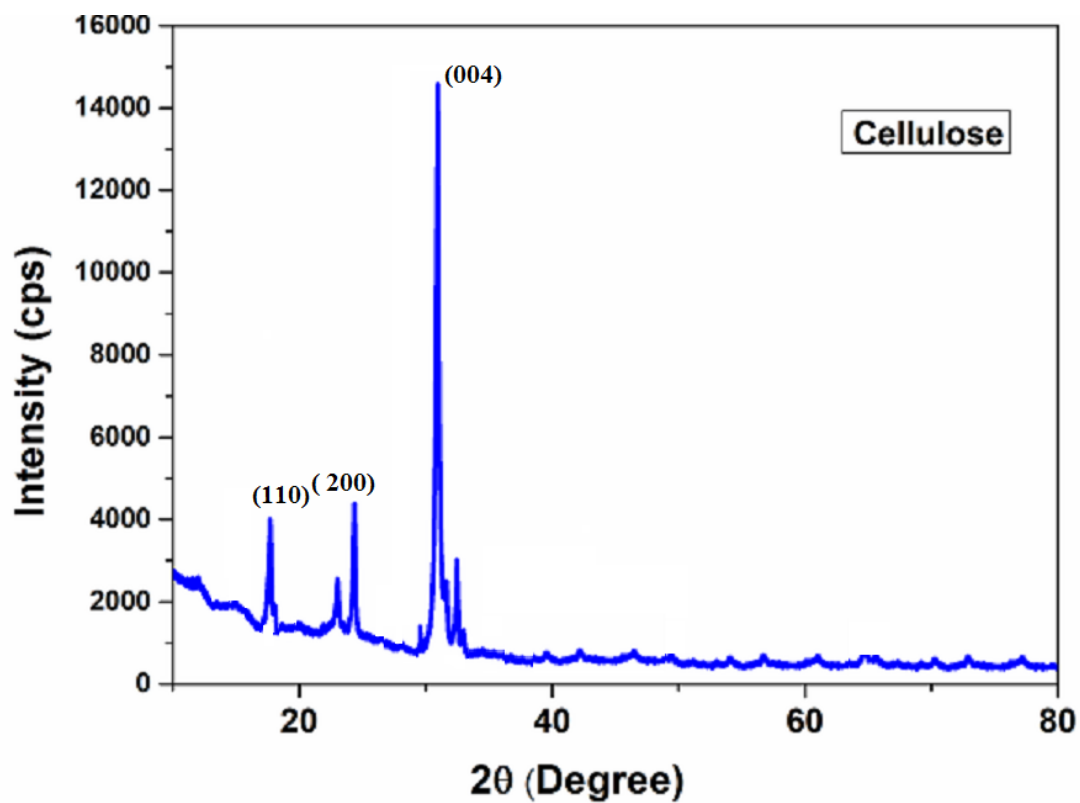


Fig.V.3 XRD diffractogram of cellulose extracted from water hyacinth

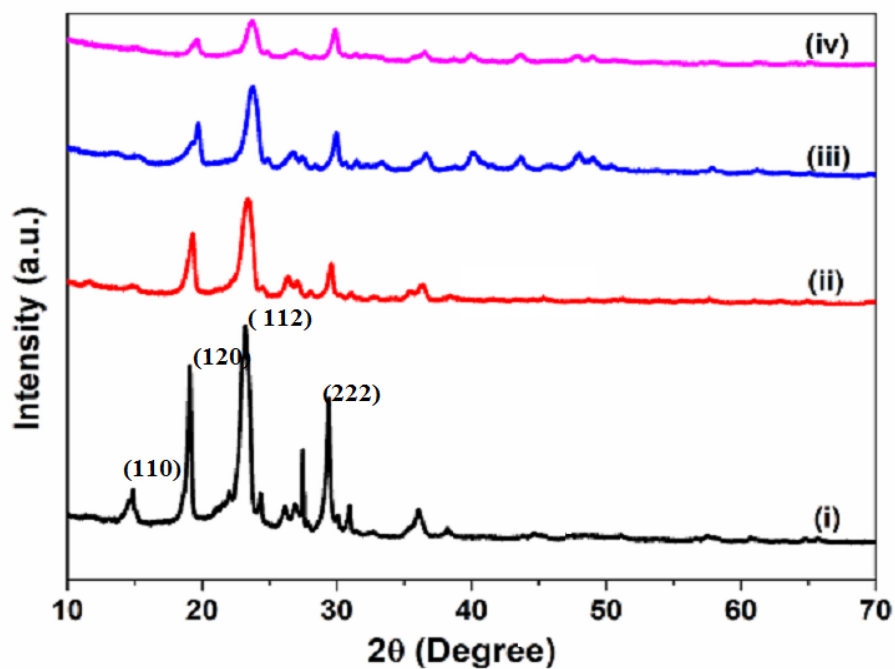


Fig.V.4 XRD diffractogram of i) PC_w ii) PC_wCD_w iii) PC_wH iv) PC_wCD_wH

Fig.V.4 represents the X-ray spectra of fabricated nanofibers. In Fig.V.4i The diffraction peak at 23° is due to (112) plane of PEO and other more intense peaks at 18.5° , 27.3° are assigned to (120) and (222) planes⁵ [PCPDF File Nos. 49-2200 and 49-2201] respectively. The spectrum of PCw shows well-defined two diffraction peaks at 18.5° and 23° , which confirms the semicrystalline nature of blend. In addition to peaks of PEO, the peak at 15.7° is due to the (110) plane of cellulose. After blending this peak is shifted to slight low angle which may be attributed to the interactions between cellulose and PEO.

XRD analysis of PCwCDw nanofibers filled with CDs is shown in Fig.V.4ii. The intensity of diffraction peaks decreases in PCwCDw and does not produce any additional peaks when compared with PCw. The diffraction pattern remains the same. This can be assigned to the non-crystalline or amorphous nature of CDs which is further confirmed by the XRD spectra of CDs. With increasing the content of nanofillers, there is a dramatic decrease in the intensity of main diffraction peaks in PCwH and PCwCDwH. This implies an increase in the amorphous regions in the polymeric matrix. The matrix became random indicating a decrease in the degree of crystallinity. This observation indicates that interaction between the nanofillers and the polymers existed in the amorphous regions. The peaks of nHAP at 26.1° (002), 31.7° (211) and 32.4° (112) are not clearly seen in Fig.V.4iii and iv as these peaks overlap with polymer diffraction peaks. But the low intensity peaks between $2\theta = 40^\circ$ to 50° clearly shows the encapsulation of nHAP in the polymer matrix.

5.2 FTIR Spectra

To ensure composition of cellulose extracted from water hyacinth, the sample was characterized using FTIR spectral studies to investigate the cellulose functional groups and compared with the pure cellulose spectra (Fig.V.5). The FTIR spectra of the extracted cellulose (Fig.V.5i) showed significant peaks at 3340 and 2885 cm^{-1} , due to the -OH stretching and C-H stretching, respectively. The bands at 1445 , 1309 , 1285 and 1011 cm^{-1} is due to -CH₂ scissoring, -OH bending, C-H asymmetric stretching, and the C-O-C pyranose ring respectively⁶⁻⁸. All the bands mentioned above correspond to the pure cellulose structure as in Fig.V.5i. The absence of peak around 1740 and 1215 cm^{-1} indicates the absence of hemicellulose content in the isolated product. The absence of peak at $1,640\text{ cm}^{-1}$, further confirms the absence of

carbonyl groups of hemicellulose. The peak at 1525 cm^{-1} and 864 cm^{-1} corresponds to C=C and C–C stretching in the aromatic rings of the lignin structure⁹. This indicates a minor amount of lignin is present in the cellulose extracted from water hyacinth¹⁰. The FTIR data supports the successful extraction of cellulose from water hyacinth.

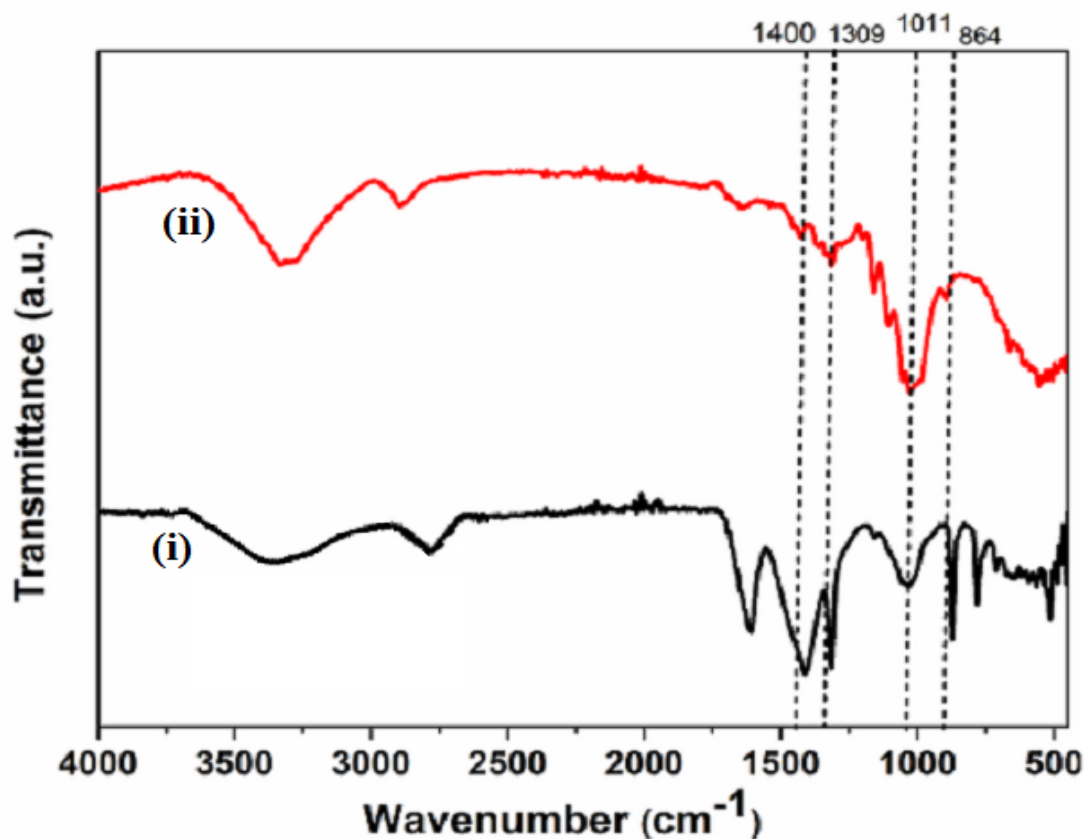


**Fig.V.5 The FTIR Spectrum of i) pure cellulose
ii) cellulose extracted from water hyacinth**

The FTIR spectrum of carbon dots synthesized is shown in Fig.V.6. Due to the stretching vibrations of the -OH groups, FTIR spectra of CDs exhibits broad peaks in the range 3300 to 3400 cm^{-1} . The stretching and bending vibrations of -CH₂ peaks are detected at 2916 and 1465 cm^{-1} respectively. The peak corresponding to 1250 cm^{-1} is due to C-O stretching inferring that carboxylic groups are present on the surface of carbon dots. Moreover, CDs exhibit the C=O and C-O-C vibrational characteristic bands at 1613 cm^{-1} and 1035 cm^{-1} respectively. The aforementioned finding indicates that the high fluorescent CDs were produced with hydroxyl, carbonyl and carboxylic

functional groups. The two peaks at 810 and 1120 cm^{-1} corresponded to the symmetrical and asymmetrical stretching vibrations of C–O–C groups¹¹.

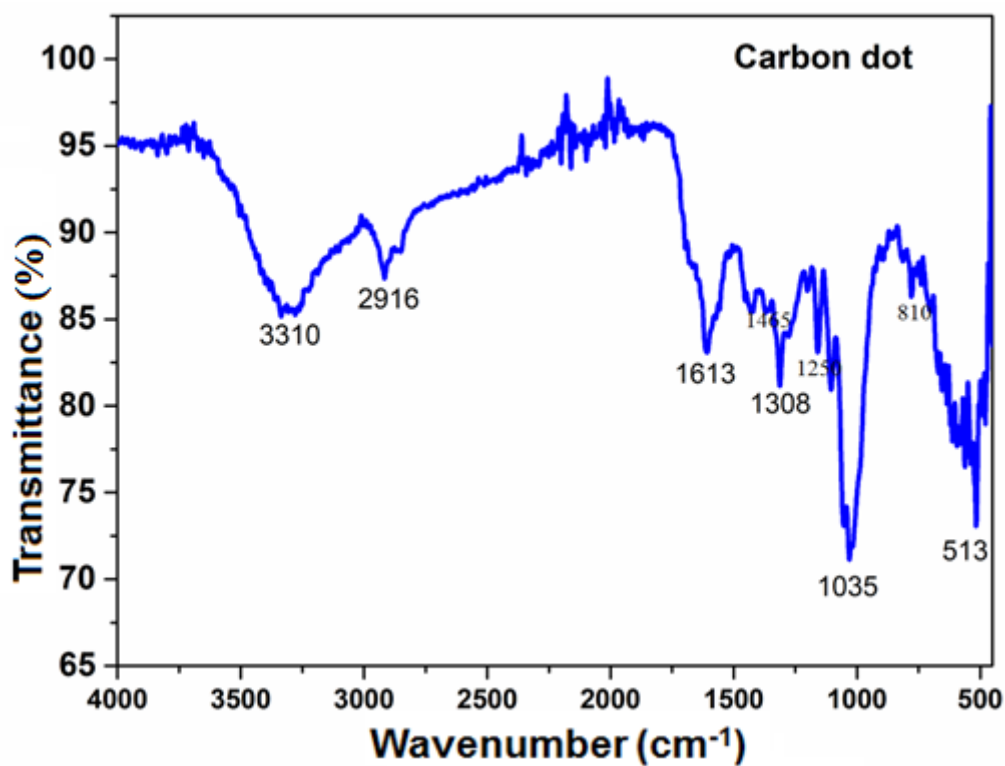


Fig.V.6 The FTIR spectrum of synthesized carbon dots

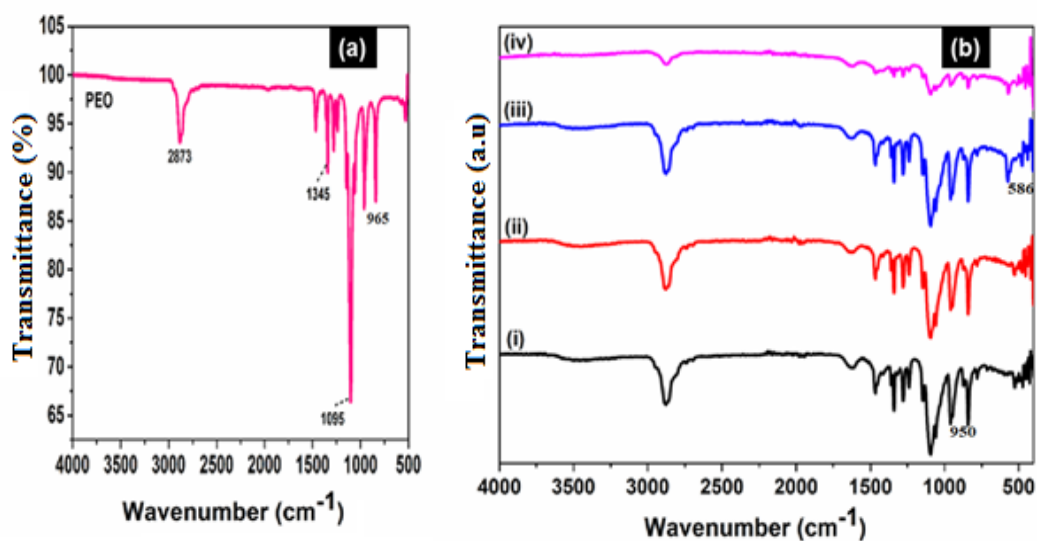


Fig.V.7 The FTIR Spectrum of a) PEO b) developed nanofibers
i) PCw ii) PCwCDw iii) PCwH iv) PCwCDwH

FTIR spectrum of PEO is shown in Fig V.7a. The absorption bands at 2873, 1463, 1150, 1095, 1060 and 965 cm^{-1} in pure PEO electrospun mat were attributed to vibrations of the CH_2 stretching, C-H bending mode and C-O-C stretching vibration respectively¹². FTIR of all blended nanofibers are shown in Fig.V.7b. It should be noted that FTIR curves of all nanofibers did not show the O-H absorption band. Due to PEO's large molecular weight, the function of its end group (-OH) might be disregarded¹³. The absorption band for the C-O-C stretching vibration was changed from 965 to 950 cm^{-1} with the addition of cellulose. The shift can be seen in the spectrum of four samples, indicating potential interactions between PEO and Cellulose¹⁴. The intensities and frequencies of peaks at 1150 cm^{-1} and 1095 cm^{-1} are influenced by the crystallinity of PEO and the intermolecular interactions (e.g., hydrogen bonding) between C-O-C and other materials^{15,16}. This shows the blending of PEO with cellulose. The C-O-C bands of pyranose ring overlaps with C-O-C bands of PEO results in change in intensities of these peaks.

Comparing with the PEO/Cellulose nanofiber (PC_w) mat, the intensity of all peaks in filler loaded nanofibers PC_wCD_w , PC_wH and $\text{PC}_w\text{CD}_w\text{H}$ found to decrease which may be due to interactions between surface functional groups of carbon dots and the polymers. The presence of a very weak peak at 585 cm^{-1} corresponds to the asymmetric bending vibration PO_4^{3-} of nHAP¹⁷ present in the spectrum of the PC_wH and $\text{PC}_w\text{CD}_w\text{H}$ (Fig.V.7b(iii) and (iv)) nanofiber mats. The main peaks of CDs and nHAP are all in the same range of major peaks of PEO and cellulose. So the broadening and decrease in intensity of peaks around this region accounts for the loading of these components in the nanofiber.

5.3 Study of Morphology

5.3.1 SEM Analysis

The morphology of four different kinds of nanofibers fabricated using the aforementioned production method is summarised in Fig.V.8. Fig.V.8(ia-iva) show that bead-free and uniform oriented nanofibers were successfully formed. This is due to uniform dispersion of CDs in the nanofiber matrix. This even distribution allows a slow release of the agrichemicals into the soil. The average nanofiber diameter for PC_w (Fig.V.8(ia)) and PC_wCD_w (Fig.8(ia)) was 276 nm and 214 nm respectively. The diameter of nanofiber is decreased by the addition of CDs. The

mean fiber diameter of nHAP loaded nanofibers PC_wH and PC_wCD_wH decreased as depicted in Fig.V.8(iia) and Fig.V.8(iva). The average fiber diameter of PC_wH and PC_wCD_wH was found to be 196 nm and 112 nm respectively. Adding the CDs resulted in a reduced diameter. The smooth and bead-free morphology may be because the CDs decreased the surface tension of polymer solution. Some fiber beading was seen as a result of the nHAP addition. Some fibers in Fig.V.8(iia and iva) show agglomeration due to the presence of nHAP and the fiber diameter becomes non uniform and the average fiber diameter of the samples decreases¹⁸.

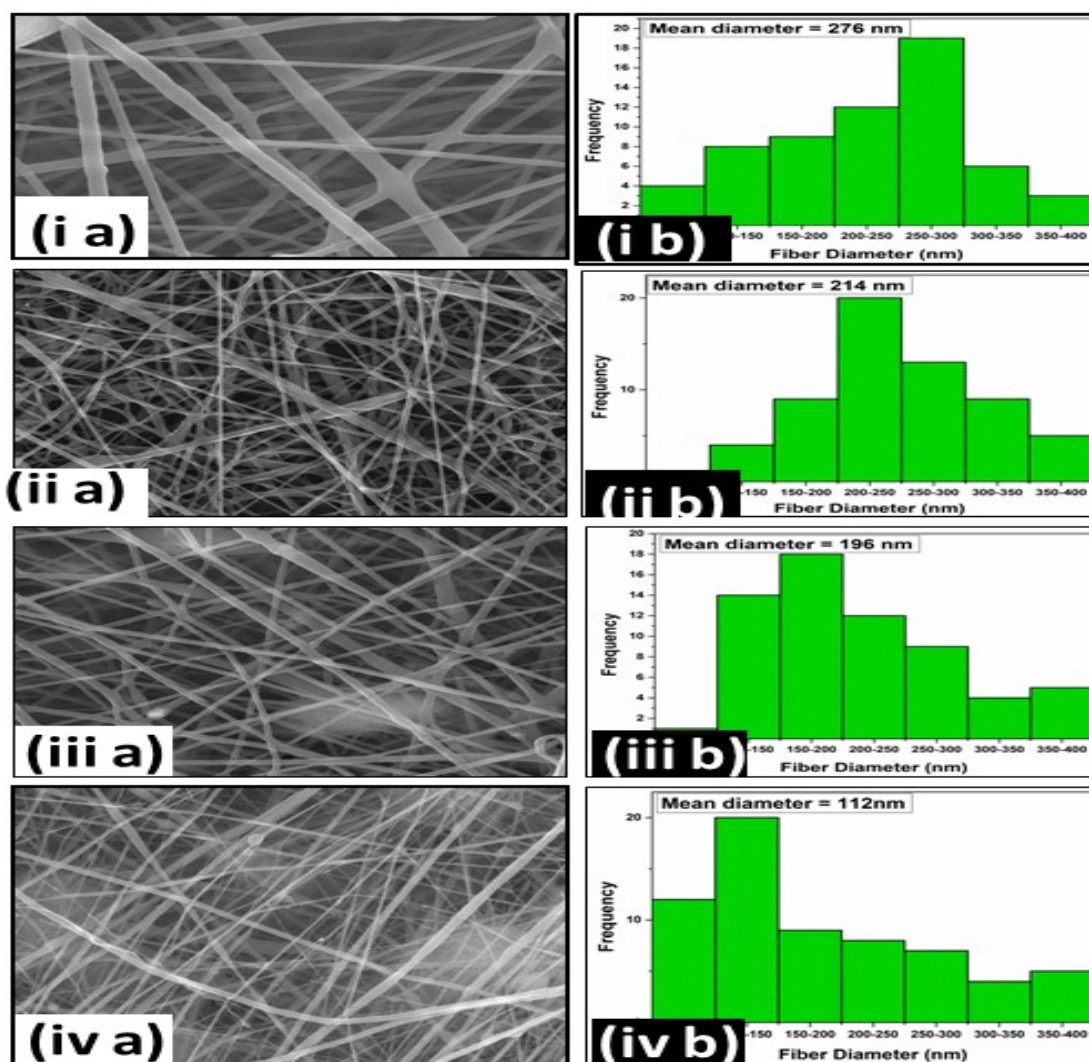


**Fig.V.8 (ia - iva) The morphology of different electrospun nanofibers
 ia) PC_w iia) PC_wCD_w iia) PC_wH iva) PC_wCD_wH
 (ib - ivb) Histogram bar chart of ib) PC_w iib) PC_wCD_w
 iiib) PC_wH ivb) PC_wCD_wH**

It is well known that increase in conductance of solution will decrease the fiber diameter. The inclusion of nHAP and CDs boosted the solution's conductivity¹⁹, which in turn caused the jet's ejection to have a higher charge density. Straight and thin nanofibers are produced as a result of the extra charges' self-repulsion and the increased elongation pressures caused by the high charge density. As a result, it was found that the average diameters of the nanofiller-incorporated fibers were smaller than those of PCw. Fig.V.8(ib- ivb) displays a histogram bar chart of the fiber diameter of nanofibers. The addition of CDs and nHAP cause a decrease in the fiber diameter in the case of PCwCDw, PCwH, PCwCDwH.

5.3.2 EDX Spectrum of PCwCDwH Nanofibers

The EDX of PCwCDwH nanofibers are shown in the Fig.V.9. Carbon, oxygen, phosphorous and calcium are all present on the surface of the nanofiber composite. It infers that all of the fillers have been loaded successfully and are present on the surface.

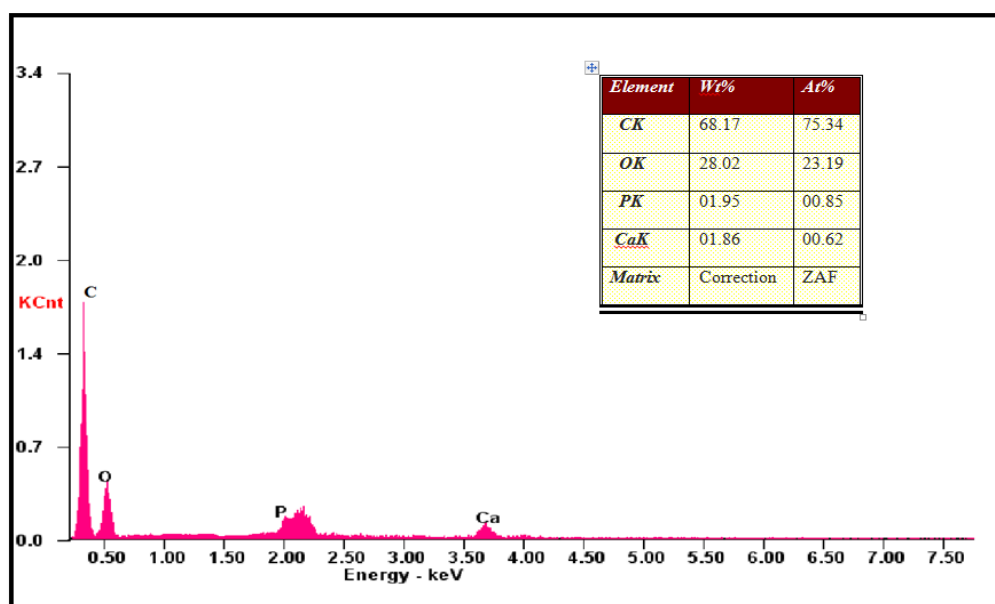


Fig.V.9 EDX spectrum of PCwCDwH nanofiber

5.3.3 TEM Analysis of CDs and PCwCDwH Nanofibers

The synthesized CDs showed a spherical shape with a mean diameter of 6.8 nm as shown in the TEM image of CDs (Fig.V.10a). The presence of dark and

light regions in the TEM image of PCwCDwH nanofibers (Fig.V.10b) shows the uneven distribution of agrichemicals. There are some agglomeration of nanofillers added which is in agreement with SEM data obtained.

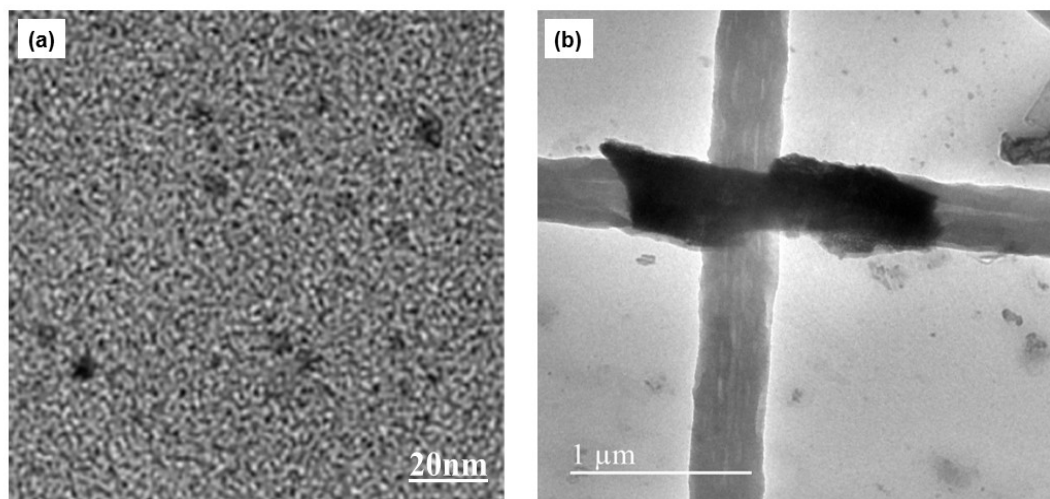


Fig.V.10 TEM image of a) CDs b) PCwCDwH nanofiber

5.4 Thermal Analysis

The thermal stability of the cellulose extracted from WH was investigated using thermogravimetric analysis (TGA). The thermogravimetric (TG) curve of the extracted cellulose is shown in Fig.V.11. A single major thermal decomposition stage was observed for cellulose and minor decomposition took place at higher temperature. The absence of hemicellulose content is confirmed by the absence of decomposition around 220-300°C. This is further confirmed by the FTIR spectra. From Fig.V.11, it is clear that the cellulose subsequently decomposes at 350–400°C due to the decarboxylation, depolymerization and decomposition of glycosidic linkages²⁰. More than 50% of the mass loss happens during the primary thermal degradation, which takes place between 340°C and 440°C. The onset degradation temperature of untreated cellulose was reported as 298.5°C in a previous study, which was lower than that of the chemically treated cellulose obtained here. The lower thermal stability of the untreated cellulose was attributed to the presence of hemicellulose with the low thermal degradation temperature^{21,22}.

With a limited amount of solid residues, cellulose is almost pyrolyzed at temperatures above 400°C. As cellulose is a linear polysaccharide polymer with a

larger molecular weight and higher order of arrangement than hemicellulose, it is more stable at high temperatures. Additionally, because of the many functional oxygen groups in its structure, including aromatic carbons, phenolics and hydroxyphenolics, which have variable thermal stabilities, lignin decomposes over a broader temperature range (250 -650°C) than hemicelluloses and cellulose^{23,24}. The small decompositions at 567°C and 655°C may be due to decomposition of organic compounds in lignin. The small weight loss % at higher temperature may be due to trace amount of lignin.

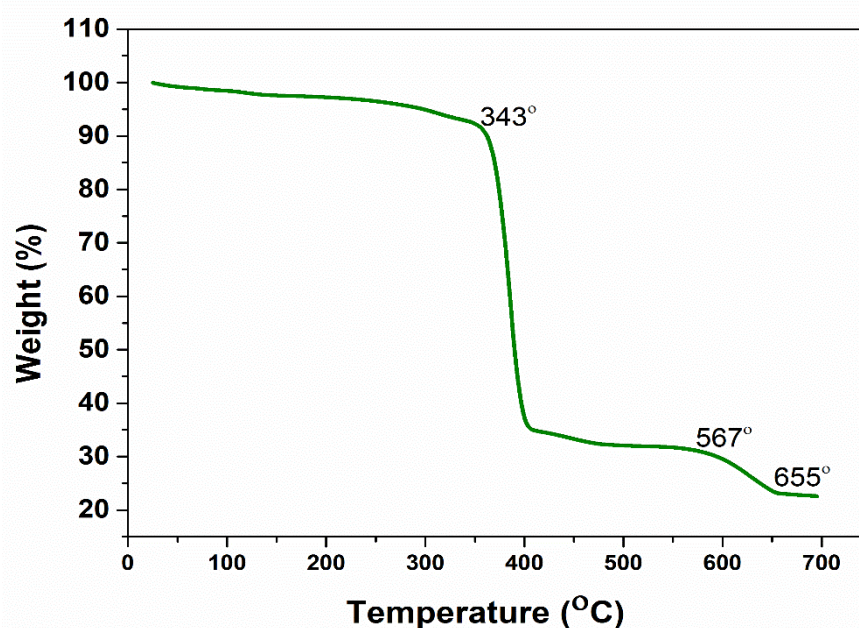


Fig.V.11 TG curve of isolated cellulose

The thermal stability of the electrospun nanofibers was investigated using TGA. (Fig.V.12). All samples had the most intense thermal decomposition process within the range of 280 – 360°C. The nanofillers such as nHAP and CDs shift the degradation slightly towards higher temperatures. The TGA curve of pure PEO Fig.III.12ii showed major weight loss at about 268°C and decomposes completely at 341°C. The decomposition of the PEO matrix may be due to thermal degradation or random chain scission of C-O bonds in PEO. An increased thermal stability was observed for PEO/Cellulose (PCw) nanofibers, increasing the decomposition temperature. This could be due to the bonding interactions between PEO and cellulose. The PCw nanofiber degradation occurred at 288°C (Fig.V.12i) and above

that temperature, the thermal stability gradually decreased and decomposition of the fibers occurred²⁵. High thermal stability observed in PCwCDwH nanofiber loaded with nHAP and CDs (Fig.V.12iv)) than PCwCDw and PCwH. The decomposition temperature of PCwCDwH nanofiber was found to be 359.7°C. The degradation temperature for PCw is 316°C and 343°C for PCwH (Fig.V.12iii and iv). It is observed in the thermogram that the weight loss for all samples remains almost unchanged after 600°C indicating the completion of decomposition of polymer matrix. The residual mass at 700°C is less for the PCw nanofibers and highest for PCwCDwH.

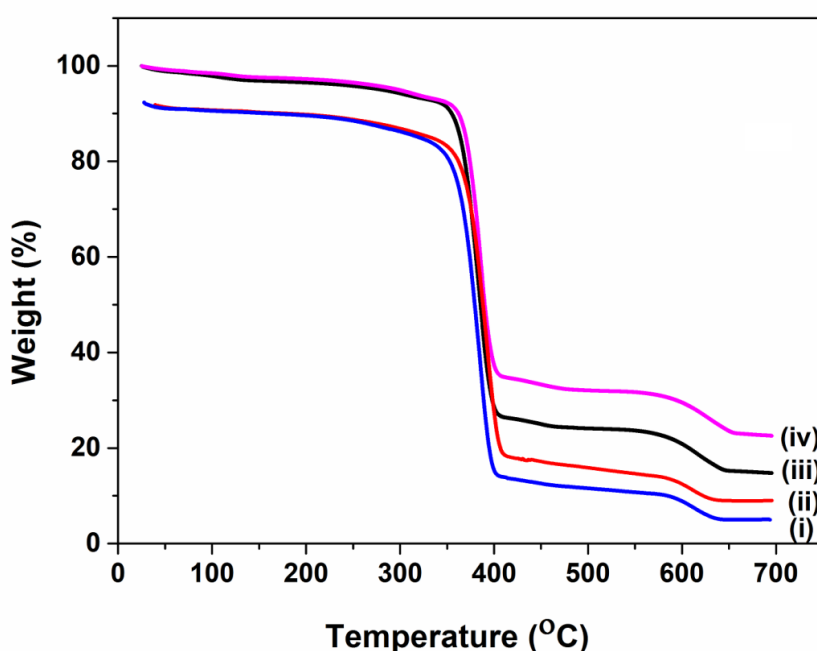


Fig.V.12 TG curves of the nanofibers i) PCw ii) PCwCDw
iii) PCwH iv) PCwCDwH

5.5 Surface Wetting Properties of the Electrospun Fibers

The static water contact angle measurements are shown in Fig.V.13. A Pristine PEO electrospun nanofiber produced a contact angle of 50.3° (Fig.V.13a), indicating that the surface is hydrophilic. The blending with hydrophobic cellulose increases the contact angle to 65.7° (Fig.V.13b). Plasticized cellulose has been found to exhibit a comparable rise in hydrophobicity²⁶. Fig.V.13c shows that hydrophilic OH group in nHAP has again increased the surface wettability and causes a small decrease in the water contact angle in PCwH compared to PCw. PCwH shows a contact angle of

57.7°. However, presence of CDs in PCwCDw and PCwCDwH nanofiber causes an increasing trend in the contact angles of the fibers thus suggesting a decrease in the wettability of the films. PCwCDw shows a strong reduction in the hydrophilicity of the nanofiber. As observed in contact angle measurement in Fig.V.13d the contact angle of PCwCDw increased to 80.6°. The nanofiber PCwCDwH exhibits a water contact angle of 66.8° (Fig.V.13e) which is greater than the contact angle of PCwH. This may be due to the presence of CDs. Here the increase in water contact angle of the PCwCDwH fibers, within the given range is favourable for its utility as seed coats²⁷.

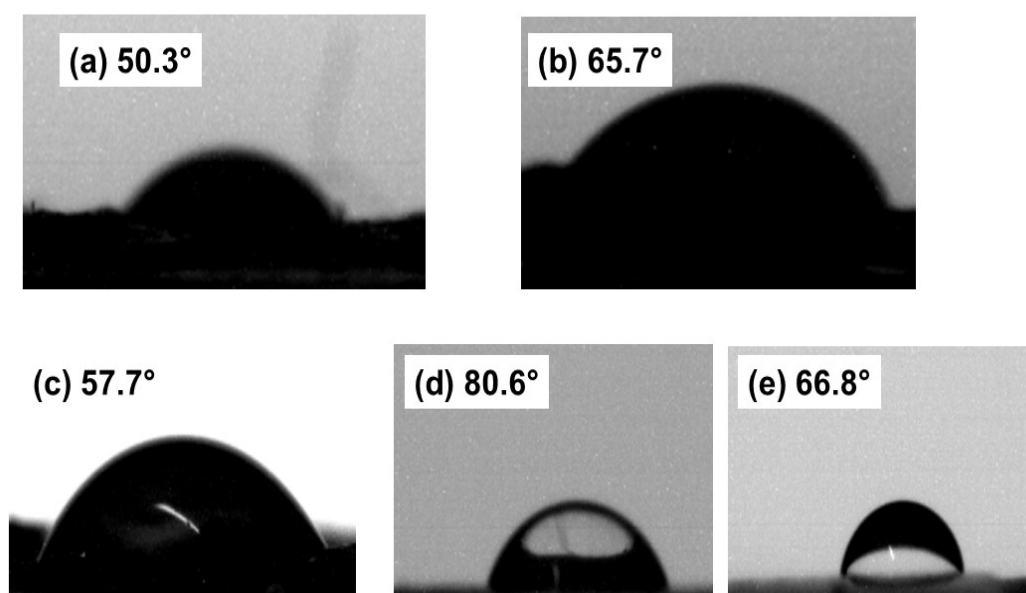


Fig.V.13 Static water contact angle measurements of nanofibers PEO

b) PCw c) PCwCDw d) PCwH e) PCwCDwH

5.6. UV-Visible Spectra of Synthesized Carbon Dots

The synthesized carbon dots (CDs) were characterized using UV-Visible spectroscopy. The CDs show two prominent electronic transitions (Fig.V.14), the sharp absorption signal at 262 nm was caused by the $\pi - \pi^*$ transition, which shows the conjugation of C=C bonds in the CDs structure demonstrating the presence of the aromatic π - system in the core of CDs²⁸. A peak between 350 nm and 380 nm was connected to the C=O bonds' n - π^* energy transition. Due to the excited

state energy being trapped by the surface states, this peak produces intense fluorescence emission. The dual peak in the UV range of CDs confirms the formation of CDs²⁹.

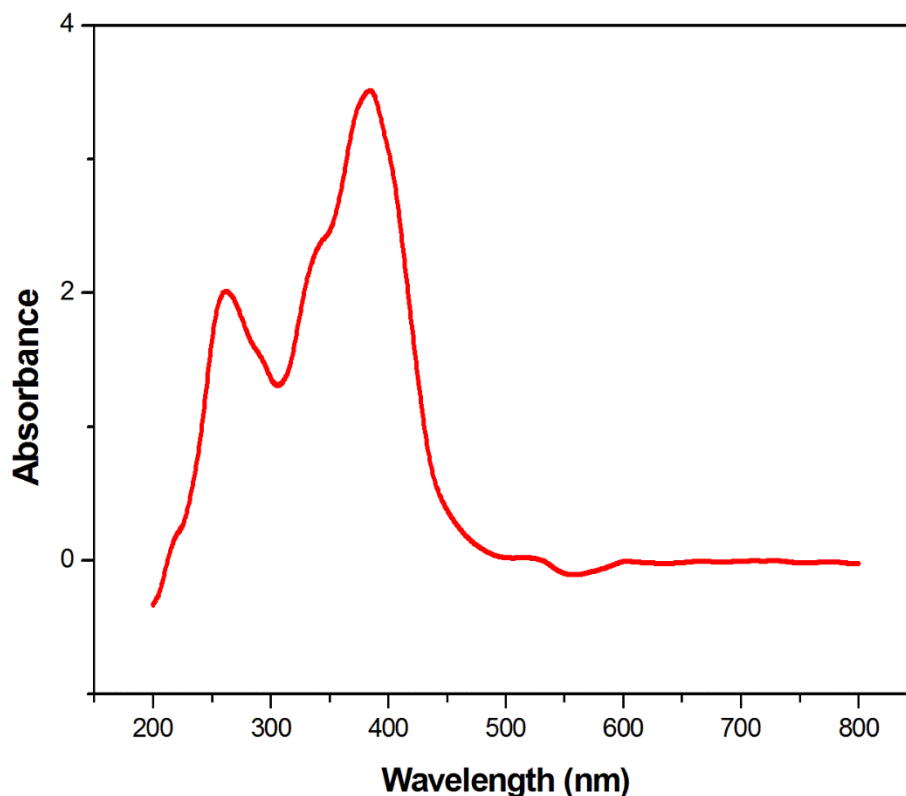


Fig.V.14 UV-Visible spectra of CDs

5.7 Photoluminescence Spectroscopy (PL Spectra)

The PL spectra of the CDs and CDs incorporated nanofiber PCwCDw were examined to better define optical characteristics. The PL spectra of synthesized CDs recorded at an excitation wavelength of 290 nm and 360 nm (Fig.V.15). It shows the excitation dependent emission of CDs. Using an excitation wavelength of 290 nm, a prominent PL emission peak at 330 nm was seen. With the increase in excitation wavelength, the emission peak was subsequently moved to a higher wavelength. The emission peak at 437 nm obtained for an excitation wavelength of 360 nm. Because of the complexity of the mechanism, it is currently not clear how PL spectra of carbon dot functions. The distribution of the numerous carbon dot surface energy traps and the occurrence of different particle sizes are the most likely causes of the PL

behaviour. In contrast to bigger particles, which are stimulated at longer wavelengths, smaller particles are excited at shorter wavelengths.

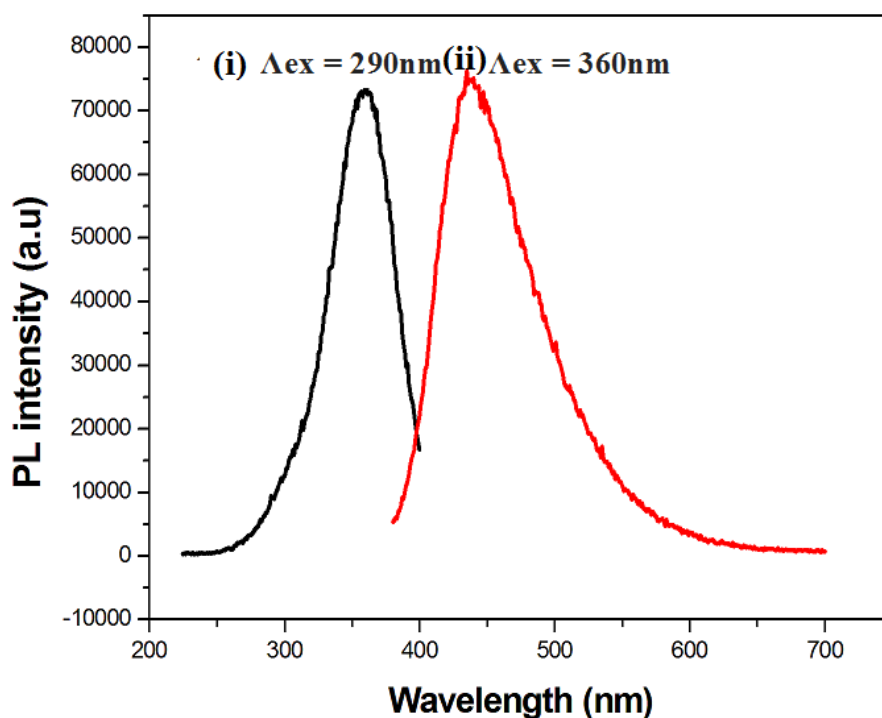


Fig.V.15 The PL emission spectra of CDs at two excitation wavelength
(i) $\Delta_{ex} = 290\text{nm}$ (ii) $\Delta_{ex} = 360\text{nm}$

The properties of the surface of carbon dots can potentially be responsible for their excitation-dependent PL behaviour. The existence of various functional groups on the surface of the carbon dots may lead to the formation of a series of emissive traps between $\pi - \pi^*$ of C-C. When the carbon dots are excited at a particular excitation wavelength, the emission results from the formation of a surface energy trap.

The PL emission spectra of the CDs and CDs incorporated nanofiber at an excitation wavelength of 360 nm is shown in Fig.V.16. For pure CDs and PCwCDw nanofiber samples the ideal emission wavelength is around 440 nm. The typical marker of carbon dots is emission wavelength- and size-dependent photoluminescent activity. PL is one of the most fascinating characteristics of carbon dots, both theoretically and practically. When exposed to UV light, the synthesised carbon dots in the aqueous solution glow green, as seen in Fig.V.17.

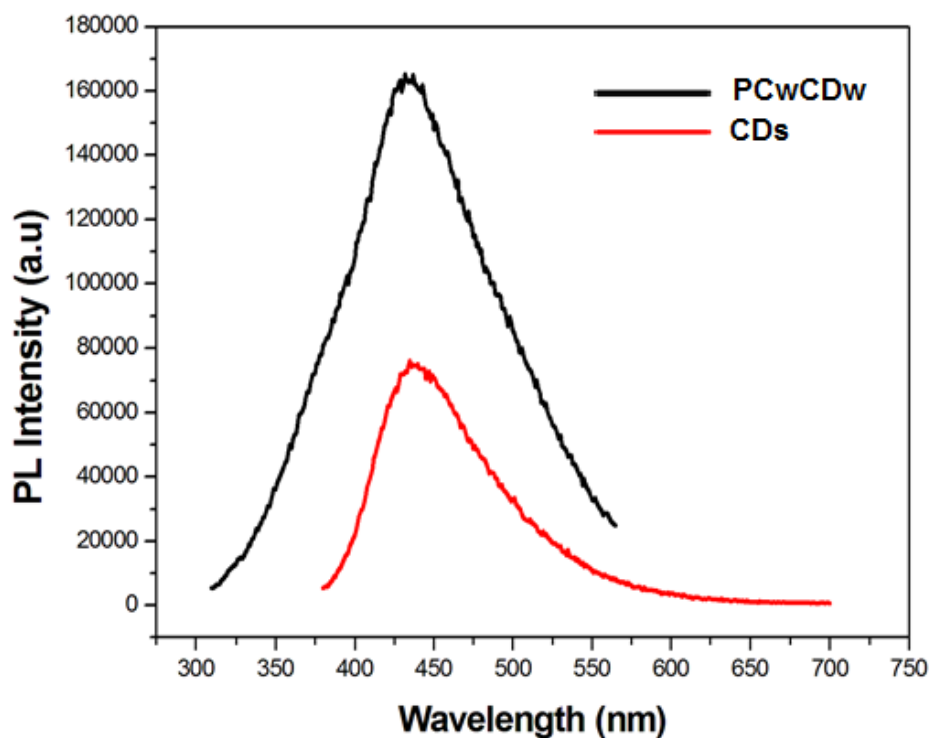


Fig.V.16 The PL emission spectra of CDs and PCwCDw nanofiber

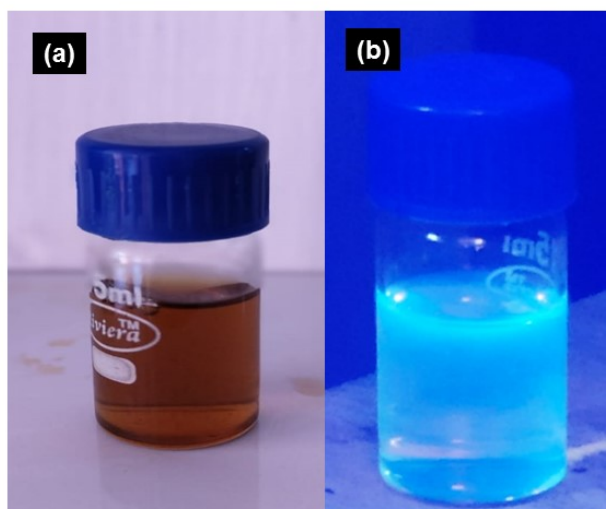


Fig.V.17 Aqueous solution of carbon dots under a) day and b) UV light

From the PCwCDw and CDs photoluminescent spectra, it is clear that the PL intensity depends on the carbon dot concentration. As the concentration of carbon dots decreases in PCwCDw the PL spectra's intensity rises significantly. At low concentrations there may be a decrease in interactions between the various polar

groups³⁰. Agglomeration is facilitated at high concentrations by the existence of a significant quantity of polar functionality. The existence of various particle sizes and the distribution of the various surface energy traps of the carbon dots are the likely causes of the PL behaviour.

5.8 Porosity Measurements

Table V.1 shows the porosity measurements of developed nanofibers. The porosity of membranes increases with the addition of nanofillers. Highest porosity observed for PCwCDwH nanofiber due to the efficient incorporation of nHAP and CDS. The SEM data also supports this. The SEM image (Fig.V.8) shows that all of the electrospun membranes displayed a consistent, three-dimensional interwoven structure with a high porosity. The porosity increased gradually, from 78.6 to 97%.

Table V.1 Porosity values of developed membranes

Polymer membrane	PCw	PCwCDw	PCwH	PCwCDwH
P(%)	78.6	83	90	97

5.9 Study of Aqueous Solution of Fibers and Seeds

5.9.1 Study of pH

The developed nanofibers and seeds coated with nanofibers were kept in distilled water at a pH of 7.0. The pH is noted for 5 days and plotted against time (Fig.V.18a and b). The addition of CDs and nHAP maintained the pH in the range 6.2 - 7.1 which is suitable for corn seed germination. The release of agrichemicals from the fibers into aqueous system causes variation in the pH of the system. Plant toxicity results from significant pH range fluctuations³¹. The consistency in pH in the current investigation was a benefit for seed germination and plant growth even while fertilizer and micronutrients were present. The nanofiber PCwH shows pH increase from 7.5 to 8.5. The release of phosphate ions from nHAP is responsible for the increase in pH for PCwH and PCwCDwH. A growing amount of attention is being given to hydroxyapatite (HAP), particularly nano-hydroxyapatite (n-HAP), as a fertilizer. Review on this topic shows that, the zeolite NaP1/hydroxyapatite

nanocomposite may release nutritional ions for a prolonged period of time, making it effective as an inorganic fertilizer³². When compared to normal P fertilizer [$\text{Ca}(\text{H}_2\text{PO}_4)_2$], nHAP has a longer persistence in soils, which benefits plants³³. The change in pH of the PC_wCD_w nanofibers loaded with CDs and PC_wCD_wH nanofibers loaded with nHAP and CDs showed similar trend as unloaded PC_w nanofibers. Up to 4 days more agrichemicals are released. Also the water absorption rate was high during the initial hours. Hence the electrospun nanofibers considered to be efficient seed coats. Fig.5.18b shows that the pH of uncoated seed increases from 5.9 to 6.4 over the 24 h period, whereas the pH of coated seeds except PC_wH was in the range of 6.2 to 7.8. The drastic change in pH initially in the case of uncoated seeds may cause toxicity. Developed nanofiber seed coats proved as an effective treatment for protection of seeds and crops from highly acidic soils.

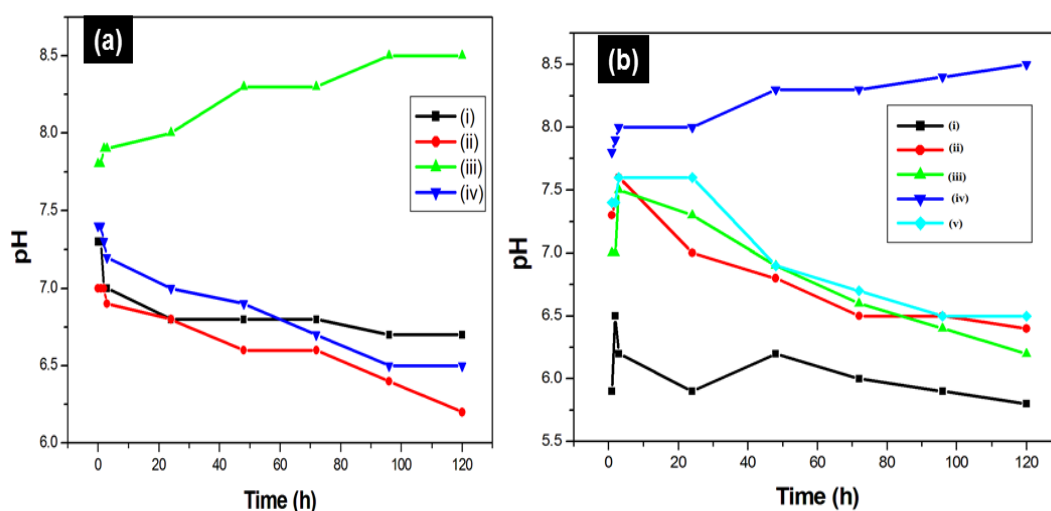


Fig.V.18 a) pH of aqueous solutions of fibers i) PC_w ii) PC_wCD_w iii) PC_wH iv) PC_wCD_wH pH of i) uncoated seeds ii – v) seeds coated with nanofibers ii) PC_w iii) PC_wCD_w iv) PC_wH v) PC_wCD_wH

5.9.2 Conductance of the Aqueous Solution of Fibers and Seeds

20 mL of distilled water were mixed with known weights (0.1 g) of the fibres. The PC_w, PC_wCD_w, PC_wH and PC_wCD_wH nanofibers were examined for variations in conductivity over time (Fig.V.19a). The conductivity values of the PC_w are almost zero and remain constant throughout study. This is because of the absence of agrichemicals in PC_w. The conductivity of PC_wCD_w, PC_wH and PC_wCD_wH

nanofibers in solutions were found to increase initially. After 48 h, a gradual decrease in conductivity is noticed. The conductivity of PCwCDwH nanofibers is highest of all. It is because of the combined release of agricultural nHAP and CDs. The metal release studies and swelling studies are in good agreement with observed conductance data for nanofibers. Every plant species has a limit for conductance above which they become vulnerable and produce less. The highest conductance values were recorded in the steep water of the uncoated seed (Fig.V.19b). Although for coated seeds' change in conductivity increased, it remained lower than that of the untreated seeds. This demonstrates the efficacy of the developed seed coats.

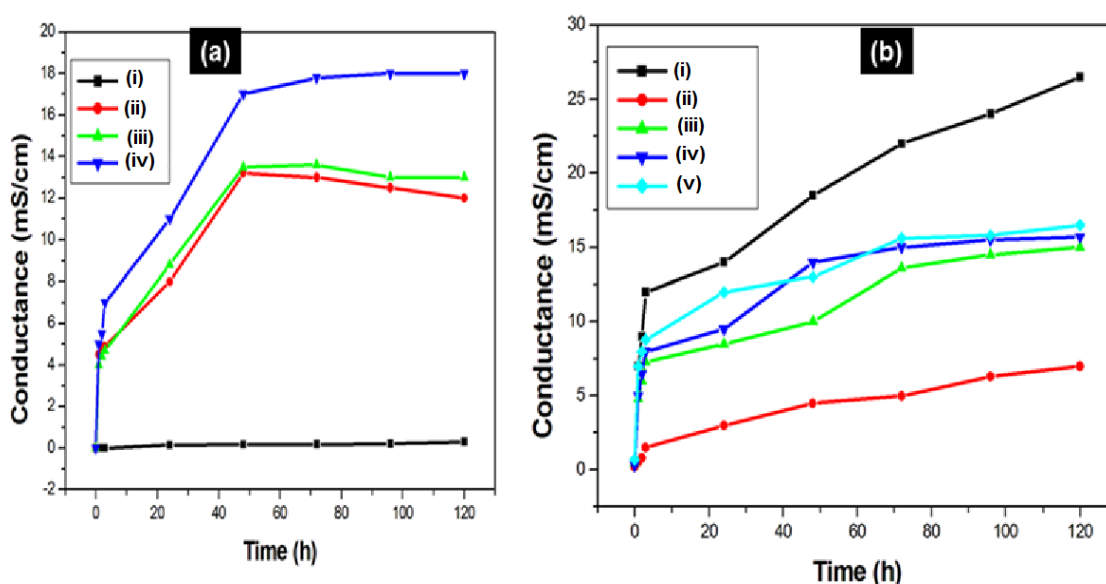


Fig.V.19 a) Electrical conductance of aqueous solutions of fibers
 i) PCw ii) PCwCDw iii) PCwH iv) PCwCDwH **b) Electrical conductance of**
 i) uncoated seeds ii-v) seeds coated with nanofibers ii) PCw iii) PCwCDw
 iv) PCwH v) PCwCDwH

5.9.3 Swelling and Stability Studies

Nanofibers can swell in water because of the porosity of nanofiber morphology. Fig.V.20 shows the swelling studies of the PEO/Cellulose (PCw) nanofibers and composite fibers. Swelling rate for PEO is high initially as it is water soluble but decreases with time. But the presence of cellulose in PCw nanofiber allows holding water for 8 h. Swelling of PCw decreases after 8 h. The interaction between cellulose and PEO increases the hydrophobicity of the fiber. The nanofiber

PC_wCD_w showed an increased and sustained swelling with addition of carbon dots. Wettability of nanofiber is low as indicated by the contact angle. The PC_wCD_w and PC_wCD_wH allow a sustained swelling even after 12 h. Thus the nanofiber seed coats of PC_wCD_w and PC_wCD_wH allow the seed to be hydrated during the entire germination stages.

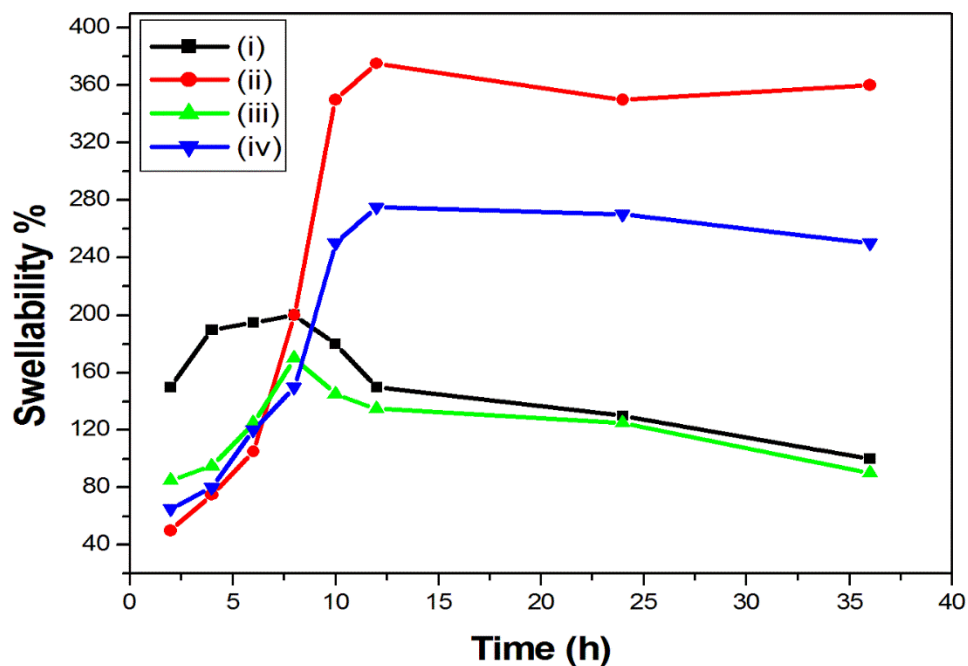


Fig.V.20 Swelling studies of i) PC_w ii) PC_wCD_w iii) PC_wH iv) PC_wCD_wH

Water contact angle analysis also confirms the decreasing wettability nature of the PC_wCD_w and PC_wCD_wH upon the addition of CDs. PC_wH nanofiber shows initial slow rate of swelling in initial hours compared to PC_w, the presence nHAP renders more porosity and uptake of water takes place in a controllable manner than PC_w. Swellability decreases with time in PC_wH than in PC_w which is due to combined effect of dissolution of PEO along with release of ions as confirmed by the metal ion release study. The high swelling percentage makes the loaded nutrients in the samples to deliver to crops in a programmed manner for use as a nanofertilizer.

The stability of the blends was investigated and is plotted in Fig.V.21. The blending with cellulose which is insoluble in water, decreases the solubility of PEO in PC_w blend nanofiber. The results showed 82% solubility of PC_w after 8 h. Carbon dots impart hydrophobic surface on nanofibers, Therefore PC_wCD_w was expected to remain after 36 h. The solubility was found to be 82%, 35%, 84% and 40

% for the PC_w, PC_wCD_w, PC_wH and PC_wCD_wH respectively. The least weight loss was seen in PC_wCD_w followed by PC_wCD_wH, PC_w and PC_wH. PC_w and PC_wH follow almost similar trend in stability. Previous studies reported that organic carbon dot coating, which serves as both a low-surface-energy modifier and a component of rough structure, is applied after the production process to generate super hydrophobic surfaces³⁴.

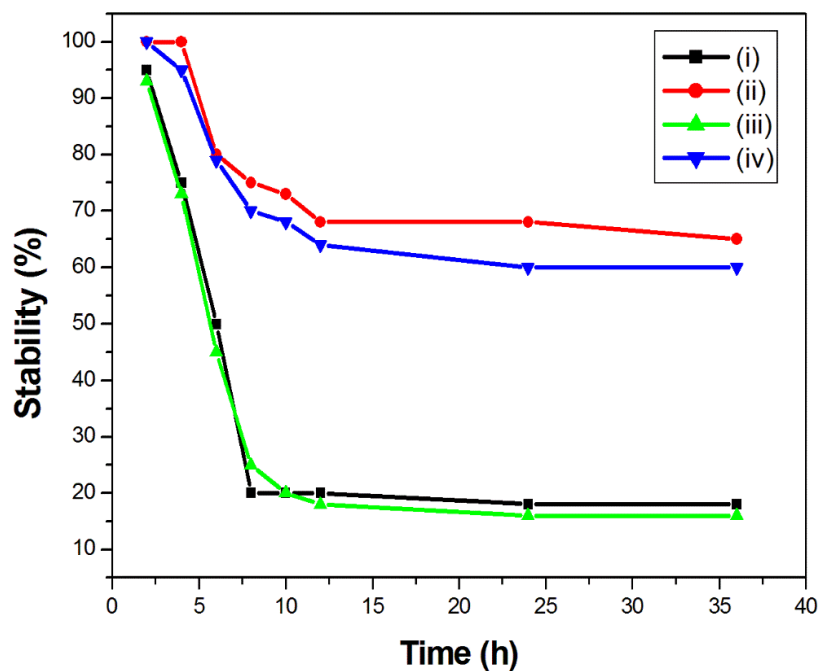


Fig.V.21 Stability studies of i) PC_w ii) PC_wCD_w iii) PC_wH iv) PC_wCD_wH

The swelling and stability studies proved that the synthesis of nanofibers of PEO with cellulose and the dispersion of CDs and nHAP allow regulated release of nutrients despite the fact that PEO is water soluble. An initial burst release followed by a controlled flow of nutrients to the seed during germination is anticipated, since the integrated nutrients are present on both the surface and the interior of the nanofibers.

5.9.4 Imbibition Studies

Imbibition studies were done by soaking the seeds in water, and the weight change was monitored in every half an hour. Fig.V.22 showed that the highest amount of water was absorbed during the first three hours for uncoated seeds and 5 h for coated seeds. Electrical conductance measurements again support this. Seeds imbibe more water in the early 3 h³⁵. Imbibition of seeds in water, which transforms the

dormant seed into a developing embryo, is the first and most important stage of seed germination. Germination is triggered by water absorption via the seed coat. Corn kernels must absorb about 30% water by their weight prior to germination. If water absorption is less than adequate due to a rapidly drying seed zone, germination may be slowed down or prevented. The uncoated seeds exhibit the maximum imbibition rate of 50% within the first two hours. Uncoated seeds may decay as a result of this sharp rise in imbibition rate. The coated seeds showed a sustained absorption rate within 8 h as required for the germination conditions of corn seeds. The polymer nanofibers are assumed to be suitable as seed coats since it permits controlled water absorption and reduced imbibitional decay. Corn seed germination starts in between 24 h to 48 h. The controlled absorption rate of water in all nanofiber coated seeds studied here allows dissolution of fertilizers and micronutrients so as to reach the seed in right amount at right time. Thus nanofiber coated seeds ensures better performance, easy application and less expensive without being toxic³⁶. The imbibition rate of PC_wCD_w and PC_wCD_wH were found to be almost same. Controlled water absorption allows the seed to have sufficient water during complete germination stages.

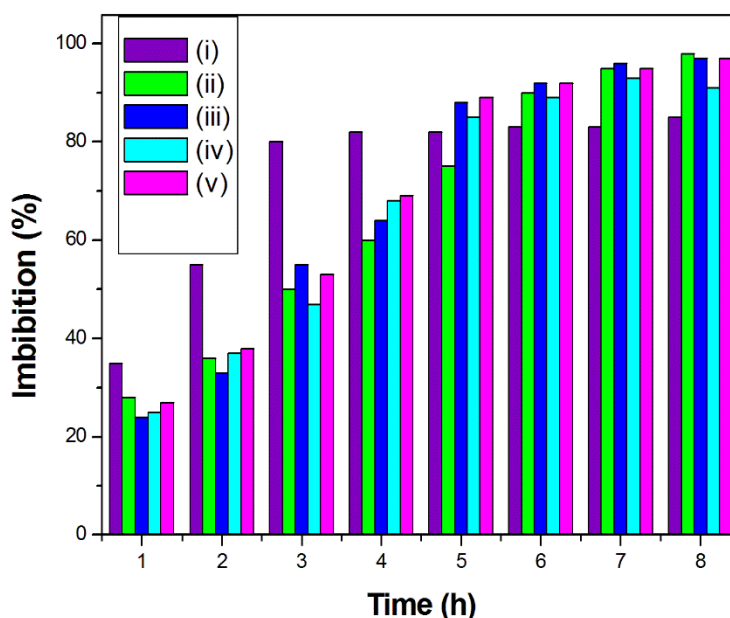


Fig.V.22 Water absorption rate of i) uncoated seeds
ii – v) seeds coated with nanofibers ii) PC_w iii) PC_wCD_w
iv) PC_wH v) PC_wCD_wH

Higher rate of imbibition was due to nanoformulation coating polymer having a capability of water absorption even under very low moisture content. It induces the fast activation of hydrolysing enzymes which are involved in seed germination process.

5.10 Metal Release Studies

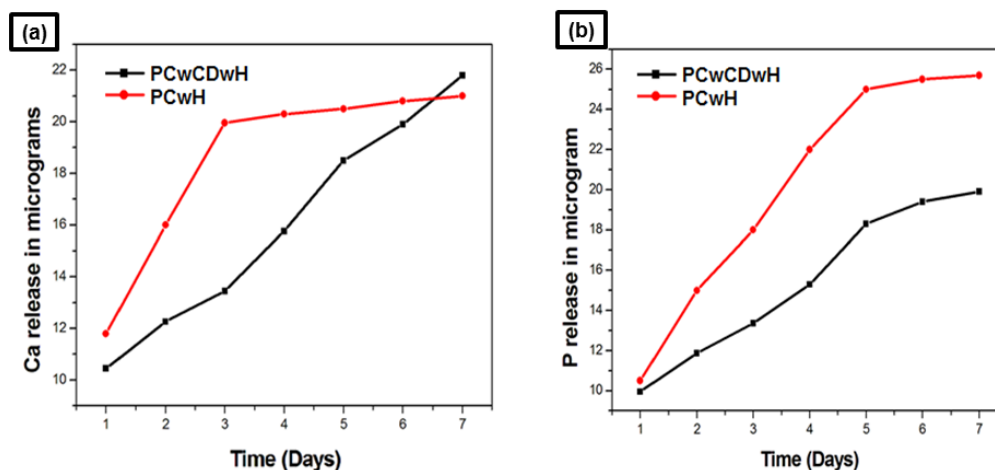


Fig.V.23 a) Ca release from PCwH and PCwCDwH
b) P release from PCwH and PCwCDwH

Fig.V.23a and b displays the Ca and P release profiles of developed nanofibers in water using ICP-OES for PCwH and PCwCDwH as these are the fibers loaded with mineral nutrients. Release of both Ca and P ions from PCwH exhibited a fast release in initial 3 days and the release rates for both the ions gradually decreased. But for PCwCDwH, the pattern follows a regular controlled path. Over the course of the experiment, calcium ion release from the PCwH and PCwCDwH scaffolds was little higher than that of phosphorus. The low solubility of nanoformulation of HAP might be the reason for the slow release of calcium and phosphorous from the nanofibers. The fast and irregular trend in PCwH is due to the high degree of wettability compared to PCwCDwH. The contact angle measurements support these results.

It is crucial to keep in mind that different seed types could necessitate different nutritional dosages for seedling growth. It is essential to develop a versatile polymer-based nanoplatform with adjustable agrichemical release kinetics that can be

tailored for different kinds of seed. The findings show that by modifying the chemical composition of the nanofibers, the release of nutrients from the created nanoplatform may be further controlled. The findings demonstrate that phosphorus availability to plants is increased by nanohydroxyapatite fertilizer and phosphorus loss is avoided by encapsulating nHAP in nanofibers. The plant received nutrients from nanofertilizers employed in this study during its growth period. At same time prevented these compounds from leaching.

5.11 Germination Studies

Germination studies were conducted for a period of 5 days. This study evaluated the role of the electrospun fiber seed coats to support the germination of seeds. The response of germinating maize seeds coated with developed nanofibers and without agrichemicals was assessed. The observation shows that maize seeds were successfully germinated on each of the germinating petri dishes. The germination stages of maize seeds with various seed coatings are depicted in Fig.V.24 and Fig.V.25. From each lot, the best ones were chosen for comparison. Radicle and plumule length of seedlings were recorded and plotted in Fig.V.26a and b for various coatings. It is evident that combined fertilizer (nHAP and CDs) loaded nanofiber, PCwCDwH exhibits high germination parameters compared to other nanofiber coatings. The germination parameters for PCwCDw nanofiber are slightly higher than PCwH nanofiber which might be due to the easy diffusion of CDs across the matrix than less soluble nHAP. The germination potential and coating efficiency follows the order

Uncoated < PCw nanofiber coated seeds < PCwH nanofiber coated seeds < PCwCDw nanofiber coated seeds < PCwCDwH nanofiber coated seeds

It is worth mentioning that the beneficial trends of the nanofertilizer loaded nanofiber coating for maize seeds improved germination parameters. It may be due to the targeted delivery and regulated release of active ingredients. The current study demonstrates the positive benefits of CDs on corn plant development and disease resistance. The growth of corn seedling is increased after treatment with CDs than nHAP.

Literature review shows that CDs penetrate into every component of rice plants, including the cell nuclei and systematic analyses shed light on the several mechanisms that promote glucose synthesis, root elongation and seed germination³⁷. In the meantime, CDs penetrate the cell, travel to the nucleus, relax the DNA structure and raise the expression of the thioine gene, which ultimately improved the rice plant's capacity for disease resistance. The previous studies further showed that the concentration of surface-oxygen-containing groups and the graphite structure of CDs were key contributors to the development of the plant disease³⁸. The results of present investigation are in good agreement with previous reports. Moreover, the CDs break down into CO₂ and plant hormone analogues that stimulate plant development. The CO₂ is then transformed into carbohydrates through photosynthesis' Calvin cycle³⁹. In acidic and highly P sorbing soils the availability of P fertilizers to plants decreases due to leaching. In this case phosphorous fertilizers made with nanotechnology might be more effective. Nano-sized particles may be able to move through the soil and can reach the plant roots. Hydroxyapatite nanoparticles (nHAP) were investigated as a potential fertilizer to increase P efficiency^{33,40}. All developed nanofiber seed coatings loaded with CDs and nHAP are found to be very effective in improving crop productivity. The pH studies again confirm the application of seed coats in highly acidic soil for improved P uptake to solve the current P demand.

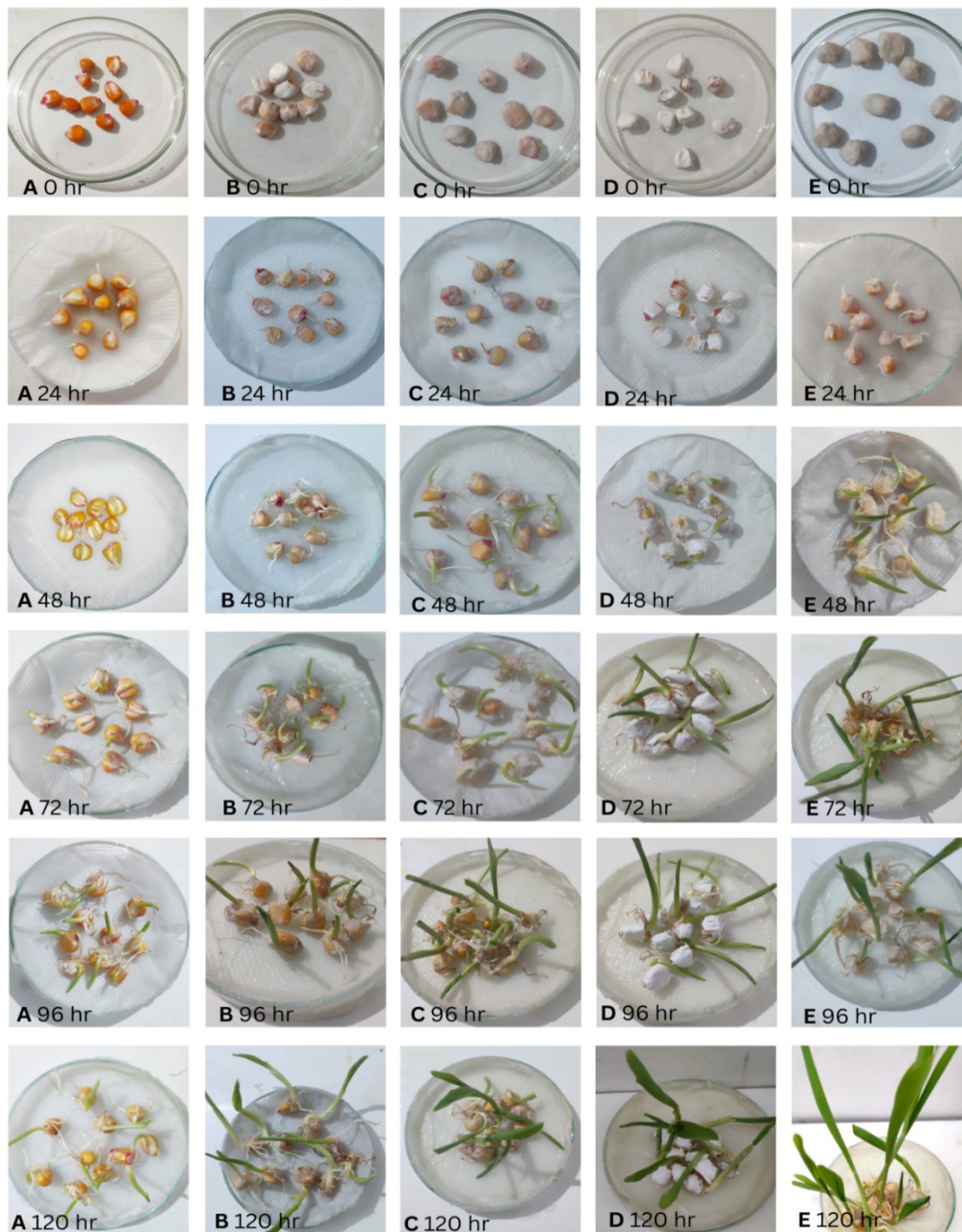


Fig.V.24 The optical photographs of corn seed germination of A) uncoated seeds B-E) seeds coated with nanofibers B) PCw C) PCwH D) PCwCDw E) PCwCDwH

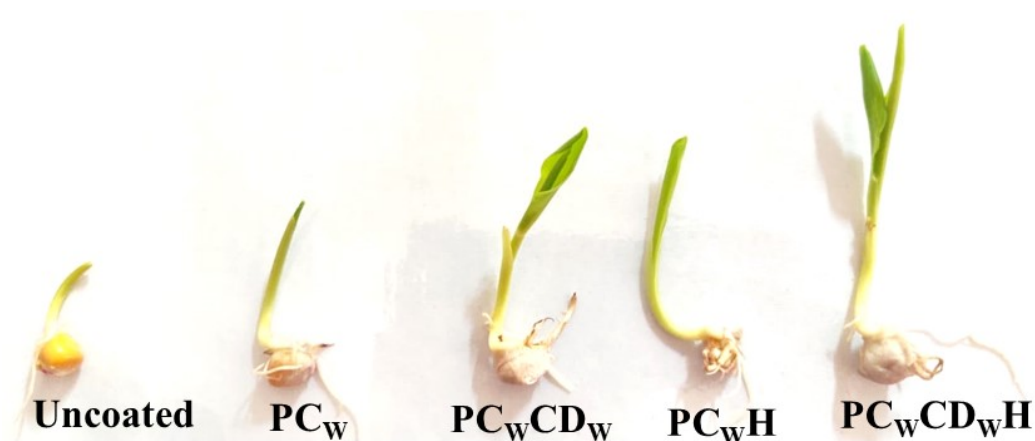


Fig.V.25 The optical photographs of germinated corn seeds coated with developed nanofibers after 5days

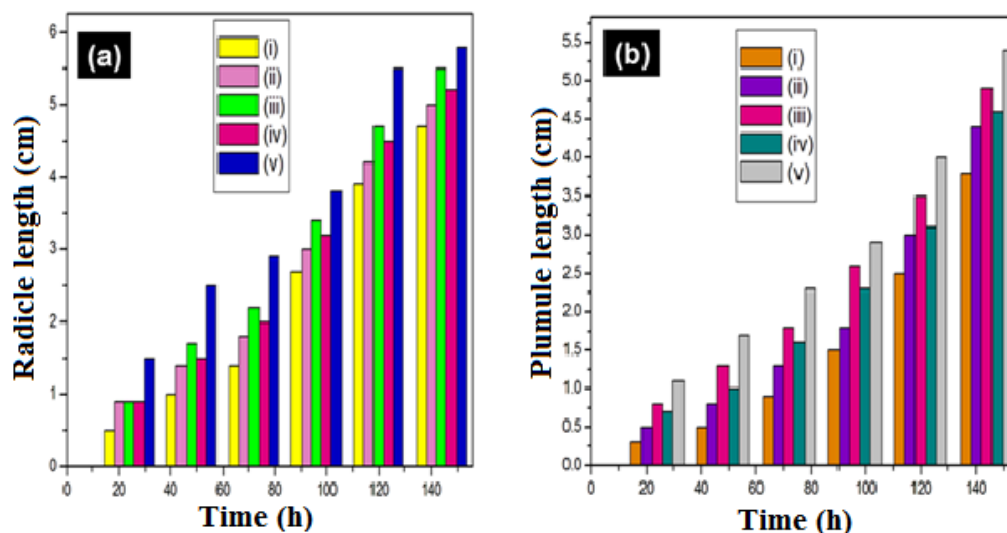
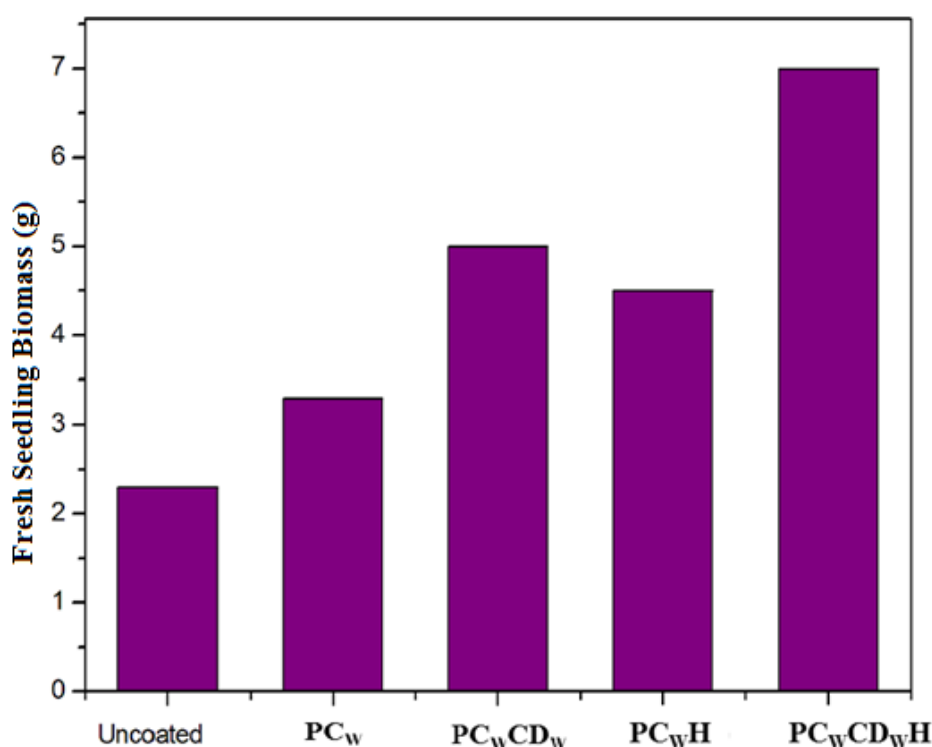


Fig.V.26 a) Radicle and b) Plumule length of seedlings i) Uncoated seeds ii – v) seeds coated with nanofibers ii) PCw iii) PCwH iv) PCwCDw v) PCwCDwH

5.11.1 Fresh Biomass Seedling

All treated seedlings' root, shoot and overall biomass were measured after 15 days of germination. Data were adjusted to the tissue mass of the untreated control plants to make comparisons easier. Without adding fertilizer, PCw nanofiber covering is not anticipated to significantly increase biomass on its own. It is interesting to notice that increase in germination rate was accompanied by an increase

in seedling biomass, as shown in the Fig.V.27 below. Also, the PC_wCD_wH nanofiber coating considerably boosted overall biomass compared to untreated seeds when loaded with the combination nanofertilizers nHAP and CDs. These results are in agreement with the studies where nHAP serves as a slow-release P fertilizer and a carrier for another macronutrient⁴⁰. Reports show that CDs promote the root vigour and moisture level of seeds, which may lead to the promotion of plant growth and development^{37,42}. Therefore the addition of nontoxic biofertilizers in to the nanofiber matrix as superior seed coatings is proved to be a cost effective and eco-friendly solution to enhance germination and crop yield.



. Fig.V.27 Fresh seedling biomass after 15 days of germination

5.11.2 Statistical Analysis

The germination parameters of five sub samples and their five replicates were examined. Following a homogeneity test, a one-way ANOVA was performed on the findings. The results of statistical analysis for germination parameters are given in Table V.2. An entirely random design was used for the statistical analysis of the data using analysis of variance. The main and interaction effects were assessed using Tukey's HSD test at a 0.05 level of probability when the F values were significant.

Using Levene's test, a homogenous results were found. The addition of nutrients nHAP and CDs had a substantial impact on the germination percentage. Graphical representations of the statistical analysis of germination parameters for each treatment are shown in Fig.V.28. The length of the seedling was used to determine the germination index and seed vigour index. According to the Tukey HSD test, the growth of the seedlings for nutrient loaded coated seeds was clearly significant (TableV.2). The alteration brought on by CDs and nHAP was substantial.

Table V.2 Estimated marginal mean of germination parameters

Sample		% Germination (%G)	Germination Index (GI)	Seed Vigour Index (SVI)
Uncoated seeds	Mean	72.00	72.00	275.20
	(SD)	(4.472)	(4.472)	(21.159)
PC _w nanofiber coated seeds	Mean	78.00	90.20	344.60
	(SD)	(4.472)	(4.142)	(17.487)
PC _w CD _w nanofiber coated seeds	Mean	94.00	120.56	460.80
	(SD)	(5.477)	(7.608)	(31.634)
PC _w H nanofiber coated seeds	Mean	86.00	103.80	395.80
	(SD)	(5.477)	(6.834)	(21.429)
PC _w CD _w H nanofiber coated seeds	Mean	98.00	139.00	531.00
	(SD)	(4.472)	(7.071)	(21.331)

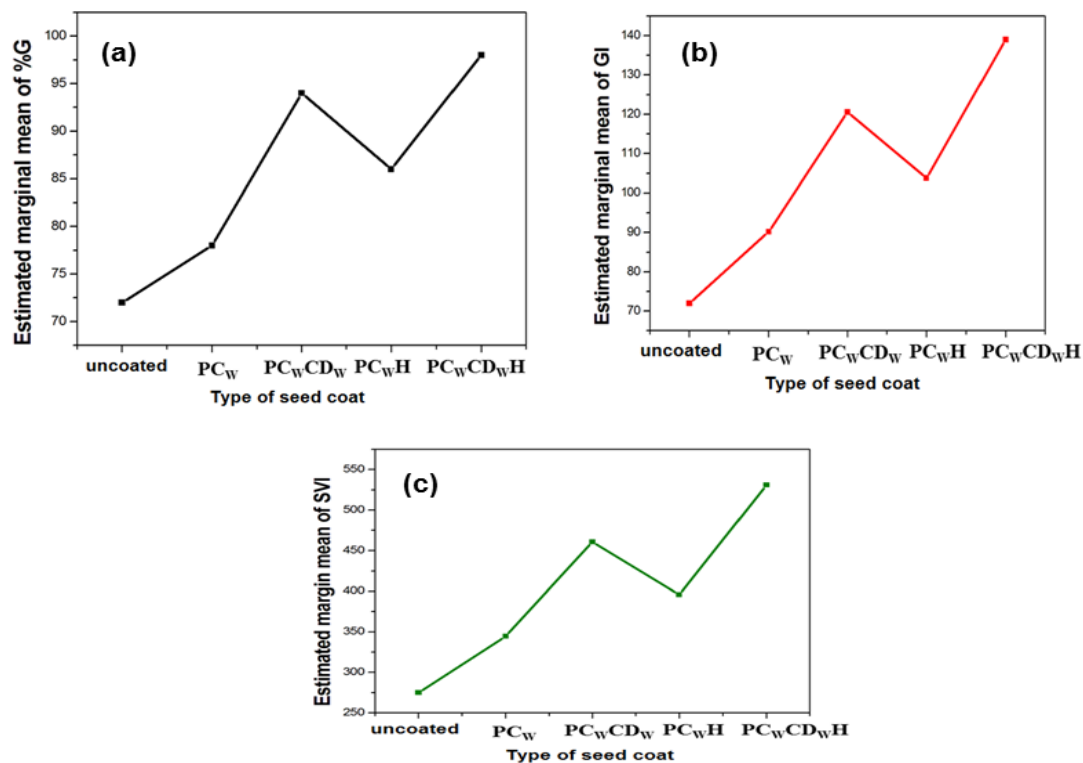


Fig.V.28 Estimated marginal mean of a) Germination percentage
b) Germination Index c) Seed Vigour Index

5.12 Antioxidant Property of Developed Nanofibers

The antioxidant power of nanofibers was evaluated with the DPPH inhibition assay. The results are plotted in Fig.V.29. The determination is based on the action of the DPPH free radical on the antioxidant, which donates a hydrogen atom to the free radical species from the surface functional groups $-OH$ and $-COOH$ ^{43,44}. The resulting radical on the nanoparticle can be stabilised in one of two ways: by delocalizing the unpaired electron through resonance in the aromatic environment of the CD core, or by rearranging the chemical bonds of the surface functional groups. Reactive oxygen species (ROS) are produced when pro-oxidative activities are increased relative to anti-oxidative (enzymatic and non-enzymatic) activities, causing oxidative stress, which is a physiological state (response) in cells, tissues, and organs⁴⁵. The decline in vigour in plant tissues has been linked to oxidative stress⁴⁶.

Antioxidants can be encapsulated to increase their bioavailability to shield them from environmental factors. Electrospun nanofibers can provide the ideal

environment for antioxidant encapsulation, making electrospinning a great choice for applications in nanotechnology. The antioxidant activity of fabricated PC_wCD_w, PC_wH and PC_wCD_wH nanofibers were evaluated and recorded in Table V.3. The scavenging activity was calculated based on the Equation 2.9.

Table V.3 Antioxidant activity of nanofibers

Sample	OD at 517 nm (A ₀)	DPPH free radical scavenging activity (%)
Control	1.848	0
PC _w CD _w	0.139	92.3
PC _w H	0.285	84.6
PC _w CD _w H	0.095	94.8

Fig.V.29 proved that both CDs and nHAP are efficient antioxidants and the application of this as nanofertilizers through nanofiber seed coats would enhance seed establishment and germination potential under oxidative stress of soil.

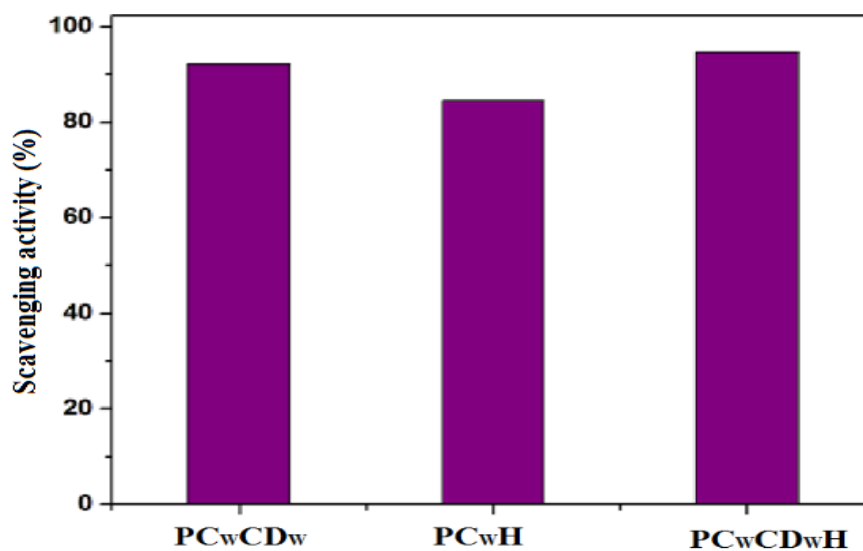


Fig.V.29 Antioxidant activity of developed nanofibers using DPPH assay

Conclusion

Electrospinning was employed to create biopolymer-based nanoplatform for seed coating. According to the outcomes of the current research, electrospun PEO/Cellulose nanofibers help corn seedlings grow rapidly because of their high surface area, good fluid absorption capacity and interconnected pore structure. Within 120 h of the germinating phase, the length of the radicle and plumule of corn seeds grew substantially due to the application of nanofertilizers such as CDs and nHAP incorporated nanofiber seed coating. CDs might have boosted the resistance of crops to diseases which is revealed from free radical scavenging abilities. The CDs showed a favourable impact on crop production. The combined use of hydroxyapatite nanoparticles with CDs resulted in a notable improvement in early plant development. This innovative nanofertilizer loaded nanofiber seed coating has such favourable impacts on plant growth, together with inherent biocompatibility, straightforward manufacturing which make it a potential material for widespread use in the agronomic field.

References

1. Bouyer, E., Gitzhofer, F., & Boulos, M. I. (2000). Morphological study of hydroxyapatite nanocrystal suspension. *Journal of Materials Science: Materials in Medicine*, 11(8), 523-531.
2. De, B., & Karak, N. (2013). A green and facile approach for the synthesis of water soluble fluorescent carbon dots from banana juice. *Rsc Advances*, 3(22), 8286-8290.
3. Setyaningsih, L., Satria, E., Khoironi, H., Dwisari, M., Setyowati, G., Rachmawati, N., & Anggraeni, J. (2019). Cellulose extracted from water hyacinth and the application in hydrogel. In *IOP Conference Series: Materials Science and Engineering* 673, (1), 012017.
4. Rosa, S. M., Rehman, N., de Miranda, M. I. G., Nachtigall, S. M., & Bica, C. I. (2012). Chlorine-free extraction of cellulose from rice husk and whisker isolation. *Carbohydrate Polymers*, 87(2), 1131-1138.
5. Dey, A., Karan, S., & De, S. K. (2009). Effect of nanofillers on thermal and transport properties of potassium iodide–polyethylene oxide solid polymer electrolyte. *Solid State Communications*, 149(31-32), 1282-1287.
6. Sundari, M. T., & Ramesh, A. (2012). Isolation and characterization of cellulose nanofibers from the aquatic weed water hyacinth—*Eichhornia crassipes*. *Carbohydrate Polymers*, 87(2), 1701-1705.
7. Reddy, K. O., Maheswari, C. U., & Shukla, M. (2013). Physico-chemical characterization of cellulose extracted from ficus leaves. *Journal of Biobased Materials and Bioenergy*, 7(4), 496-499.
8. Halib, N., & Amin, M. C. I. M. (2012). Physicochemical Properties And Characterization Of Nata De Coco From Local Food Industries As A Source Of Cellulose. *Sains Malaysiana*.
9. Chen, W., Yu, H., Liu, Y., Hai, Y., Zhang, M., & Chen, P. (2011). Isolation and characterization of cellulose nanofibers from four plant cellulose fibers using a chemical-ultrasonic process. *Cellulose*, 18, 433-442.
10. Wang, B., & Li, D. (2015). Strong and optically transparent biocomposites reinforced with cellulose nanofibers isolated from peanut shell. *Composites Part A: Applied Science and Manufacturing*, 79, 1-7.
11. Yang, L., Jiang, W., Qiu, L., Jiang, X., Zuo, D., Wang, D., & Yang, L. (2015). One pot synthesis of highly luminescent polyethylene glycol anchored carbon dots functionalized with a nuclear localization signal peptide for cell nucleus imaging. *Nanoscale*, 7(14), 6104-6113.

12. Zhou, C., Chu, R., Wu, R., & Wu, Q. (2011). Electrospun polyethylene oxide/cellulose nanocrystal composite nanofibrous mats with homogeneous and heterogeneous microstructures. *Biomacromolecules*, 12(7), 2617-2625.
13. Pielichowska, K., Głowinkowski, S., Lekki, J., Biniaś, D., Pielichowski, K., & Jenczyk, J. (2008). PEO/fatty acid blends for thermal energy storage materials. Structural/morphological features and hydrogen interactions. *European Polymer Journal*, 44(10), 3344-3360.
14. Kakade, M. V., Givens, S., Gardner, K., Lee, K. H., Chase, D. B., & Rabolt, J. F. (2007). Electric field induced orientation of polymer chains in macroscopically aligned electrospun polymer nanofibers. *Journal of the American Chemical Society*, 129(10), 2777-2782.
15. Xu, X., Jiang, L., Zhou, Z., Wu, X., & Wang, Y. (2012). Preparation and properties of electrospun soy protein isolate/polyethylene oxide nanofiber membranes. *ACS Applied Materials & Interfaces*, 4(8), 4331-4337.
16. Xu, X., Liu, F., Jiang, L., Zhu, J. Y., Haagenson, D., & Wiesenborn, D. P. (2013). Cellulose nanocrystals vs. cellulose nanofibrils: a comparative study on their microstructures and effects as polymer reinforcing agents. *ACS applied materials & interfaces*, 5(8), 2999-3009.
17. Choi, D., Marra, K. G., & Kumta, P. N. (2004). Chemical synthesis of hydroxyapatite/poly (ϵ -caprolactone) composites. *Materials Research Bulletin*, 39(3), 417-432.
18. Cacciotti, I., Bianco, A., Pezzotti, G., & Gusmano, G. (2011). Synthesis, thermal behaviour and luminescence properties of rare earth-doped titania nanofibers. *Chemical Engineering Journal*, 166(2), 751-764.
19. Bhardwaj, N., & Kundu, S. C. (2010). Electrospinning: A fascinating fiber fabrication technique. *Biotechnology advances*, 28(3), 325-347.
20. Naduparambath, S., & Purushothaman, E. (2016). Sago seed shell: determination of the composition and isolation of microcrystalline cellulose (MCC). *Cellulose*, 23, 1803-1812.
21. Yang, H., Yan, R., Chen, H., Lee, D. H., & Zheng, C. (2007). Characteristics of hemicellulose, cellulose and lignin pyrolysis. *Fuel*, 86(12-13), 1781-1788.
22. Nair, S. S., & Yan, N. (2015). Effect of high residual lignin on the thermal stability of nanofibrils and its enhanced mechanical performance in aqueous environments. *Cellulose*, 22(5), 3137-3150.
23. Jiao, Y., Wan, C., Qiang, T., & Li, J. (2016). Synthesis of superhydrophobic ultralight aerogels from nanofibrillated cellulose isolated from natural reed for high-performance adsorbents. *Applied Physics A*, 122, 1-10.

24. Brebu, M., & Vasile, C. (2010). Thermal degradation of lignin—a review. *Cellulose Chemistry & Technology*, 44(9), 353. Brebu, M., & Vasile, C. (2010). Thermal degradation of lignin—a review. *Cellulose Chemistry & Technology*, 44(9), 353.
25. Fatema, U. K., Uddin, A. J., Uemura, K., & Gotoh, Y. (2011). Fabrication of carbon fibers from electrospun poly (vinyl alcohol) nanofibers. *Textile Research Journal*, 81(7), 659-672.
26. Rychter, P., Kot, M., Bajer, K., Rogacz, D., Šišková, A., & Kapuśniak, J. (2016). Utilization of starch films plasticized with urea as fertilizer for improvement of plant growth. *Carbohydrate polymers*, 137, 127-138.
27. Pang, J., Liu, X., Zhang, X., Wu, Y., & Sun, R. (2013). Fabrication of cellulose film with enhanced mechanical properties in ionic liquid 1-allyl-3-methylimidazolium chloride (AmimCl). *Materials*, 6(4), 1270-1284.
28. Ansi, V. A., & Renuka, N. K. (2018). Table sugar derived Carbon dot—a naked eye sensor for toxic Pb²⁺ ions. *Sensors and Actuators B: Chemical*, 264, 67-75.
29. Zhu, S., Song, Y., Zhao, X., Shao, J., Zhang, J., & Yang, B. (2015). The photoluminescence mechanism in carbon dots (graphene quantum dots, carbon nanodots, and polymer dots): current state and future perspective. *Nano research*, 8, 355-381.
30. Sahu, S., Behera, B., Maiti, T. K., & Mohapatra, S. (2012). Simple one-step synthesis of highly luminescent carbon dots from orange juice: application as excellent bio-imaging agents. *Chemical communications*, 48(70), 8835-8837.
31. Mickelbart, M.V., Stanton, K.M., Camberato, J.M., & Lee, B.D. (2007). *Purdue extension publication*, HO-240-W, 1-4
32. Szameitat, A. E., Sharma, A., Minutello, F., Pinna, A., Er-Rafik, M., Hansen, T. H., & Husted, S. (2021). Unravelling the interactions between nano-hydroxyapatite and the roots of phosphorus deficient barley plants. *Environmental Science: Nano*, 8(2), 444-459.
33. Montalvo, D., McLaughlin, M. J., & Degryse, F. (2015). Efficacy of hydroxyapatite nanoparticles as phosphorus fertilizer in andisols and oxisols. *Soil Science Society of America Journal*, 79(2), 551-558.
34. Peng, H., Li, L., Wang, Q., Zhang, Y., Wang, T., Zheng, B., & Zhou, H. (2021). Organic carbon dot coating for superhydrophobic aluminum alloy surfaces. *Journal of Coatings Technology and Research*, 18(3), 861-869.
35. Rathinavel, K. (2015). Extension of shelf life of cotton (*Gossypium hirsutum* L.) seeds through polymer coating under ambient storage condition. *Indian Journal of Agricultural Research*, 49(5), 447-451.
36. Farooq, M., Wahid, A., & Siddique, K. H. (2012). Micronutrient application through seed treatments: a review. *Journal of soil science and plant nutrition*, 12(1), 125-142.

37. Li, H., Huang, J., Lu, F., Liu, Y., Song, Y., Sun, Y., & Kang, Z. (2018). Impacts of carbon dots on rice plants: boosting the growth and improving the disease resistance. *ACS Applied Bio Materials*, 1(3), 663-672.
38. Kang, Z., Liu, Y., & Lee, S. T. (2012). Themed issue: nanomaterials for energy conversion and storage. *J. Mater. Chem*, 22, 24230-24253.
39. Priyam, A., Yadav, N., Reddy, P. M., Afonso, L. O., Schultz, A. G., & Singh, P. P. (2022). Fertilizing benefits of biogenic phosphorous nanonutrients on *Solanum lycopersicum* in soils with variable pH. *Heliyon*, 8(3), e09144.
40. Kottegoda, N., Munaweera, I., Madusanka, N., & Karunaratne, V. (2011). A green slow-release fertilizer composition based on urea-modified hydroxyapatite nanoparticles encapsulated wood. *Current science*, 73-78.
41. Wang, H., Zhang, M., Song, Y., Li, H., Huang, H., Shao, M., & Kang, Z. (2018). Carbon dots promote the growth and photosynthesis of mung bean sprouts. *Carbon*, 136, 94-102.
42. Wang, A., Kang, F., Wang, Z., Shao, Q., Li, Z., Zhu, G., & Li, Y. Y. (2019). Facile Synthesis of Nitrogen-Rich Carbon Dots as Fertilizers for Mung Bean Sprouts. *Advanced Sustainable Systems*, 3(3), 1800132.
43. Zhao, S., Lan, M., Zhu, X., Xue, H., Ng, T. W., Meng, X., & Zhang, W. (2015). Green synthesis of bifunctional fluorescent carbon dots from garlic for cellular imaging and free radical scavenging. *ACS applied materials & interfaces*, 7(31), 17054-17060.
44. Das, B., Dadhich, P., Pal, P., Srivas, P. K., Bankoti, K., & Dhara, S. (2014). Carbon nanodots from date molasses: new nanolights for the in vitro scavenging of reactive oxygen species. *Journal of Materials Chemistry B*, 2(39), 6839-6847.
45. Hendry, G. A. (1993). Oxygen, free radical processes and seed longevity. *Seed Science Research*, 3(3), 141-153.
46. Demidchik, V. (2017). Reactive oxygen species and their role in plant oxidative stress. In *Plant stress physiology*, 64-96, Wallingford UK: CABI.

Summary and Conclusions

Agriculture is one of the essential sectors where nanotechnology needs to be applied as it directly affects the availability of food. Over several cycles of intense farming, the soil quality deteriorates owing to nutrient depletion, making all agricultural methods completely dependent on fertilizers to increase the output from the soil. For the control of plant diseases and to prevent crops from suffering substantial losses, modern agriculture heavily relies on the use of pesticides, but many of the most crucial tools for disease control are rapidly losing their effectiveness as a result of the emergence of resistance. The usage of pesticides can have side effects that could be harmful to human health and the environment. To promote agricultural production, more sustainable techniques are required to prevent the crop loss, plant diseases and deterioration of arable lands. The goal of this research is to increase food security by creating a cutting-edge agricultural practices using nanotechnology. This investigation is an attempt to increase the effectiveness of nutrient utilization and to reduce fertilizer leaching, which would reduce agricultural production systems' nonpoint sources of pollution and lower fertilizer costs. The agrichemicals are encapsulated inside the polymer and applied as seed coats in order to achieve the goal of controlled release or gradual release. Ultrathin nanofibers formed using the electrospinning technique is the polymer morphology selected for the application. The nanofibers exhibit exceptional qualities like high surface to volume ratio, high porosity, easy tunability and processing. Nanofibers are produced when electrical forces are applied to a viscoelastic polymer solution to cause unidirectional elongation. Fabrication of the porous film was carried out to compare the feasibility of polymer film for the specified application. Polycaprolactone, poly(ethylene oxide) and cellulose are the organic polymers selected for this study. All polymers are biocompatible, biodegradable, safe and FDA-approved. The work provided seed producers a novel and sustainable seed coating technology which will increase crop yields and food production by reducing the rate of toxic fertilizer application. The developed seed coating technology helps to protect seeds and seedlings from varying climatic conditions, soil borne and seed borne pathogens.

Study of Fibers and Film of Nanohydroxyapatite, Zinc Oxide Nanoparticles and *Trichoderma Viride* Incorporated PCL and PCL/PEO Blend Nanofibers

Zinc oxide nanoparticles, nanohydroxyapatite and *Trichoderma viride* were incorporated into the polycaprolactone and polycaprolactone/poly(ethylene oxide) blend nanofibrous seed coating which allowed access to micronutrient and macronutrient in the proximity of the seed in very small but sufficient quantities. The nontoxic nanofiber coating acts like protective covering. ZnO NPs are synthesised by fuel approach in solution combustion method using Zinc nitrate hexahydrate and Urea as the fuel. The wet chemical method was used to synthesize hydroxyapatite nanoparticles. The FTIR and XRD studies indicated the formation of ZnO NPs and nHAP. SEM images revealed the synthesized ZnO NPs and nHAP are spherical with average diameters 98.72 nm and 95.36 nm respectively. Prepared hydroxyapatite nanoparticles are agglomerated. The PCL nanofibers was prepared using a 10% (w/v) PCL solution in 4:1 solvent mixture of chloroform and DMF. This resulted in the formation of fibers with an average diameter of 276 nm. The optimised percentage of nHAP, ZnO NPs and *T.viride* added were 20%, 10% and 10% respectively with respect to weight of PCL. A blended nanofiber was fabricated using PCL and PEO with an aim to reduce the high hydrophobicity of PCL. This was optimised by taking three different composition ratios of PCL and PEO. The blend B3 with PCL: PEO ratio of 30:70 resulted in smooth, uniform bead free nanofibers. This composition was used to fabricate composite nanofiber with nHAP, ZnO NPs and *T.viride*. The FTIR spectra of the fibers showed no change in PCL due to electrospinning. The presence of peaks corresponding to nHAP, ZnO NPs and *T.viride* confirmed the incorporation of fillers into the PCL scaffold.

The TGA study revealed that the addition of nutrients increased the decomposition temperature and char yield. The XRD analysis and morphological studies SEM, EDX and TEM analysis confirmed the loading of components in PCL matrix. The static water contact angle was found to decrease with the incorporation of nHAP, ZnO NPS and *T.viride* compared to pristine PCL. The blending of PCL with PEO resulted in a nanofiber with optimum surface wettability as required for seed coating applications. The swelling and stability investigations revealed that the

BHZT fibers swelled by about 200% in the first few hours, significantly higher than the PCL fibers. After 10 hours, every nanofiber enabled a consistent pattern for stability and swellability. On dissolving nanofibers in water, more than 50% of the material was retained even after 30 min, as opposed to film, where only 30% of the material was retained. Comparing the fibers with the film, electrospinning method reduced the burst release resulting in regulated release of agrichemicals in fibers. Comparing the ZnO NPs, nHAP and *T.viride* integrated PCL/PEO film and nanofiber release characteristics, a burst release of over 50% is observed in the film whereas only a controlled release is noted in the fibers. Porosity measurements of nanofibers were conducted using n-butanol uptake method. The nanofibers exhibited high degree of porosity with a maximum porosity of 98% for BHZT fiber. The analogous polymer film showed very low porosity of 25%. Hence it can be concluded that the large surface area and porosity of nanofibers made them more effective in promoting plant growth. With addition of active ingredients, the diameter of the fibers are varied. Nutrients are added to the electrospun polymer nanofibers to increase the availability of fertilizer for the seed which improve germination potential. The pH and conductivity studies showed a slow release of nutrient from the fiber mats. The aqueous solution of nutrient incorporated PHZ, PHZT and BHZT fibers showed a pH range between 5.4 and 6.5. The pH of the soil containing most vital plant nutrients ideal for plant growth was found to be in the range of 5.5-6.2. The conductivity studies revealed lower conductivity for coated seeds than for untreated seeds, indicating that the seeds are well protected during storage. The prepared nanofertilizer loaded fibers enhanced the growth of corn seedlings. This is due to the slow release of Zn, Ca and P as confirmed by metal release study using ICP-OES. The slow release of calcium and phosphorous from nanofibers indicates the low solubility of nanoformulation of HAP. In addition to providing nutrients to the plant during its growth period, the nanofertilizers employed in this study prevented excessive amounts of these compounds from leaching.

To determine the importance of the addition of nutrients and nanofertilizers, as well as how they interacted, germination studies were conducted over a five-day period. The findings are analysed using one way ANOVA. The use of developed polymer nanofibers as seed coats has significantly increased the growth of radicle and plumule length of *Zea mays* seeds within 120 h of the germinating period. The

three parameters germination percentage (G %), germination index (GI), seed vigour index (SVI) were studied. Nutrient supplementation was observed to boost the germination parameters significantly.

PCL coating provide a sustainable environment to developing embryo by providing optimum retention of moisture and protecting the seed directly from harmful pathogens. The porous polymer film, BHZT_F had not shown any improvement in germination and seedling biomass. The developed nanofiber seed coating significantly improved seedling biomass than conventional film coating approaches utilized by the industry, which inhibited gas and water exchange and hindered radicle and plumule emergence during the germination. The efficiency of the seed coating can be graded as follows:

BHZT_F film coated < Uncoated < PCL nanofiber coated < PHZ nanofiber coated < PHZT nanofiber coated < BHZT nanofiber coated seeds

The antagonistic activity of immobilized *T.viride* spores, a plant beneficial microorganism against *Aspergillus* pathogenic fungi proved the use of such nanofiber seed coating protection as a powerful and versatile platform to enable plant growth in pathogen infested soils.

Study of PCL Nanofiber Loaded with Free α -Amylase and α -Amylase Immobilized on MCM-41 in Presence of Plant Growth Promoters

The application of nanofiber immobilized alpha-amylase for seed germination was done. PCL nanofibers with immobilized alpha-amylase in presence of essential micronutrient, MgO NPs and plant growth regulator, gibberellic acid were applied as seed coats. The use of soluble alpha-amylase in industry is restricted by pH and temperature variations. This caused negative effects on the stability of the enzyme and activity. Alpha-amylase immobilization on inorganic-organic matrix is an effective means of enzyme stabilization. α -Amylase is a crucial biocatalyst for starch hydrolysis in seed germination. The encapsulation of α -amylase enzyme was done through electrospinning. Immobilization was carried out in two ways. PCL and free α -amylase are directly spun into nanofibers which resulted in direct entrapment of enzyme in nanofiber matrix. As a second approach α -amylase was covalently grafted

on MCM-41 via glutaraldehyde as a cross linker, then loaded in PCL solution for electrospinning. MCM-41 was synthesized using sol gel method followed by hydrothermal treatment. The characterization of synthesized MgO NPs, MCM-41, MCM-41 immobilized α -amylase and nanofibers were done using FT-IR, XRD, TG, SEM, EDX and TEM analysis. All the results indicated the successful synthesis and incorporation of components. The aim of the present study was to evaluate the effects of exogenously applied alpha-amylase immobilized nanofibers as seed coats in germination of corn seeds. The contact angle of nanofibers PA was found to be 101.3° and MCM-41 immobilized α -amylase loaded nanofibers PMA, PMMA and PMMG showed hydrophilic property with contact angle less than 90° value. The decrease in the water contact angle to 74.3° in PMMG compared to high hydrophobicity in pristine PCL and high hydrophilicity of water soluble polymers is considered advantageous as the nanofibrous seed coating would assist water absorption in a controlled rate without making the seed dry. All the three scaffolds PMA, PMMA, PMMG show comparable swelling rates. The membrane PA absorbs the solution slowly compared to other nanofibers. Stability studies of PA, PMA and PMMA showed almost 100% stability even after 12 h. It is acceptable to conclude that the weight loss of the composite fiber mats is primarily caused by the deterioration of the composite bulk, which is aided by the release of fillers and accelerated ester bond breakage caused by more amorphous regions. The pH variation of PBS buffer solution of nanofibers was found to be controlled by the PCL matrix degradation rate as well as dissolution profile of MgO nanoparticle. The extent of decrease in pH is low in MCM-41 immobilized α -amylase loaded nanofibers compared to directly entrapped amylase in PCL, which might be due to covalent grafting of α -amylase on MCM-41 restricts the diffusion of enzyme. Thus reduces the degradation of PCL membrane. Out of the nanofibers the pH range for the PMMG nanofiber seems to be the most suitable seed coat since optimum pH range for corn seed germination is found to be 5.8 – 6.5. Mg ion release pattern was analysed using ICP-OES for PMMA and PMMG. The release increased gradually reaching a maximum of $44\ \mu\text{g}$ for PMMA and $32\ \mu\text{g}$ for PMMG at the end of the incubation period. The germination percentage, germination index and seed vigour index are all calculated in order to study the germination rate. The germination trials are carried out for a period of 5 days. The germination potential and coating efficiency follows the order

Uncoated < PA nanofiber coated seeds < PMA nanofiber coated seeds < PMMA nanofiber coated seeds < PMMG nanofiber coated seeds

The high growth rate and more seedling biomass in PMMA and PMMG is due to the presence of MgO NPs. In PMMG additional enhancement is due to the presence of GA. Statistical analysis confirmed that the addition of nutrients and enzyme had a substantial impact on the germination percentage. The α -amylase enzymatic activity of developed nanofibers was measured with time. The results showed that the enzymatic activity increased initially from 103 U/mL to 127U/ml till 20 minutes of incubation time for PA. But MCM-41 supported enzyme incorporated fibers exhibited slow activity in the initial 30 minutes. In contrast to directly loaded enzyme, it was discovered that immobilized enzyme on MCM-41 required a longer incubation period for maximum enzyme activity, up to 40 min. The MCM-41 grafted enzyme loaded nanofibers were also capable of retaining its activity throughout the incubation period with no appreciable loss of activity. There was no drastic decrease in activity compared to the directly encapsulated enzyme in PA. The stability of immobilized enzyme in PCL nanofibers with regard to pH, temperature, reusability and storage were studied.

Nanofibers where α -amylase anchored via covalent grafting on MCM-41 performs better at low and high pH than α -amylase loaded directly in PCL matrix. The optimum pH for both methods was found to be 6.5. Immobilization through covalent grafting enzyme activity maintains almost constant even at pH 7.5 without any significant decrease. pH stability of nanofibers is one of the major advantages to promote seed germination under different soil pH. The optimum temperature for maximum activity for all nanofibers was observed at 40 °C and the activity maintains high for PMMG, PMMA and PMA even at 50°C due to covalent immobilization through inorganic carrier MCM-41. The reuse of enzyme-loaded nanofibers was investigated for up to five runs; almost 56% of the initial activity of PMMG was retained. The storage stability of immobilized α -amylase was examined by monitoring the enzyme activity in every 10 days for a period of 8 weeks. The directly encapsulated PA nanofiber shows 45% activity after 60 days but in PMMA where enzyme incorporated in inorganic silica support lost only 28% activity even after 60 days. The process of seed germination is influenced by various environmental

factors, including soil, pH, moisture and temperature. In addition, the enzymes are essential for seed germination, growth, and development. The germination process can't go on without enzymes. These results indicated that immobilized α -amylase into PCL nanofiber can be used for seed coating for better germination parameters and seedling growth. The PCL with α -amylase immobilized on MCM-41 imparts more stability and proved to be superior organic-inorganic composite seed coats which can be applied for entire lifetime of seedling development.

Study of PEO/Cellulose Nanofibers Incorporated with nHAP and CDs

As a next step, to overcome these economic and environmental obstacles, the research focus is shifted towards incorporation of biopolymers and biofertilizers from biomass for controlled release of fertilizers. The majority of polymers after complete nutrient release are not easily biodegradable, which leads to an unfavourable build-up of plastic residues and a new source of soil contamination. The aim of the present work is the extraction of a biopolymer, cellulose from water hyacinth which then blended with PEO and electrospun into nanofibers. This blend was incorporated with carbon dots derived from water hyacinth and nanohydroxyapatite as nanofertilizer and spun into different composition of fertilizer loaded nanofibers. The study is focused on the promising properties of developed fibers as seed coating for agricultural applications. The efficiency of new and smart biobased seed coating are explored for the controlled release of fertilizers and enhanced germination parameters. Carbon dots are successfully synthesized from HTC process liquid obtained from Hydrothermal Carbonization of water hyacinth stem. Nanohydroxyapatite was synthesized as mentioned by wet precipitation method. The electrospinning solution was prepared by 50:50 PEO/Cellulose blend with 20% nHAP in presence and absence of CDs. The solutions are electrospun to generate nanofibers. The synthesized CDs, cellulose and nanofibers are characterized using the same techniques used in previous studies. IR, XRD, TGA, SEM, EDX AND TEM analysis revealed the incorporation of fillers. IR and XRD spectrum of composite nanofibers showed additional peaks of CDs and nHAP. The synthesized carbon dots (CDs) are characterized using UV-Visible spectroscopy, Photoluminescence spectroscopy and TEM analysis. The PL spectra of CDs incorporated nanofiber showed emission peak around 440 nm. This confirmed the incorporation of CDs within nanofiber matrix. TGA showed that all samples had

the most intense thermal decomposition process within the range of 280–360°C. In this temperature range, the nanofillers such as nHAP and CDs shift the degradation temperature slightly toward higher temperatures. The thermal stability of nanofibers increased upon the addition of fillers. The decomposition temperature for PC_w, PC_wCD_w, PC_wH and PC_wCD_wH nanofibers were found to be 288°C, 316°C, 341°C and 359.7°C respectively. The SEM images of fibers showed formation of uniform, beadless fibers with the EDX images showing presence of phosphorus and calcium on the surface. Fiber diameter decreased upon the addition of fillers.

Water contact angle of prepared nanofibers gives a measure of wettability which is less compared to pristine PEO. This would be beneficial since the nanofibrous seed coating prevents seed degradation due to water absorption. Variation of pH and conductance of aqueous solution of nanofibers were analysed to understand the efficiency of nanofibers for controlled release of agrichemicals. The pH of coated seeds was in the range of 7.4 to 6.8. The release of agrichemicals from the fibers into aqueous system causes variation in the pH of the system. The PEO/Cellulose nanofiber seed coats with biofertilizer CDs and nHAP proved as an effective treatment for protection of seeds and crops from highly acidic soils. The conductance values of nanofibers showed an initial increase but after 48 h the conductance followed a constant pattern. The swelling and stability investigations showed that even though PEO is water soluble, composite nanofibers of PEO with cellulose and the dispersion of CDs and nHAP allow the controlled release of active ingredients. Since the combined nutrients are present on the surface and in the interior of the nanofibers, a burst release of nutrients followed by a controlled flow to the seed during germination is expected.

Metal release study from PC_wH and PC_wCD_wH conducted using ICP-OES for Ca and P release. Ca and P release pattern follows a regular controlled path. The fast and irregular trend in PC_wH is due to the high degree of wettability compared to PC_wCD_wH. The slow release of calcium and phosphorous from nanofibers indicates the low solubility of nanoformulation of HAP. Germination studies are performed using nanofiber coated seeds with uncoated seeds as control. Germination parameters are calculated. Statistical analysis further confirmed the results of germination. Germination potential and fresh biomass seedling follows the order

Uncoated seeds < PC_w nanofiber coated seeds < PC_wH nanofiber coated seeds < PC_wCD_w nanofiber coated seeds < PC_wCD_wH nanofiber coated seeds

Hydroxyapatite nanoparticles (nHAP) were investigated as a potential fertilizer to increase P efficiency. The present study demonstrated the positive benefits of CDs on corn plant development. The antioxidant properties of nanofibers were investigated using DPPH assay. The nanofibers PC_wCD_w, PC_wH and PC_wCD_wH showed high DPPH free radical scavenging activity. The nanofiber PC_wCD_wH exhibited high activity of 94.8%. Antioxidant studies proved that both CDs and nHAP are efficient antioxidants and the application of this as nanofertilizers through nanofiber seed coats would enhance seed establishment and germination potential under oxidative stress of soil.

This study concluded that all nanofibers developed with added fertilizers can release the nutrients within the seed coat during germination in a controlled manner. This attempt in agronomical sector is more advantageous because nontoxic materials such as nHAP, CDs, ZnO NPs, MgO NPs, α -amylase and gibberellic acid were applied as plant growth promoters. This strategy can replace conventional toxic, synthetic chemical fertilizers. Furthermore, to broaden the application of seed coats in addition to germination studies, *Trichoderma viride* was immobilized in the seed coating matrix as biocontrol agent and ability of seed coats in pathogen infected conditions are explored. Further studies are done to identify whether the use of the proposed bio-derived materials offers any significant benefit over existing materials in seed germination and seedling development. With a view to reduce the cost and increase the biocompatibility, biopolymers and biofertilizers derived from biobased materials are employed in the present work as efficient seed coats. Therefore the seed coats are promising to expand the application to agronomic industry. The roles of seed coats to alleviate abiotic stress conditions such as drought, salinity and oxidative stress were investigated in this study. The results are promising lines of research for seed coating. The ultimate goal of introducing a novel crop management product into the agricultural market which will reduce reliance on synthetic agricultural chemicals, plant diseases and in turn increase the profitability for seedling producers is accomplished using the developed nanofibrous seed coating systems.

Future Scope

The selection of the best formulation for polymers and inoculants in seed coating can be quite difficult; the research should be expanded by altering the composition of coating materials and plant beneficial materials for specific crops. Further studies are needed to explore the use of this innovative method in applications like elemental analysis of fresh biomass of seedling to measure the rate of absorption of nutrient elements. After the application of nanofibers in the soil, the water that has leached over a period of time must be analyzed to determine whether the scaffolds have caused any water pollution. An agricultural field experiment must be carried out to evaluate the impact of fiber mats on the entire life cycle of the plant. This study is expected to open the door for new advancements in fertilizer types, administration methods and dosage used in sustainable agriculture. These data will serve as the foundation for expansion into other crop-disease management systems. An in-depth evaluation of the suggested seed treatment's overall effects on the root system will enable us to determine whether the method is viable.

List of Publications

(i) Articles in journals

- **Nonu Davis Chakkalakkal**, Mini Thomas, Pearly Sebastian Chittillapilly, A. Sujith and P.D. Anjali, “Electrospun polymer nanocomposite membrane as a promising seed coat for controlled release of agrichemicals and improved germination: Towards a better agricultural prospect”, *Journal of Cleaner Production*, **2022**, 377, 134479 (IF: 11.072)

(ii) Published contributions in academic conferences

- Presented a paper entitled “Tailoring ecologically sustainable electrospun porous membranes and their potential use as seed coats” at National Seminar on Novel research methodology in chemical science and intellectual property rights organized by Research and PG Department of Chemistry, St. Joseph’s college, Irinjalakuda, Thrissur, Kerala on 9-10 March 2023
- Presented a paper entitled “Synthesis and Characterization of MCM-41 supported Palladium Schiff base complex” at Science Academies’ lecture workshop on “Advances in Supramolecular chemistry and Nanoscience” organized by Research and PG Department of Chemistry, St. Joseph’s college, Irinjalakuda, Thrissur, Kerala on 3-4 March 2017
- Presented a paper entitled “Comparison of catalytic activity of Cobalt(II) schiff base complex immobilized on MCM-41 over the homogeneous analogue towards benzyl alcohol oxidation” international conference on Science and Technology for National Development, organized by the Indian Science Congress Association Cochin Chapter at KUFOS on 25-26 October 2016

- Presented a paper entitled “Immobilized nickel(II)Schiff base complex act as efficient catalyst towards cyclohexanol oxidation over homogeneous analogue” at National Seminar on “Organic synthesis” organized by Research and PG Department of Chemistry, St. Joseph’s college, Irinjalakuda, Thrissur, Kerala on 28-29 January 2016
- Presented a paper entitled “Novel benign solid catalysts for oxyfunctionalization of organic compounds” at National Seminar on Modern Trends in Chemistry organized by Research and PG Department of Chemistry, St. Joseph’s college, Irinjalakuda, Thrissur, Kerala on 22,23 January 2015
- Presented a paper entitled “Enhanced Catalytic Activity of Immobilized Copper(II) Schiff Base Complex over the Homogeneous Analogue towards Cyclohexanol Oxidation” at 25th Swadeshi Science Congress” Organised by Swadeshi Science Movement at Sree Sankaracharya university of Sanscrit, Kalady,Kerala on 16-18 December 2015
- Presented a paper entitled “Transition metal Complexes of Schiff’s Base Derived from 6-aminouracil & 2-hydroxybenzaldehyde as Efficient Catalysts for Cyclohexanol Oxidation” at National Seminar on “Supramolecules and Nanomaterials: Basic Concepts and Architectural Assemblies” organized by Department of Chemistry Sacred Heart College Chalakudy , Thrissur, Kerala on 17-18 November 2015